GaAs/langmuir-blodgett film mis devices

Nicholas John Thomas

GaAs/LANGMUIR-BLODGETT FILM MIS DEVICES

by

NICHOLAS JOHN THOMAS

A thesis submitted in candidature
for the degree of Doctor of Philosophy

UNIVERSITY OF DURHAM

Department of Applied Physics and
Electronics

1986

The copyright of this thesis rests with the author. No quotation from it should be published without his prior written consent and information derived from it should be acknowledged.

I hereby declare that the work reported in this thesis has not previously been submitted for any degree and is not being currently submitted in candidature for any other degree.

Signed

The work reported in this thesis was carried out by the candidate

Signed

ACKNOWLEDGEMENTS

I would like to thank Dr. H. Y. Hall, Dr. G. Hill and Dr. J. H. Marsh, of the SERC Central Facility for 3-5 semiconductors, Department of Electronic and Electrical Engineering, University of Sheffield, who were most cooperative in ensuring the supply of semiconducting material. I am also grateful for the useful discussions I had with them and Professor P. N. Robson.

I am grateful for the cooperation I received from the technical and workshop staff of the Department of Applied Physics, who were under the capable direction of F. Spence.

For the preparation of Langmuir-Blodgett films I am indebted to C. Pearson in particular and also to Dr. T. M. Ginnai, Dr. S. Baker and Dr. Y. L. Hua.

During my time at Durham University I received much help and advice from my many colleagues. In particular I must mention Dr. J. Batey, Dr. J. P. Lloyd, Dr. P. Christie, Dr. I. W. Archibald and D. Buchanan. I apologise to those who I have failed to mention, as they all helped to make my stay an enjoyable one.

I would like to thank Mrs. P. Morrell for typing this thesis and Mrs. J. Smart for preparing the photographs.

It was a great pleasure to work under the supervision of Professor G. G. Roberts and Dr. M. C. Petty. I wish them as much success in their new roles as they enjoyed in their years together.

Finally, I would like to express my gratitude for the help, advice and encouragement I received from my parents.

ABSTRACT

Langmuir-Blodgett (LB) films have previously been used as organic insulating layers in compound semiconductor metal-insulator-semiconductor devices, with promising preliminary results. This thesis describes the first investigation of the use of LB films in gallium arsenide metal-insulator-semiconductor devices. Diodes incorporating thin layers of ω-tricosenoic acid or substituted copper phthalocyanine possessed 'leaky' electrical characteristics, i.e. there is some conduction through the LB film.

This 'leaky' behaviour was exploited to produce the first metal-insulator-semiconductor-switch (MISS) incorporating an LB film. MISS devices on n-p^+ GaAs were produced with good switching characteristics and a high yield ($\sim$90%), using LB film thicknesses between 9 and 33 nm. It was shown that the 'punchthrough' mechanism was responsible for the switching behaviour. p-n^+ GaAs/LB film MISS diodes behaved rather differently, with good switching characteristics only found at reduced temperature. Some degradation of the characteristics of LB film MISS devices was noted, although this was reduced by using the more robust phthalocyanine LB films.

Metal-tunnel-insulator-semiconductor diodes were produced on the ternary alloy $Ga_{.47}In_{.53}As$, using LB film monolayers. The barrier height was apparently larger than that of Schottky barriers on this material, with a very substantial reduction in current density due to tunnelling through the LB film. Using this technique it may be possible to produce very high performance GaInAs field-effect-transistors, which are analogous to GaAs metal-semiconductor field effect transistors.

CONTENTS

CHAPTER 1

INTRODUCTION

Gallium Arsenide is becoming increasingly important to the semiconductor device industry. The principal reason for this is that electrons travel at higher velocities in this material than in silicon; thus devices fabricated in GaAs can operate at higher frequencies. GaAs is expensive and it is more difficult to use than silicon, however there are applications which demand the higher performance that can be achieved using GaAs. GaAs devices are now widely used in analogue microwave applications, and gigabit/s digital integrated circuits have become commercially available. In addition, interesting experimental developments are exploiting two other valuable attributes of GaAs, which silicon does not possess. The first of these is the direct bandgap, which allows integrated optoelectronic devices to be constructed. The second development is the production of high quality hetrostructures, by depositing epitaxial AlGaAs layers, which permit the tailoring of material properties and structures to produce new devices such as the high-electron-mobility transistor (HEMT). These two developments will inevitably become very important in this era of high speed lightwave communications.

The greatest difference between GaAs and silicon technologies is perhaps the widespread use of metal-oxide-semiconductor (MOS) structures in silicon processing. High quality silicon dioxide layers can be grown on silicon, and the electrical properties of the silicon-silicon dioxide interface are excellent. This fortunate state of affairs has enabled Si MOS devices to take over a large and growing sector of the market.

Recently, experimental devices using insulating layers thin enough to conduct, by quantum-mechanical tunnelling or other mechanisms, have been investigated. These come in a variety of different structures, including memory devices, the metal-insulator-semiconductor-switch (MISS), solar cells and light emitting diodes. Unfortunately, it has not proved possible to develop a metal-insulator-semiconductor technology for GaAs, because of a lack of compatible insulating films. Oxides grown on GaAs are nonstoichiometric, with poor mechanical and electrical properties. Good insulators, such as silicon dioxide and silicon nitride, can be deposited onto GaAs. However, the properties of the insulator-semiconductor interface are generally very poor, which may be due to disruption of the GaAs surface caused by the energetic deposition process. One possible route to solving this problem is to use an insulating layer which can be deposited without disturbing the semiconductor surface, for example Langmuir-Blodgett (LB) films.

Certain organic materials can form layers upon the surface of a liquid which are a single molecule thick; these are called Langmuir films. These layers can be transferred onto a solid substrate by passing it through the surface of the liquid; by repeating this process multilayer Langmuir-Blodgett (LB) films can be built up, one monolayer at a time. These LB films are highly ordered and uniform organic layers, whose thickness is directly related to the number of monolayers deposited. This room temperature technique is not aggressive, therefore it should not damage the surface upon which the film is deposited. The electrical properties of the LB film can be very good, if care is taken to control the deposition process. A unique asset of LB films is the excellent uniformity of, and control over, their thickness, which is determined by the molecular dimensions. This may prove of particular

importance when applied to ultra-thin metal-insulator-semiconductor structures, because these are highly sensitive to variations in insulator thickness. Indeed, it is extremely difficult to reliably form ultra-thin insulating films using other techniques, because the layers required are only a few atoms thick. This is the case even for the growth of silicon dioxide on silicon, which has been exhaustively researched. The preliminary investigation of metal-insulator-semiconductor (MIS) devices incorporating LB films, on a variety of elemental and compound semiconductors, has yielded some promising results, which suggest that it may be possible to exploit the advantages of the Langmuir-Blodgett technique.

The object of this work was to investigate the suitability of LB films for use as the insulating layer in metal-insulator-semiconductor (MIS) devices based on GaAs (or related materials). Conventional MIS structures using thick insulating layers (such as those which are required for use in insulated gate field effect transistors) were briefly investigated, but the results obtained were not promising. Therefore it was decided to concentrate on thin layer MIS structures; this offered several interesting possibilities, including the metal-insulator-semiconductor-switch (MISS), which was the subject of a major part of this study. Also of interest was the use of an LB film layer to modify the effective barrier height of Schottky contacts. This is particularly desirable on materials with a low barrier height, such as $Ga_{.47}In_{.53}As$, which is potentially even better than GaAs for use in high performance devices. One other area which was briefly examined was the use of 'active' LB film layers to produce chemically sensitive MIS devices. It is possible, using the LB technique, to deposit thin, uniform and reproducible chemically sensitive layers, and this could

allow improvements in the accuracy, speed of response and sensitivity of microelectronics sensors to be obtained.

In chapters 2 and 3 the basic physics required for an understanding of this work is covered, including the theory of Schottky barriers, metal-thin-insulator-semiconductor devices, and the metal-insulator-semiconductor switch. The following chapter describes the physics and applications of Langmuir-Blodgett films. The experimental techniques used to fabricate and characterise devices are detailed in chapter 5. The first of the two results chapters covers the basic characterisation of the GaAs/LB film MIS system. Schottky barriers were used to test the efficacy of the preparation of clean GaAs surfaces. They were also used to determine how the LB film deposition process affects the GaAs surface, which must be clearly established before the effects of the LB film can be quantified. The effects of variations of LB film thickness and composition upon the electrical characteristics of GaAs MIS devices were studied. The work on GaInAs is also described in this chapter. Chapter 7 describes the results of the study of GaAs/LB film metal-insulator-semiconductor-switches. The dependence of their characteristics upon both the LB film and the GaAs substrate were investigated. An attempt was made to provide a simple explanation for the behaviour of these MISS devices, utilising all the available data for the GaAs/LB film system. Silicon/LB film MISS diodes and the work on LB film sensors are also covered in this chapter. The final chapter discusses the conclusions drawn from this work and puts forward some suggestions for future work.

CHAPTER 2

SCHOTTKY BARRIER AND TUNNEL MIS DIODES

2.1 Introduction

Rectification at point contacts between metals and semiconductor crystals was first observed by Braun in 1874[1]. From about 1905 to 1925 these 'cat's whiskers' were in widespread use as detectors in radio receivers. However, at this time, the operation of these devices could not be satisfactorily explained. In the early 1930's it was realised that the potential drop occurred almost entirely at the contact[2], and Wilson proposed a theory based on the newly discovered quantum-mechanical tunnel effect[3]. However, it was soon realised that this predicted the opposite polarity of rectification to that observed[4]. In 1938 Schottky[5] and Mott[6] independently proposed that this behaviour could be explained by diffusion of carriers over an energy barrier in the semiconductor, and that this barrier could arise from work function differences between the metal and the semiconductor. The term 'Schottky barrier' specifically refers to the most common case of a uniformly doped semiconductor, however it is now also widely used to denote any metal-semiconductor contact.

Point contact diodes again became important in the 1940's due to the need for low noise microwave detectors, and during this period two important theoretical advances were made, Bethe's Thermionic Emission Theory[7] and Bardeen's Surface State Model[8]. In the 1950's and 1960's studies of Schottky barriers were stimulated by the increasing use of evaporated metal contacts in semiconductor devices and by a better appreciation of the importance of the properties of interfaces. Progress

continued into the 1970's, when the emergence of U.H.V. techniques first permitted detailed studies of both clean semiconductor surfaces and the initial stages of Schottky barrier formation.

Today Schottky barriers are playing an increasingly important role in semiconductor device technology, for example as photodiodes and in MESFETs (Schottky gate FETs). There is also considerable interest in modifying contact properties by introducing a thin insulating layer, hence producing a tunnel MIS diode, which can significantly improve photovoltaic, electroluminescent or electrical characteristics. It is not possible, or desirable, to comprehensively cover this immense field in this thesis, therefore the reader is referred to the many books and reviews on the subject[9-17]. The first of the three main sections of this chapter covers the physics of Schottky barrier formation, commencing with the simple models of Schottky and Bardeen, before discussing more recent developments. Following this is a description of the electrical characteristics of nearly ideal, abrupt, Schottky diodes. However, interfacial layers occur in many practical metal-semiconductor contacts, or they may be intentionally introduced, resulting in the slightly different behaviour which is discussed in the final part of this chapter.

2.2 Schottky Barrier Formation

In this section we first consider Schottky's original model, which demonstrated that a barrier could result purely from the requirements for thermal equilibrium between metal and semiconductor. We continue by describing Bardeen's model, which takes into account the effects of surface states. Although these models are widely used they are not totally satisfactory, and the recent progress in this area is discussed in the section on further developments. It should be noted that only n-type material is considered in this chapter, for convenience and clarity, as the generalisation to p-type is straightforward.

2.2.1 The Schottky Model

Schottky established that a potential barrier could arise at a contact between an ideal metal and an ideal semiconductor, even if both materials remained uniform up to an abrupt boundary[4,18]. This can be most easily explained by considering the metal and semiconductor to be initially separated, but electrically connected to maintain thermal equilibrium, and then being brought into intimate contact. Band diagrams for the two ideal surfaces are shown in fig. 2.1a and 2.1b, ϕ_m and ϕ_s are the work functions of the metal and semiconductor, χ_s is the electron affinity of the latter and $\zeta(=\phi_s - \chi_s)$ is the energy of the Fermi level of the semiconductor below the conduction band minimum (c.b.m.).

The case where electrical connection has been established, but the separation is large, is shown in fig. 2.1c. In this case $\phi_m > \phi_s$, as is most common in practice. The work function difference gives rise to an electric field, E, which requires a negative charge on the metal surface and an equal positive charge on the semiconductor surface. The charge on the metal can be accommodated close to the surface because of the large density of states at the Fermi level. Therefore the penetration of the field into the metal is negligible (it is equal to the Thomas-Fermi screening length $\sim$.05 nm). However, in the semiconductor the charge can only be accommodated by conduction band electrons receeding from the surface, which leaves uncompensated donors in a region depleted of electrons. As the separation is reduced and the charge required increases, the surface of the semiconductor becomes completely depleted to a depth, w, (fig. 2.1d). When the separation approaches zero then the potential drop across the gap must go to zero and then the work function difference must be accommodated entirely by the depletion region of the semiconductor (fig. 2.2). The band bending in the semiconductor is V_{do},

the (zero bias) diffusion potential. By inspection

$$V_{do} = \phi_m - \phi_s \tag{2.1}$$

Therefore if $\phi_m > \phi_s$ there is a potential barrier and the contact is rectifying, but if $\phi_m < \phi_s$ the bands are bent downwards and, as there is no barrier, the contact is ohmic. (For p-type material the contact is rectifying if $\phi_m < \phi_s$.) The barrier height between metal Fermi level and semiconductor conduction band, ϕ_b, is given by

$$\phi_b = \phi_m - \chi_s \tag{2.2}$$

as first stated by Mott[6]. We have assumed that there are no dipole layers at the surfaces, but this is unlikely due to boundary effects. However, the model is still valid providing the dipoles are unaffected when contact is made.

The shape of the potential barrier is determined by the space charge density. If the band bending is greater than 3kT/q then the electron density in the conduction band is reduced by an order of magnitude, giving a space charge almost entirely due to uncompensated donors. The calculation of the barrier profile is simplified if the transition region is ignored and if the space charge density is assumed to change abruptly from qN_d to zero at the edge of the depletion region. In this 'depletion approximation' the shape of the barrier is determined entirely by the distribution of ionised donors. Schottky described the most common case of constant donor density throughout the semiconductor. Applying Gauss's theorem we find that the electric field increases from zero at the edge of the depletion region (at x=w), to a maximum at the

interface (at x=0), which is given by

$$E_{max} = \frac{q N_d w}{\varepsilon_s} \tag{2.3}$$

From Poisson's equation the band bending in the semiconductor follows a parabolic profile and the depletion width is given by

$$w = \left(\frac{2 \varepsilon_s V_d}{q N_d} \right)^{\frac{1}{2}} \tag{2.4}$$

When an external bias is applied these equations still hold, however the diffusion potential changes to accommodate the bias.

Schottky's model explained the observed rectification at metal-semiconductor contacts. However, it soon became apparent that the variation in contact properties with metal work function was much smaller than predicted. This was not satisfactorily explained until 1947, when Bardeen proposed a model that included the effects of surface states.

2.2.2 Bardeen Model

Bardeen[8] proposed a model which could explain the discrepancy between Schottky's theory and experimentally observed barrier heights. In his model the height of the barrier is controlled by surface (or interface) states in the semiconductor band gap, which arise from the abrupt termination of the lattice. The model also requires a thin interfacial insulating layer, of atomic dimensions, which is assumed to be completely transparent to electrons and therefore have no effect on carrier transport in the contact.

Fig. 2.3 shows the band diagram of a metal-semiconductor contact with an interfacial layer of thickness δ and permittivity ε_i; V_i is the

potential drop across the layer and ϕ_o is the energy, measured from the valence band maximum (v.b.m.), to which all interface states must be filled for charge neutrality at the semiconductor surface. It is assumed that the density of interface states per unit energy, N_{ss}, is constant over the range of interest. In equilibrium there must be overall charge neutrality, therefore

$$Q_m = -(Q_{ss} + Q_{sc}) \tag{2.5}$$

where Q_m, Q_{ss} and Q_{sc} are the charge densities per unit area on the metal surface, in surface states and in the depletion region, respectively. This equation has been solved for the zero bias case by Cowley and Sze[19]. However, if a sufficient forward bias is applied such that the flat band case is reached (fig. 2.4), then $Q_{sc} = 0$ as there is no space charge region[12]. It is assumed that the charge in the interface states is controlled by the Fermi level in the metal, as would be expected because the interfacial layer is thin. Therefore, applying Gauss's theorem, the flat band barrier height, ϕ_{bo}, is given by

$$\phi_{bo} = \gamma\ (\phi_m - \chi_s) + (1 - \gamma)\ (E_g - \phi_o) \tag{2.6}$$

where γ is defined as

$$\gamma = \frac{\varepsilon_i}{\varepsilon_i + q\delta N_{ss}} \tag{2.7}$$

This result was first derived by Cowley and Sze as an approximation to the zero bias case. These authors also showed that the transition

between the 'Schottky limit' of negligible surface state density (i.e. γ=1) and the 'Bardeen limit' of very large density (i.e. γ=0) occurs over a reasonable range of values.

In this model the barrier height is a function of applied bias because of the presence of the interfacial layer. It can be shown that the barrier height change is proportional to the electric field at the semiconductor surface, E_{max}, that is

$$\phi_b = \phi_{bo} - \alpha E_{max} \tag{2.8}$$

where

$$\alpha = \frac{\delta \varepsilon_s}{\varepsilon_i + q \delta N_{ss}} \tag{2.9}$$

Taking the worst case of zero surface state density and for a moderately heavily doped semiconductor ($N_d \sim 10^{17}$ cm^{-3}), then $\phi_{bo} - \phi_b \sim .06$ eV. This small variation of barrier height has only minor effects (see section 2.3.1).

This simple model has been widely used and provides an explanation of barrier formation that is satisfactory as a first order approximation. Considerable efforts have been made to promote a more complete understanding of Schottky barriers. These studies, including the large body of work on 3-5 semiconductors and in particular GaAs, are described in the next section.

2.2.3 Further Developments

In their analysis of the Bardeen model Cowley and Sze[19] noted a reasonable degree of agreement with the observed barrier height dependence on metal work function, especially when the variability of

work function measurements was taken into account. The fit was often better for chemically etched semiconductor surfaces than for those prepared by vacuum cleavage; this might be expected as the former always leaves an interfacial layer which isolates the semiconductor surface from the metal. Although, on initial examination, it seems difficult to apply the Bardeen model to intimate contacts, such as those prepared by vacuum cleavage, Heine[20] argued that even in this case an interfacial region must exist. This is created by mixing of metal and semiconductor wavefunctions; interface states arise due to tunnelling of metal wavefunctions into the semiconductor bandgap (Metal Induced Gap States). Although this demonstrates the utility of Bardeen's model, it must be noted that Archer and Yep[21] found that the variation in barrier height with the doping concentration of silicon substrates was much smaller than expected, thus demonstrating a limitation on the validity of Bardeen's formulation.

Studies on covalent semiconductors showed that the barrier height (on n-type material) was often approximately two thirds of the bandgap for a wide range of metals and semiconductors[22]. It was soon realised that ionic semiconductors possessed very different characteristics, showing large variations in barrier height, as expected from the Schottky model[23]. Kurtin and coworkers[24] formalised this by defining an interface parameter, S ($= \partial\phi_b/\partial X_m$ where X_m is the electronegativity of the metal). They found a sharp transition between $S \sim 0$, the Bardeen limit, for covalent materials and $S \sim 1$ for ionic materials, which they ascribed to the Schottky limit (fig. 2.5). This gives a fair indication of trends in contact behaviour, however the validity of this approach has been questioned[25,26]. In particular, it is often not possible to obtain a linear fit for S, therefore this model is not universally applicable.

Andrews and Phillips first demonstrated that strong bonding at the interface could influence Schottky barrier formation[27]. They found a strong correlation between the barrier height of transition metal - silicon diodes and the heat of formation of the silicide. The importance of interfacial reactions in barrier formation on other semiconductors, including GaAs, has been shown by the work of Brillson[28,29]. A sharp transition between unreactive and reactive cases was found when barrier height was plotted against heat of reaction (between metal and semiconductor) (fig. 2.6). A strong correlation between interface thickness and the heat of reaction was also noted, however the basis of this latter observation has been questioned[26].

Spicer and coworkers discovered that the Fermi level at cleaved (110) surfaces of 3-5 semiconductors becomes pinned by submonolayer coverages of metals or oxygen[30,31] (fig. 2.7). The pinning position was almost independent of the metal and was in agreement with reported Schottky barrier heights. These authors proposed a 'Unified Defect Model', which explained these observations as being due to defects characteristic to the semiconductor, created by the energy released as the metal condensed on the surface. Although the nature of these defects is not yet certain there is some evidence that they are associated with anion vacancies. This model conflicts in some respects with that of Brillson, and the interpretation of the available data is still the subject of some controversy[26,32,33]. Different approaches to the barrier formation conundrum have included the 'Effective Work Function' model of Woodall and Freeouf[34]. This proposed that the GaAs-metal interface consists of microclusters of different phases which modify the effective work function and hence the barrier height. In addition, Lee et al[35] suggested that their results on GaP Schottky barriers could be

explained by the presence of a relatively thick amorphous layer at the interface.

In conclusion, we find that at present there is no satisfactory universal model of Schottky barrier formation. Several theories have had some success in explaining the details of a limited range of contact systems. However, even in these cases there are opportunities for differing interpretations of the data. Undoubtedly part of this problem is due to the sensitivity of surface and interface properties to the details of their preparation. As this area is of great technological importance there is a large and growing research effort, as can be seen in the recent review by Brillson[15] which includes over 1000 references.

2.3 Near-Ideal Schottky Barriers

We will define a near-ideal Schottky barrier as one in which the interfacial region between metal and semiconductor is thin enough to have negligible effects on carrier transport or the capacitance of the device. Many contacts fabricated on chemically prepared or cleaved semiconductor surfaces will be near-ideal, although some chemical treatments leave substantial interfacial layers. The discussion of the characteristics of near-ideal Schottky diodes commences with the mechanisms of current transport, then the capacitance of these devices is considered and finally methods of measuring the barrier height are described and compared.

2.3.1 Current Transport

Possible current transport mechanisms in Schottky barriers are illustrated in fig. 2.8. The dominant process in most devices is thermionic emission of majority carriers over the barrier. In these unipolar devices minority carrier injection is usually insignificant (cf. p-n junction behaviour), and it will not be considered in this section.

In heavily doped semiconductors thermally assisted tunnelling, thermionic-field emission, becomes important, and for degenerate material direct tunnelling, field emission, can occur. These processes are of little relevance to this work and are not discussed in detail. If the mobility of the semiconductor is sufficiently low then diffusion in the depletion region, not thermionic emission, may limit current flow. In addition, recombination and generation in the depletion region may be significant in low lifetime materials for reverse and low forward bias. However, before describing these processes we must first consider image force barrier lowering, which can play an important role in carrier transport over the barrier.

Image Force Barrier Lowering

Image force lowering, also known as the Schottky effect, is due to the attractive force which acts on a charged particle near a metal surface. This causes an effective lowering of the potential barrier for electrons (or holes), although there is no change in the barrier profile in the absence of charge carriers. The simple model used here assumes that screening effects are negligible, i.e. the carrier density at the top of the barrier is small.

For an electron at a distance x from a metal surface the attractive 'image force' is given by

$$\frac{q^2}{4\pi \varepsilon_s' (2x)^2}$$

Note that ε_s', the high frequency permittivity, is used because electrons approach the barrier with thermal velocities. However in practice we may

assume $\varepsilon_s' = \varepsilon_s$, the static value. The lowering of the potential must be added to the potential energy of the barrier, in order to find the true potential felt by an electron (fig. 2.9). This gives a potential maximum at x_o and a barrier lowering of $\Delta\phi_{bi}$. Since the image force is only significant close to the metal then it may be assumed that the field in the semiconductor is constant and equal to E_{max}; this gives

$$\Delta\phi_{bi} = \left(\frac{q\, E_{max}}{4\pi\, \varepsilon_s'} \right)^{\frac{1}{2}} \qquad (2.10)$$

For a doping density, $N_d = 10^{17}\ cm^{-3}$ and a diffusion potential of 1 volt, then $\Delta\phi_{bi} \sim .05eV$, which is large enough to affect current transport over the barrier. In the remainder of this section we will use ϕ_e to signify the effective barrier height when referring to transport of carriers over the barrier, where

$$\phi_e = \phi_b - \Delta\phi_{bi} \qquad (2.11)$$

Thermionic Emission Theory

This theory of carrier transport in metal-semiconductor contacts was formulated by Bethe[7], who assumed that the current limiting process is the thermionic emission of electrons over the potential barrier. In this model the effects of drift and diffusion in the depletion region are assumed to be negligible, and the electron quasi-Fermi level of the semiconductor is therefore flat (fig.2.10). At the semiconductor side of the boundary the electron concentration is given by

$$n = N_c \exp\left[-q\,(\phi_e - V)/kT\right] \tag{2.12}$$

where the effective density of states in the conduction band, N_c, is defined as

$$N_c = 2(2\pi\, m^*\, kT/h^2)^{3/2} \tag{2.13}$$

If we can assume an isotropic Maxwellian velocity distribution for the conduction band electrons at the top of the barrier then, from elementary kinetic theory, the electron current from semiconductor to metal is given by

$$J_{sm} = A^*\, T^2 \exp\left(\frac{-q\,\phi_e}{kT}\right)\exp\left(\frac{qV}{kT}\right) \tag{2.14}$$

A^* is the effective Richardson constant of the semiconductor ($= m^*/m_e$ times the Richardson constant, A^*)and is given by

$$A^* = \frac{4\,\pi\, m^*\, qk^2}{h^3} \tag{2.15}$$

At zero bias the current from metal to semiconductor, J_{ms}, must be equal to J_{sm}. The barrier to electrons passing from metal to semiconductor is constant ($=\phi_b$), therefore J_{ms} is constant and the total current is given by

$$J = A^* T^2 \exp\left(\frac{-q\,\phi_e}{kT}\right)\left(\exp\left(\frac{qV}{kT}\right) - 1\right) \tag{2.16}$$

For forward bias, V, of greater than 3kT/q volts J_{ms} is negligible and the total current is given, approximately, by equation 2.14.

An alternative approch was proposed by Henisch[9] and Spenke[10], in which a Maxwellian distribution of electron velocities is assumed to occur at the edge of the depletion region. If the mean free path, λ, is greater than w, the depletion width, then electron emission occurs from this plane. In fact, if we can chose a reference plane which is in equilibrium with the bulk, possesses a Maxwellian velocity distribution and is also less than a mean free path from the interface, then the current is limited by thermionic emission. It is sometimes proposed that the validity of the thermionic emission regime is set by the condition $\lambda > w$, however the above argument shows that this limit is too stringent.

In practice, for most common semiconductors, the observed current transport characteristics are in good agreement with the predictions of the thermionic emission theory. Some refinements of this theory are discussed later, but first it is necessary to briefly describe the original diffusion theory of carrier transport in Schottky barriers.

Diffusion Theory

In the diffusion theory of Schottky and Spenke[18] the current is assumed to be limited by carrier transport in the depletion region, as governed by the usual processes of drift and diffusion. The current due to diffusion and drift of electrons in a semiconductor is given by

$$J = q.n.\mu.\varepsilon + q.D_e \frac{\partial n}{\partial x} \qquad (2.17)$$

where μ is the electron mobility and D_e is the diffusion coefficient for electrons. These are linked by the Einstein relationship, enabling the current to be restated as

$$J = q.\mu.n. \frac{\partial \zeta}{\partial x} \qquad (2.18)$$

where we define an electron quasi-Fermi level of energy, ζ , by the equation

$$n = n_c \exp\left[-q\,(E_c - \zeta)/kT\right] \qquad (2.19)$$

where E_c is the energy of the conduction band minimum.

In the diffusion theory the current is determined by integrating equation 2.18 across the depletion region (using the depletion approximation to obtain the barrier profile). The limits for the integration are given by assuming that the electron quasi-Fermi level is aligned with metal Fermi level at the interface and aligned with bulk Fermi level at the edge of the depletion region (fig. 2.11). This is equivalent to the initial assumption of this theory, that the current is limited by diffusion and drift in the depletion region. The current-voltage relationship thus obtained is given by

$$J = qN_c\,\mu\,E_{max}\exp\left(\frac{-q\,\phi_b}{kT}\right)\left(\exp\left(\frac{qV}{kT}\right) - 1\right) \qquad (2.20)$$

This is almost of the same form as the thermionic emission result (equation 2.16), apart from the preexponential term; this also has a slight voltage dependence, since $E_{max} \propto (V_{do} - V)^{\frac{1}{2}}$, which prevents saturation of the reverse characteristics.

As the thermionic emission and diffusion theories give very similar current-voltage relationships, then the only indication of which process dominates is the magnitude of the preexponential term. For nearly all diodes studied the thermionic emission theory gives a better fit to the results. It is reasonable to assume that both processes act in series, therefore several combined thermionic emission - diffusion theories have been proposed, and these are considered below.

Thermionic Emission-Diffusion Theory

The most developed theory combining thermionic emission and diffusion processes is that of Crowell and Sze[36]. This assumes that the current is diffusion limited on the semiconductor side of the boundary (at x_m when image force effects are included) and thermionic emission limited between this point and the metal. The current due to thermionic emission is given by

$$J = q\, v_r\, (n-n_o) \tag{2.21}$$

defining a 'recombination velocity', v_r; $(n - n_o)$ is the change in electron concentration, at x_m, from that at equilibrium. The diffusion current on the semiconductor side of x_m is calculated as in the original diffusion theory. These two currents can then be equated giving (after some rearrangement)

$$J = \frac{q\, N_c v_r}{1 + v_r/v_d} \exp\left(\frac{q\,\phi_e}{kT}\right)\left(\exp\left(\frac{qV}{kT}\right) - 1\right) \tag{2.22}$$

v_d, the effective 'diffusion velocity', is approximately equal to

$$v_d = \mu\, E_{max} \tag{2.23}$$

If we assume a Maxwellian distribution of electron velocities at the top of the barrier (at x_m) then, since v_r is due to thermionic emission.

$$v_r = \frac{\bar{v}}{4} = \frac{A^* T^2}{q\, N_c} \tag{2.24}$$

We can now see that equation 2.22 is equivalent to the thermionic emission case (equation 2.16), if $v_d >> v_r$. This inequality is roughly equivalent to Bethe's condition for the validity of the thermionic emission theory of $E_{max} > kT/q\lambda$.

Crowell and Sze extend their theory to include the effects of optical phonon scattering in the boundary region and quantum mechanical reflection at the interface. In this case the current can be described by a modified thermionic emission equation,

$$J = A^{**} T^2 \exp\left(\frac{-q\phi_e}{kT}\right)\left(\exp\left(\frac{qV}{kT}\right) - 1\right) \tag{2.25}$$

where A^{**} is given by

$$A^{**} = \frac{f_p f_q A^*}{1 + f_p f_q v_r/v_d} \tag{2.26}$$

f_q is the quantum mechanical transmission coefficient and f_p is the phonon induced probability of emission. The overall result of this theory is the replacement of the effective Richardson constant A^* with a new constant A^{**}. Reasonable estimates give $f_p f_q \sim .5$ and, since $v_d >> v_r$ for most semicondutors, we then find that A^{**} is approximately half the value of A^*. Although this well developed theory agrees quite well with experiment it is still not comprehensive; this is because a satisfactory treatment of electron transport in rapidly varying potentials is not available.

Non-Ideal Current Transport

Experimental studies of Schottky diodes show deviations from the ideal characteristics described above. It is found that in general

$$J \propto \exp\left(\frac{qV}{nkT}\right) \tag{2.27}$$

where n is the ideality factor. For the ideal cases described above n = 1, however experimentally n is always greater than 1 (although for near-ideal diodes n is usually less than 1.1). Also, in reverse bias, the expected current saturation is rarely observed. The most important causes of these effects are described below.

The effective barrier height, ϕ_e, appears in an exponential term in the current-voltage relationship, therefore even a small bias dependence can have a significant effect. Two possible causes of a bias depenence have been discussed previously. The first of these occurs in all diodes and is due to image force barrier lowering (equation 2.10). This is proportional to $E_{max}^{\frac{1}{2}}$ and is therefore a function of bias. The second effect arises when a interfacial layer is present (as in the Bardeen model, equations 2.8 and 2.9), which gives a barrier lowering proportional to E_{max}. These effects, although small, cause an increase in the ideality factor. These mechanisms can also be important under reverse bias, which increases E_{max}; the resultant barrier lowering may be the cause of non-saturation of the reverse characteristics.

If thermionic field emission is significant then the ideality factor, n, can be much larger than unity, in addition the reverse current will not saturate[37]. However, this process only becomes important at low temperature, or for high doping densities. Another process that can cause an increase in the ideality factor is recombination in the space

charge region. Yu and Snow[38] demonstrated that this can be significant in Schottky barriers on low lifetime semiconductors, especially for low forward bias. The theory was initially developed for p-n junctions[39], and for the case of forward bias

$$J \propto \exp\left(\frac{qV}{2kT}\right) \tag{2.28}$$

If this component is small it may cause an apparent increase in the ideality factor, n. If the effect is more significant a separate region in the log J versus V characteristic, with an n value of 2, will be found. Under reverse bias the corresponding generation current, which is proportional to depletion width, may be a cause of non-saturated characteristics.

It can be concluded that the current-voltage characteristics follow equation 2.26 with an ideality factor, n, greater than, but usually close to, one. This non ideality can be caused by several mechanisms and these also prevent saturation of the reverse current. It must be pointed out that the electric field may be greatly enhanced at the edges of contacts unless special precautions are taken (e.g. guard rings). This can greatly increase the non-idealities caused by field dependent processes and is especially important for reverse bias.

2.3.2 Capacitance

The capacitance of Schottky barriers arises because of the space charge in the semiconductor depletion region and the equal and opposite charge on the metal surface. Since the depletion width is a function of applied bias, the capacitance must be voltage dependent. If the depletion approximation is used then the charge in the depletion region,

Q_{sc}, (due entirely to ionized donors) is given by

$$Q_{sc} = (2\ \varepsilon_s q\ N_d\ V_d)^{\frac{1}{2}} \tag{2.29}$$

The capacitance is usually measured by superimposing a small a.c. signal on a d.c. bias; this is the differential capacitance. The capacitance per unit area is given by

$$C = \frac{\partial Q_{sc}}{\partial V} = \left(\frac{q\ \varepsilon_s N_d}{2\ (V_{do} - V)} \right)^{\frac{1}{2}} \tag{2.30}$$

where V is the applied bias (forward positive). A more rigorous analysis, taking into account the effect of the transition region at the edge of the depletion region, yields

$$C = \left(\frac{q\ \varepsilon_s\ N_d}{2\ (V_{do} - V - kT/q)} \right)^{\frac{1}{2}} \tag{2.31}$$

In both cases $1/C^2$ is proportional to the bias and the slope is inversely proportional to donor density.

The above analyses both assume that the space charge is due solely to a constant density of ionized donors and that any interfacial layer is negligible. The first assumption will not hold if the surface of the semiconductor is inverted, or if there is a large density of deep trap levels. The effects of interfacial layers are discussed later in this chapter in section 2.4.2.

2.3.3 Barrier Height Measurement

The barrier height at a metal-semiconductor contact can be obtained from three types of measurement. The techniques measure either current-voltage, capacitance-voltage, or photoresponse characteristics.

The results of these methods are complementary, and ideally at least two techniques should be compared to ensure that misleading results have not been obtained.

Current-Voltage Measurements

In section 2.3.1 it was shown that the barrier height determines the current-voltage characteristics of Schottky diodes. In theory the barrier height can be found from either forward, or reverse, bias characteristics. However reverse bias measurements may be unreliable because the current often differs from the ideal case (see section 2.3.1). In forward bias, for $v > 3kT/q$, the current is given by

$$J = J_o \exp\left(\frac{q\,V}{nkT} \right) \tag{2.32}$$

where (from equation 2.25)

$$J_o = A^{**} \exp\left(\frac{-q(\phi_b - \Delta\phi_{bi})}{kT} \right) \tag{2.33}$$

Therefore a plot of ln J against bias should form a straight line of slope q/nkT, with an intercept on the current axis at J_o. If A^{**} is known then ϕ_b can be calculated; however an approximate value of A^{**} can be used, since a factor of two change in this gives an error of less than kT/q in ϕ_b.

If A^{**} or the active area of the device are unknown, then ϕ_b can be found by determining J_o as a function of temperature. An activation energy plot, of $\ln (J_o/T^2)$ versus T^{-1}, should yield a straight line of slope $-q\,(\phi_b - \Delta\phi_{bi})/k$, with an intercept at $1/T = 0$ of $\ln A^{**}$. If the barrier height is a slowly varying function of temperature then this technique yields the zero temperature barrier height. Techniques have also been devised for determining the barrier height even when a large

series resistance causes the plot of ln J versus V to become nonlinear[40-42]. Unfortunately, they are all of limited utility, either because they assume n = 1, or due to their use of tedious calculations.

I-V methods for obtaining barrier heights are only reliable if the interfacial layer is thin enough not to interfere with carrier transport. A high ideality factor ($n > 1.1$) is usually due to the presence of a substantial interfacial layer. However a low ideality factor ($n < 1.1$) is not always an indication of an intimate contact, and under certain conditions a small n value can be obtained despite the existence of a significant interfacial layer[43].

Capacitance Measurements

It can be seen from equation 2.31 that a plot of $1/C^2$ versus reverse bias voltage has a slope of $2/(q\epsilon_s N_d)$ and an intercept on the voltage axis of $(-V_{do} + kT/q)$. Once the zero bias diffusion voltage, V_{do}, and the doping density, N_d, are known it is possible to calculate, ϕ_b, the barrier height. Image force effects do not need to be taken into account with capacitive measurements, unlike other techniques of barrier height measurement. This is because capacitance is a function of barrier profile and is unaffected by transport of carriers over the barrier. However the technique is unreliable where there is a significant interfacial layer at the contact, as will be demonstrated in section 2.4.2. A good review of the practical difficulties of this method has been given by Goodman[44]; the effects of deep traps, effective area variations and circuit considerations are covered.

Photoelectric Effect

If light of energy $h\nu > \phi_b - \Delta\phi_{bi}$ is incident on the metal then electrons can be excited and pass over the potential barrier into the semiconductor (fig. 2.12). This generates a photovoltaic E.M.F., causing

a current to flow. The photoelectric theory was developed by Fowler[45] for the emission of electrons from a metal into a vacuum, but it applies equally well to this case. It was assumed that the current is directly proportional to the 'number of available electrons', N_b. Fowler showed that for $h\nu - \phi_e >> kT$ then

$$N_b \propto (h\nu - \phi_e)^2 \qquad (2.34)$$

Therefore a plot of (photocurrent/applied photon)$^{\frac{1}{2}}$ against photon energy, $h\nu$, should yield a straight line, with an intercept on the energy axis at $h\nu_o = \phi_b - \Delta\phi_{bi}$. As the photon energy approaches the bandgap this relationship must break down, because an additional photocurrent due to band to band excitation is then generated.

To observe the photoelectric effect the metal can be illuminated either through the semiconductor or, if thin ($\lesssim$ 50 nm), directly. The latter is possible because the mean free path of hot electrons in a metal is fairly long ($\sim$74 nm in gold for an energy of 1eV[46]). The photoelectric technique is generally considered the most accurate method of determining the barrier height, and it has the advantage of yielding the result directly. This method can be used for contacts with interfacial layers, however the magnitude of the current may be greatly reduced by the quantum mechanical tunnelling effect. Excitation of electrons from interface states may also cause problems, although this can be minimised by the use of thick ($\sim$50nm) gold electrodes combined with direct illumination[47].

2.4 Metal Tunnel-Insulator Semiconductor Diodes

In the preceeding sections we have largely ignored the effects of interfacial layers in Schottky barriers. Here we consider the behaviour

of diodes which have a thin insulating layer, of thickness in the range where quantum mechanical tunnelling is important (<6nm), between metal and semiconductor. These tunnel MIS structures are of great interest, not only because many practical Schottky barriers possess significant interfacial layers, but also because considerable changes in device characteristics can be obtained by deliberately forming an insulating film at the contact. These structures are being studied for use in improved solar cells[48], electroluminescent MIS diodes[49] and for the reduction of leakage currents in MESFETs (Schottky gate FETs)[50].

2.4.1 Current Transport

The most widely used treatment of tunnel MIS diode characteristics is due to Card and Rhoderick[51]; they described the four main effects of the insulating layer. The first of these is a reduction in the current through the device, caused by tunnelling through the insulator which impairs electron emission into the metal. As in the Bardeen model, the potential across the insulating layer is a function of applied bias, and this causes a reduced dependence between diffusion potential and bias, therefore increasing the ideality factor, n. The zero bias diffusion potential can be affected by the charge in the insulator. Finally, charging of interface states can be controlled either by tunnelling to the metal or the interaction with the semiconductor bands; the relative importance of these competing processes is determined by the thickness of the insulator. In this approach it is arbitrarily assumed that surface states can be divided into two groups, one in equilibrium with the metal (of density D_{sa} per unit energy) and the other in equilibrium with the semiconductor (of density D_{sb} per unit energy). D_{sa} and D_{sb} are functions of the insulator thickness, δ; for thin films the interface states communicate mainly with the metal ($D_{sa} > D_{sb}$) and for thick films the converse is true.

Card and Rhoderick modified the thermionic emission theory, allowing for the finite transmission probability for quantum mechanical tunnelling through the insulator, and obtained

$$J = A^{*} T^{2} \exp(-\chi^{\frac{1}{2}}\delta) \exp\left(- \frac{q}{kT} (V_d + \Im) \right) \qquad (2.35)$$

for forward bias, $V > 3kT/q$. χ is the mean barrier height presented by the insulator (fig. 2.13); other symbols have been defined previously. Image force effects are assumed to be negligible. The second principle assumption of this model is that the potential barrier of the insulator can be approximated to a rectangular profile, with a transmission probability that remains constant over the bias range considered. It should be noted that χ is unlikely to correspond to the bulk properties of the insulating material. This is because thin insulating films are often of inhomogenous composition and thickness; tunnelling is very sensitive to these variations and hence χ is an effective 'averaged' value.

The diffusion potential, V_d, can be related to the bias, V, by an ideality factor, n, such that

$$n = \frac{- V}{V_d - V_{do}} = \frac{- V}{\Delta V_d} \qquad (2.36)$$

For a truly exponential current-voltage relationship n will be constant, and this is the only case considered here. Using this relation then

equation 2.34 may be reformulated as

$$J = A^{*} T^{2} \exp(\chi^{\frac{1}{2}}\delta) \exp\left(\frac{-q\phi_b}{kT}\right) \exp\left(\frac{qV}{nkT}\right) \qquad (2.37)$$

We can see that this is very similar to the near-ideal diode case (equation 2.16), apart from an additional term in $\chi^{\frac{1}{2}}\delta$; this term equals the probability of an electron tunnelling through the insulator. To determine the ideality factor, n, and thereby provide a complete description of the current voltage behaviour, it is necessary to calculate the relation between applied bias and diffusion potential. Card and Rhoderick showed that

$$n = 1 + \frac{\left(\delta/\varepsilon_i\right)\left(\varepsilon_s/w + qD_{sb}\right)}{1 + \left(\delta/\varepsilon_i\right) qD_{sa}} \qquad (2.38)$$

From this it can be seen that the ideality factor is reduced by interface states in equilibrium with the metal, and increased by those in equilibrium with the semiconductor . Therefore, in general, n increases as the insulating film thickness is increased.

In this section, it has been demonstrated that the forward bias characteristics of tunnel MIS diodes are similar in some respects to those of Schottky diodes. However, for the same metal-semiconductor barrier height, the introduction of an insulating film may greatly reduce the magnitude of the current because the electrons must tunnel through the film. Also, the ideality factors of tunnel MIS diodes tend to be significantly larger than those observed for near ideal Schottky diodes.

2.4.2 Capacitance

The first analysis of the capacitance of thin MIS diodes was by Cowley[52], who sought to explain the behaviour of metal-interfacial layer-GaP diodes. In his experiments it was found that plots of $1/C^2$ versus bias were linear and had a similar slope to that expected for ideal Schottky barriers (see section 2.3.2); however the intercept on the voltage axis increased for increased interfacial layer thickness. This intercept no longer corresponded to the zero bias diffusion potential, and was occasionally several times greater than that value. It was shown that the characteristics of these diodes could not be explained in terms of a MIS model without interface states. When a constant density of interface states was added to the model then the behaviour of these diodes could apparently be explained. However, this analysis and subsequent ones based upon it make a fundamental error, which was corrected by Fonash[53]. These analyses are discussed below and their predictions are compared to experiment.

As before, the interface states are divided into two groups, those in equilibrium with the metal (D_{sa}) and those in equilibrium with the semiconductor (D_{sb}). It can be shown that

$$\left(\frac{\partial V_d}{\partial V}\right)_{qs} = - \frac{1 + \alpha''}{1 + C_{sc}/C_i + \alpha' + \alpha''} \qquad (2.39)$$

where we define

$$\alpha' = q\delta D_{sb}/\epsilon_i \qquad (2.40)$$

and

$$\alpha'' = q\delta D_{sa}/\varepsilon_i \qquad (2.44)$$

C_{sc} is the capacitance of the depletion region (section 2.3.2) and C_i is the capacitance of the interfacial layer = δ/ε_i. Equation 2.39 relates a change in diffusion potential to a small quasistatic change in bias, denoted by the letters qs. However for a small high frequency bias change, as occurs in capacitance measurement, the interface state charge is unable to respond. For this high frequency, a.c., case then

$$\left(\frac{\partial V_d}{\partial V} \right)_{ac} = - \frac{1}{1 + C_{sc}/C} \qquad (2.42)$$

The capacitance of a MIS diode is given by

$$C = - \frac{\partial Q_{sc}}{\partial V} = - \frac{\partial Q_{sc}}{\partial V_d} \cdot \frac{\partial V_d}{\partial V} = - C_{sc} \frac{\partial V_d}{\partial V} \qquad (2.43)$$

This is where the theories of Fonash and Cowley diverge. Cowley's approach is equivalent to inserting equation 2.39 into equation 2.43, which yields

$$C = \frac{(1 + \alpha'') C_{sc}}{1 + C_{sc}/C_i + \alpha' + \alpha''} \qquad (2.44)$$

As noted by Fonash, this is clearly in error because the quasistatic derivative (calculated assuming that the interface states can respond to the bias change) has been used, although we are considering the high frequency case (where the states cannot respond). The correct analysis must substitute equation 2.42 into equation 2.43, which yields

$$C = \frac{C_{sc} C_i}{C_{sc} + C_i} = \left(\frac{1}{C_{sc}} + \frac{1}{C_i} \right)^{-1} \qquad (2.45)$$

This result, as obtained by Fonash, appears to be more physically realistic as the capacitance is now a series combination of the depletion region and insulating layer capacitances.

Fonash also considered many other possible cases, such as states following the signal, $D_{sa} = 0$, $D_{sb} = 0$ or the possibility of variations in the densities of states with energy. In general the $1/C^2$ versus bias behaviour is nonlinear and the slope of the curve is expected to be equal to, or less than, that of an ideal Schottky barrier (except for certain restrictive cases). This is rather perplexing as many studies have shown linear behaviour over a wide bias range and slopes significantly larger than expected (for example[54,55]). It is apparent that the present theory does not satisfactorily explain this behaviour, and the problems in this area clearly merit further study.

2.5 Summary

This chapter begins with a discussion of the formation of Schottky barriers, starting with the simple Schottky and Bardeen models. Although these are very useful they are inadequate in some respects, therefore more recent developments are briefly discussed. In the next section, we define a near-ideal diode as one with a negligible interfacial layer and

discuss the electrical characteristics of these diodes. It is noted that near-ideal characteristics (e.g. $n \sim 1$ and linear $1/C^2$ vs. bias plots) are not always indicative of a near-ideal structure. The characteristics of the tunnel MIS diode are then considered. A conflict between theoretical and experimental capacitative behaviour is pointed out; this obviously merits a thorough investigation. Metal-thin insulator-semiconductor diodes are also considered in the next chapter, in connection with their use in MISS structures.

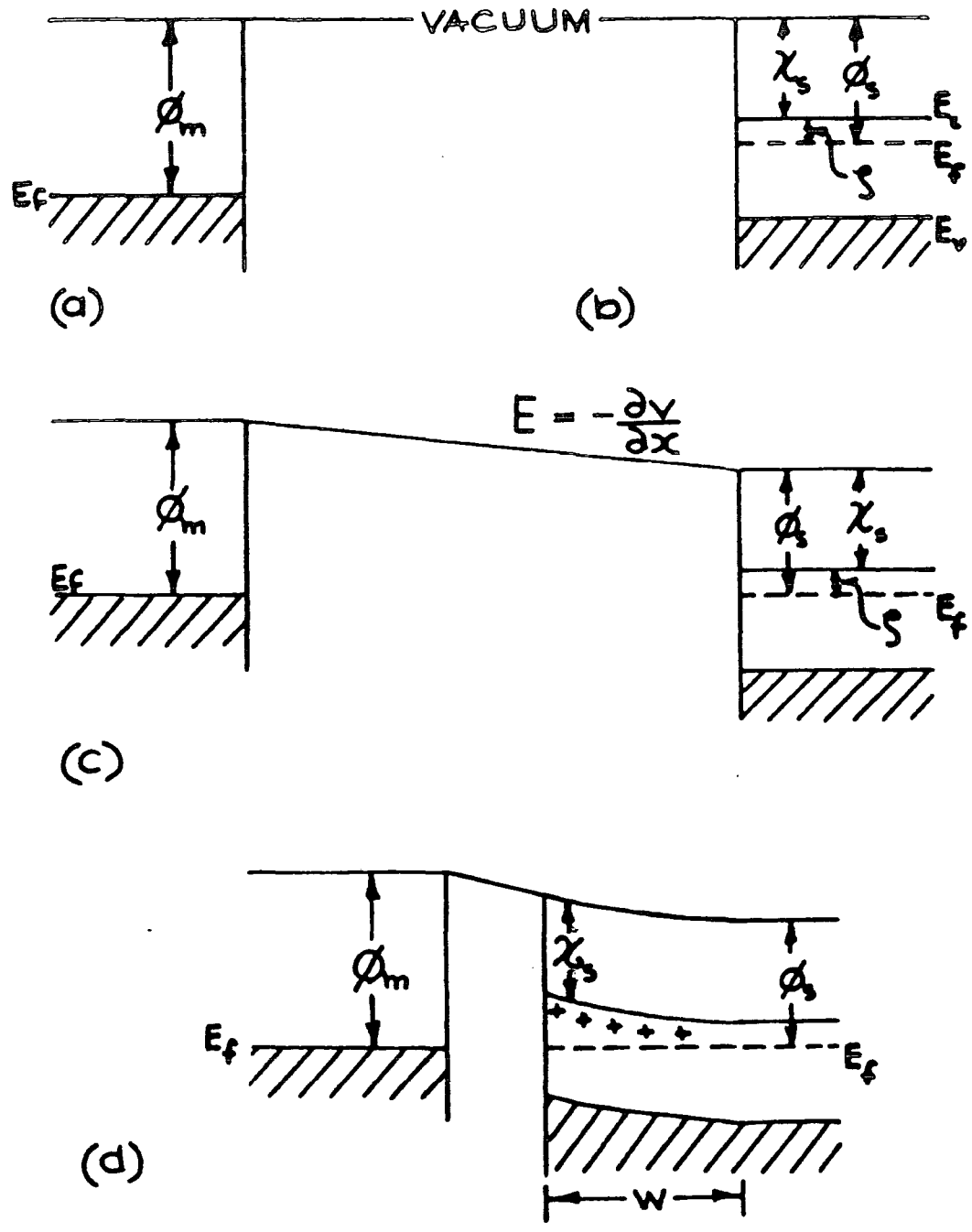

Figure 2.1 Band diagrams illustrating the formation of a Schottky barrier between a metal and an n-type semiconductor.

(a) Ideal metal surface; E_f is the Fermi level and ϕ_m is the workfunction of the metal.

(b) Ideal n-type semiconductor surface; E_f is the Fermi level, ϕ_s is the workfunction of the semiconductor, χ_s is its electron affinity and ζ is the energy of the Fermi level below the conduction band minimum.

(c) Metal and semiconductor when electrically connected in order to maintain thermal equilibrium, yet remaining spatially separated. Note the electric field, E, in the intervening space.

(d) Metal and semiconductor in close proximity (whilst remaining electrically connected). This shows the penetration of the electric field into the semiconductor. The surface of the semiconductor is depleted of conduction band electrons, thus revealing a positive space charge due to uncompensated donors.

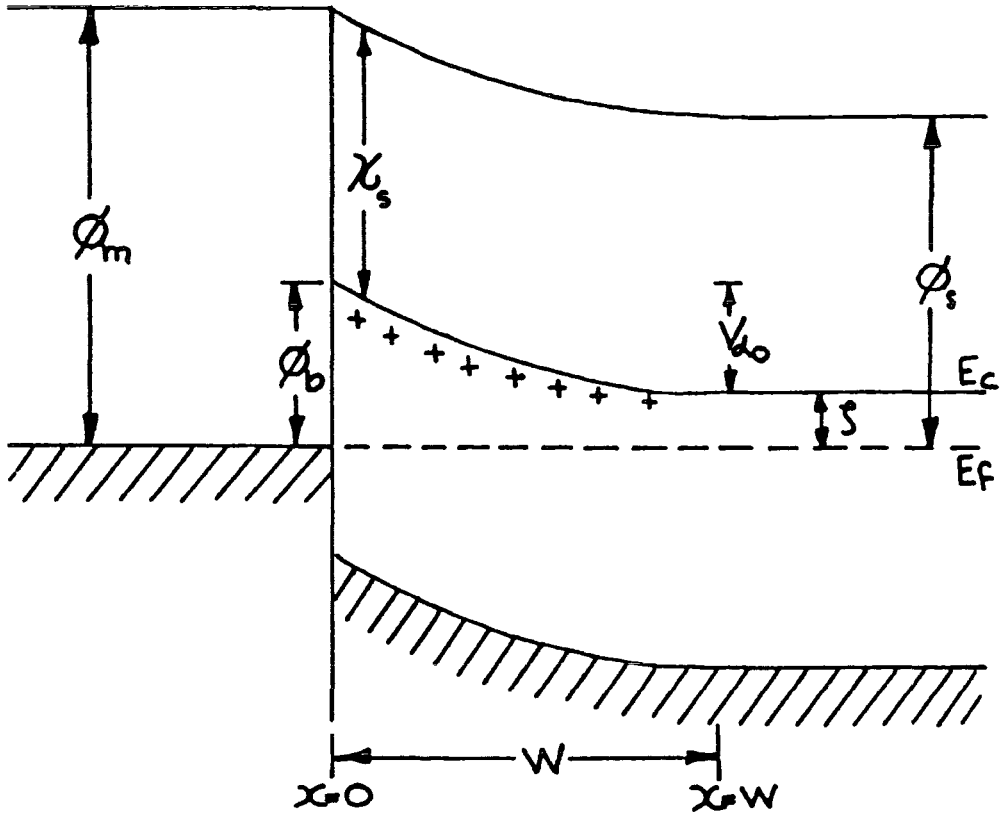

Figure 2.2 Band diagram of an intimate Schottky contact between a metal and a n-type semiconductor. The Schottky barrier height is given by ϕ_b. V_{do}, the zero bias diffusion potential, is equal to the bandbending in the semiconductor, and W is the width of the depletion region.

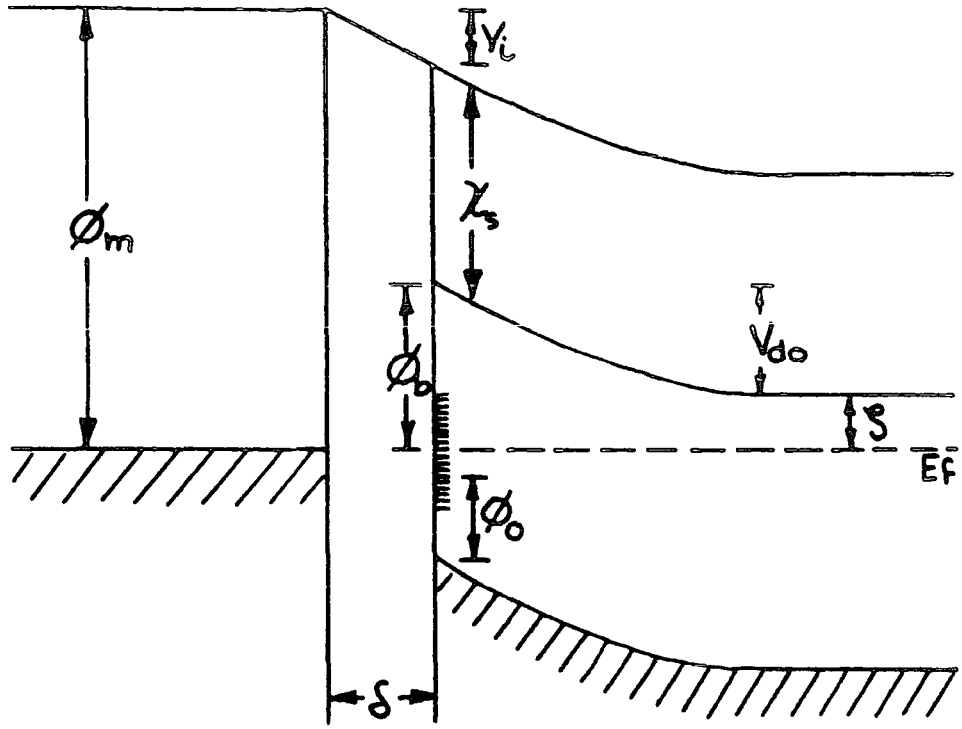

Figure 2.3 The Bardeen model of a metal-semiconductor contact is shown in this band diagram. There is a thin interfacial layer of thickness δ. The potential drop across this layer is V_i. The interface states at the surface of the semiconductor must be filled to an energy ϕ_o for charge neutrality.

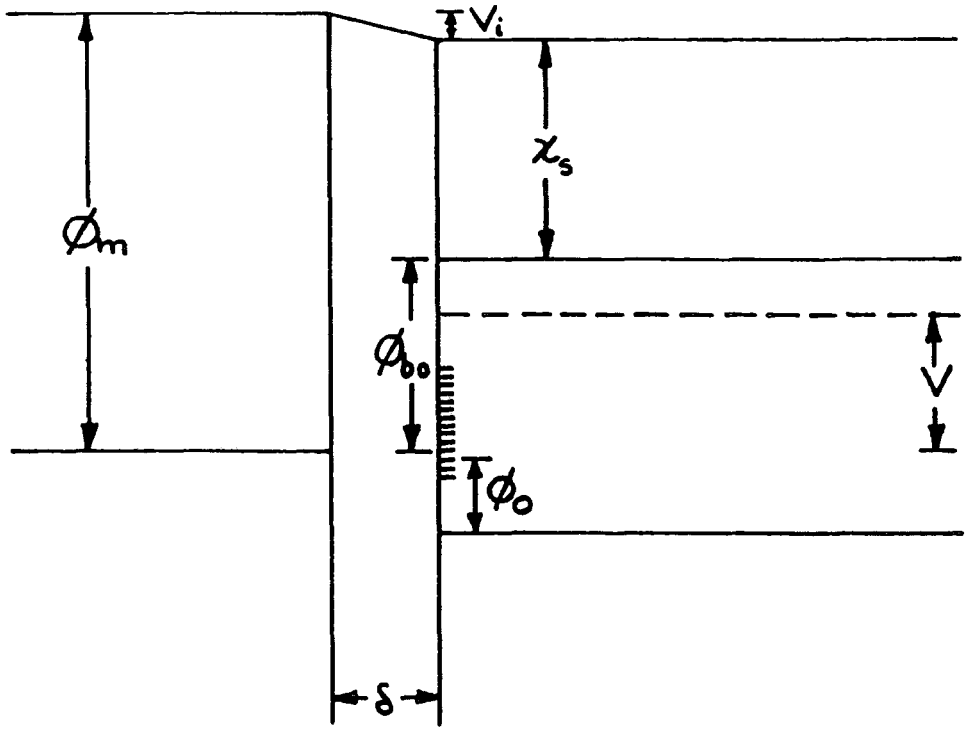

Figure 2.4 Band diagram for the Bardeen model with sufficient forward bias, V, applied to flatten the bands. Note that the barrier height is now ϕ_{bo}, which does not equal the zero bias barrier height, ϕ_b.

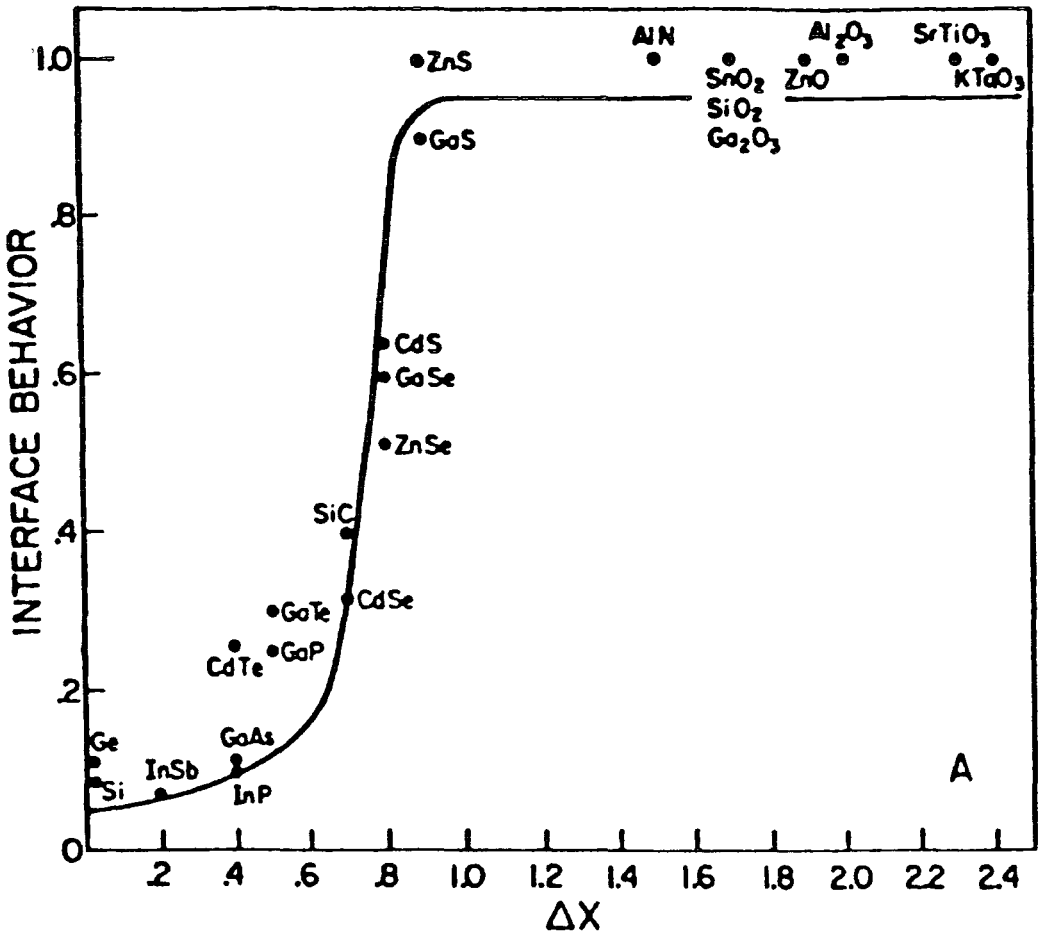

Figure 2.5 The index of interface behaviour, S, plotted as a function of the ionicity of the semiconductor, ΔX (see text for definitions). This shows a sharp transition between Schottky model like behaviour for ionic semiconductors (ΔX large) and Bardeen model like behaviour for covalent semiconductors (ΔX small). (from ref. 24)

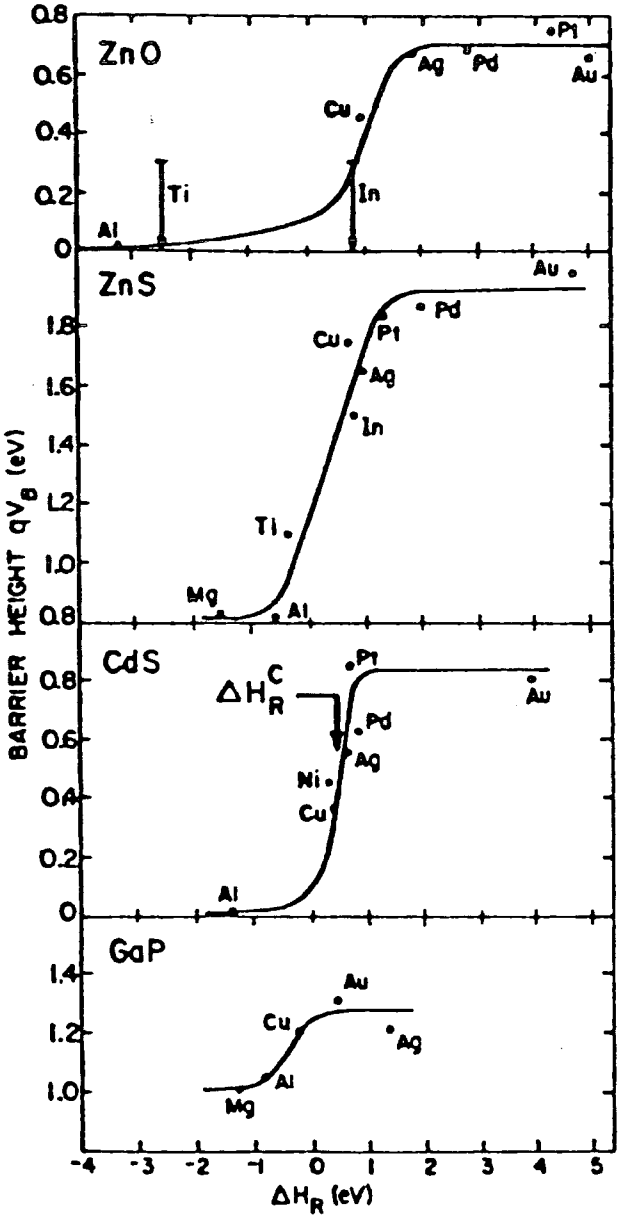

Figure 2.6 Barrier height, ϕ_b, plotted against the heat of chemical reactivity between metal and semiconductor, ΔH_R. A distinct difference between reactive and unreactive interface behaviour can be discerned. (from ref.28)

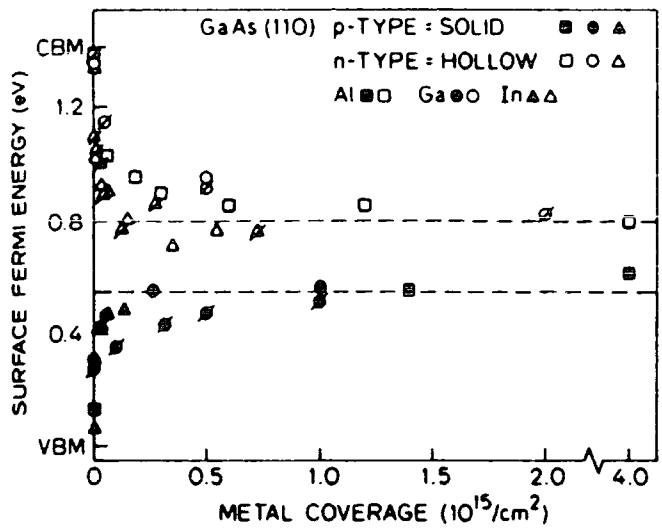

Figure 2.7 Surface Fermi level position for (110) GaAs (both n and p type) for various coverages of metal adatoms. The Fermi level is completely pinned by less than 20% of a monolayer of metal. (from ref. 31)

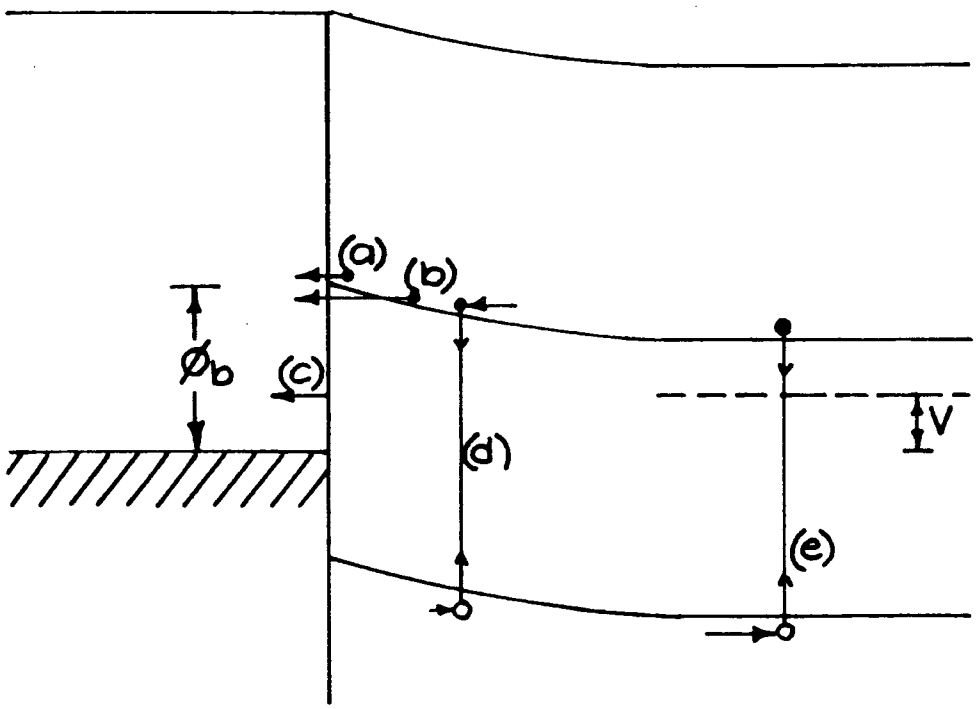

Figure 2.8 Band diagram illustrating the possible conduction mechanisms in an ideal Schottky barrier;
(a) thermionic emission or diffusion
(b) thermionic field emission
(c) field emission
(d) recombination in the depletion region (generation for reverse bias)
(e) minority carrier injection.

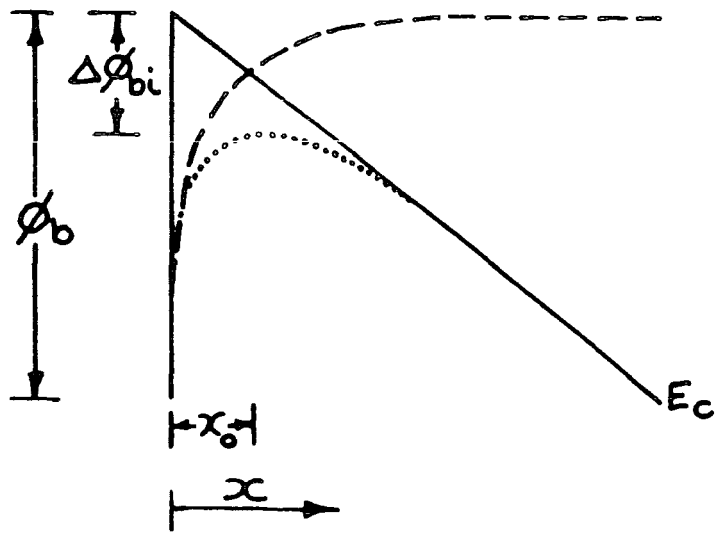

Figure 2.9 Potential profile at the top of a Schottky barrier, illustrating image force barrier lowering, $\Delta\phi_{bi}$.
—— barrier without image force effect
---- potential of electron due to image force
.... combined potential including image force effect.

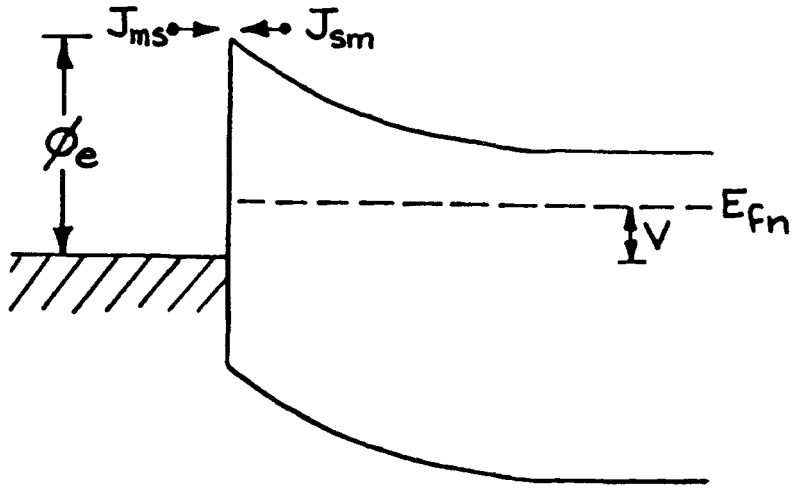

Figure 2.10 Band diagram showing thermionic emission over a Schottky barrier. J_{ms} and J_{sm} are the electron currents passing from metal to semiconductor and vice versa. V is the voltage applied to the diode.

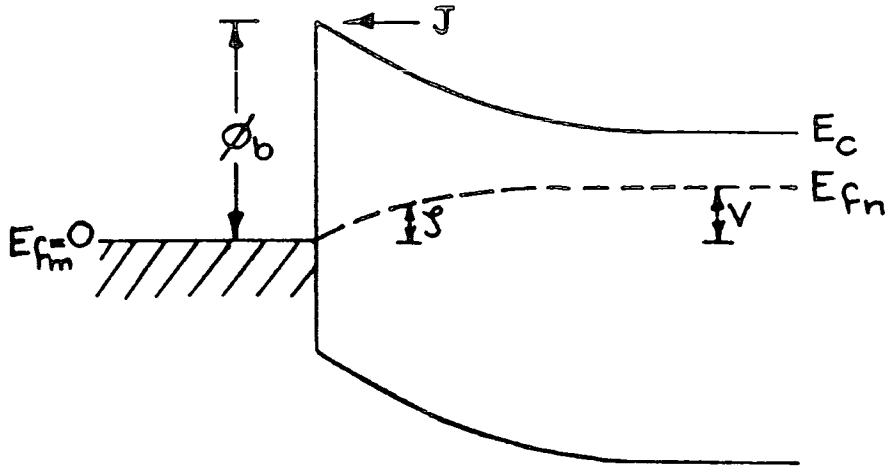

Figure 2.11 Current transport in a Schottky barrier controlled by diffusion in the depletion region. Note that the energy of the Fermi level in the semiconductor, ζ , is defined with respect to the metal fermi energy ($E_{fm} = 0$).

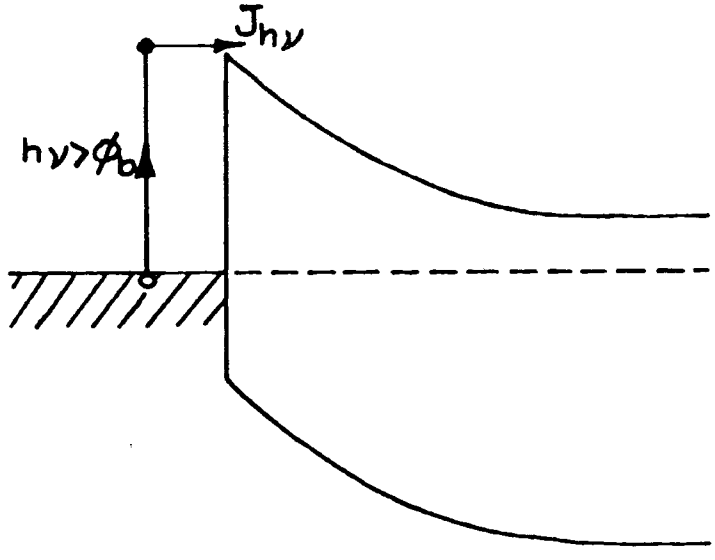

Figure 2.12 The photoelectric effect as used to measure the barrier height (in the Fowler plot technique). Electrons in the metal are excited by light of energy $h\nu > \phi_b$, enabling them to cross the potential barrier into the semiconductor hence generating a photocurrent.

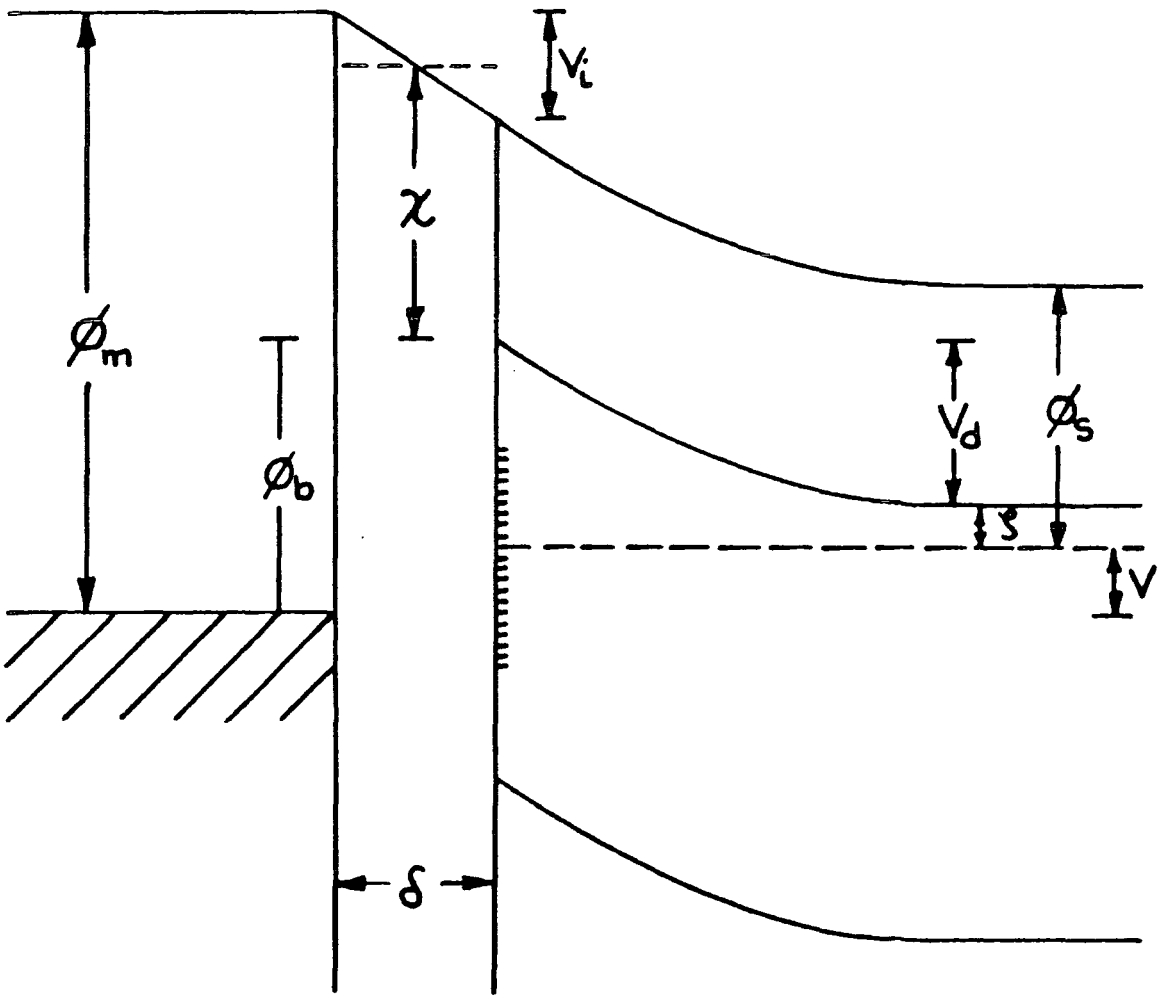

Figure 2.13 Band diagram for an idealised tunnel metal-insulator-semiconductor diode with an applied bias, V. The insulating layer, of thickness δ, presents a a barrier to electrons tunnelling from semiconductor to metal of (mean) height χ.

CHAPTER 3

THE MISS DEVICE

3.1 Introduction

The first report of negative resistance in a metal-thin insulator - $n\text{-}p^+$ semiconductor structure (fig. 3.1) was in 1972 by Yamamoto and Morimoto[1]. Their devices consisted of a thin SiO_2 layer (< 10nm) on silicon, and when the p layer was positively biased an S-type characteristic was observed (fig. 3.2). Similar characteristics were found for complementary metal-thin insulator - p-n devices. It was noted that these diodes appeared to switch much more rapidly than other devices exhibiting S-type negative resistance behaviour (for example the Shockley diode). These structures became known as MISS devices (for Metal Insulator Semiconductor Switch) or less commonly as the Inversion Controlled Switch (ICS). Considerable interest in these MISS diodes developed because of their relatively simple structure and the prospect of high speed operation.

It was discovered that other insulating layers could be used to form MISS devices, such as thin (2-20 nm) silicon nitride[2,3]; thicker 'semi-insulating' films such as silicon oxynitride, amorphous silicon, amorphous germanium, tin oxide and polysilicon were also suitable[4,5]. Switching has also been briefly reported for a GaAs MISS diode[6]. Three terminal MISS devices were developed[6-9] in which a third (ohmic) connection is made to the upper semiconductor layer (fig. 3.3). By varying the current through this 'base' terminal it is possible to control the switching voltage (fig. 3.4). As these characteristics are similar to those of thyristors, these structures are often referred to as

Metal - Insulator - Semiconductor - Thyristors (MIST). Three terminal devices with MOS gates have also been reported[10,11].

From the first reports of the switching phenomena it was realised that some kind of regenerative or internal feedback process was involved[1], that the high impedance state corresponded to deep depletion of the semiconductor surface and that the surface was inverted in the on state[2]. Simmons and El-Badry[12,13] recognised that switching often corresponded to either 'punchthrough' of the surface depletion region to the p-n junction, or the onset of avalanche multiplication in the depletion region. However for many MISS devices the switching voltage does not correspond to either of these limits. Buxo et al[14] first modelled an alternative process, where switching arises from a multiplication mechanism that occurs in MIS diodes, obtaining agreement with experimental switching voltages (in fact the mechanism had first been suggested by Yamamoto et al[6]). It should be noted that the three processes mentioned above all involve similar regenerative mechanisms; more than one of these may be of importance in a particular device if the conditions of operation are varied (e.g. in three terminal devices). Calculations of MISS device characteristics have been made using models of the regenerative process; however, due to the complexity of the system agreement with experiment is often poor.

Many applications for MISS devices have been proposed, although there are considerable technological problems to be overcome before any of these become practicable. One possible application is in logic circuits, where a device with two distinct states is highly desirable. Some simple logic circuits have been fabricated, including simple gates[15], shift registers[6,16] and RAM cells[17]. Other proposed applications are as oscillators[17], photodetectors[17-19] and palladium

hydrogen sensors[20]. At the present stage of development it is not clear whether MISS devices will be able to compete with conventional device structures. There are also other two state devices, with similar characteristics, that may rival the MISS diode for certain uses. One example is the Shockley diode, which has been integrated into RAM cells[21]. Another two state device is the Planar Doped Barrier Switch, a device fabricated using M.B.E., consisting of a triangular $n^- - p^+ - n^-$ barrier and a p-n junction[22,23].

In this chapter we commence with a description of the physics of the switching process. The two active components of the device, the p-n junction and the MIS diode, are initially considered in isolation. It is then explained how their interaction causes switching (N.B. for convenience only M-I-n-p^+ devices will be considered). The next section reviews the results of detailed modelling of MISS devices, making some comparisons with experiment and also discussing their dynamic characteristics. Finally, conduction mechanisms in thin insulating films are outlined.

3.2 Physics of the MISS Device

As the title suggests, we are here concerned with the essential features of the operation of MISS devices. Although some simple quantative expressions have been included, a full numerical analysis has not been attempted. Indeed, it is shown later in this chapter that the present quantitative models are of limited utility; this may be due to either a lack of agreement with experiment or, in more comprehensive models, sensitivity to a large number of parameters (which are often not well known). It is hoped that the approach taken here will enable the salient features of MISS diode operation to be discerned. The discussion is broken into three sections. The first two of these describe the

components of the structure, the MIS diode (reverse biased) and the p-n junction (forward biased). Finally, we consider the regenerative feedback mechanism that links them together and causes switching.

3.2.1 Metal - Semi-insulator - Semiconductor Diodes

Introduction

In the previous chapter we considered one limiting case of the MIS diode, where the characteristics are Schottky diode like. In that case the insulator is thin enough (< 4nm) to allow appreciable tunnel currents to flow and, at the semiconductor surface, minority carriers are in equilibrium with the metal. The other limit of MIS diode behaviour is for a perfect (thick) insulator. In this case both majority and minority carriers are in thermal equilibrium with the bulk of the semiconductor. A major difference between this case and that of Schottky-like behaviour (apart from the obvious absence of current flow) is the limit imposed on the surface potential (ψ_s) by the onset of strong inversion at the semiconductor surface (fig. 3.5). This occurs when

$$\psi_s \text{ (inversion)} \sim 2\psi_b \tag{3.1}$$

where ψ_b is the difference between the bulk Fermi level and the intrinsic level, given by

$$\psi_b = \frac{kT}{q} \ln\left(\frac{N_D}{n_i}\right) \tag{3.2}$$

where n_i is the intrinsic electron concentration. This is in contrast to Schottky type behaviour where ψ_s can increase without limit (until breakdown is reached). It must be noted that for a material, such as GaAs, where MIS structures possess large surface state densities[24] the range of ψ_s may be further restricted.

In MISS devices we are interested in the intermediate area between these two limits; this will occur for various insulator thicknesses, depending on the conduction mechanisms involved. Most studies of this non-equilibrium (Schottky like) to equilibrium (ideal MIS) transition have been on the SiO_2/Si system[25-28], where conduction is by quantum mechanical tunnelling and a very narrow thickness range is involved (∿3-5nm). The most important feature of these non-equilibrium MIS diodes, especially as regards their application in MISS devices, is the possibility of the semiconductor surface being either deeply depleted or inverted; factors affecting this may include the bias or, more importantly, external injection of minority carriers.

Characteristics

We first consider deep depletion, as shown in fig. 3.6. For the two limiting cases, of Schottky like and ideal MIS like behaviour, it can be shown that the quasi-Fermi levels are nearly flat throughout the depletion region[25], therefore we will assume that the quasi-Fermi levels are also flat in these 'non-equilibrium' diodes. In deep depletion, the minority carrier current is limited by generation, and the parameter ϕ, the separation between the hole quasi-Fermi level and the metal Fermi level, is small. The majority carrier current is also small and is determined either by the field in the insulator, or the metal-semiconductor or metal-insulator barrier, depending on the transport mechanism. As the insulator is thin, most of the potential across the device is dropped across the depletion region. Therefore, we may approximate the surface potential to

$$\psi_s \sim V - \psi_{so} \tag{3.3}$$

where ψ_{so} is the zero bias band bending. The depletion width is similar to that of a Schottky barrier and is given by

$$w_d = \left(\frac{2\,\varepsilon_s}{q\,N_d} \right)^{\frac{1}{2}} \psi_s^{\frac{1}{2}} \qquad (3.4)$$

In this deep depletion, or semiconductor limited, case the current is small and the potential drop occurs mainly across the semiconductor.

A nonequilibrium MIS diode is shown in strong inversion in fig. 3.7. Unlike in the ideal MIS diode, the quasi-Fermi levels are separated. In this case the inversion criterion, found by inspection of fig. 3.7 is given by

$$\psi_s \sim 2.\psi_b + V - \phi \qquad (3.5)$$

where ϕ is the separation between the minority carrier quasi-Fermi level and the metal Fermi level, as defined by Jen et al. who obtained the above expression[29]. In this case the hole current is limited by conduction through the insulator, due to the availability of holes from the inversion layer, therefore the separation of the quasi-Fermi levels ($= V - \phi$) is small. Once the semiconductor surface is inverted any additional bias increases the field in the insulator and lowers the metal-semiconductor barrier, hence augmenting the majority carrier current. However the increased field also augments the minority carrier current, therefore significant currents will only flow if the supply of holes to the semiconductor surface, by generation or injection, is sufficient to sustain inversion. Some MIS diodes may be inverted for small reverse bias, yet become deeply depleted at higher bias as the minority carrier current becomes semiconductor limited[27].

The degree to which a nonequilibrium MIS diode is semiconductor or insulator limited may be varied by changing the supply of minority carriers, for example by illumination. Thus increasing the minority carrier supply causes the semiconductor surface to become more heavily inverted. This enhances the field in the insulator, offering the possibility of an increase in the majority carrier current. This was first observed by Shewchun and Clarke[30] in tunnel - SiO_2/Si structures. The multiplication factor, M, defined as the rate of increase in total current for increased minority carrier supply current, could be as high as 1000[31,32] (fig. 3.8). Yamamoto et al. first suggested that this mechanism was important in MISS switches[6], and we will see that this linkage between minority carrier injection and majority carrier current is a crucial part of the regenerative process, even if the linkage is weak.

In summary, we have described the non-equilibrium MIS diode, defined by the limits of Schottky barrier like and ideal MIS like behaviour. It has been shown that the semiconductor surface may be deeply depleted or inverted, dependent on the supply of minority carriers. We have outlined the link between minority and majority carrier currents, giving the possibility of a large multiplication factor.

3.2.2 The p-n Junction

At the boundary between p and n type regions of a semiconductor there is a potential step. The field in this region causes the boundary to become depleted of free carriers (fig. 3.9). The profile of this depletion region is determined by the space charge density, which is due to uncompensated donors and acceptors. When an external bias is applied across the junction the potential profile is changed, disturbing the carrier concentrations in the junction region and a current flows (fig.

3.10). The electron and hole currents are determined by the normal processes of diffusion and drift (equation 2.25).

Shockley first solved these equations, assuming negligible recombination in the depletion region and low injection conditions (i.e. minority carrier density << majority carrier density), obtaining the ideal rectifier equation

$$J = J_s \ (\exp \ (qV/kT) \ -1) \tag{2.6}$$

J_s is given by the celebrated Shockley equation[33]

$$J_s = \frac{q \ D_p p_{no}}{L_p} + \frac{q \ D_n \ n_{po}}{L_n} \tag{3.7}$$

where p_{no} and n_{po} are the equilibrium minority carrier concentrations in the bulk n and p type regions respectively and L_p ($= \sqrt{D_p \ \tau_p}$) and L_n ($= \sqrt{D_n \ \tau_n}$) are the diffusion lengths for holes and electrons (τ_n and τ_p are the electron and hole lifetimes). In forward bias, minority carriers are injected into the bulk of the semiconductor and recombine within a diffusion length of the junction. In high purity n-type GaAs this distance, L_p, is of the order of a few microns[34]. It can be shown that the first term in the Shockley equation represents the hole current in the depletion region and the second term the electron current. Therefore, if we define a hole injection ratio, α, as the ratio of hole current to electron current, at the edge of the depletion region, then

$$\alpha = \frac{D_p \ p_{no} \ L_n}{D_n \ n_{po} \ L_p} \tag{3.8}$$

For efficient hole injection a large value of p_{no}/n_{po} is required, which will occur if the doping on the p side of the junction is much heavier than that on the n side. In such a p^+-n junction α can be much greater than 1.

In practical p-n junction diodes the current only agrees with the Shockley theory over a restricted region of forward bias. At high current levels the injected minority carrier densities approach the majority carrier density and this is referred to as high injection. this causes an increase in majority carrier density and the current is then given by $J \propto \exp(qV/2kT)$[35]. Of more interest in the context of MISS devices is the low forward bias region, where recombination in the depletion region becomes important reducing the injection ratio, α. Sah et al.[36] showed that this additional recombination current (for $V > 3kT/q$) is given by

$$J_R = J_o \exp(qV/2kT) \tag{3.9}$$

where J_o is a constant. For low forward bias this will be the dominant component of the current flow. At the edge of the depletion region the majority carrier current is then approximately equal to J_R, however the minority carrier current is still given by the Shockley theory. Therefore, for small forward bias, the hole injection ratio is given by

$$\alpha = \frac{q D_p p_{no}}{L_n J_o} \exp\left(\frac{qV}{2kT}\right) \propto J \tag{3.10}$$

from equations 3.6, 3.7 and 3.9.

It can be seen from equations 3.8 and 3.10 that as the current through the p^+ -n junction is increased then the hole injection ratio, α, increases, until a maximum value is reached, as shown in fig. 3.11. It can also be seen in this diagram that at low current levels little hole injection occurs and at high current levels hole injection dominates. We can now begin to discern the role the p-n junction plays, by controlling the supply of minority carriers to the semiconductor surface, in the MISS device. In the next section we combine the p-n junction with the MIS diode and discuss the effects of the coupling between the devices.

3.2.3 Regenerative Switching

Here we commence by describing the off state of the MISS, which is followed by an outline of the regenerative process occurring in the negative resistance region and then the on state is covered. Finally two special conditions are described which limit the possible range of switching voltage.

The Off State

The band diagram of the MISS device in the high impedance state is shown figure 3.12. The semiconductor surface is deeply depleted because the insulating layer is thin, allowing minority carriers to 'leak' to the metal. As described in section 3.2.1, the current is small because the electron current, J_e, is limited by the metal-semiconductor barrier height or by the insulator. The hole current, J_h, is limited by thermal generation (J_g). This assumes that hole injection, J_h^*, is negligible. This assumption is reasonable since minority carrier injection at p-n junctions is minimal at low current levels (see section 3.2.2). The potential across the p-n junction, V_j, is small because the current is also small. Therefore, as we saw earlier (section 3.2.1), most of the potential is dropped across the depletion region at the semiconductor

surface. We can conclude that, in the off state, the p-n junction has little effect and the MISS device behaves like a non-equilibrium MIS diode in deep depletion.

The Regenerative Mechanism

Before describing the feedback process we state two necessary conditions for feedback to occur. Firstly holes injected by the p-n junction must be able to reach the semiconductor surface, therefore the n epilayer width, w_e, must not be significantly larger than the hole diffusion length, L_p. Secondly, the MIS diode must be of the non-equilibrium type described in section 3.2.1. If these criteria are satisfied then a feedback loop will exist, similar to the one shown in fig. 3.13. Feedback occurs because the electron and hole currents are linked at both the p-n junction (by minority carrier injection) and at the semiconductor surface (through the MIS multiplication effect). These two processes can provide a net gain round the loop, despite losses such as those due to recombination. If there is net gain round the loop we can see that either the current will increase without limit (and the device breakdown) or a new stable state must be reached. This new state arises because of the build up of inversion charge at the semiconductor surface, which increases the field in the insulator and decreases the band bending in the semiconductor.

The On State

In the low impedance state of the MISS device the semiconductor surface is strongly inverted, limiting the band bending (ψ_s) in the depletion region (fig. 3.14). The field in the insulator is large, permitting substantial current flow. However, as the insulating layer is thin, the voltage drop, V_i, is relatively small. The p-n junction is forward biased, therefore V_j is also small and the total potential across

the device has fallen to a few volts. The on state is stable because the losses in the feedback loop, due to the hole current to the metal (J_n) and recombination in the epilayer (J_R^*), are large. The current is limited by the insulator, and since a small increment in applied bias greatly increases the field in the oxide then the impedance in the on state is low. In some materials (e.g. GaAs) the high density of surface states prevent inversion of the surface, and it might be thought that this would prevent the occurrence of an on state; however in this case the inversion charge can be replaced by surface state charge, giving similar results.

We have not yet described how the device returns to the off state. The turn off process can be visualised as the feedback mechanism operating in reverse; as the current through the device is reduced a point will be reached where the inversion charge cannot be sustained, due to reduced minority carrier injection, and this triggers the turn off process. Although the regenerative mechanism has now been described, the magnitudes of the switching and holding voltages (and currents) have not been considered. These are determined by the gain in the feedback loop and in principle they could occur at any, essentially arbitary, points. However, two special conditions are defined below, which together define the maximum switching voltage for a given epilayer structure.

Avalanche

When the MISS device is in the off state the field in the depletion region may be very large, and if the doping density is high this field may become sufficient to cause avalanche multiplication. This occurs because electrons accelerated by the field can gain enough kinetic energy to generate electron-hole pairs by impact ionisation (fig. 3.15). The holes generated by this process are swept towards the semiconductor

surface and we can see that this auguments the feedback mechanism. Indeed this may be considered as forming another feedback loop[37] (in concert with the MIS multiplication effect) which may allow three separate stable states to exist[38]. As the avalanche gain may become very large we can expect switching to occur. The potential across the depletion region required for the avalanche gain to become very large, V_a, is given by the approximate expression[39].

$$V_a \sim 60\left(\frac{E_g}{1.1}\right)^{3/2}\left(\frac{N_b}{10^{16}}\right)^{-3/4} \qquad (3.11)$$

where E_g is the semiconductor bandgap in eV and N_b is the background doping in cm^{-3}. For MISS devices where this mechanism is important, the switching voltage is approximately equal to V_a because, in the off state, most of the applied bias is dropped across the depletion region at the semiconductor surface.

Punchthrough

The second limit on the switching voltage is due to 'punchthrough', which occurs when the depletion region at the semiconductor surface begins to encroach upon the depletion region of the p-n junction (fig. 3.16). If the bias is increased beyond this point then the band bending in the p-n junction is reduced, thereby increasing minority carrier injection from the p region. The hole injection actually begins to increase before punchthrough is reached because the width of the neutral n-type region, w_n, is reduced, thus altering the boundary conditions for diffusion from the p-n junction. When w_n is less than a hole diffusion length (L_p) then the Shockley equation (equation 3.7) is modified and, to a good approximation, L_p is replaced by w_n[40]. From equations 3.8 and

3.10 we can see that this will increase the hole injection ratio, α. Therefore hole injection is enhanced as punchthrough is approached, becoming very large at punchthrough. This greatly increases the gain in the feedback loop, consequently triggering switching. At punchthrough $w_d = w_e - w_j$, where w_d is the MIS depletion width, w_e is the epilayer thickness and w_j is the p^+-n junction depletion width (i.e. a one sided abrupt junction). w_d can be found from equation 3.4 and if it is assumed that the potential across the device is mainly dropped across the depletion region, then

$$V_{pt} \sim \frac{q N_d}{2\epsilon_s}\left(w_e - w_j \right)^{\frac{1}{2}} \qquad (3.12)$$

where V_{pt} is the voltage across the MISS device at punchthrough (N.B. w_j must be calculated for a small forward bias).

Summary

It is unfortunate that this explanation of switching in MISS devices is rather recondite due to the complexity of the process. However, it is hoped that the main features of MISS diode operation have been emphasised. The first of these features are that the high and low impedance regions correspond to deep depletion and inversion of the semiconductor surface respectively. Switching between these states is due to regenerative feedback between the two components of the MISS device, the p-n junction and the MIS diode. Upper limits on the switching voltage are defined by punchthrough or the onset of avalanche multiplication, depending on epilayer doping and thickness. In the above discussion a detailed treatment of the characteristics has not been attempted. As will be seen in the next section, although it is possible to perform such calculations the results are of limited utility.

3.3 A Review of MISS Characteristics

In this section the previously reported work on modelling MISS device characteristics is reviewed and those factors found to be significant are emphasised. In addition, the dynamic characteristics of MISS devices are covered as they become of great importance in many applications.

3.3.1 Detailed Switching Characteristics

The approach usually taken when modelling MISS device characteristics is to solve the continuity equations for electrons and holes. As the structure of the device is complex, with conduction and recombination/generation processes occurring in several distinct regions, it is not usually possible to find analytic solutions, therefore numerical methods must be used to compute the solution. There are many problems with this approach, even when the well characterised SiO_2/Si system is being studied (as in the great majority of cases discussed below). The principal problems arise because many of the parameters are not well known, for example surface state distributions, carrier lifetimes and insulator characteristics. This problem is obviously even more serious where less studied (or more variable) materials are concerned. In addition, many of the models ignore two dimensional effects and this is often unrealistic, as has been shown in experimental studies of devices with different geometries[41,42]. Many models are also grossly simplified, for example by ignoring surface states. As a result of these shortcomings, few successful comparisons of experimental and theoretical characteristics have been published, which perhaps indicates that the results of the theoretical models discussed below should be treated cautiously.

The first attempt at a quantative MISS model was made by Buxo, Millan and co-workers[14,43]. They considered devices switching before punchthrough or avalanching occurred and found a reasonable fit to experimentally observed switching voltages. Independently, Habib and Simmons formulated models for switching near punchthrough[44] and switching by avalanche multiplication[38]. It was found that switching only occurred over a limited range of oxide thicknesses and even within this range the characteristics varied significantly, as is shown for punchthrough devices in fig. 3.17. These authors also noted a reasonable agreement between the calculated switching voltage and the approximate expression for punchthrough voltage (equation 3.11). For MISS diodes switching due to avalanche multiplication, it was found that under certain circumstances a three state characteristic was obtained (fig. 3.18). Habib and Simmons further extended their model and noted that for thicker oxide films the off state could correspond to deep depletion with a clamped inversion charge[45].

Sarrabayrouse et al. extended the original regenerative model[46,47]. They found that the calculated variations in switching voltage with illumination and temperature were in agreement with their experimental results. Habib and Eltoukhy modelled the effects of a single surface state level[48] and demonstrated the significant effects that these states had on MISS characteristics (fig. 3.19). Faraone et al.[42] proposed a simple two dimensional model, which accounted for the experimentally observed variation in switching voltage with device area by assuming that the effective p-n junction area was larger than the metal contact area.

Although these models gave a good fit to experimentally observed switching voltages the calculated current levels in the off state were

much smaller than found in practice. Millan et al. were able to obtain a better fit using a model that incorporated resonant tunnelling via traps in the insulator[49] (fig. 3.20). The same authors also calculated the effects of changing the insulator thickenss, metal-semiconductor barrier height, epilayer doping and p-n junction injection efficiency, all of which resulted in marked changes in the switching voltage. Zolomy modified previous models by including two-dimensional effects, surface states, inhomogeneity in the insulator and some other details[50]. Not surprisingly, substantial variations in the calculated characteristics could be obtained by varying the many parameters of this model. Martinez and Piqueras modelled the polysilicon MISS device[51] and found that the operation was somewhat similar to that of a Shockley diode. Finally, we note that Fiori de Mattos and Sarrabayrouse, in a recent study of the effects of variations in several critical parameters, concluded that any attempt to fit theory to experiment was purely speculative due to the sensitivity of MISS characteristics to these variations[52].

We can conclude that theoretical models of MISS devices are at present inadequate, largely due to the complexity of the structure. This also emphasises a major problem with practical devices since it is necessary to control many parameters in order to obtain repeatable and stable devices. In addition it is not clear which critical factors must be improved for optimum results.

3.3.2 Dynamic Characteristics

The first reports of MISS diodes noted that the switching action was perhaps faster than for other S-type negative resistance diodes[1,2,6]. The turn on time was possibly as short as a few nanoseconds. Later studies of the turn on characteristics showed three distinct phases in the process[5,14,53,54] as shown schematically in fig. 3.21. The first

of these (1), the capacitive rise time, arises because the device is charged up through a series resistance, R_s (the resistance is essential to prevent destruction of the device in the on state). This part of the turn on process is shortened if the value of R_s is reduced. The second stage (2) is thought to be due to the time required to build up inversion at the semiconductor surface. This 'Inversion Charge Delay Time' is inversely related to pulse amplitude and ranges between a few ns and several hundred ns. The final phase (3), the 'Feedback Regeneration Time', corresponds to the rapid collapse of the depletion region in the semiconductor as the regenerative process takes effect. The overall turn on times observed range down to a few tens of nanoseconds for reasonable series resistances and pulse amplitudes[14,53,54]. It would be expected that the switching speed could be increased by reducing device capacitances and epilayer width (and by increased mobility), however studies of the optimisation of dynamic characteristics of MISS devices have not yet been carried out. Simmons and Taylor[55] studied the limitations and practical viability of MISS devices. They concluded that, for memory applications, the MISS device did not compare favourably with conventional MOSFETs when switching speeds were taken into account. This limitation may also apply for other potential applications of the MISS diode.

3.4 Conduction in Insulating Films

Electronic conduction in thin insulating films plays a very important role in the MISS device, therefore the conduction mechanisms are briefly described in this section. We can distinguish between barrier limited or bulk limited processes, and these are discussed separately. However, in general, the conduction mechanism may be field and temperature dependent, therefore both types of process could be of

importance in some materials. Characteristics of thin insulating layers are often controlled by high densities of defect levels and can therefore differ significantly from those of bulk material. High field effects are also relevant, even for relatively small potentials, because the layers are usually extremely thin.

3.4.1 Barrier Limited Conduction

There are two types of barrier limited conduction process, thermal excitation of carriers over the barrier into the insulator conduction band and quantum mechanical tunnelling through the potential barrier presented by the insulator.

The first of these conduction processes, often called Schottky emission, is directly comparable to thermionic emission in Schottky barriers. Again, we must take into account the effects of image force barrier lowering. This is given by equation 2.18, and if we define

$$\beta_s = (q^3/4\pi\ \varepsilon_i')^{\frac{1}{2}} \tag{3.13}$$

where ε_i' is the high frequency permittivity of the insulator, then the current over the barrier is given by

$$J = AT^2 \exp\left(- \frac{q\phi_o}{kT} \right) \exp\left(\frac{\beta_s E^{\frac{1}{2}}}{kT} \right) \tag{3.14}$$

where A is the Richardson constant, ϕ_o the barrier presented by the insulator and E the electric field in the insulator. Therefore for Schottky emission the log of the current is directly proportional to the square root of the field.

Stratton analysed tunnelling currents for thin insulating films[56] and found that the current was given by an equation of the form

$$J = \frac{4\pi\, mq \exp(-b_1)}{c_1^2\, h^3} \cdot \frac{\pi\, c_1\, kT}{\sin(\pi\, c_1 kT)} [1 - \exp(-c_1\, V)] \qquad (3.15)$$

where b_1 and c_1 are auxilliary functions dependent on barrier profile and applied voltage. Tunnel currents are only significant for very thin films (< 6nm) and their most important characteristic is a very weak temperature dependence. Resonant tunnelling via defect states can also occur, which can greatly enhance the tunnel current[57]. At high fields the metal-insulator barrier is narrowed and even in thick films tunnelling may become important (fig. 3.22). This process is called Fowler-Nordheim emission[58]. In this case the current is given by

$$J = \frac{q^2}{8\pi h} \cdot \frac{E^2}{\phi_o} \exp\left(- \frac{4(2m^*)^{1/2} (q\phi_o)^{3/2}}{3qhE} \right) \qquad (3.16)$$

and the log of [current/(field)^2] is directly proportional to the field.

3.4.2. Bulk Limited Conduction

In low mobility materials conduction may be better described by hopping between localised states[59] or by polaron conduction[60] than by electronic band conduction, although only the latter process is considered here. If the carrier density is controlled by donor or trap levels we must consider the Poole-Frenkel effect[61]. This is due to the lowering of the coulombic potential barrier of the trap by the electric field (fig. 3.23). Although this mechanism is, in a certain sense, a barrier limited process it is considered here because conduction is

limited in the bulk of the insulator and not by the metal-insulator barrier. Since the coulombic potential is four times the image force potential, the barrier lowering is twice that given by the Schottky effect (eq. 2.18). Therefore the current - voltage relationship is of the form

$$J = J_o \exp (\beta_{PF} E^{\frac{1}{2}}/kT) \qquad (3.17)$$

where

$$\beta_{PF} = (q^3/\pi\epsilon_i')^{\frac{1}{2}} \qquad (3.18)$$

This is similar to the case of Schottky emission, apart from a factor of two in the exponent (i.e. $\beta_{PF} = 2\ \beta_s$). However in a system with both neutral trap and donor levels the Poole-Frenkel effect may exhibit the same slope as the Schottky effect[62]. It should be noted that these calculations of Poole-Frenkel behaviour are rather approximate; Hill has considered the process in more detail[63].

If the contact to the insulator is ohmic then the current may be space charge limited. This would give a power law relationship between current and voltage for a trap free insulator[64]. However Rose[65] has shown that in a defect insulator the current is considerably reduced because most of the space charge is trapped and therefore immobile. He found that for trap densities of $\sim 10^{18}$ cm^{-3} space charge limited currents were reduced to almost immeasurable levels. We will not consider this effect further, except to note that modulation of other conduction mechanisms can occur if the space charge significantly alters the electric field.

3.5 Summary

In the first part of this chapter the principles governing the operation of MISS devices are discussed. We begin by considering the two 'components' of the device in isolation; these are the MIS diode and the p-n junction. It is then shown that the interaction between them gives rise to a regenerative feedback process and that this is responsible for the switching behaviour. Switching often occurs at punchthrough or due to avalanche breakdown, although in many cases the devices may switch before either of these points is reached. The review of published models of MISS devices shows that there are serious limitations on their use. These arise because of the complex nature of the device and they make it difficult to meaningfully fit theory to experiment. The speed of a MISS device is a function of the applied voltage and the (external) series resistance. However it is not clear how the intrinsic speed of the MISS structure can be optimised. In the final part of the chapter we find that conduction in the thin insulating layers used in these devices may be due to one of several mechanisms. Conduction processes in LB films are considered in the next chapter.

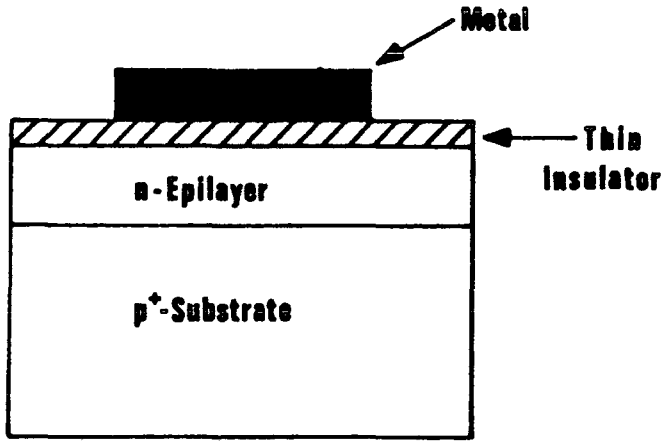

Figure 3.1 Schematic diagram showing the structure of a MISS diode, in this case on an n on p^+ semiconductor.

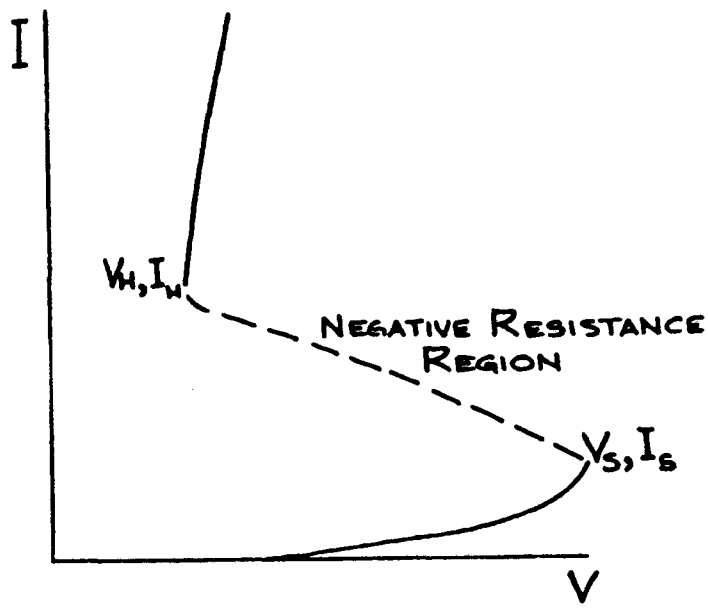

Figure 3.2 Current-voltage characteristics of a typical MISS diode. The negative resistance region is bounded by the switching (V_s, I_s) and holding (V_H, I_H) points. The off state is the high impedance region below I_s, and the on state is the low impedance region above I_H.

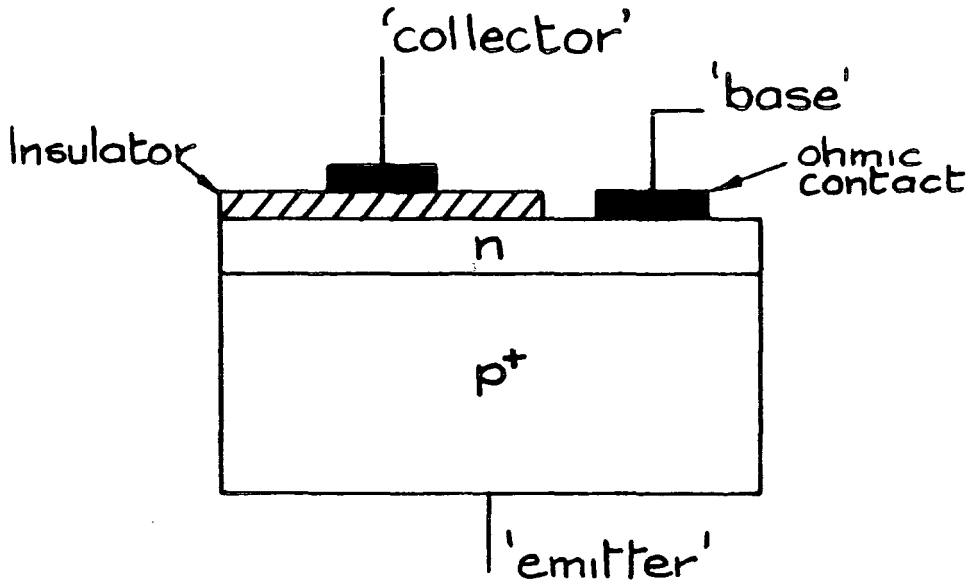

Figure 3.3 Schematic illustration of the structure of a three terminal MISS device, the metal-insulator-semiconductor thyristor (MIST).

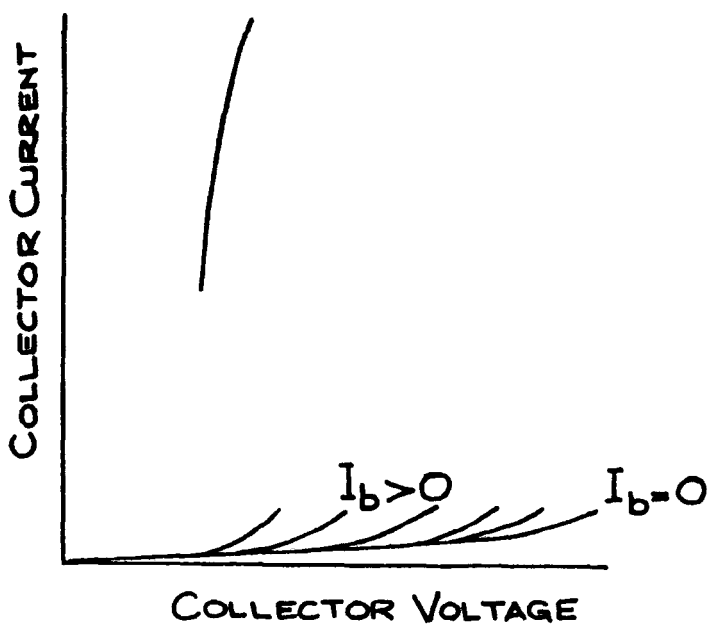

Figure 3.4 Current-voltage characteristics of a typical MIST. The base current controls the switching voltage, as in a conventional thyristor. For an n on p^+ device both collector and base are positively biased with respect to the emitter.

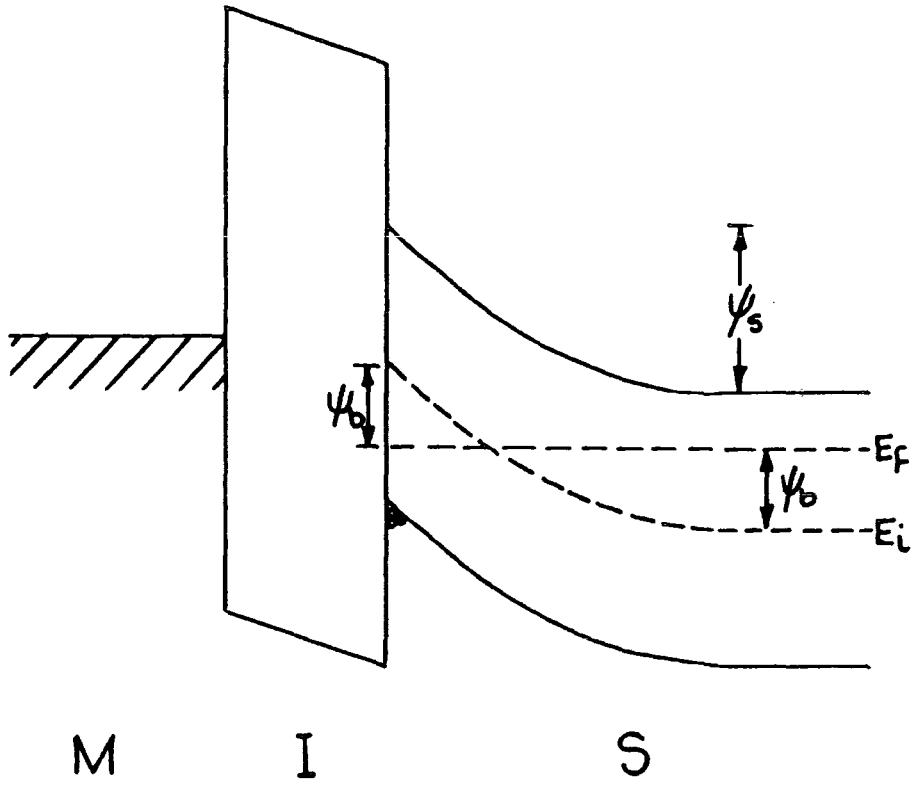

Figure 3.5 Band diagram for an ideal MIS diode at the onset of strong inversion. E_f is the Fermi level in the semiconductor, E_i is the intrinsic level, ψ_s is the band bending in the semiconductor (the surface potential) and ψ_b is defined as $E_f - E_i$.

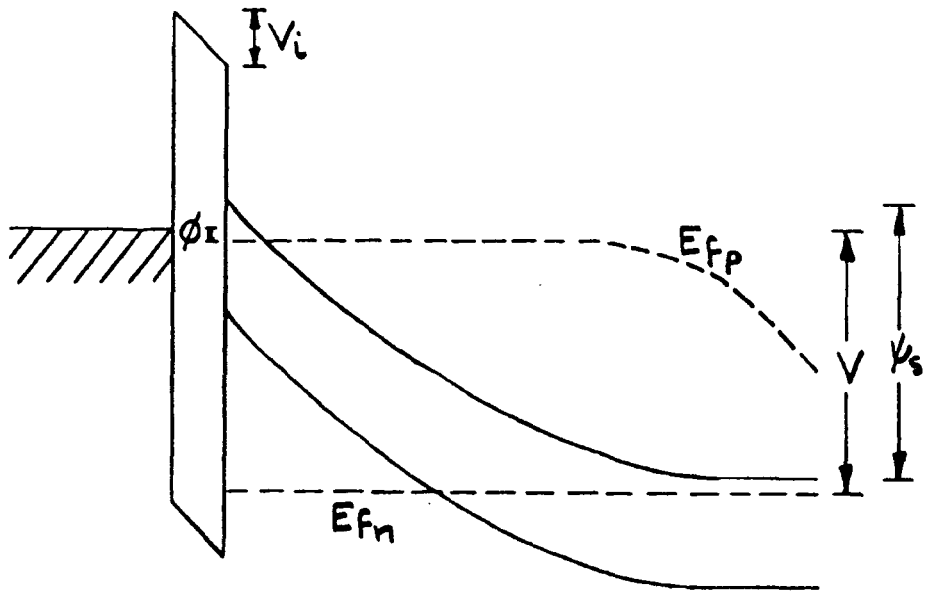

Figure 3.6 Band diagram showing a 'nonequilibrium' MIS diode in deep depletion (i.e. the band bending, ψ, is greater than that required for inversion in an ideal MIS diode). Note the splitting into separate quasi-Fermi levels for the conduction (E_{fn}) and valence (E_{fp}) bands. V is the potential across the device, and V_i is the potential across the insulating layer.

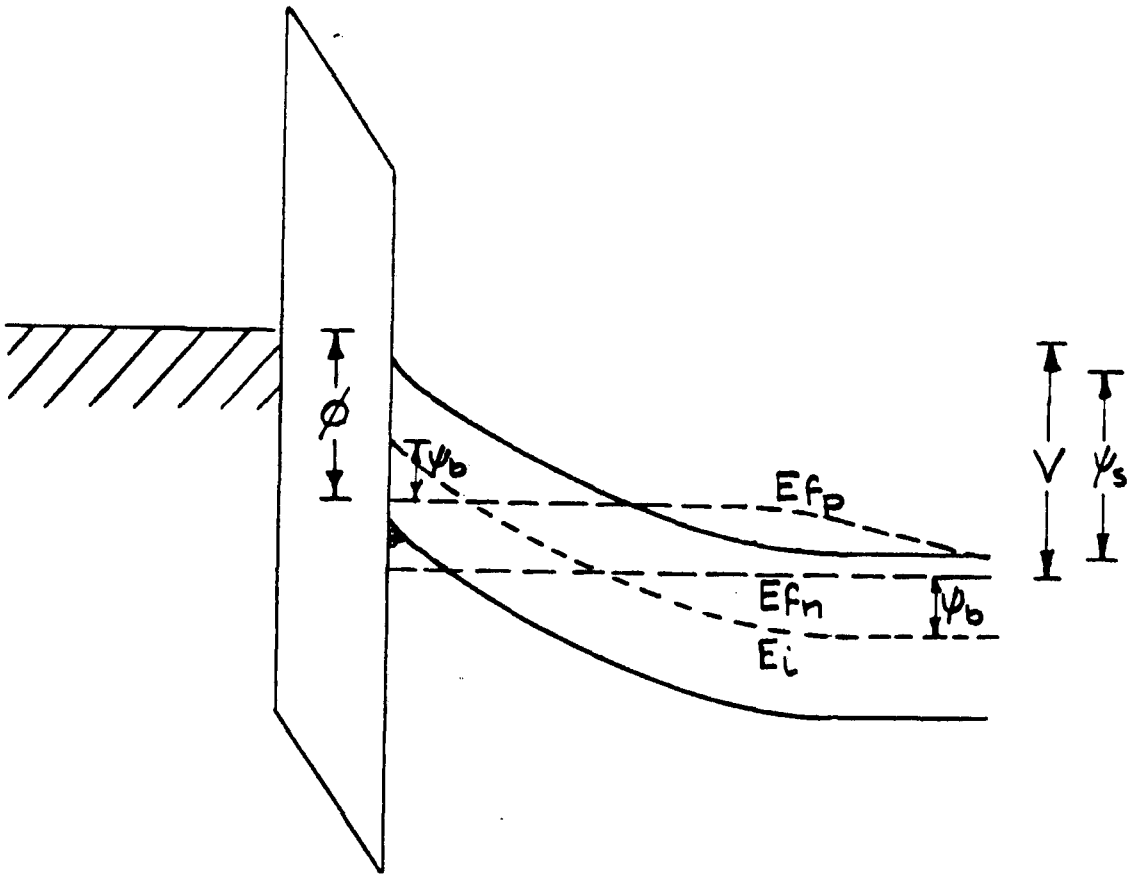

Figure 3.7

Band diagram for a 'non-equilibrium' MIS diode in inversion. For this structure ψ_s at inversion is greater than $2\psi_b$, because of the splitting of the quasi-Fermi levels, which is in marked contrast to the behaviour of an ideal MIS diode. Note that in this case the parameter ϕ is large (c.f. fig. 3.6).

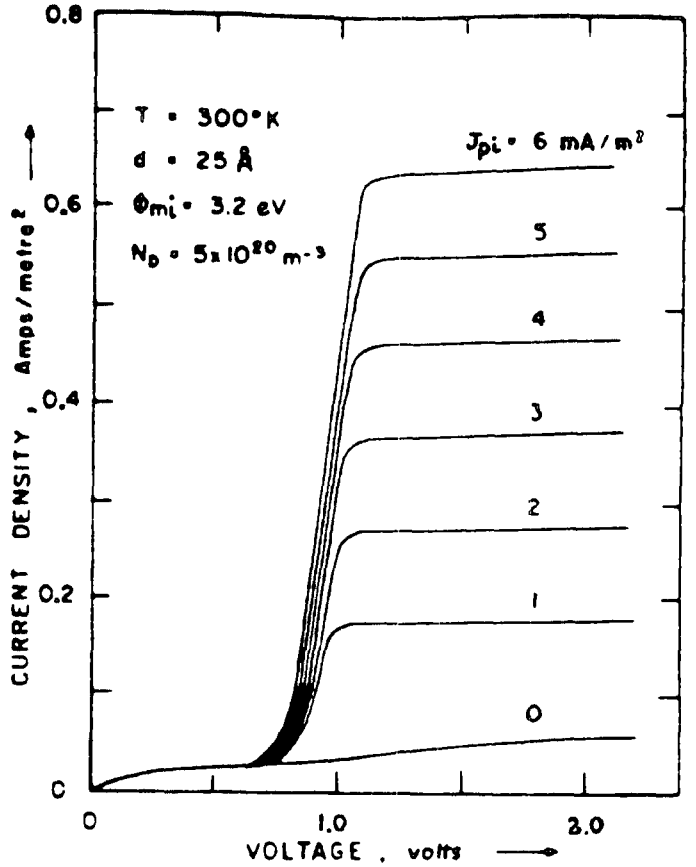

Figure 3.8

The calculated reverse bias current-voltage characteristics for an Al-SiO_2-Si tunnel MIS diode, for varying supply rates of injected minority carriers, J_{pi}. The current multiplication effect can be clearly seen, and in this case the gain is greater than 100. (from ref 31).

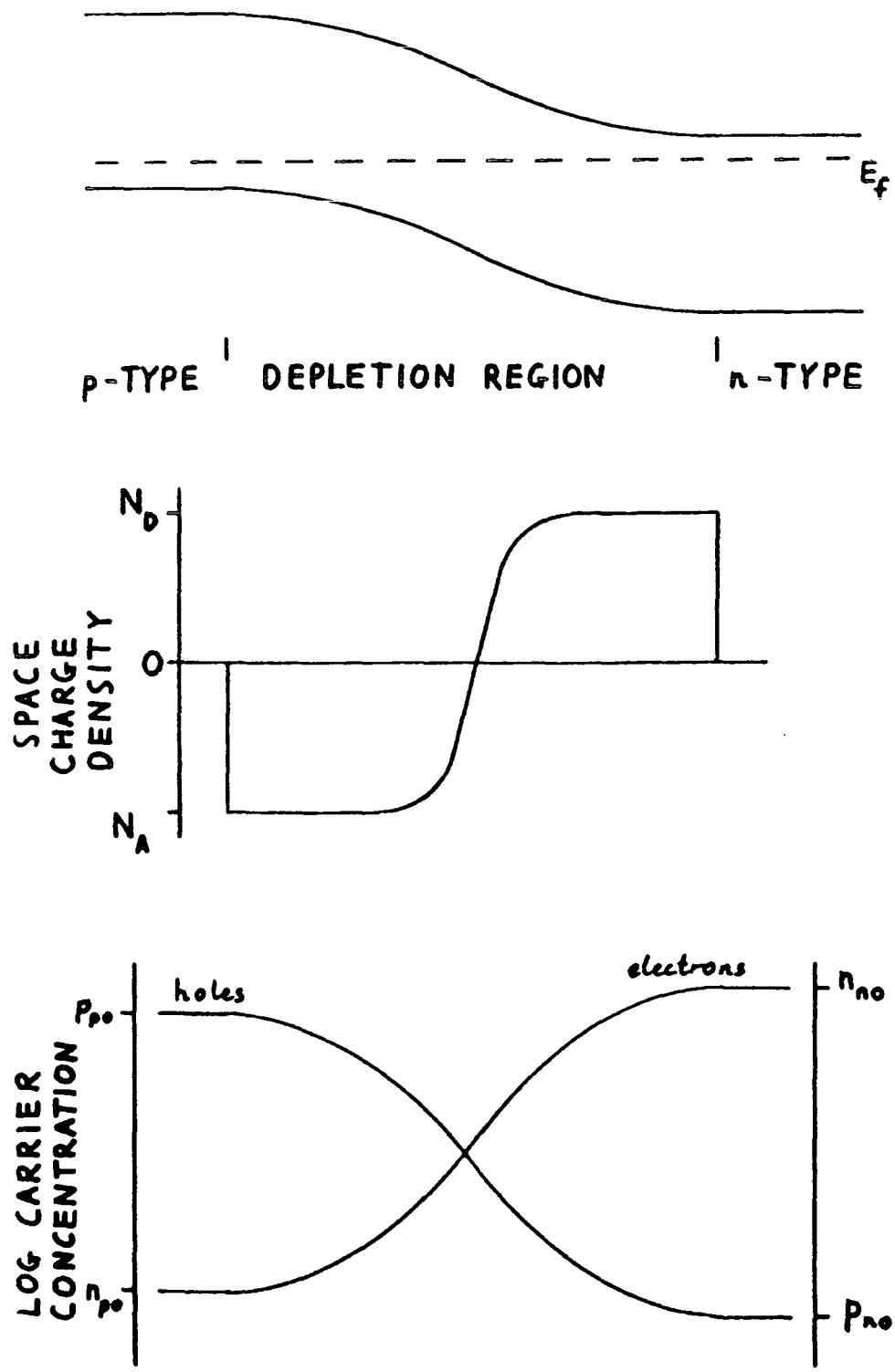

Figure 3.9 The p-n junction at zero bias. The top of this diagram is the band structure of the junction. The middle section shows the corresponding space charge density. The lower part of this figure plots the electron and hole concentrations across the junction.

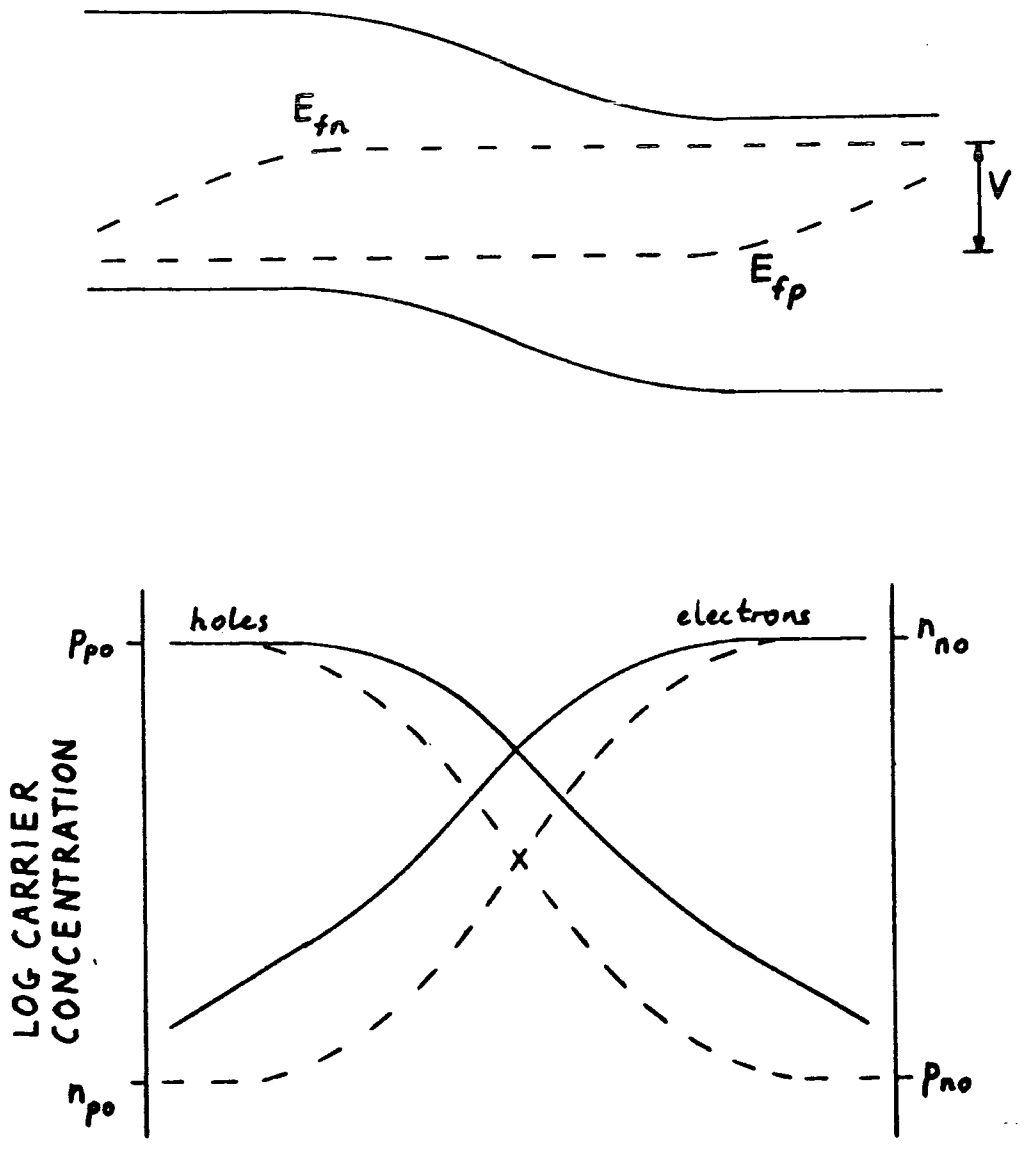

Figure 3.10 The forward biased p-n junction. The upper half of this diagram shows the band structure, with the electron (E_{fn}) and hole (E_{fp}) quasi-Fermi levels marked. In the lower half, the corresponding electron and hole concentrations are shown; the dashed lines show the equilibrium (zero bias) concentrations. The increase in minority carrier concentrations due to minority carrier injection can be clearly seen.

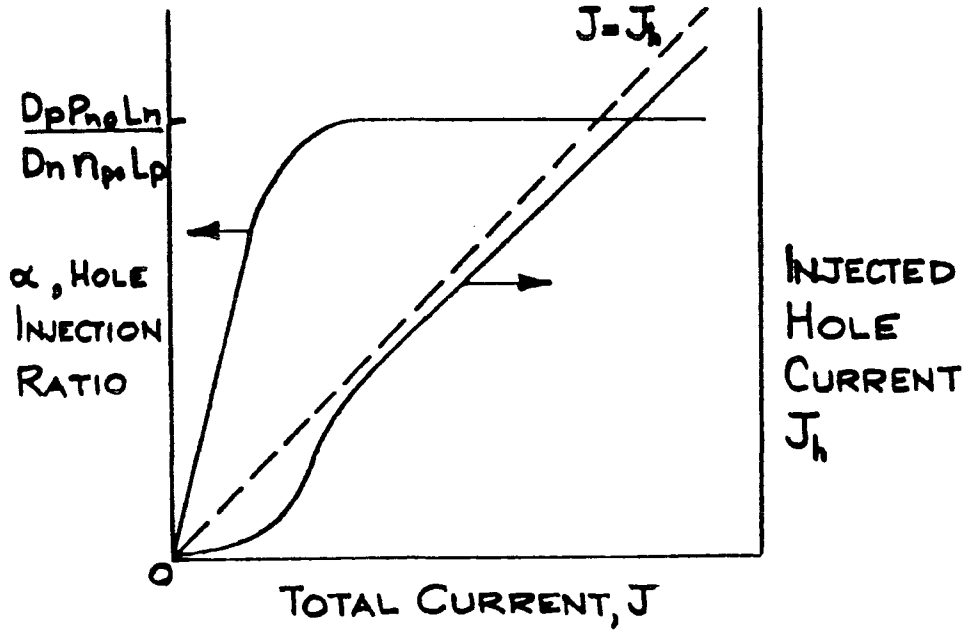

Figure 3.11 Graph of hole injection ratio, α, (as defined in text) and injected hole current as a function of the total current through a p^+-n junction. At low current levels little minority carrier injection occurs, because most of the current is due to recombination in the depletion region. At high current levels hole injection is dominant, because the p side of the junction is more heavily doped than the n side, thus suppressing electron injection.

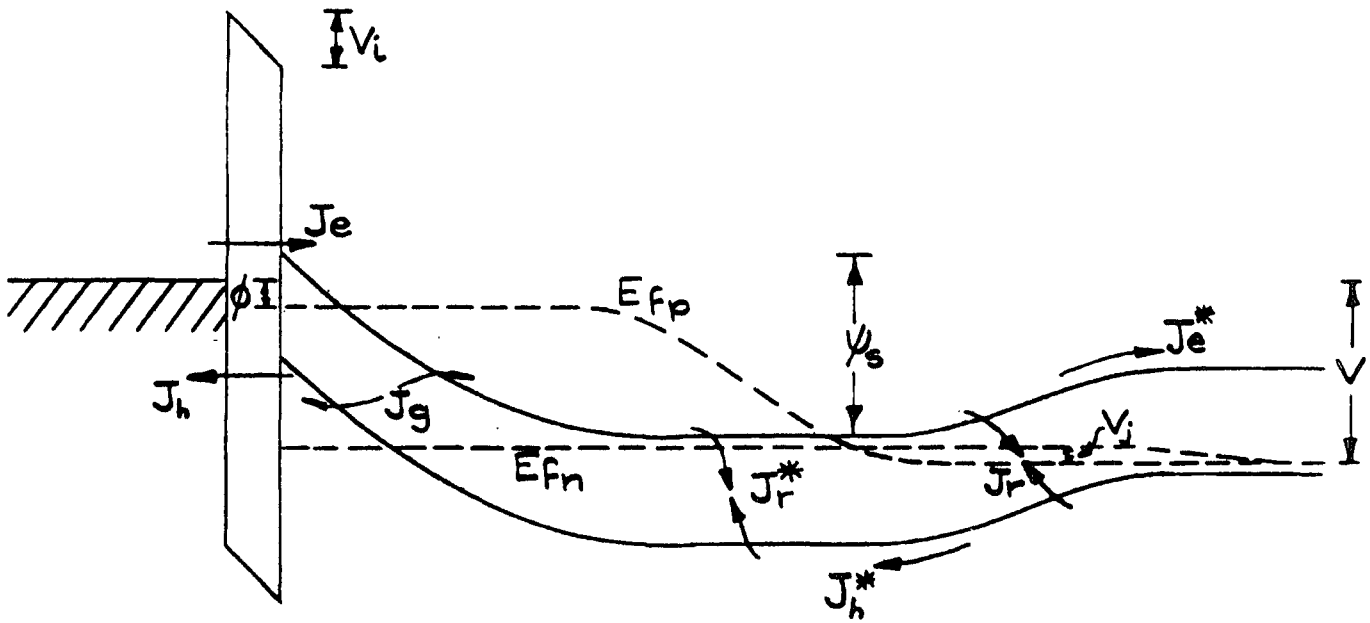

Figure 3.12 Band diagram illustrating the off state of the MISS device. The arrows indicate the direction of carrier flow. J_e and J_h are, respectively, the electron and hole currents through the thin insulating layer. J_g is the generation current in the depletion region. The recombination currents in the neutral (n-type) epilayer and the p-n junction are denoted by J_r and J_r^*, respectively. J_e^* and J_h^* represent the currents due to electron and hole injection at the p-n junction.

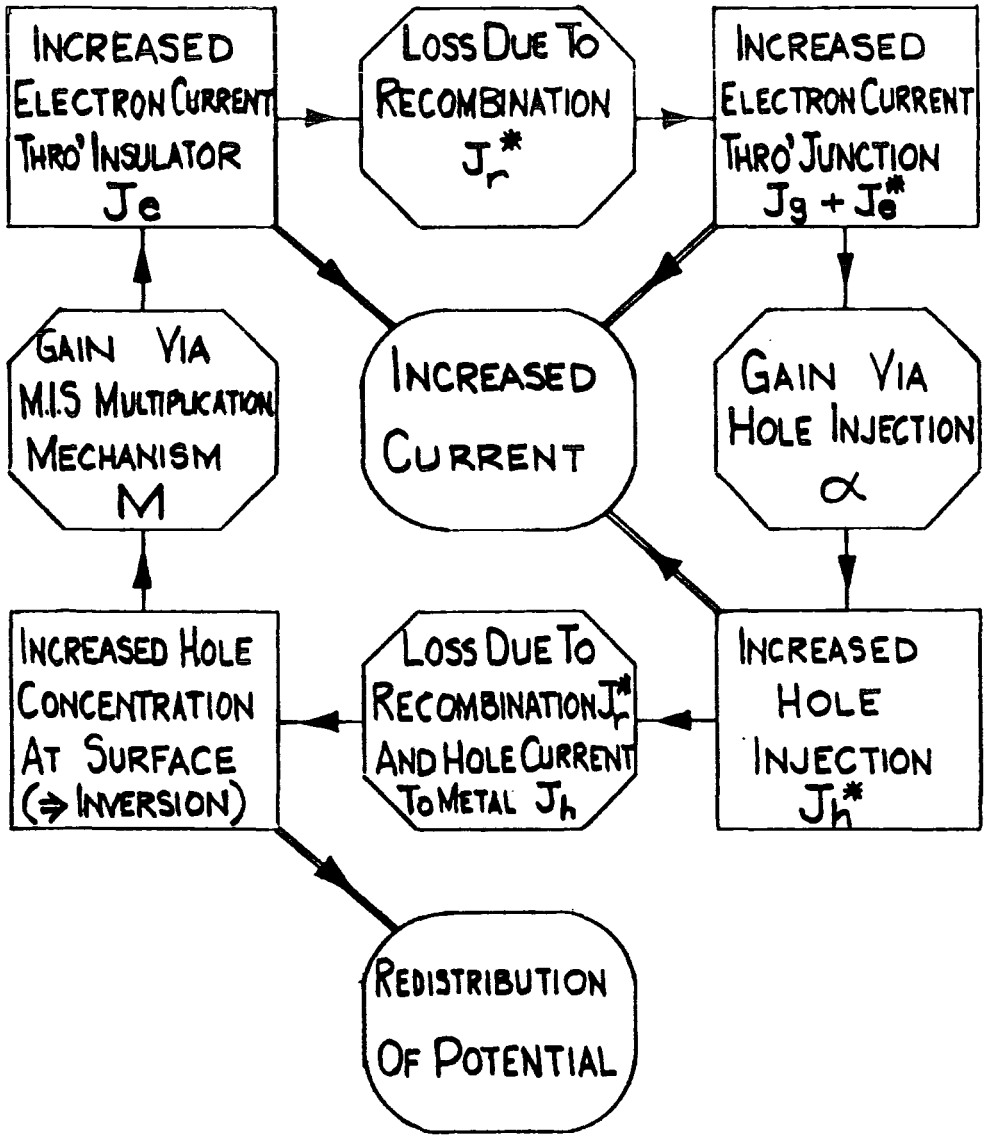

Figure 3.13 This flow chart is for the feedback process in MISS devices. If there is a net gain round this loop then there are two principal effects, an increase in the current through the device and a redistribution of the potential within the device. The latter leads to a reduction in the voltage that can be sustained by the device, which results in a negative impedance region in the I-V characteristics.

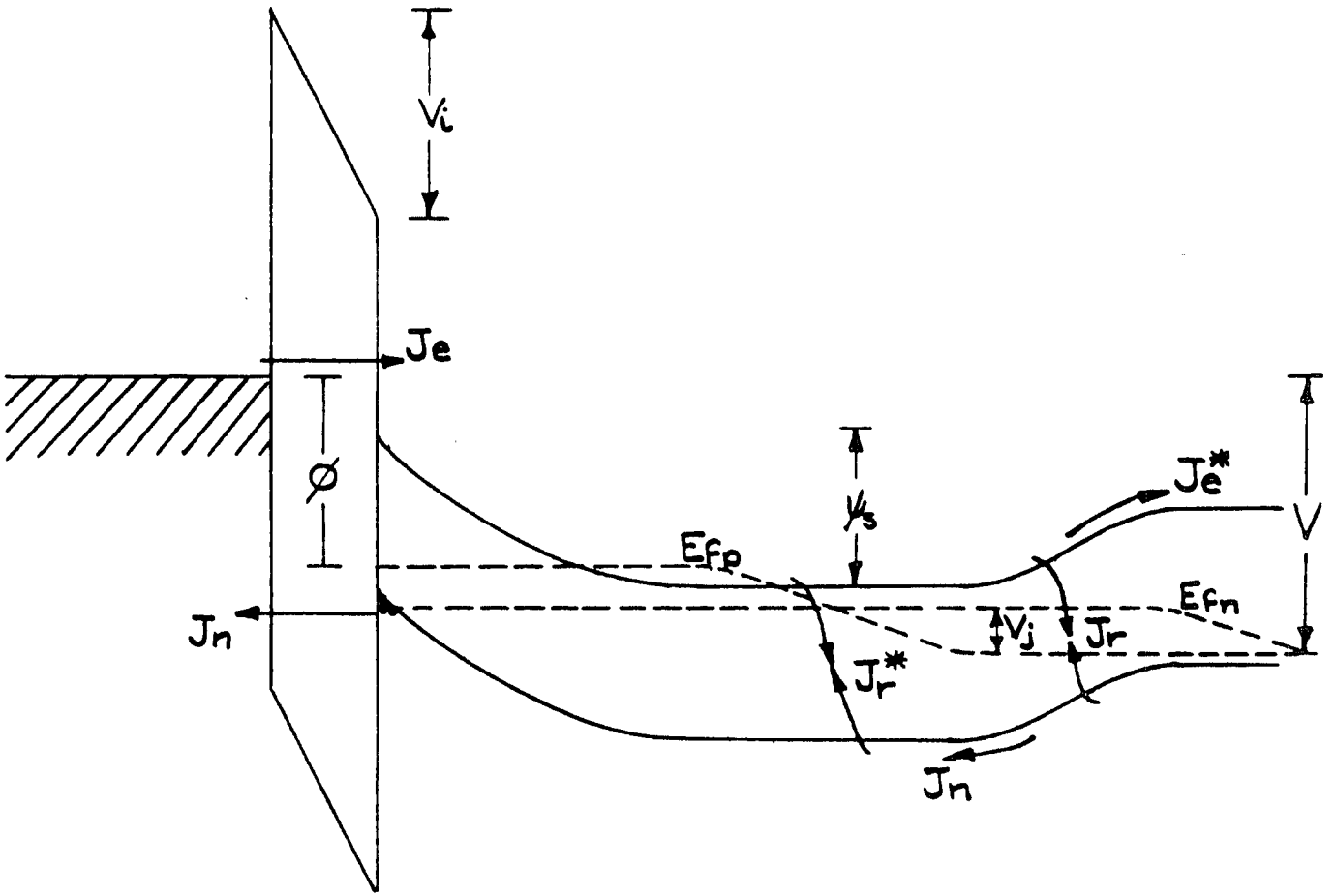

Figure 3.14 This band diagram shows the MISS device in the on state. Comparison with the off state (fig. 3.12) shows that the voltages across the insulator, V_i, and the p-n junction, V_j, have increased, while the band bending at the surface of the semiconductor, ψ, has decreased markedly. The net effect is that the voltage across the device, V, has fallen.

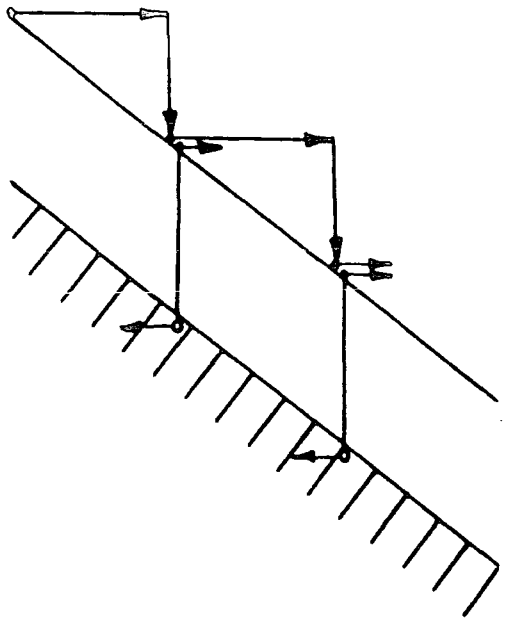

Figure 3.15 Avalanche multiplication occurs if the electric field in a semiconductor is sufficiently high, as is shown schematically in this diagram. The field accelerates electrons to kinetic energies that are large enough to generate electron hole pairs via impact ionisation. The generated electrons and holes are themselves accelerated, and the process repeats itself. In this way a single electron may generate a shower of many electrons (and holes), which corresponds to a large current multiplication.

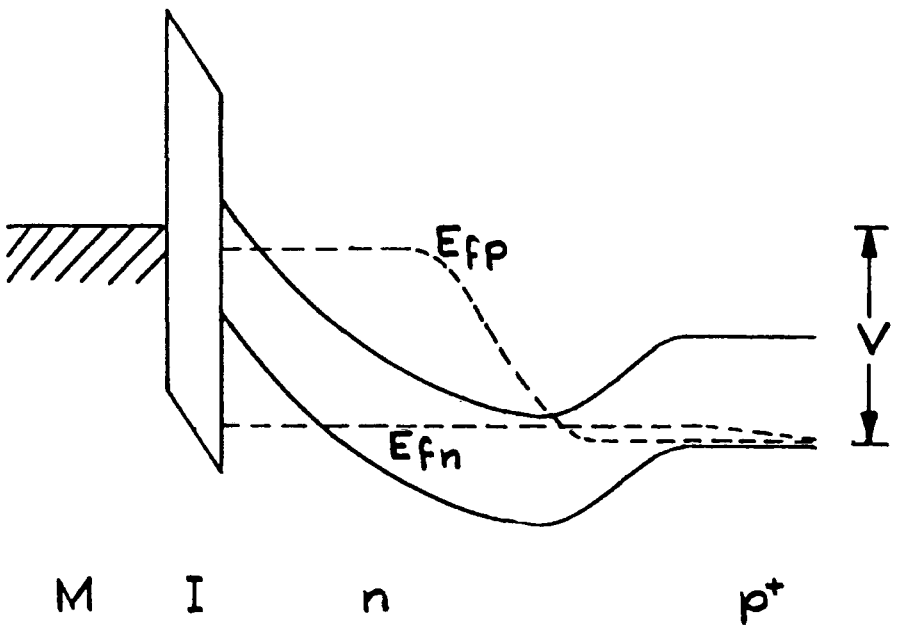

Figure 3.16 Band diagram of a MISS diode at 'punchthrough'. Note that the n-type epilayer is completely depleted, therefore any additional bias will tend to flatten the bands in the p-n junction region.

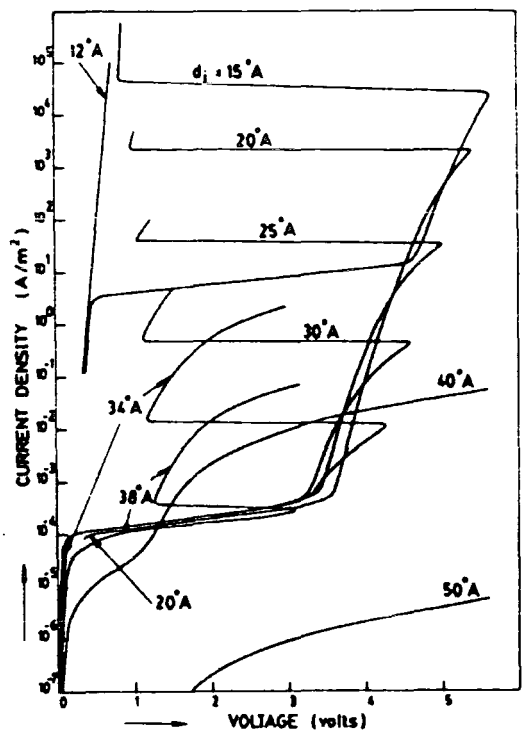

Figure 3.17 Calculated current-voltage characteristic for a punchthrough mode MISS device for different oxide thicknesses (from ref. 44).

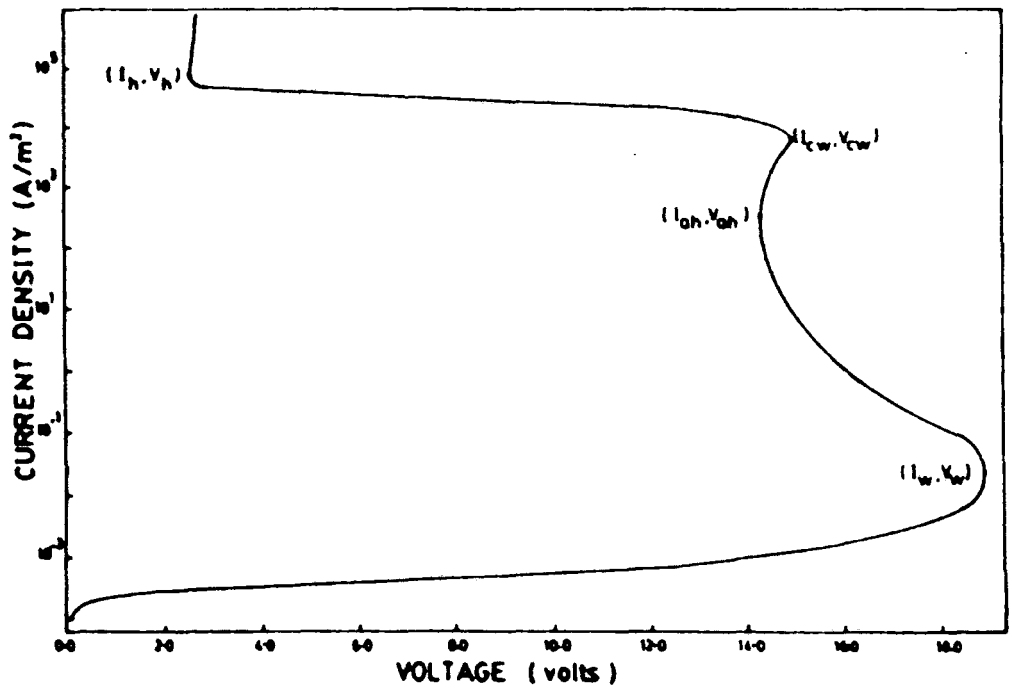

Figure 3.18 Calculated current-voltage characteristic for an avalanche mode MISS device which possesses three stable states (from ref. 38).

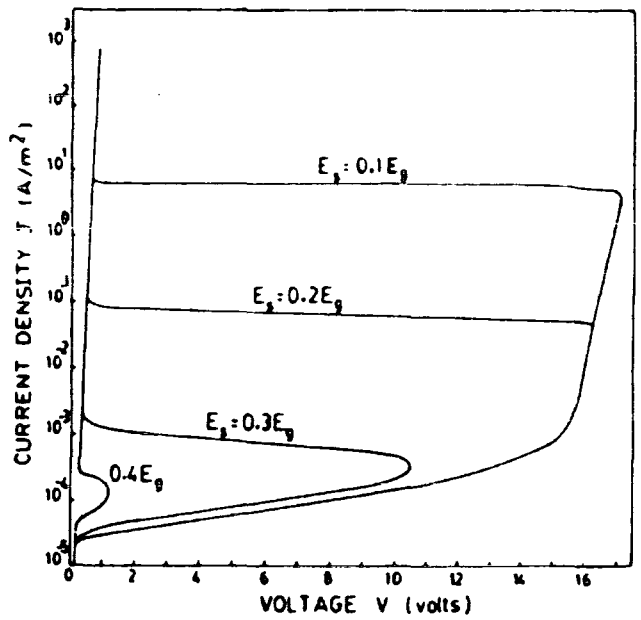

Figure 3.19 Calculated current-voltage characteristic for a MISS diode with a single surface state level of density 6×10^{12} cm^{-2}. The position of this level in the bandgap has very significant effects on the characteristic (from ref. 48).

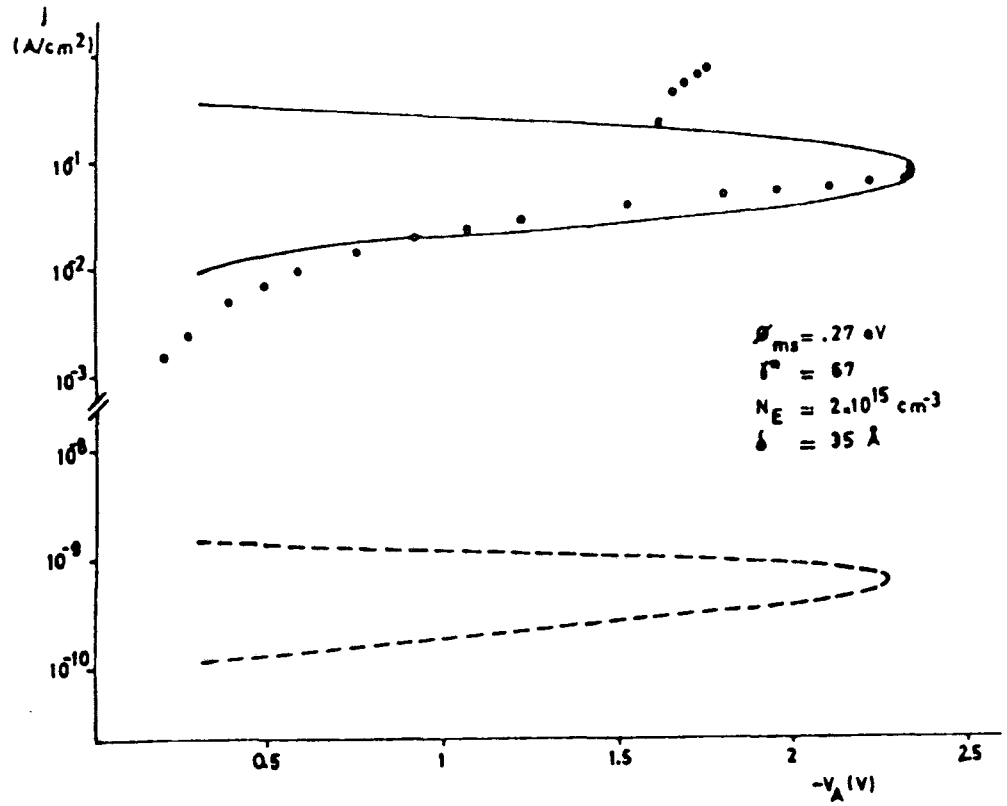

Figure 3.20 Comparison of the theoretical and experimental current-voltage characteristics of a MISS diode. The circles represent experimental data. The lines are from numerical models, the dotted line is for direct tunnelling through the insulator and the continuous line is for a model which also incorporates resonant tunnelling effects. The fit is much better for the resonant tunnel model (nb. this model is not valid in the on state). (from ref. 49)

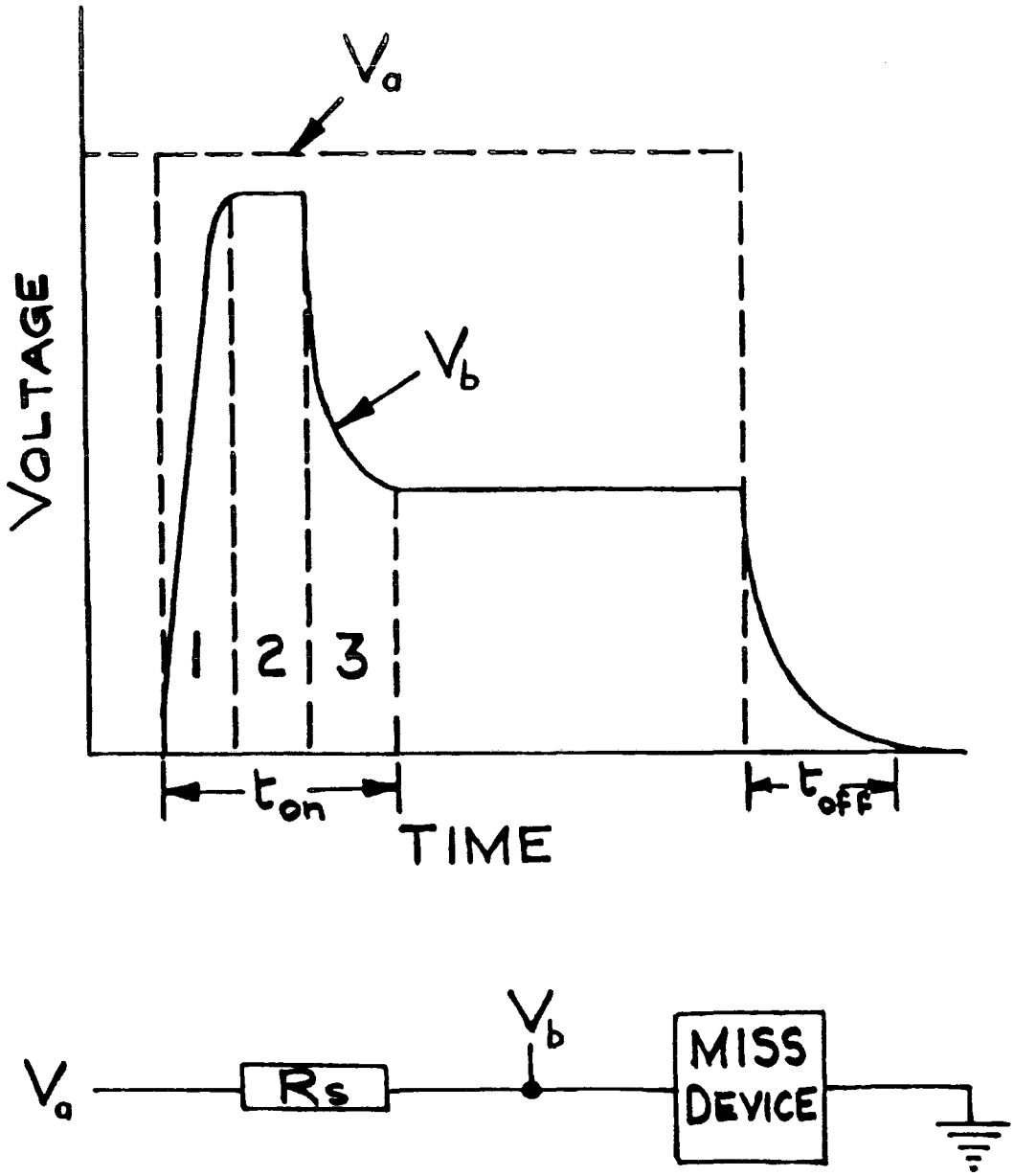

Figure 3.21 The upper part of this diagram illustrates the response of a MISS device to a pulsed signal. The lower part of the diagram shows the circuit, with the pulse, V_a, applied across a series resistor, R_s, producing a voltage, V_b, across the device. The three distinct phases of the turn on process are; (1) the capacitive rise time, (2) the inversion charge delay time, and (3) the feedback regeneration time.

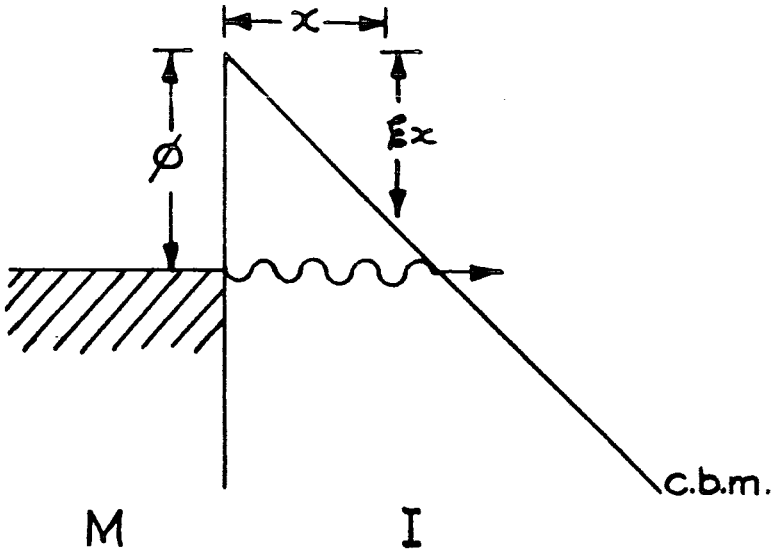

Figure 3.22 Band diagram for Fowler-Nordheim tunnelling. The large electric field in the insulator produces a triangular potential barrier. At very high fields electrons can tunnel from the metal into the conduction band of the insulator, giving rise to a current.

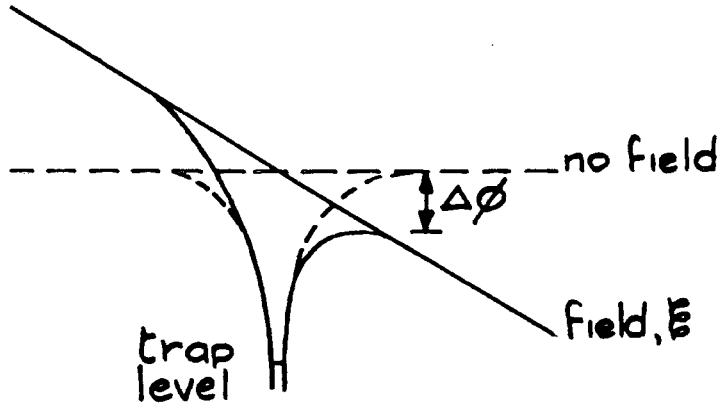

Figure 3.23 The Poole-Frenkel effect is illustrated by this band diagram. The potential barrier of the coulombic trap level is lowered due to the high external field in the insulator. The barrier lowering is $\Delta\phi$.

CHAPTER 4

LANGMUIR-BLODGETT FILMS

4.1 Introduction

It has long been known that certain oils will spread on the surface of water, and the quantitative observations of Benjamin Franklin suggested that the resulting films were extremely thin[1]. Scientific study of these films began in the 1880's with the experiments of Agnes Pockels, who invented the basic techniques for manipulating them. Her work was first published as the result of correspondence with Lord Rayleigh[2], who was the first to suggest that the films were of one molecule thickness.

The foundations of modern studies of monomolecular films were laid down by Irving Langmuir and Katharine Blodgett at the General Electric Research Laboratories. During the First World War, theoretical concepts to explain previous observations were developed; in particular studies of long chain fatty acids showed that the molecules were oriented vertically on the water surface[4]. Later, during the 1930's, Langmuir and Blodgett investigated the transfer of these monomolecular films from the water surface onto solids. It was discovered that multiple layers could be built up[5] and these possessed useful optical properties. The outbreak of World War Two curtailed studies of these multiple layer 'Langmuir-Blodgett' films, and interest in them remained subdued for two decades. The recent revival of interest stems largely from the elegant work of Kuhn, who exploited the possibilities offered by the LB technique to construct organised systems of molecules[6].

In this chapter we first discuss the preparation of LB films, including the details of the necessary apparatus. Details of the deposition conditions used in this work are not covered here (see section 5.3.4). The next section describes some of the properties of these layers, with particular emphasis on their electrical characteristics. Finally we consider some potential applications for LB films; the discussion in this section concentrates on semiconductor devices incorporating LB films.

4.2 Preparation

A detailed description of the intricacies of LB film preparation is not attempted here; instead we concentrate on the basic principles. A more comprehensive discussion of the behaviour of monomolecular films is contained in the excellent book by Gaines[7]. Also covered in this section is the apparatus used to produce these films, the Langmuir trough.

4.2.1 Basic Principles

Fatty acids, such as stearic acid (fig. 4.1), are typical Langmuir film forming materials. They are amphiphlic, that is they possess distinct hydrophilic and hydrophobic regions. The latter consists of the long hydrocarbon chain, and the hydrophilic head group is in this case a carboxylic acid unit. Other long chain molecules with polar headgroups, such as alcohols and amines, also form Langmuir films. The film material is usually spread upon the water surface using a volatile solvent that is immiscible with water. Once the solvent has evaporated an expanded film is left on the surface, as shown in fig. 4.2(a). In this situation the molecules are widely separated, thus behaving like a two dimensional gas.

As a Langmuir film is compressed the surface pressure rises (surface tension falls); a phase diagram for the two dimensional film can be

obtained by plotting surface pressure against film area (this is usually referred to as an isotherm). A typical isotherm for a fatty acid material is given in fig. 4.3, showing the three distinct regions that are often observed. For large areas the surface pressure is low - the 'gaseous phase'. As the area is reduced and the molecular area becomes small, the surface pressure begins to rise and the film behaves as a two dimensional liquid. On further compression the molecules become closely packed and the surface pressure increases rapidly. This 'solid phase' is stable up to a threshold pressure, above which collapse occurs. In the compressed 'solid' films the molecules are aligned vertically (fig. 4.2(b)) and a high degree of order may also occur in the plane of the film. The area per molecule, A_o, is comparable with the molecular cross section, demonstrating that a truly close packed monolayer has been formed. Isotherms are very sensitive to the pH and purity of the subphase, therefore extremely pure water must be used if repreatable results are to be obtained. It should be noted that many materials do not exhibit distinct phases (unlike the fatty acids); this is especially true of complex molecules such as dyes and polymers, which usually give very rounded and featureless isotherms.

Under certain circumstances it is possible to transfer a compressed Langmuir film from the water surface onto a solid. The most common method used to do this is to vertically dip the solid into the subphase; by repeatedly inserting and withdrawing the substrate it is possible to build up a Langmuir-Blodgett film with a thickness of many monolayers. Three types of deposition have been recognised. The most common of these is 'Y type', in this case pickup occurs on both the upstroke and downstroke, as shown in fig. 4.4. Pickup on the initial insertion is dependent on the solid substrate; if the surface is hydrophilic (as

shown) no film transfer occurs, however for a hydrophobic surface a monolayer is deposited during this first insertion. On each subsequent insertion and withdrawal a monolayer is deposited and a head to head, tail to tail structure is built up (fig. 4.4d). At high pH levels fatty acids may pickup on the downstroke only and a head to tail multilayer would be expected (fig. 4.5a). However X-ray measurements on these 'X type' films indicate that the structure is identical to that of Y-type films. It is believed that this is due to molecules flipping over during deposition[7]. Z-type deposition, involving pickup only on the upstroke (fig. 4.5b), had been postulated by Langmuir, although it was not observed until recently[8]. Successful deposition is dependent on many factors, especially the cleanliness of the substrate, the subphase purity and it's pH. Other factors may also be important, for example when dipping fatty acid films it is usual to add divalent cadmium ions to the subphase ($\sim 10^{-4}$ molar); this enhances the stability of the monolayer and facilitates film deposition[9].

4.2.2 The Langmuir Trough

At its simplest the Langmuir trough comprises a basin containing the subphase, barriers to confine and compress the monomolecular film and some means of measuring surface pressure. The troughs in use at Durham are a development of a design first proposed by Blight et al[10]; a typical example is shown in the photograph fig. 4.6. A motor driven constant perimeter, variable area compression system is employed[11], consisting of a PTFE coated glass fibre belt located on PTFE rollers (fig.4.7 inset). The trough itself is made of glass and is supported by a metal framework which also supports the dipping mechanism, a motor driven micrometer screw to which the sample may be clamped. The surface pressure is monitored using a Wilhelmy plate[12], consisting of a 1 cm

wide strip of filter paper, suspended by a thread from a microbalance head (mounted above the trough). Where possible the structure is made from stainless steel and PTFE, with other metal chrome plated or anodised, to minimise the risk of contamination and to prevent corrosion. The complete structure is housed in a glass doored cabinet which is fitted with an extractor fan to aid solvent evaporation.

The peripheral equipment associated with the trough comprises a purpose built control box, a Beckman LM600 microbalance, Bryans 312 2 channel Y-t and 2900 X-Y chart recorders and a Pye-Unicam PW 9409 pH meter. The control box regulates barrier and dipping head movements and in particular maintains constant surface pressure using a differential feedback system (fig. 4.7). The introduction of feedback systems to maintain constant surface pressure[13,14] was an important technological advance and is essential for the repeatable production of high quality LB films. Using the chart recorders pressure-area isotherms and plots of pressure and area versus time could be obtained, the latter allowing the dipping process to be recorded.

Cleanliness is of great importance in any device processing technology, therefore the Langmuir troughs are housed in a class 10000 microelectronics clean room. The purity of the subphase is a critical factor in the deposition of high quality LB films. At Durham a two stage water purification system is used, comprising an Elga reverse osmosis unit followed by a Millipore 'Milli Q' polish; the water supplied by this system has a resistivity of > 10 MΩ cm. Analysis of the freshly purified water shows low levels of contamination, especially when compared with the impurities leached from the glass trough in a 24 hour period[15] (see table 4.1).

4.3 Characteristics

Many different molecules have been used to form LB films including dyes, biological materials and polymers or their precursors. Many of these substances possess interesting optical, electrical or chemical properties. In this section we do not attempt to describe all these characteristics, instead we concentrate on the relevant properties of the materials used in this work.

4.3.1 General

The bulk of this work concerns LB films of ω-tricosenoic acid (ω-TA), a fatty acid with a vinyl double bond at the end of the carbon chain (fig. 4.8). Films of this material are similar in many respects to the 'classic' LB film materials, the saturated fatty acids such as stearic acid. However high quality films of ω-TA can be produced without the addition of cadmium to the subphase[16]. Fig. 4.9 shows a transmission electron diffraction pattern for an ω-TA LB film[17], demonstrating that structures produced by this technique can be highly ordered in the plane of the film. Fatty acid multilayers are also highly ordered normal to the plane of the film; this is illustrated in figure 4.10, which shows the neutron reflectivity profile of an 29 layer fully deuterated cadmium arachidate LB film[18]. Physical parameters are reproducible from one monolayer to the next, as can be seen from the data plotted in figure 4.11. In fig. 4.11(a) the reciprocal capacitance of metal-cadmium arachidate LB film - metal structures is plotted against the number of monolayers in the film[19]; the linear relationship indicates that each monolayer has the same dielectric thickness. A band in the infra-red reflection spectrum of the same material has been used to demonstrate the uniformity of successive monolayers[20] (fig. 4.11b). Fig. 4.11(c) shows the count rate of ^{14}C β rays as a function of the

number of monolayers of barium stearate labelled with ^{14}C[21], again confirming the uniformity of the deposition process. Finally fig. 4.11(d) shows the attenuation of X-ray photoemission signals from a substrate coated with cadmium dimethyl arachidate[22].

Fatty acid LB films are not mechanically robust and have low melting points. They are therefore easily damaged and this may be a significant limitation on their use. As a consequence of this there is considerable interest in less delicate LB film materials. The most promising materials in this respect are the phthalocyanines (Pc). These are highly conjugated heterocyclic structures which are stable up to 400°C, in addition they possess interesting optical and electronic properties that can be modified by substituting different metals into the centre of the ring. However preparation of LB films of these materials is not a simple task as they are almost completely insoluble in common solvents. The molecules also lack distinct hydrophobic and hydrophilic regions and are therefore less likely to form ordered monolayers on the water surface. These difficulties can be partially overcome by the use of substituted derivatives[23-25], such as the asymmetric copper phthalocyanine (Cu:Pc) shown in figure 4.12. Films of these materials adhere tenaciously to the substrate, however they are much less ordered than the classical fatty acid LB films.

4.3.2 Conduction Mechanisms

Measurements of the electrical characteristics of LB films must be treated with caution for a number of reasons. It would be desirable to deposit LB films on noble metal substrates, unfortunately this is not practicable. Therefore there is always a thin oxide layer underneath the film and this may affect the measured conductivity. The film quality is also crucial, and consistent results began to be obtained only

comparatively recently (the work up to 1980 has been reviewed by Vincett and Roberts[26]). In addition environmental effects, such as ambient and humidity, can be significant[27]. In this section we concentrate on the behaviour of fatty acid LB films because of their relevance to this work.

Fatty acid LB films are good insulators with high breakdown strengths ($> 10^6$ V cm^{-1}). For single monolayers the films are thin enough for quantum mechanical tunnelling to occur. Characteristics consistent with tunnelling have been observed[28-30], and for stearic acid monolayers Careem and Hill[31] found agreement with the expected behaviour over a wide voltage and temperature range. Tunnelling characteristics have also been observed for fatty acid monolayers between superconducting metal contacts[32-34]. Perhaps the most convincing evidence of tunnelling in LB films is the observation of inelastic tunnelling by Ginnai et al[35] in barium stearate monolayers. These data cannot be explained in terms of conduction through pinholes.

At low fields conduction in fatty acid multilayers is approximately ohmic[27,28,36,37]. Measurements of the low frequency ac conductivity show an ω^n dependence with $0.5 < \omega < 1$[36-39]; this has been interpreted in terms of hopping of carriers by thermally assisted tunnelling between localized states. Further support for this model is provided by the work of Sugi and co-workers[40,41], in particular by the observed conductivity dispersion at low frequencies in heterogeneous LB structures[42]. At high fields a log $J \propto V^{\frac{1}{2}}$ behaviour is usually observed[27,30,36,37,43]. This could be due to either Schottky emission or a Poole-Frenkel process, however there is a lack of agreement on which mechanism occurs. This could be due to differences in electrode materials, although the process may also be dependent on film thickness[31]. On some substrates different behaviour has been reported, for example a $J \propto V^2$ behaviour has

been observed on InP, indicative of space charge injection[44], while thermionic emission across the potential barrier presented by the LB film has been reported for GaP MIS structures[45]. As yet no conductivity data on ω-tricosenoic acid LB films have been published. However it is expected that the ω-double bond does not significantly alter the behaviour, particularly as the electrical characteristics of diacetylene films[46] (which contain two triple bonds per molecule) are similar to those of other fatty acid films.

In the bulk state phthalocyanines may be semiconductors (usually p-type). Their conductivity can be markedly increased upon exposure to oxidising gases, but although the process is reversible recovery is slow and may require heating. The electrical characteristics of phthalocyanine LB films have not yet been fully investigated. Fig. 4.13 shows the current-voltage behaviour for a LB film consisting of 40 monolayers of tetra-tert-butyl manganese phthalocyanine[47]. At low fields conduction is ohmic and at higher fields conduction is space charge limited. The behaviour of Cu:Pc is similar, however the high field region is less pronounced. LB films of phthalocyanines also exhibit a pronounced sensitivity to oxidising gases. The lateral conductivity of a film of Cu:Pc increases by more than an order of magnitude when exposed to a 20 VPM concentration of NO_2[24]. The recovery of these layers is much more rapid than that of vacuum deposited thin films, and this is probably due to the thinness and more ordered structure of the LB film.

4.4 Potential Applications

Interest in possible applications of LB films has only emerged in the last decade, largely due to the realisation that the LB technique allows the fabrication of organised molecular structures, which are

difficult or impossible to construct using other methods. Many applications require essentially passive layers, and in those cases the technique's advantages include the uniformity and precisely controlled thickness of the films. In addition large areas can be coated and minimal surface damage is caused by this room temperature deposition process. Other applications require active LB film layers, for example dye layers and chemically sensitive films. In LB films the molecules are oriented and highly ordered, therefore useful differences from bulk behaviour may occur. The final category of applications will utilise the unique capabilities of the LB technique to construct complex ordered systems. These may have their properties tailored to suit specific applications (Molecular Engineering). Some of the proposed applications of LB films[38,48] are summarised in table 4.2. In the remainder of this section we discuss the use of these films in metal-insulator-semiconductor devices.

The first reported MIS diodes incorporating a LB film[49] were formed on p-type silicon. The capacitance of these structures exhibited the normal accumulation, depletion and inversion regions as the bias was varied. These devices were of little practical interest as nearly ideal insulating oxide layers can be grown on silicon. The first LB film MIS diodes on a compound semiconductor, n-type InP, also possessed promising characteristics[50]. In particular, an increase in capacitance at low frequencies in the strong inversion region was observed and the calculated density of interface states was $\sim 3 \times 10^{11}$ $cm^{-2}eV^{-1}$. Roberts et al later reported the characteristics of the first transistor incorporating a LB film, a simple depletion mode InP MISFET[51]. LB film MIS devices have also been fabricated on p-type InP[52], p-type CdTe[53], p-type InSb and n-type $Hg_{.47}$ $Cd_{.53}$ Te[54]. In addition FETs have been

reported on amorphous silicon substrates[55]. All these devices used relatively thick multilayer LB films as insulating layers.

The LB film technique also enabled metal-tunnel insulator-semiconductor diodes to be fabricated, utilising films of a few monolayers thickness. The first investigation of this type of structure, on n-type CdTe, showed that MIS solar cells incorporating a thin LB film could be up to 40% more efficient than comparable Schottky barrier cells[56]. Thin film MIS devices on n-type GaP have been quite extensively studied[45,57-62]. Measurements of current-voltage, capacitance-voltage and the photoelectric characteristics of these diodes show Schottky like behaviour and the barrier heights calculated from the three techniques concur[57,58,60,61]. These barrier heights are greater than those of similar Schottky barriers (i.e. fabricated identically apart from the omission of LB film deposition), although there are some differences between the work of Tredgold et al and that of Batey et al which may be due to differences in preparation. Several models have been proposed to account for this behaviour. Perhaps the simplest of these is an increase in the barrier height due to fixed charge in the LB film, however this does not fit the observed behaviour. Winter et al have proposed that the barrier height increase is due to the intrinsic dipoles of the headgroups of the film molecules[61]. Batey et al investigated the electrical, photoelectric and electroluminescent behaviour of diodes incorporating several monolayers, and they proposed a different model in which electron transport occurs by thermionic emission from the semiconductor, via the conduction band of the LB film[45,62]. This work also demonstrated electroluminescent efficiencies approaching those of p-n junctions[45,59]. Similar LB film structures have been fabricated on ZnSeS and these offer the possibility of efficient blue

electroluminescence[63]. LB film thin MIS devices have also been reported on GaAs[64], although their characteristics are rather different from those reported in this thesis. This may be due to the use of different surface treatments before film deposition.

Investigation of LB film MIS devices has demonstrated that useful properties can be obtained, and significant improvements could result from further development. However there are many technological problems to be solved before the application of LB films in practical devices can be considered. Perhaps the most rewarding avenue for future development is the incorporation of active LB films layers in integrated sensors. Preliminary investigations using gas sensitive phthalocyanine films have shown some promise[63]. Developments in this area may soon enable physiological sensors to be produced which utilise biological LB film layers, such as proteins and enzymes, as active layers in chemically sensitive FETs (ChemFETs or ISFETs).

Table 4.1 (a) Impurity concentrations in freshly purified 'millipore' water.
(b) Impurity concentrations present after 24 hours in the Langmuir trough.

	Na	K	Sn	Fe	Al	Si	Total Organic Content
a	0.05	0.02	0.01	<0.02	<0.2	<0.5	92
b	0.3	1.05	0.06	0.21	<0.2	<0.5	145

(Values in Parts per Billion)

Table 4.2 Potential applications of LB films.

Topic	Molecular Electronics Application
Model Systems in Fundamental Research	Spectroscopy of Complex Monolayers; spectral sensitization, fluorescence quenching, energy transfer between excited states. Model membranes to mimic photosynthetic system. Modification of solid surface properties. Examination of lipids, proteins and membrane phenomena; organic semiconductors.
Applied Chemistry	Surface chemistry and behaviour of surfactants; Catalysis; Filtration/Reverse Osmosis membranes; Adhesion; Surface Lubrication.
Electron Beam Microlithography	Good sensitivity and contrast; acceptable plasma etching resistance; less scattering of electrons and therefore better resolution; negative and positive resists possible.
Integrated Optics	Film thickness plus refractive index of film and hence guided wave velocity can be controlled with great precision; acceptable attenuation loss. Possible uses in conventional optics and optical data storage.
Non-Linear Physics	Control of molecular architecture to produce asymmetric structures with high nonlinear coefficients, e.g. in electro-optics or pyroelectric detectors.
Dilute Radioactive Sources	Radioactive nuclide incorporated in conventional LB Film; used to measure the ranges of low energy electrons.
Electronic Displays	Large area capability of LB films is an advantage; the monolayers can either be the active electroluminescent layer or used to enhance efficiency of an inorganic diode; passive application to align liquid crystal display. Deposition of liquid-crystal type molecules also possible.
Photovoltaic Cells	Used as a tunnelling layer in an MIS solar cell or as an active layer in p-n junction diode, perhaps involving an inorganic/organic junction.
Two Dimensional Magnetic Arrays	Magnetic atoms e.g. Mn, periodically spaced in LB film; possible applications include magnetic control of superconducting junctions and bubble and magneto-optical devices.
Field Effect Devices	Accumulation, depletion and inversion regions possible with a variety of semiconductors; can therefore form the basis of several devices e.g. CCD, bistable switch, gas detector or pyro/piezo FET if suitable LB films are used.
Biological Membranes	Attractive supporting membranes for commercial exploitation of biological material, e.g. immobilization of membrane bound enzymes in solid state sensors; ISFET type structures.
Supermolecular Structures	Speculative work aimed at superconductors, organic metals, Esaki superlattices, 3D memory storage, molecular switches.

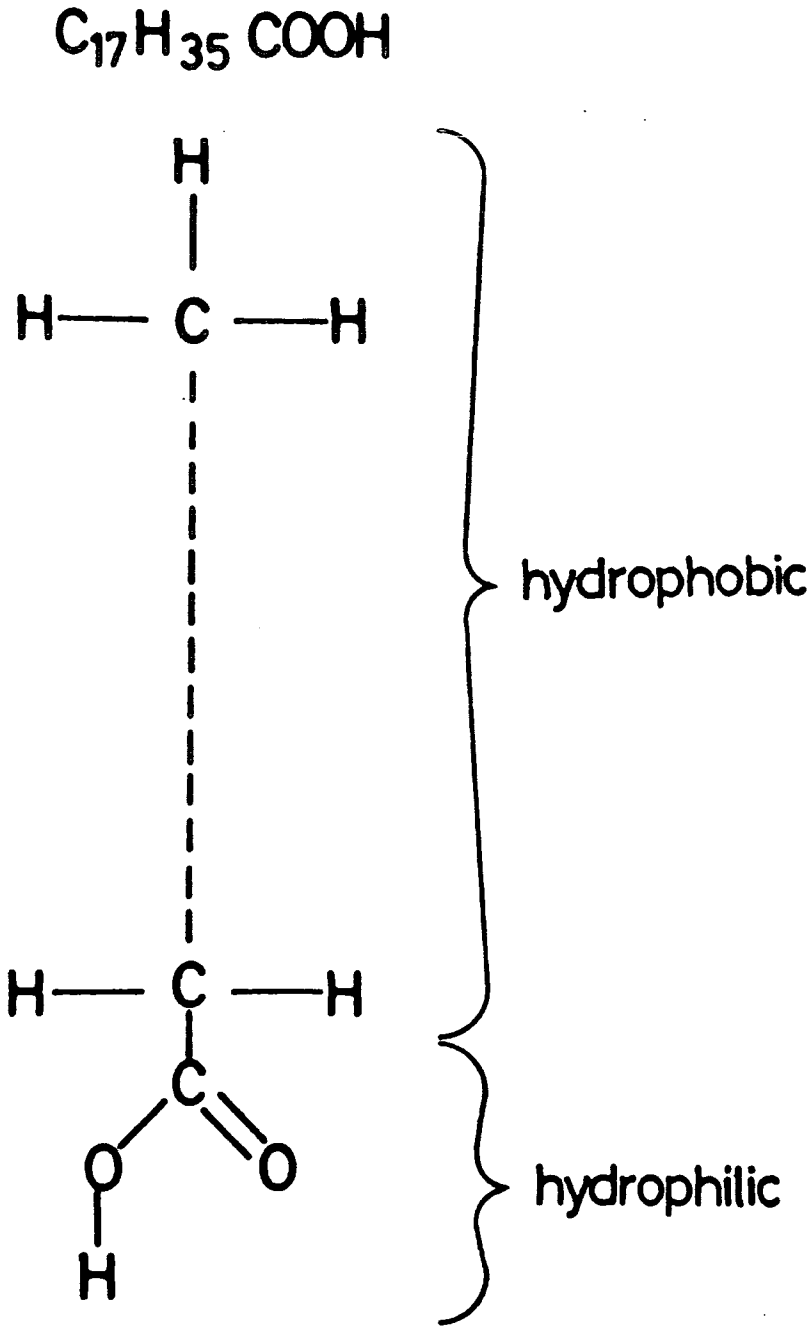

Figure 4.1 Molecular structure of stearic acid. This long chain fatty acid is a typical Langmuir film forming material. There are two distinct regions in the molecule, a nonpolar (hydrophobic) carbon chain and a polar (hydrophilic) head group.

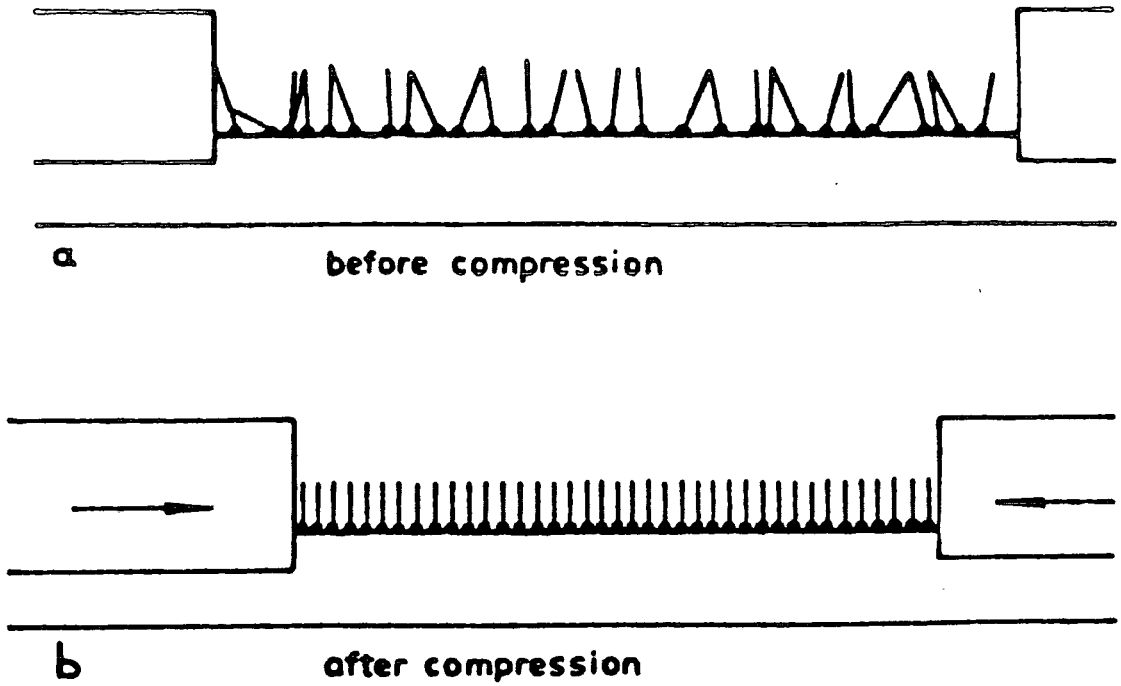

Figure 4.2 Schematic diagram showing a Langmuir film on the water surface. The molecules spread across the surface because of the attraction between the water and the hydrophilic head groups, but are prevented from dissolving by their hydrophobic 'tails'.

(a) In an uncompressed film the molecular separation is large and the molecules are aligned randomly.

(b) In a compressed monolayer the molecules are close packed and aligned in the direction normal to the surface (nb. the molecules may be slightly tilted due to packing considerations).

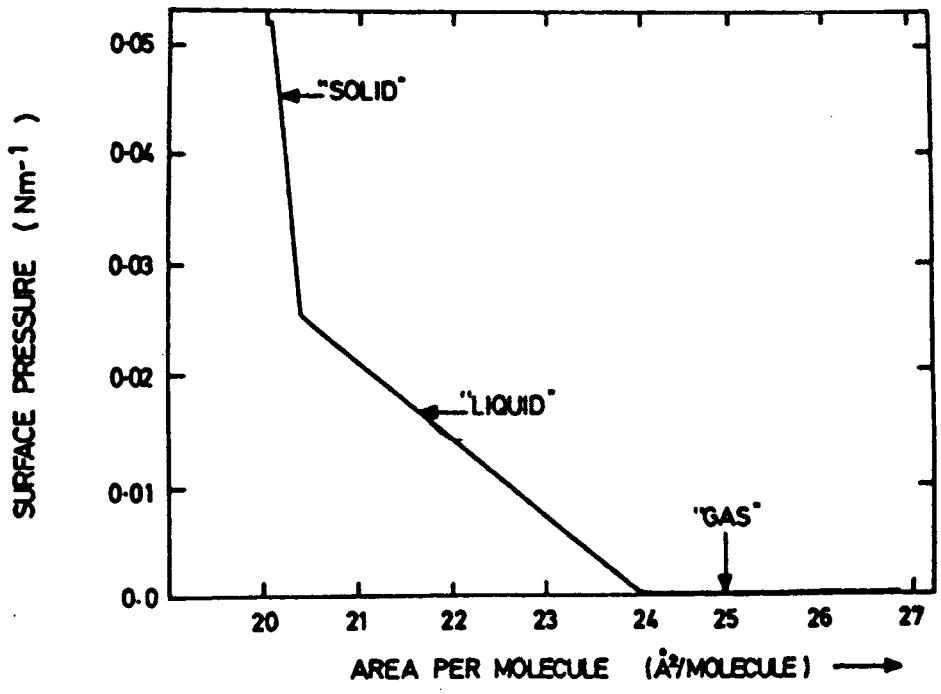

Figure 4.3 Pressure-area isotherm for a typical fatty acid Langmuir film (schematic). Three separate regions can be seen, the 'gaseous', 'liquid' and 'solid' phases. In the latter the area per molecule corresponds closely to the molecular cross section, indicating that the film is closely packed.

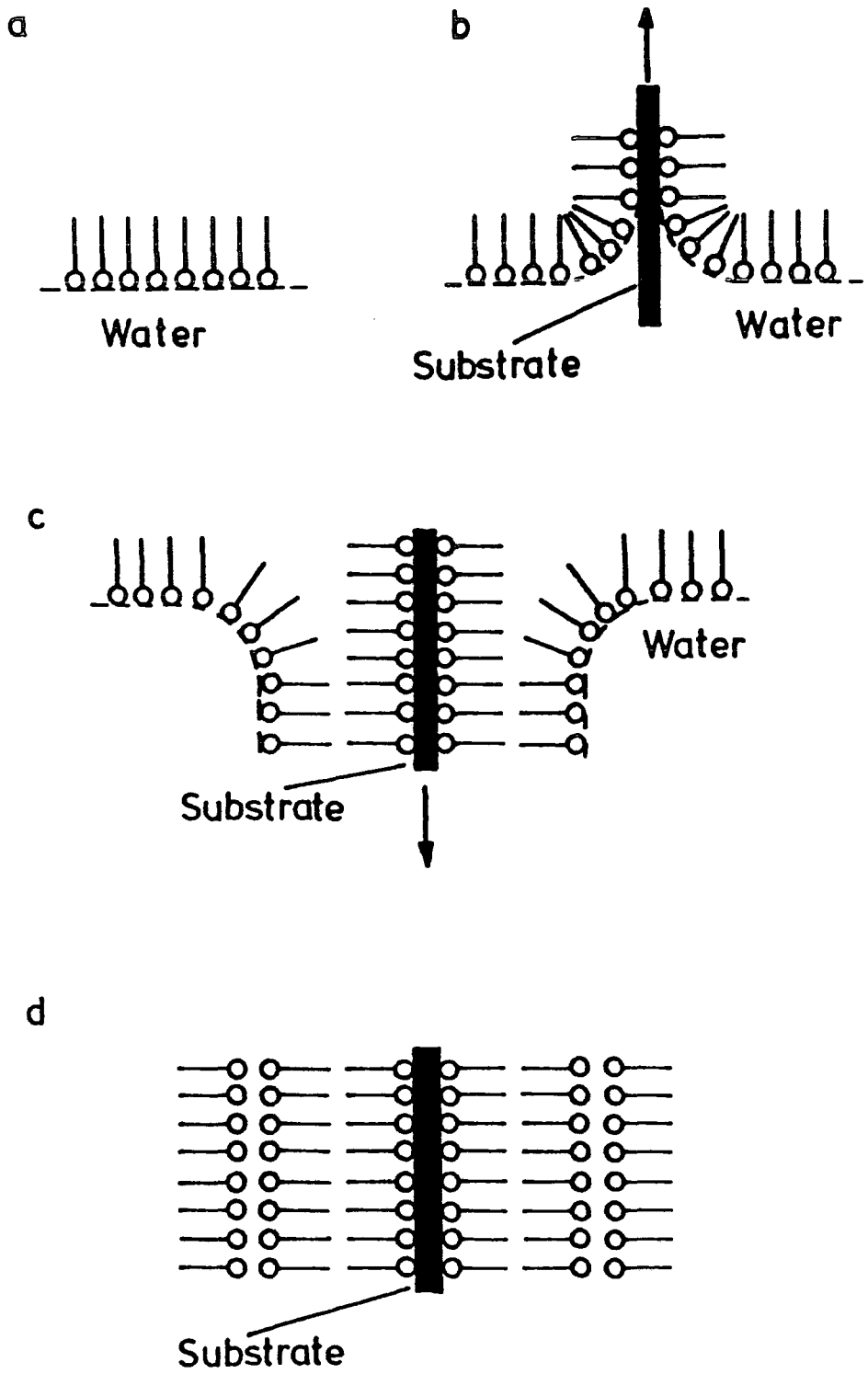

Figure 4.4 Y-type deposition of a Langmuir-Blodgett film

(a) Shows a compressed Langmuir film on a water surface. No deposition usually occurs during insertion of the solid substrate through the film.

(b) When the substrate is withdrawn from the water a monomolecular layer is picked up.

(c) As the substrate is reinserted another monolayer is deposited. This process is repeated during subsequent insertions and withdrawals.

(d) This produces a head to head, tail to tail multilayer LB film. The film thickness is proportional to the molecular length and the number of monolayers deposited.

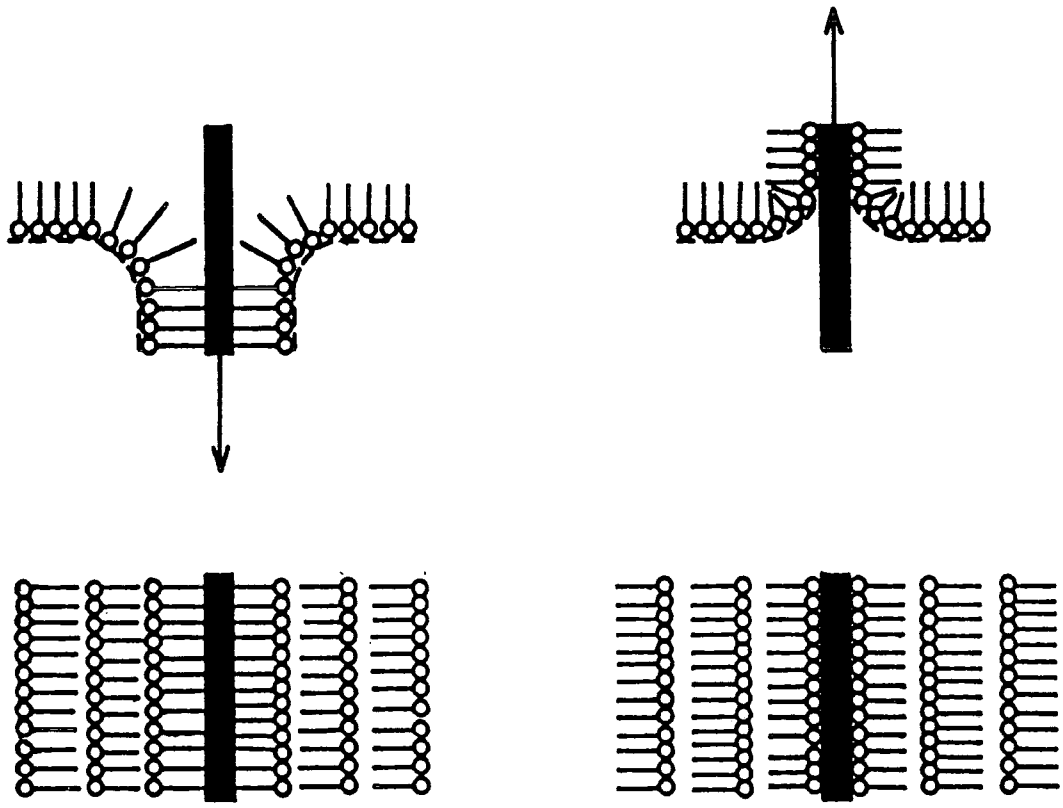

Figure 4.5 X and Z type deposition of LB films

(a) In X-type deposition material is only transferred to the substrate during insertion into the subphase. A head to tail structure would be expected to result, although in practice the structure resembles that of Y type films (see text).

(b) In Z-type deposition film transfer only occurs during withdrawal of the substrate from the subphase.

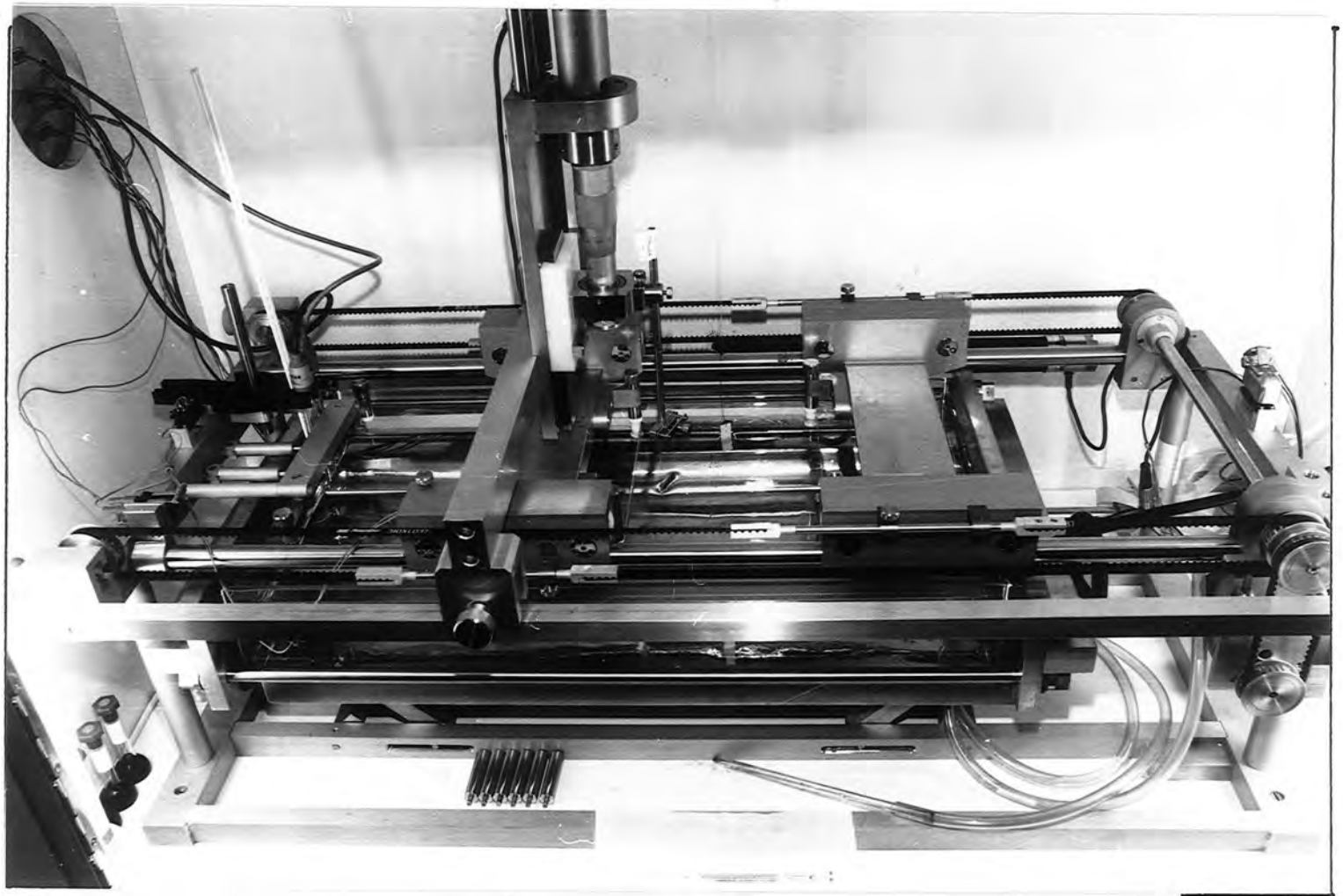

Figure 4.6 Photograph of a typical example of the type of Langmuir trough used at Durham. The belt drive for the constant perimeter barrier mechanism can be seen at the front and rear of the trough. The vertical micrometer head in the centre is the dipping mechanism.

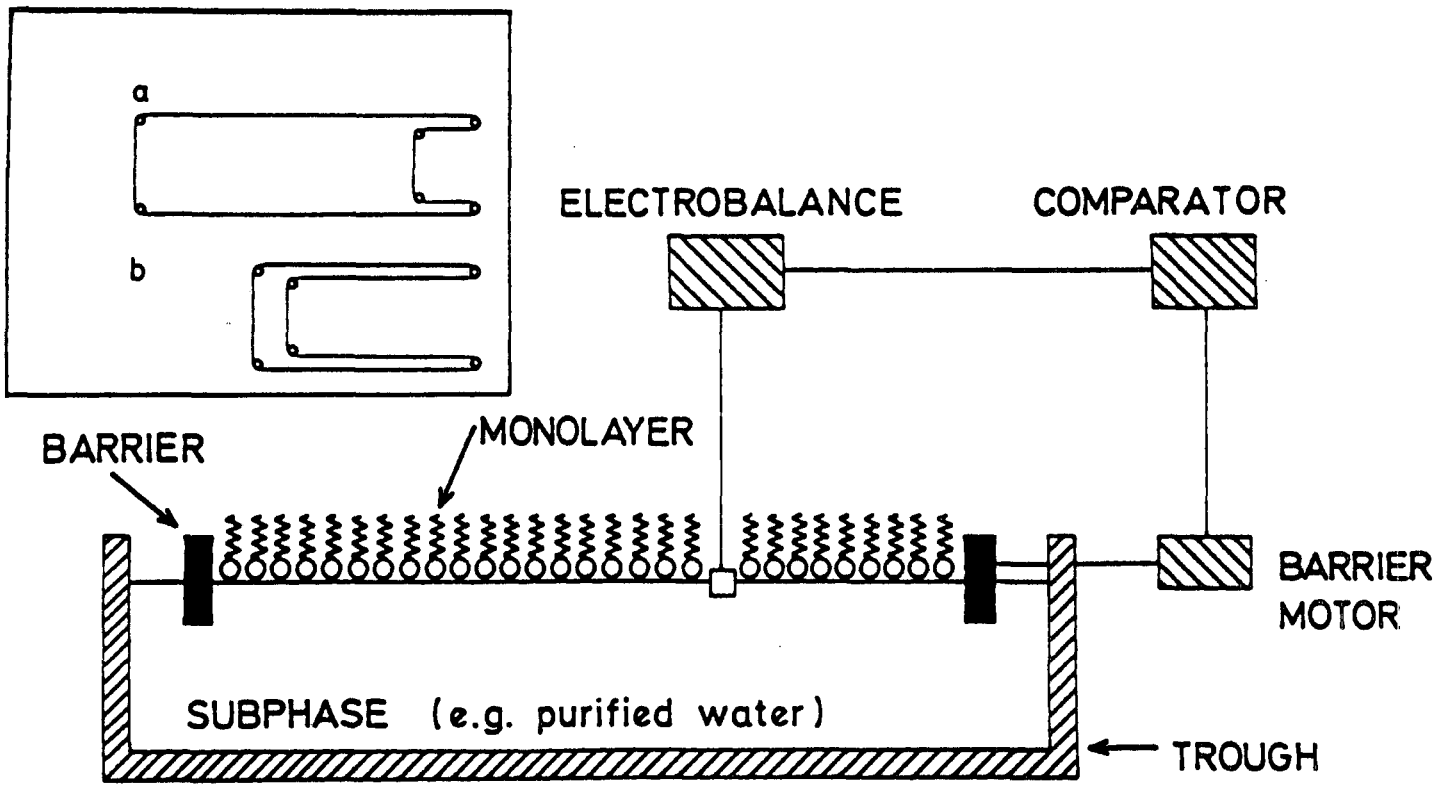

Figure 4.7 Schematic diagram showing the principal components of a modern Langmuir trough. The purified water subphase is contained in a glass trough. The Langmuir film on the water surface is confined by a constant perimeter, variable area barrier system. The inset shows this barrier opened to its maximum extent (a) and closed to its minimum extent (b). The surface pressure is controlled by a feedback system, which consists of a Wilhelmy plate connected to an electrobalance (to measure surface pressure) and a comparator which controls the barrier motor.

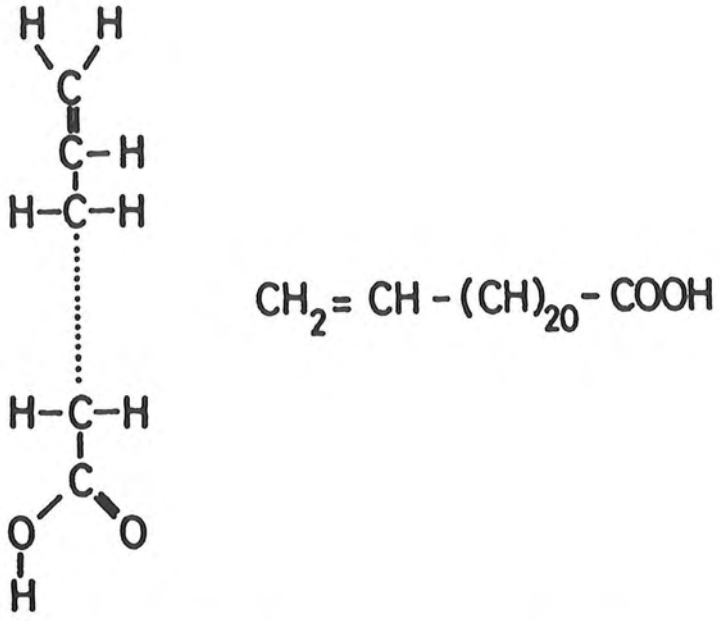

$$CH_2 = CH - (CH)_{20} - COOH$$

Figure 4.8 Molecular structure of ω-tricosenoic acid. This unsaturated fatty acid has a single double bond at the end of the hydrocarbon chain.

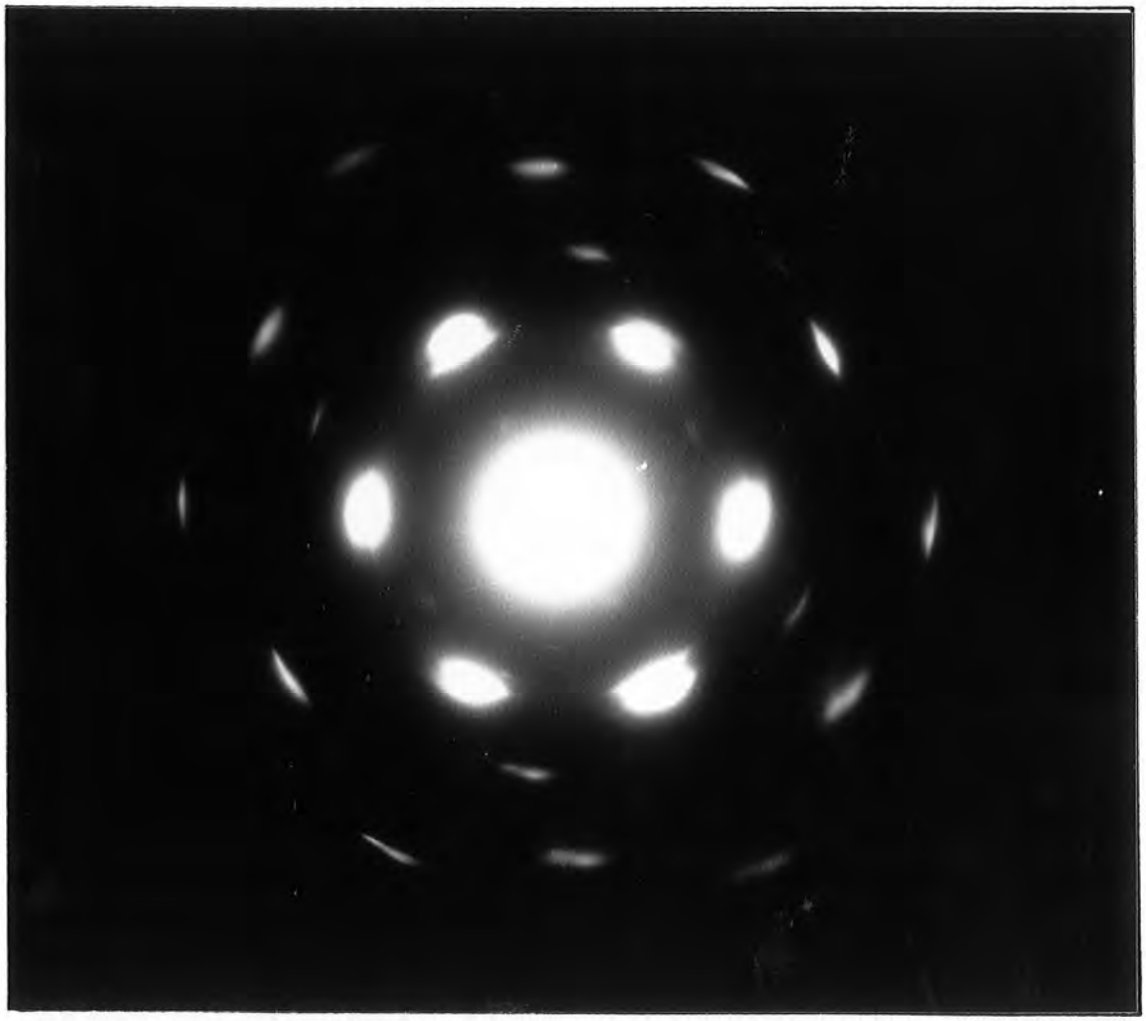

Figure 4.9 Transmission electron diffraction pattern for a 21 monolayer ω-tricosenoic acid LB film, deposited on an Al_2O_3 substrate. (from ref. 17)

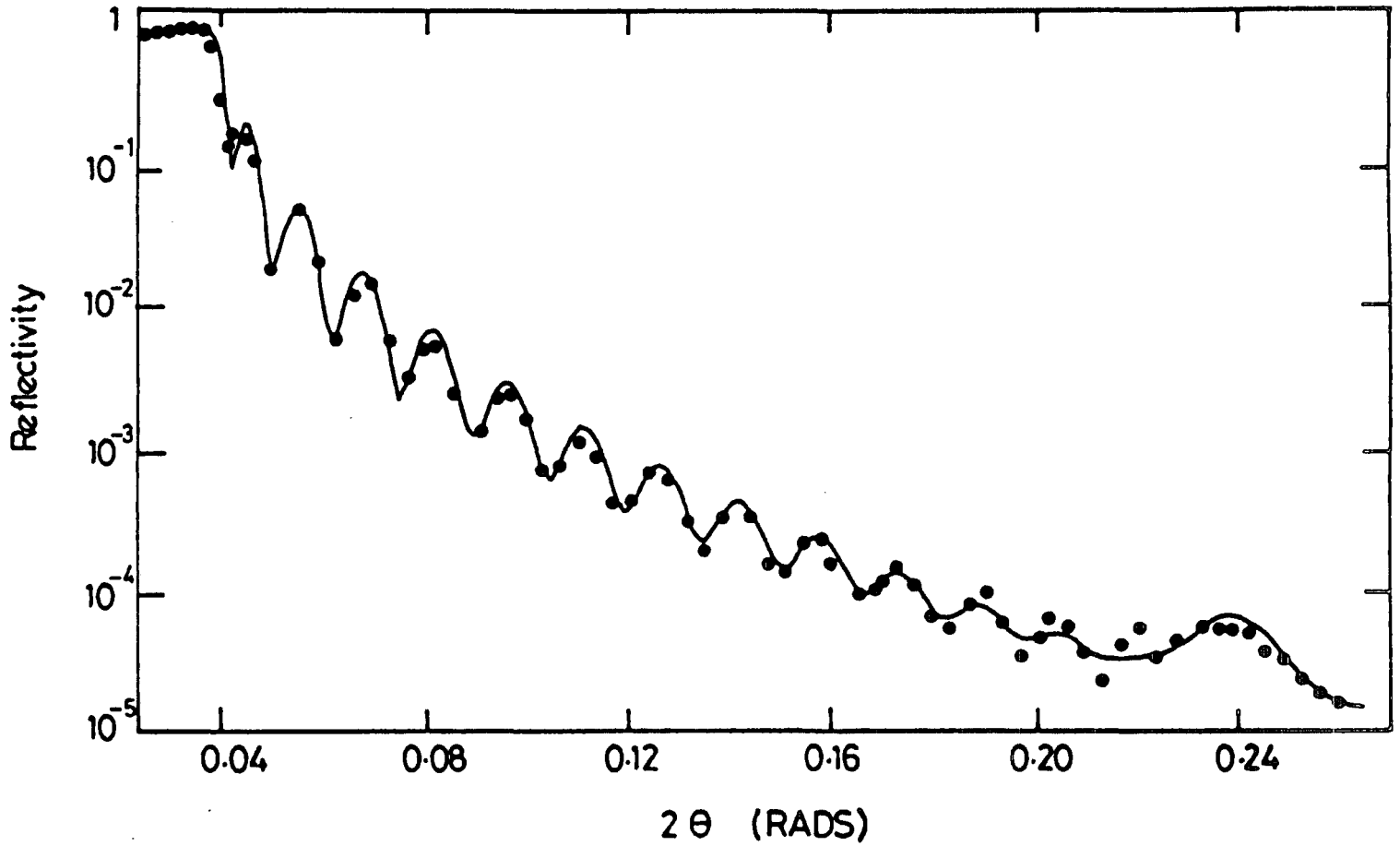

Figure 4.10 Neutron reflectivity profile for a 29 layer LB film of fully deuterated cadmium arachidate, deposited on glass. (from ref. 18).

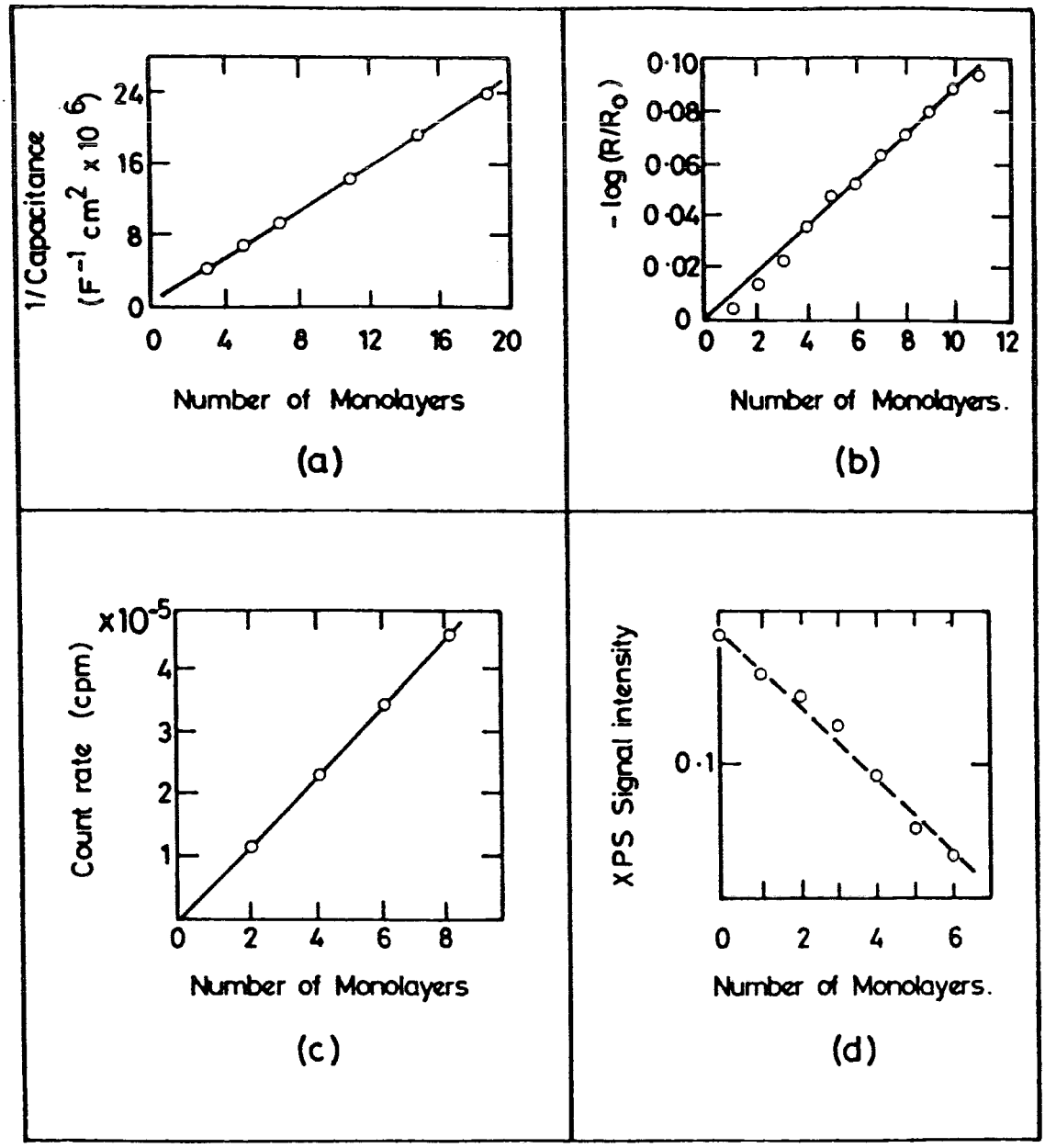

Figure 4.11 Properties of LB film layers as a function of the numbers of monolayers deposited.

(a) Reciprocal capacitance per unit area of cadmium arachidate films deposited on an aluminium substrate. (from ref. 19)

(b) Infra-red absorption for the symmetric carboxylate stretching mode (1432 cm^{-3}) in cadmium arachidate LB films. (from ref. 20)

(c) Count rate of ^{14}C β rays from barium stearate layers labelled with ^{14}C. (from ref. 21)

(d) X-ray photoelectron signal intensity from silver substrates coated with cadmium dimethyl arachidate LB films. (from ref. 21)

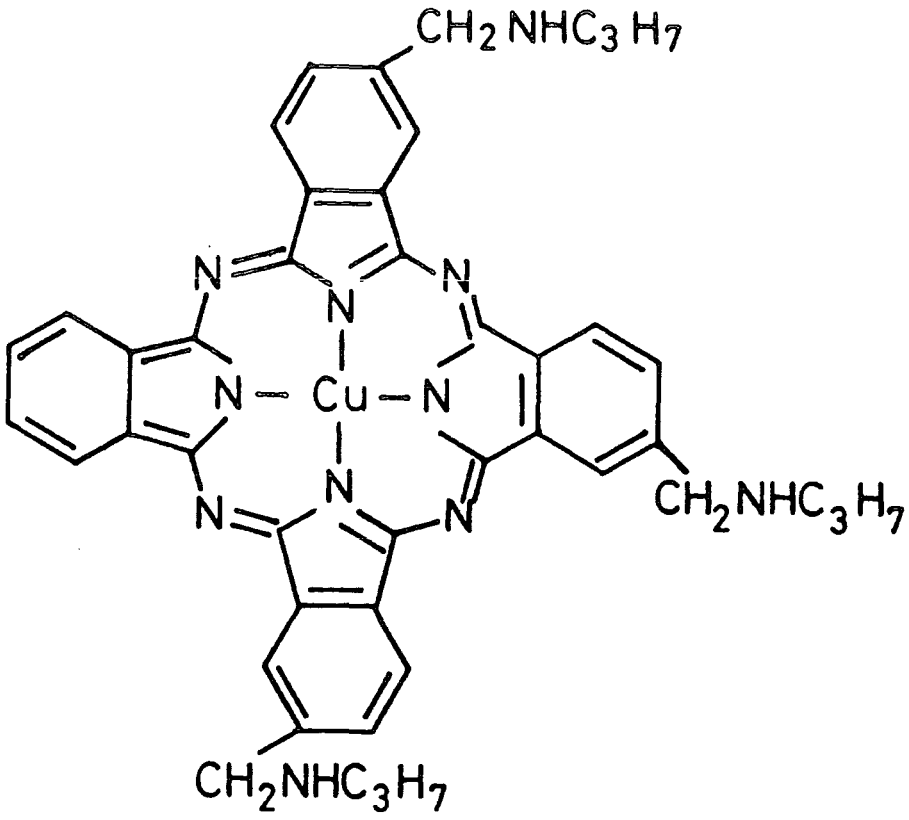

Figure 4.12 Molecular structure of the asymmetrically substituted copper phthalocyanine derivative.

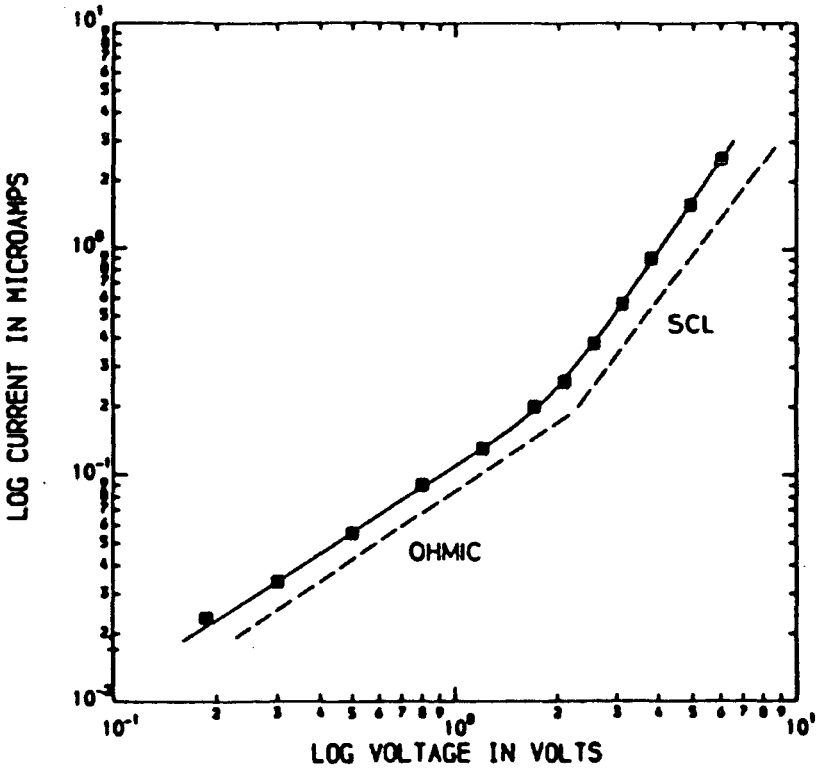

Figure 4.13 Current-voltage characteristic for a 40 monolayer thickness of tetra-tertiary butyl manganese phthalocyanine deposited on a NESA conducting glass substrate (nb. no polarity dependence) (from ref. 47)

CHAPTER 5

EXPERIMENTAL TECHNIQUES

5.1 Introduction

In this chapter the details of device fabrication and the techniques subsequently used to characterise the devices are described. Details of the semiconductor materials used are given first. This is followed by a description of the stages in the fabrication of devices; these are cleaning, ohmic contact formation, chemical polishing, LB film deposition and electrode deposition. In the final section, the techniques and equipment used for device characterisation are described.

5.2 Semiconductor Materials

The details of the semiconductor materials used in this work are summarised in Table 5.1. The majority of the compound semiconductor samples were supplied by the SERC Central Facility for 3-5 Semiconductors in the Department of Electronics and Electrical Engineering of the University of Sheffield. Epilayer thicknesses and carrier concentrations were measured using a mercury probe C-V profiler/plotter. Layers grown by liquid phase epitaxy are known to be of nonuniform thickness, therefore these figures are only approximate. All LPE samples possessed some visible surface features (e.g. meniscus lines), but these did not appear to cause any problems with device fabrication or measurement. Single crystal GaAs wafers, polished on one side, were obtained from MCP Electronics plc. The 2" wafer of epitaxially grown silicon was kindly supplied by Dr. M. J. Morant of the University of Durham. The materials supplied in wafer form were too large for convenient handling, therefore they were scribed and broken into convenient sized pieces for device fabrication.

5.3 Device Fabrication

There are four main stages in the preparation of Metal-Insulator-Semiconductor devices. Firstly, an ohmic contact must be made to the semiconductor substrate. Secondly, the semiconductor surface must be treated to make it suitable for the deposition (or growth) of the insulating layer. The insulator is then deposited, in this case using the Langmuir-Blodgett technique. Finally, metal contacts must be deposited onto the insulating film. These stages and the pre-preparation cleaning procedure are described in this section.

5.3.1 Cleaning

This first stage in the preparation of devices is to remove any organic contamination or particulates from the semiconductor surface. This was done by refluxing in organic solvents, using Soxhlet extraction apparatus. Samples were placed in clean glass extraction thimbles and refluxed in trichloroethane (BDH 'analar' grade) for several hours. This was followed by refluxing for a similar period in isopropyl alcohol (BDH 'analar' grade). Care was taken when removing samples from the solvent in order to minimise recontamination. This procedure was carried out immediately before chemically polishing or forming ohmic contacts to samples.

5.3.2 Ohmic Contacts

Many techniques have been used to make ohmic contact to semiconductors[1,2]. For the devices described in this work relatively simple techniques could be employed due to the large area of the contacts. For the compound semiconductors the samples were cleaned (as described above), then preformed soft metal contacts were placed on the unpolished back surface of the semiconductor. For n-type material indium wire (99.999%) was used for this. In the case of p-type material an alloy of indium with 5% zinc by weight was used. At least two separate contacts were made on each sample to enable the contact resistance to be

tested. Contacts to both n-type and p-type material were alloyed at a temperature of 300 °C for 5 minutes under flowing dry nitrogen. Contacts produced by this method consistently possessed low resistance ohmic characteristics.

A more complicated procedure was used for silicon samples. They were first cleaned and then treated with hydrofluoric acid (40%) as described in section 5.3.3. The samples were then mounted on a metal shadow mask to allow two separate contact areas to be evaporated. The evaporation was performed in an Edwards 306 vacuum coating system at a pressure of $< 2 \times 10^{-6}$ torr. The contacts to the p-type back face of the silicon were made by thermally evaporating aluminium (99.999%) from a tungsten filament to a thickness of $\sim$ 50 nm. The contacts were annealed at 300°C for 5 minutes in flowing dry nitrogen, producing a low resistance ohmic contact.

5.3.3 Chemical Polishing

To prepare semiconductor surfaces free from contamination and damage it is usually necessary to use a chemical polishing treatment. A great variety of different chemical compositions have been reported[3,4,5]. Chemical polishing is often sensitive to the exact conditions used and this may critically affect the quality of the surface finish. Several polishing solutions for compound semiconductors were tried during this work. Treatments discarded due to poor polishing or because they resulted in non ideal Schottky diode characteristics included:- sulphuric acid: hydrogen peroxide: water (SHH), sodium hydroxide: hydrogen peroxide: water, and aqueous citric acid solutions.

The polishing treatment finally adopted for GaAs consisted of a bromine/methanol solution, which was followed by a concentrated hydrochloric acid rinse. The 1:2000 (by volume) bromine/methanol mixture

was always freshly prepared and had an expected etching rate of ∿ .1μ/minute[6] for a (100) surface. This polish is known to leave an oxide layer on the GaAs surface, therefore a concentrated hydrochloric acid rinse was used to remove this layer[7]. The effects of omitting this stage are discussed in section 6.3.1. The quality of the polished surface was found to be critically dependent on the cleanliness of apparatus used. All glassware was cleaned before use by thoroughly rinsing with chromic acid, deionized water, and finally methanol. Before polishing the sample, the ohmic contacts were protected by a coating of 'lacomit' to prevent chemical attack. Samples were polished for 1 minute in the bromine/methanol mixture; polishing was stopped by flooding with methanol. The samples were then immersed in conc. HCl for 5 minutes, rinsed in methanol and finally dried between clean filter papers. A similar treatment was used for GaInAs, however in this case the bromine concentration was .2% by volume. The concentrated hydrochloric acid rinse was omitted because it attacks indium based materials.

A simple surface preparation was used for silicon samples. The treatment comprised a 1 minute immersion in 40% hydrofluoric acid, followed by a thorough rinse in deionised water; samples were dried between filter papers. This treatment removes any oxide layer without etching the silicon[3], and the resulting hydrophobic surface is very suitable for the deposition of LB films. Hydrofluoric acid is highly corrosive and toxic, therefore its use was restricted to within a specially designed fume cupboard.

5.3.4 LB Film Deposition

Deposition of the first monomolecular layer onto semiconductor substrates was performed as soon as possible after the etching procedure had been completed; in all cases this was less than 30 minutes. Large

samples could be clamped to the dipping head for film deposition. However it proved easier to dip small samples if they were first mounted on clean 'chance select' microscope slides using 'lacomit'. This enabled the whole of the sample to be coated with the LB film. Before use slides were cleaned by ultrasonic agitation in 'Decon 90' detergent (∿10% by volume), followed by two deionised water rinses and they were finally refluxed in isopropyl alcohol. After LB film deposition had been completed, samples were desiccated in a low pressure dry nitrogen atmosphere for two days before top contacts were deposited. This has been found necessary to ensure consistency between samples. The procedure for LB film deposition was outlined in section 4.2.1. Details are given here of the specific deposition conditions for the film materials used in this work.

ω-Tricosenoic Acid

For ω-tricosenoic acid the subphase pH was adjusted to 5.5 (± .1) at a temperature of 18 (±2)°C. No cadmium was added to the subphase. In all cases the pressure-area isotherm was obtained before dipping commenced (fig. 5.1); this gives an indication of the film quality. During dipping the surface pressure was maintained at 37 mNm^{-1}. ω-Tricosenoic acid films undergo an ageing process on the water surface[8]. Therefore the first monolayer was deposited using a freshly spread film, less than 1 hour old, at a dipping speed of ∿ 1 mm/minute. After the first insertion into and withdrawal from the subphase, the sample was allowed to dry for at least 30 minutes. This is known to improve the deposition of subsequent layers. A freshly spread monolayer was used for depositing these layers and a higher dipping speed of ∿3mm/minute was used.

Figure 5.2 shows the dipping record for an etched GaAs sample. The surface pressure and area are plotted as a function of time, enabling the dipping pressure to be monitored. Deposition does not occur during the first insertion into the subphase. The first monolayer is deposited during the first withdrawal. Subsequent layers are deposited during both insertion and withdrawal, producing a Y type film. GaInAs samples showed similar behaviour to GaAs during dipping. The behaviour of hydrofluoric acid treated silicon was rather different because the highly hydrophobic surface allows a monolayer to be deposited during the first insertion. Deposition then occurs in both directions and again a Y type film is produced.

Phthalocyanines

Two different phthalocyanines were used in this work and the structure of one, CuPc has been shown in fig. 4.12. The other, tetra-4-tert-butyl phthalocyaninatosilicon dichloride (SiPc), is shown in fig. 5.3. Similar deposition conditions were used for both these materials. The subphase pH was adjusted to $\gtrsim$ 7 at 18 (±2)°C. For dipping a surface pressure of 30 mNm^{-1} was used and the dipping speed was 2.5 mm/minute. These films are deposited only during withdrawal (Z type), however due to the rigidity of these Langmuir films some partial pickup also occurs during insertion. This undesirable behaviour can be minimised by releasing the surface pressure during insertion. In this case the solid substrate passes through the expanded film and little material transfer occurs. The film is then recompressed for the subsequent withdrawal/deposition, and the process is repeated until the required film thickness has been built up.

5.3.5 Electrode Deposition

The final stage in the preparation of Schottky barriers or MIS devices is the deposition of metal top contacts. The most common method used is thermal evaporation of the desired metal in a high vacuum. This has proved satisfactory for LB film MIS devices, providing care is taken to avoid damage to the delicate, low melting point, LB film. An Edwards 306 oil diffusion pumped vacuum coating system, with an ultimate vacuum of $\lesssim 1 \times 10^{-7}$ torr, was used. To define the electrode area samples were mounted on a metal shadow mask. The electrode material, usually gold (99.999%), was evaporated from an electrically heated molybdenum boat at a pressure of $\lesssim 2 \times 10^{-6}$ torr. The rate of evaporation was monitored using a quartz crystal film thickness monitor.

To avoid damaging the LB film the metal was evaporated in stages, and the evaporator and sample were allowed to cool between stages. This technique has been found to be preferable to evaporating onto a cooled substrate, because the latter method can cause electrode cracking due to the mismatch in thermal expansion coefficients[9]. The metal was deposited in stages of $\lesssim 2$ nm thickness, at a rate of $\lesssim 0.02$ nm s^{-1}; the interval between stages was approximately 20 minutes. The total thickness of the evaporated electrode was usually in the range 15-25 nm, with the former value being close to the minimum required to ensure a continuous metal film. A photograph of a completed device is shown in fig. 5.4.

5.4 Device Characterisation

This section describes the electrical, photoelectric and gas sensitivity characterisation of the devices studied in this work. In all cases care was taken to ensure that representative and repeatable results were obtained. Each sample was examined to ensure that

characteristics were consistent between contacts; this was usually done by measuring the currents at selected bias voltages. Many measurements could be performed in air, but vacuum or an inert gas ambient was used when necessary; in addition, samples were stored under a low pressure of dry nitrogen in order to minimise any degradation due to oxidation or water absorption.

5.4.1 Electrical Measurements

These were performed with the samples mounted in a shielded, light tight, chamber or a cryostat. The custom made shielded chambers (fig. 5.5) were gas tight and could be evacuated or filled with gaseous ambients. Trays containing silica gel desiccant were used to provide a dry atmosphere inside the chambers. Windows or an optical fibre light pipe permitted illumination of samples. For measurements at low temperatures an Oxford Instruments DN 704 liquid nitrogen exchange gas cryostat was used (fig. 5.6). An Oxford Instruments DTC2 temperature controller enabled the temperature to be controlled to a precision of 1K between 77K and 350K.

Samples were attached to small brass blocks using conducting silver paste; this made electrical connection to the ohmic contacts on the back of the samples and also enabled them to be securely mounted inside the shielded chambers. Contact to top electrodes was made using a gold ball formed on a thin gold wire, which was attached to a micromanipulator. For use in the cryostat, samples were affixed to mica sheets. Unfortunately, in this case problems were encountered in making satisfactory electrical connections to the sample. Due to the stresses imposed by thermal cycling a light pressure contact using a gold ball was not suitable; heavier pressure contacts would damage the LB film. Connection could be made using thin wire and silver paste, but it was

difficult to avoid damaging the LB film, especially if it was thicker than one monolayer. To ensure no degradation had occurred, the characteristics were measured before and after the paste contact was made. Further measurements were only carried out if no change had occurred.

For DC current-voltage measurements, a Time Electronics 2003s voltage calibrator or a Keithley 241 regulated high voltage PSU was used to supply the bias. The current was measured using Keithley 410A or 414 picoammeters. When currents above 10 mA were to be measured a Fluke 8060A DMM was used. To ensure that steady state values were recorded the current was monitored on a chart recorder. For measurement of MISS structures a series resistance was inserted using a resistance box and the voltage across the sample was measured using a DMM. Low frequency I-V characteristics of MISS devices were examined on a Tektronix 575 transistor curve tracer. Capacitance-voltage measurements were performed using a Boonton Electronics 72BD digital capacitance meter, in conjunction with the voltage sources mentioned above.

One shielded chamber was modified to allow two 10:1 oscilloscope probes and a series resistor to be mounted internally (fig. 5.7). This was necessary to allow pulsed measurements of MISS device characteristics to be performed (the probes minimise the capacitive loading, which limits the rise time). A Phillips PM5716 50 MHz pulse generator and a Hitachi V-203F 20MHz oscilloscope were used for these measurements.

5.4.2 Photoelectric Measurements

Two types of photoelectric measurement were performed in this work. The first of these, the Fowler Plot technique, uses sub-bandgap monochromatic illumination to determine the barrier height of a Schottky contact. A Bausch and Lomb 33-86-02 monochromator and a high intensity

tungsten source supplied the required illumination. A long wavelength pass filter was used to remove any higher order reflection from the grating. The output of the monochromator was either directed onto samples mounted in the cryostat, or focussed into the optical fibre light pipe to illuminate devices mounted in the shielded chamber. The illumination was calibrated using an Oriel 7102 thermopile detector and a Keithley 181 nanovoltmeter. Photocurrents were measured using synchronous detection in order to improve the resolution. The light was mechanically chopped and the photocurrent was detected by an ORTEC Brookdeal 9502 Ortholoc lock-in-amplifier.

In the second kind of photoelectric measurement, the current-voltage characteristics were examined under white light illumination. This was provided by a 60 W incandescent tungsten lamp. These measurements were not intended to investigate solar conversion devices, but were used to examine minority carrier transport in MIS devices (see section 6.4).

5.4.3 Gas Sensor Measurements

These measurements were performed using a small stainless steel chamber, because the gas used, NO_2, is corrosive and toxic. This chamber was connected to a Signal 852 gas blender using stainless steel pipework and valves, as shown in fig. 5.8. The system exhausted via a fume cupboard and could be evacuated using a rotary pump. The calibrated gas blender allowed a mixture of two gases, in the range 0.01% to 100%, to be obtained. The sample chamber was flushed with pure carrier gas (nitrogen) before admitting the gas mixture. The electrical characteristics of devices could be continuously monitored during this process, which allowed the size and speed of response to be determined.

TABLE 5.1 SEMICONDUCTOR MATERIALS

Material	Growth Technique	Type	Orientation	Epilayer Doping/cm^{-3}	Epilayer Thickness/μm	Substrate Doping/cm^{-3}	Size	Supplier
GaAs	LPE	n on n^+	(100)	$0.7\text{-}10\times10^{15}$	4-5	$\sim 10^{18}$	.5-1 cm^2	Sheffield
GaAs	LPE	n on p^+	(100)	$0.3\text{-}8\times10^{15}$	2-5	$\sim 10^{18}$	.5-1 cm^2	Sheffield
GaAs	LPE	p on p^+	(100)	$1\text{-}4\times10^{15}$	10	$\sim 10^{18}$	.5-1 cm^2	Sheffield
GaAs	LPE	p on n^+	(100)	$2\text{-}15\times10^{15}$	3-10	$\sim 10^{18}$	.5-1 cm^2	Sheffield
GaAs	Horizontal Bridgeman	n	(100)			3×10^{16}	$\sim$ 2"	MCP Electronics plc
$Ga_{.47}In_{.53}As$ on InP	LPE	n on n^+	(100)	$2\text{-}6\times10^{16}$	3	2×10^{18}	.5-1 cm^2	Sheffield
Si		n on p^+	(111)	1×10^{15}	4.3		2" diameter	

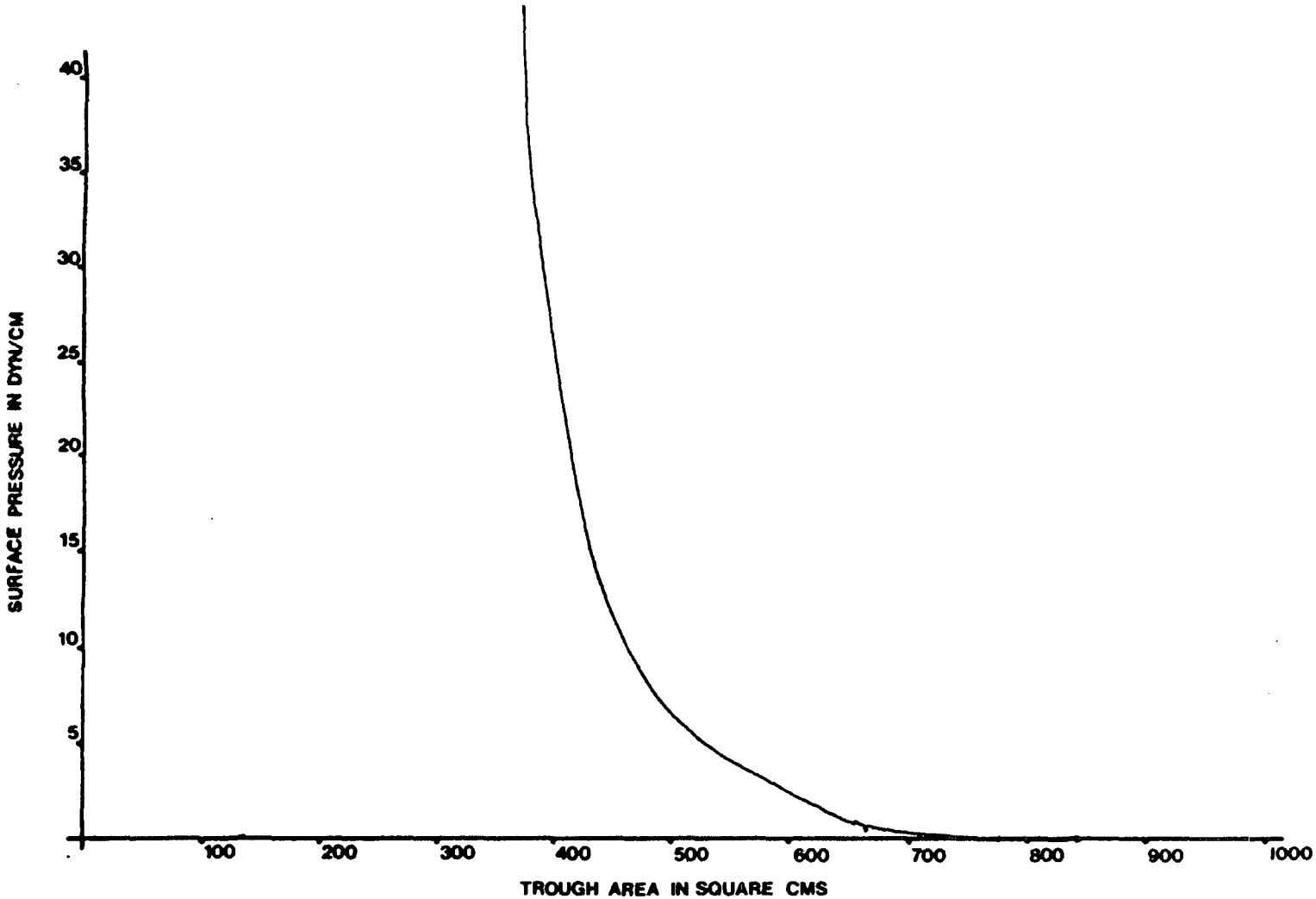

Figure 5.1 Pressure area isotherm for an ω-tricosenoic acid LB film.

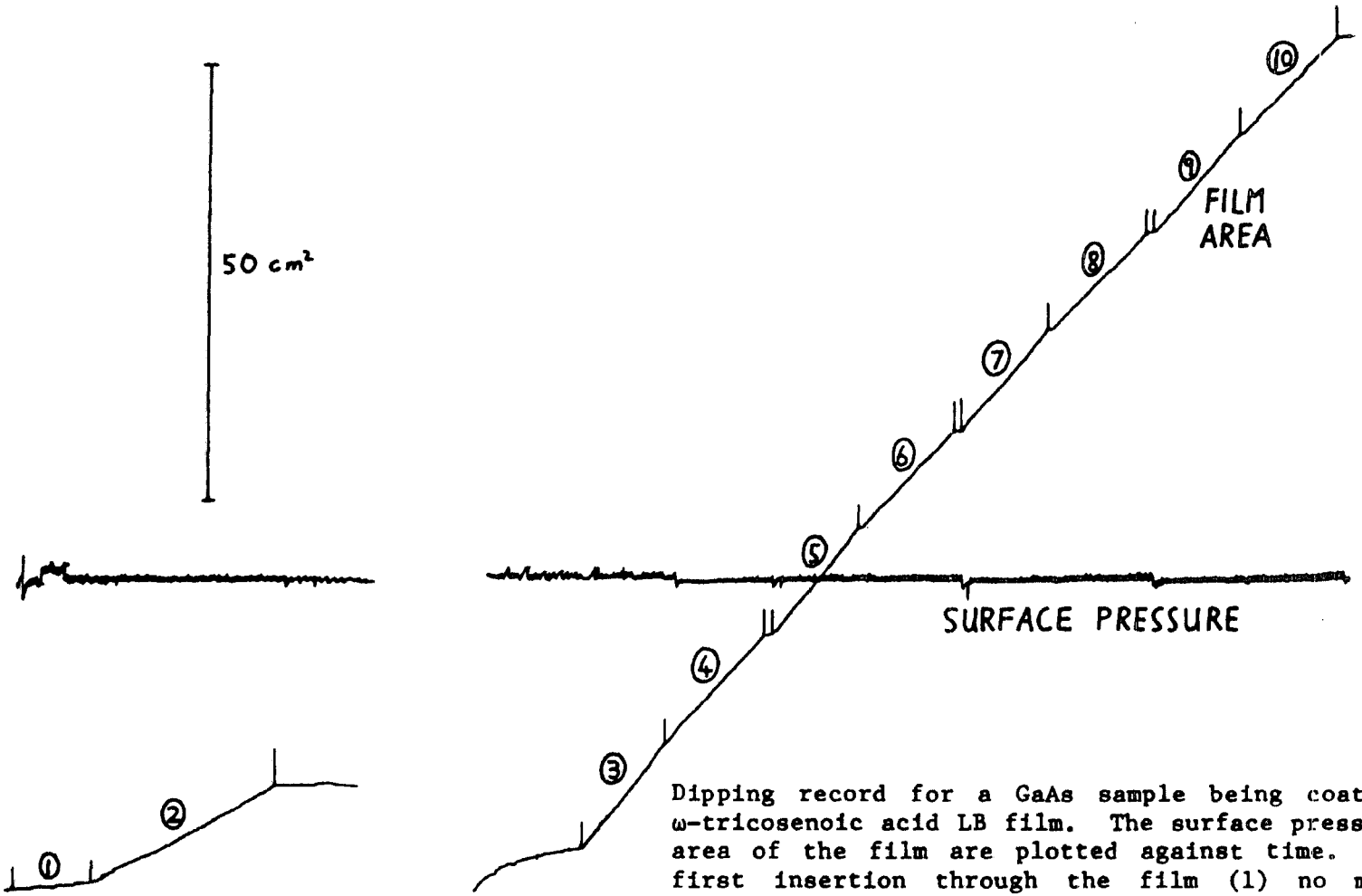

Figure 5.2

Dipping record for a GaAs sample being coated with an ω-tricosenoic acid LB film. The surface pressure and the area of the film are plotted against time. During the first insertion through the film (1) no material is deposited, but a monolayer is deposited upon withdrawal (2). A fresh Langmuir film was spread for the deposition of subsequent layers, which occurs during both insertions (odd numbers) and withdrawals (even numbers). The pickup ratio was 95±5% (≡ the ratio of film area lost to the surface area of the sample).

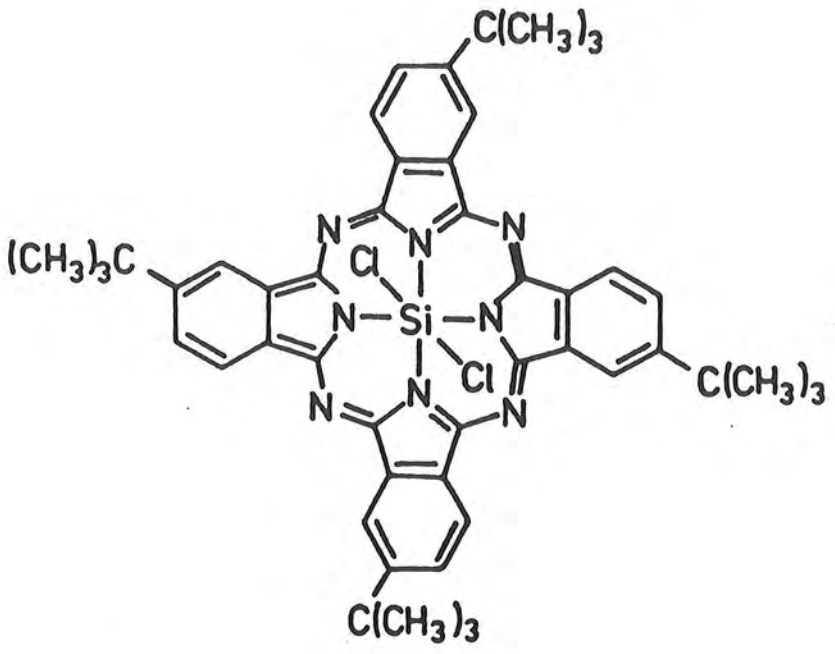

Figure 5.3 Molecular structure of SiPc (tetra-4-tert-butyl phthalocyaninatosilicon dichloride).

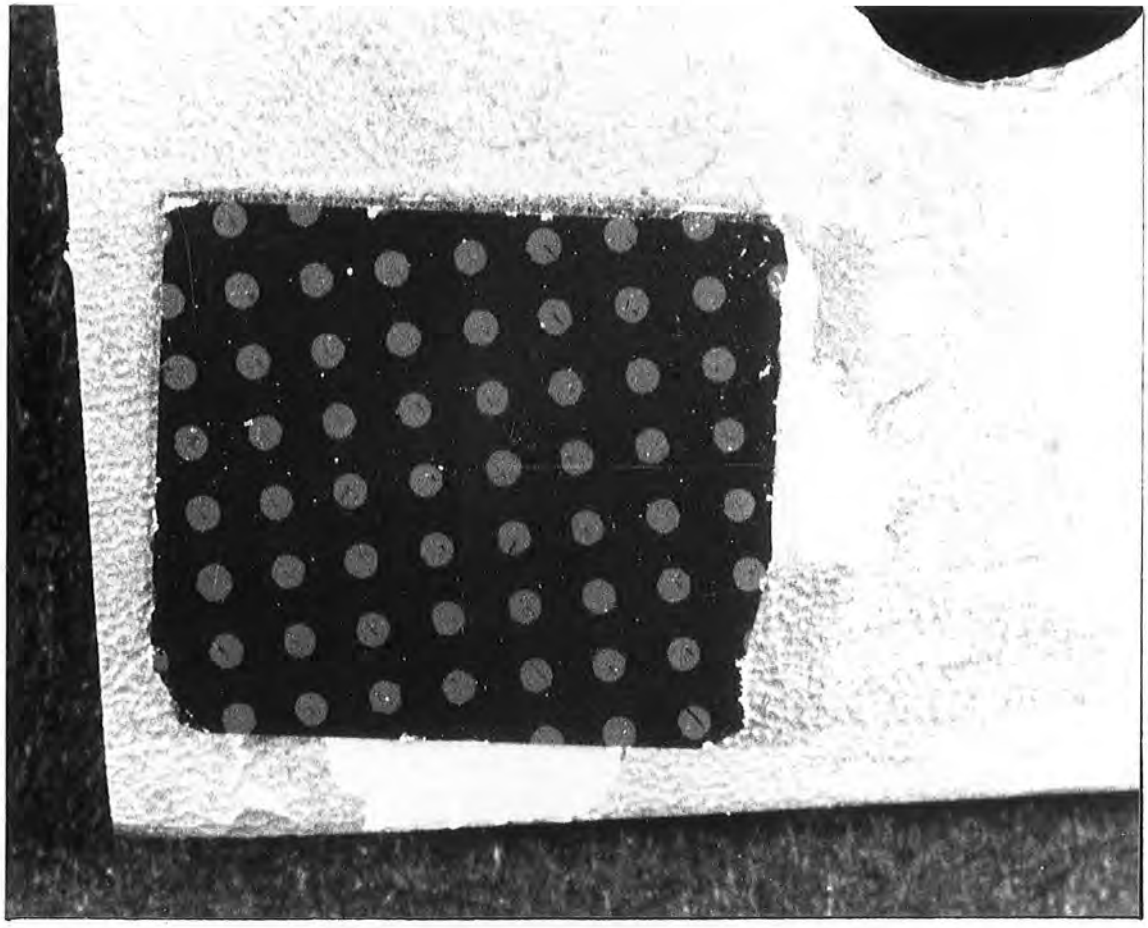

Figure 5.4 Photograph of a completed GaAs/LB film diode. The sample is approximately 1 cm square and the gold dot contacts are of ½ mm diameter. Areas of two different LB film thickness were deposited on this sample, and the dividing line between them can be faintly seen (it runs vertically up the middle of the sample).

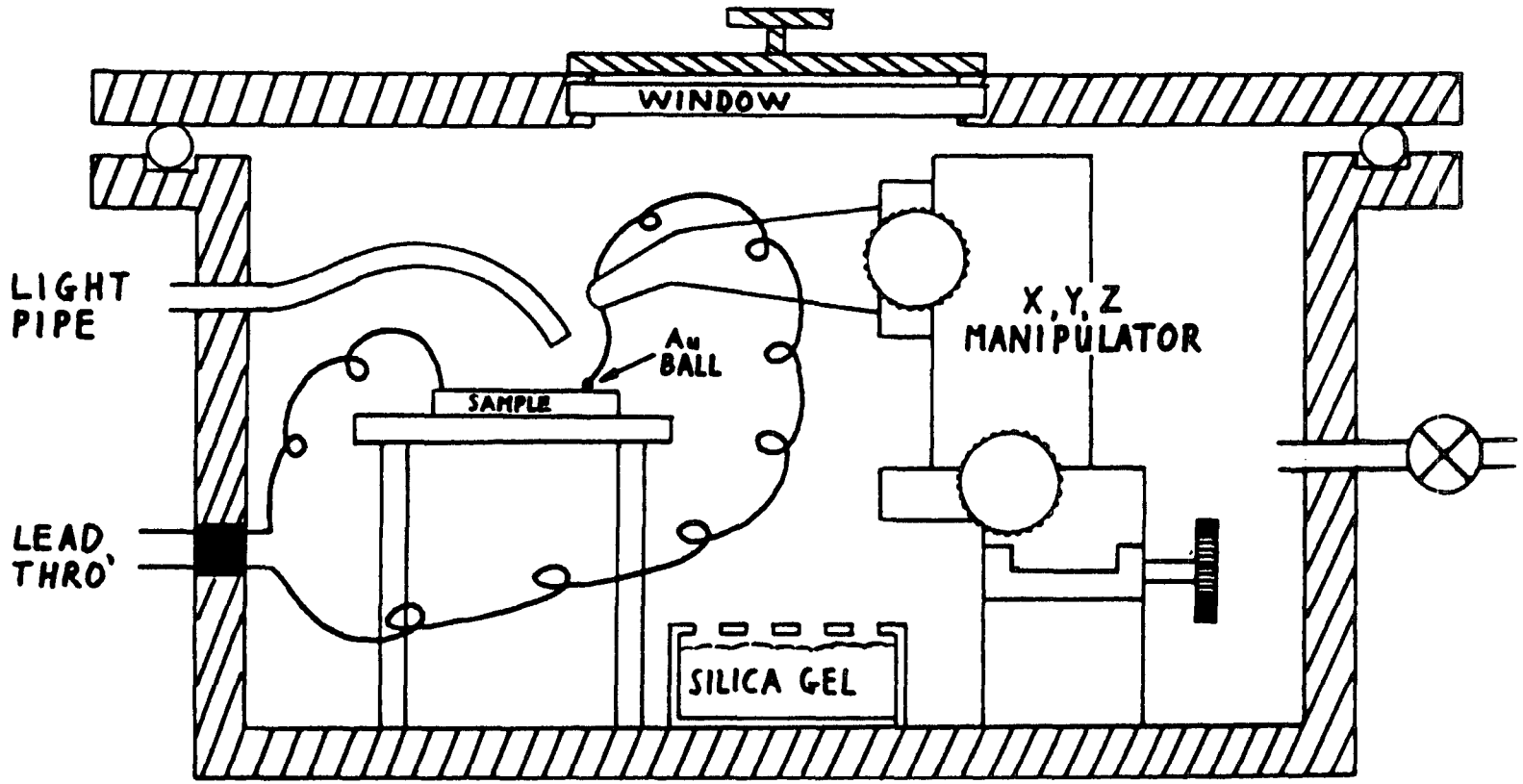

Figure 5.5 Schematic diagram of one of the shielded chambers used during electrical characterisation. The chamber is both gas and light tight.

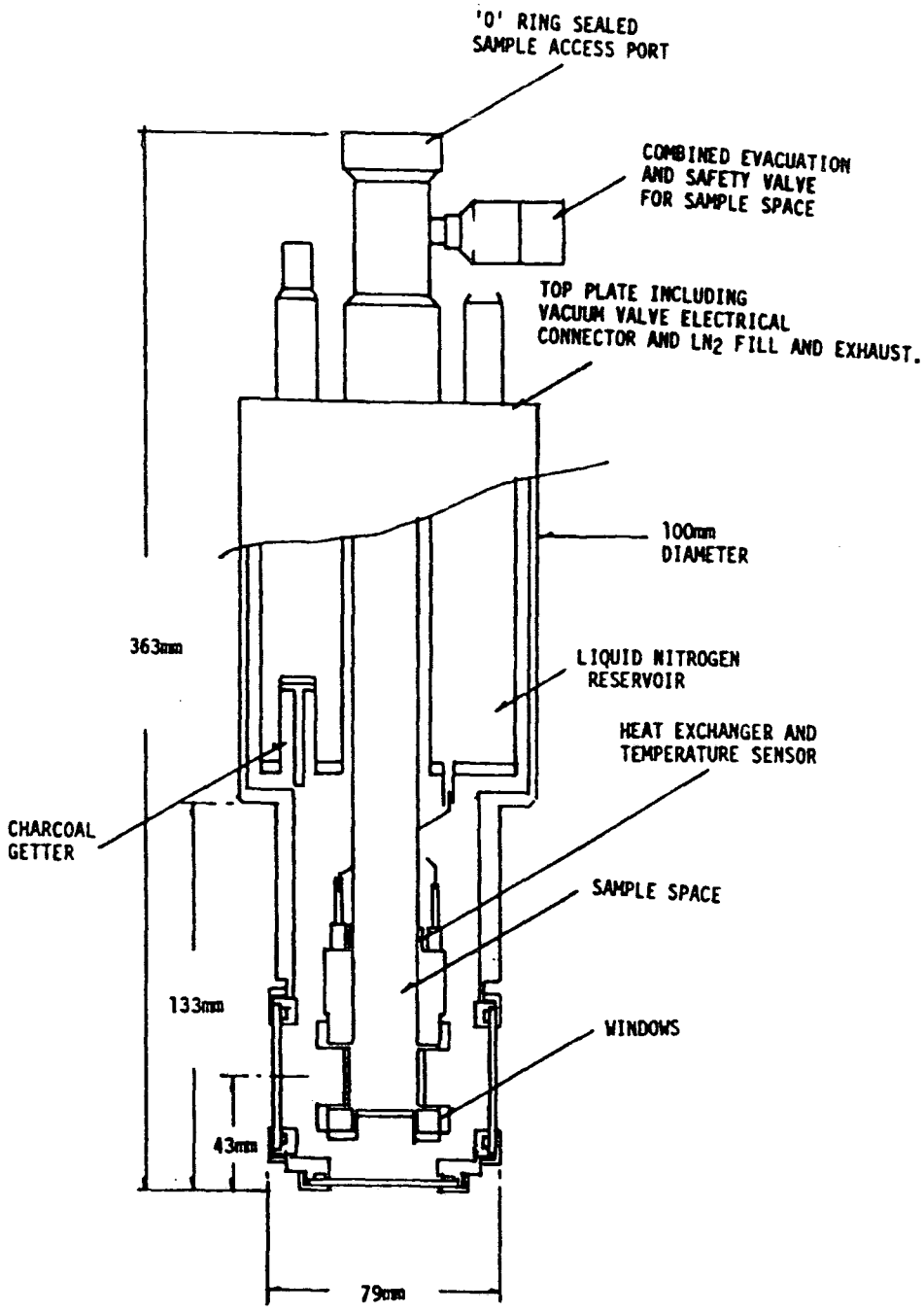

Figure 5.6 Schematic diagram of an Oxford Instruments DN704 exchange gas cryostat. Helium is used as the exchange gas to ensure good thermal coupling between the sample and the liquid nitrogen cooled heat exchanger.

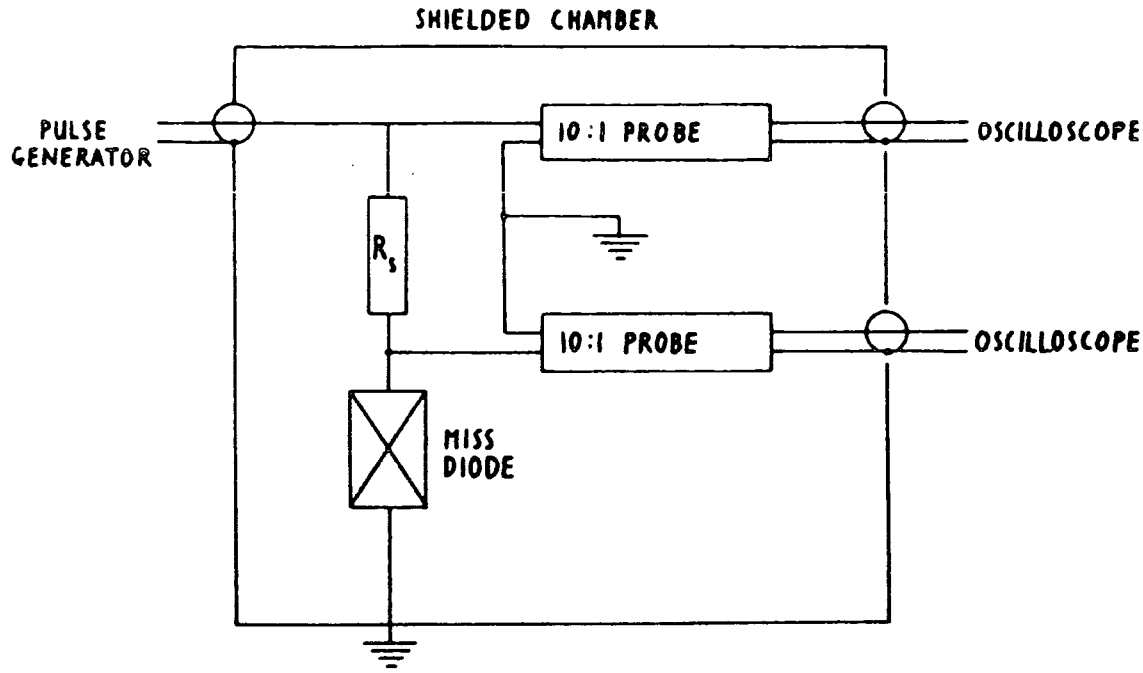

Figure 5.7 Schematic diagram of the circuit layout used to perform pulse measurements on MISS diodes.

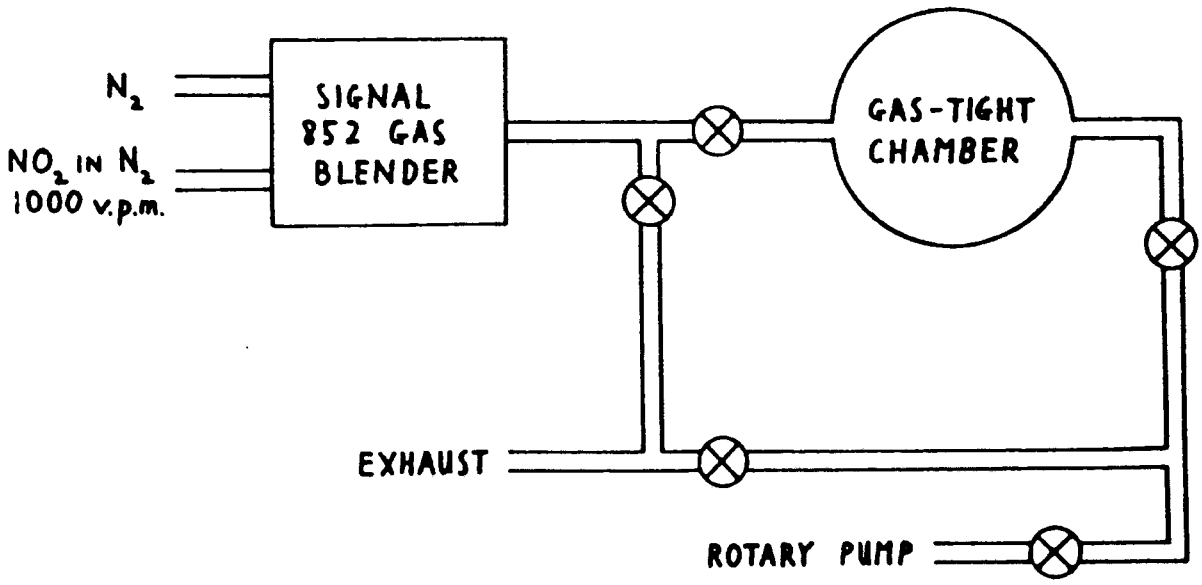

Figure 5.8 Schematic diagram showing the essential features of the apparatus used for experiments involving exposure of devices to NO_2 ambients.

CHAPTER 6

RESULTS AND DISCUSSION :

SCHOTTKY BARRIER AND MIS DIODES

6.1 Introduction

Three quarters of this chapter are devoted to the study of GaAs Schottky barriers and metal-thin-insulator-semiconductor diodes incorporating LB films. The main objective of this investigation is to provide a foundation of knowledge which could be used to underpin the work on MISS devices, which are described in chapter 7. It is obviously important to understand the behaviour of MIS diodes because of the crucial role they play in the operation of the MISS structure (see chapter 3). However, we commence with a study of Schottky barriers, since this provides useful information about the GaAs surface. Perhaps most significantly, we can use them to determine the effects of the LB film deposition process on the semiconductor. This information aids the investigation of LB film MIS devices and helps to clarify the role of the LB film. In the final quarter of this chapter we consider $Ga_{.47}In_{.53}As$/LB film MIS devices. This ternary semiconductor has very desirable transport properties and offers the promise of very high speed operation. One of the principle technological limitations of this material is the very low barrier height of Schottky contacts; this prevents the fabrication of practical MESFETs because the gates would be too 'leaky'. By replacing the Schottky gate with a thin MIS diode the reverse leakage current can be substantially reduced, which will allow practical devices to be produced.

6.2 Near-Ideal GaAs Schottky Barriers

In this section we describe the characteristics of near-ideal Au-GaAs Schottky barriers on both n-type and p-type material. These

diodes can be regarded as a benchmark to which other diodes can be compared. In addition, it is instructive to compare the results obtained with previous reports of Schottky diode behaviour, as this allows the quality of sample preparation to be assessed.

6.2.1 n-type GaAs

Small pieces of GaAs, cleaved from bulk n-type wafers, were prepared as described in section 5.3. The thermally evaporated gold top electrodes were of ∿50 nm thickness and of 1.3 mm diameter. The devices were electrically characterised over a temperature range of 150 - 350 K. Room temperature photoresponse measurements were also used to determine the barrier height.

Current-Voltage Characteristics

Typical room temperature log J vs. V behaviour, for both forward and reverse bias, is shown in fig. 6.1. The forward bias characteristic is linear over more than 5 decades of current, with an ideality factor of ∿1.06. At low forward bias there is an excess current; this is probably due to recombination in the depletion region (see section 2.3.1). If the Richardson constant is assumed to equal the theoretical value of $A^* = 8$ A cm^{-2} K^{-2}, then the effective barrier height ($\phi_e = \phi_b - \Delta \phi_{bi}$) is .86eV, as calculated from the intercept on the current axis.

Forward bias measurements were performed over the temperature range 150-350K. The results are given in fig. 6.2 and table 6.1. The characteristics remain linear over the whole temperature range, except for the excess current at low bias; this becomes more significant at low temperatures, as would be expected from the temperature dependences of thermionic emission and recombination currents (see section 2.3.1). The ideality factor remains small down to 190K, and the effective barrier height remains constant, with a value of .839 ± .006eV (assuming $A^* = 8$

$Acm^{-2}\ K^{-2}$). Below 190K a significant increase in ideality factor occurs and the barrier height appears to decrease. One possible cause of this is the onset of thermionic-field emission. Padovani and Stratton derived an approximate upper limit for the thermionic-field emission regime[1]; this can be written as

$$V < V_d - \frac{3}{2} \cdot E_{oo} \cdot \frac{\cosh^2 (E_{oo}/kT)}{\sinh^3 (E_{oo}/kT)} \qquad (6.1)$$

where

$$E_{oo} = \frac{q\hbar}{2} \left(\frac{N_d}{m^* \epsilon_s} \right)^{\frac{1}{2}} \qquad (6.2)$$

The doping density of the n-type GaAs, N_d, is $3 \times 10^{16}\ cm^{-3}$, giving E_{oo} = 3.4 meV. This limit is plotted in fig. 6.3 for a diffusion voltage, V_d, of .8 volts. Comparison with fig. 6.2 shows that at the two lowest temperatures the characteristics encroach upon the thermionic-field emission regime. Therefore, the increase in ideality factor, n, and the apparent reduction in barrier height that occurs below 190K can be confidently ascribed to the effects of thermionic-field emission. The activation energy plot for this Schottky barrier is shown in fig. 6.4. A good straight line fit is obtained, except at low temperature (see above). The slope yields an effective barrier height (ϕ_e) of .839 ± .005eV, and the intercept on the vertical axis (at ln A^*) gives a Richardson constant of $A^* = 9 \pm 5\ A\ cm^{-2}\ K^{-2}$.

Capacitance

The reciprocal of capacitance squared (at 1 MHz) is plotted against bias in fig. 6.5. The linear relationship expected from theory (see section 2.3.2) is not observed, instead a curve with a downwards facing

concavity is obtained. Borrego et al[2] have observed a $1/C^2$ characteristic with a change in slope occurring at approximately 1.3 volts for Au-n-GaAs Schottky diodes. This was attributed to the uncovering of a deep trap level, which lies between .9 and 1.2eV below the c.b.m. However this does not give a good fit to the data in fig. 6.5. Pellegrini and Salardi assumed that the 'effective' dielectric constant is a function of the electric field[3]. They proposed that this nonlinear dielectric susceptibility is due to the lack of inversion symmetry in GaAs and to imperfections of the lattice. Their model yields

$$C = C_d + C_o \tag{6.3}$$

where C_d is the depletion region capacitance (equation 2.33) and C_o is a constant 'excess capacitance'. C_o can be obtained from the intercept of a graph of capacitance vs. $(V_{do} - V)^{-\frac{1}{2}}$ (fig. 6.6). Taking V_{do} = .8 V, we obtain C_o = 4600 pF cm^{-2}. If we now plot $(C - C_o)^{-2}$ against bias (fig. 6.5) we obtain the expected straight line. This gives an intercept on the voltage axis (= V_{do} - kT/q) at .78 V, therefore the (zero bias) diffusion voltage V_{do} = .805 ± .01 V. The doping density, calculated from the slope of this line, is $N_d = 3.9 \times 10^{16}$ cm^{-3}, which is close to the quoted value of 3×10^{16} cm^{-3}.

Photoresponse

The photoresponse was measured using monochromatic illumination, chopped at 106 Hz, covering a wavelength range of .9 to 1.6 μm. The Fowler function ([photoresponse/applied photon]$^{\frac{1}{2}}$) is plotted against photon energy in fig. 6.7. The expected linear dependence (see section 2.3.3) is observed over the energy range between ϕ_b and E_g. The intercept yields an effective barrier height, ϕ_e, of .800 ± .005 eV.

Discussion

To permit comparison of the above results, the true barrier height, ϕ_b, must be calculated from either the effective barrier height ($\phi_e = \phi_b - \Delta\phi_{bi}$) or the diffusion voltage ($V_{do} = \phi_b - \zeta$). The doping density and diffusion voltage obtained from the capacitive measurements (N_d = 3.9 x 10^{16} cm^{-1} and V_{do} = .805 V) can be inserted into equation 2.10, yielding an image force lowering, $\Delta\phi_{bi}$, of .03 eV. From the doping density, the energy of the Fermi level below the c.b.m., ζ, can be calculated to be .06 eV. We can now calculate the true barrier height as determined from the various measurement techniques; these results are shown in table 6.2. The values of barrier height lie within a range of .04 eV. Although this is slightly larger than the experimental errors, the agreement is quite good when the approximations of the theoretical models are taken into account. However, the room temperature results agree with the activation energy result (which should give the zero temperature barrier height); this appears to indicate that the temperature dependence of ϕ_b is unexpectedly small.

The Richardson constant, as measured from the activation energy plot, is 9 ± 5 A cm^{-2} K^{-2}, which is in excellent agreement with the theoretical value (8 A cm^{-2} K^{-2}). This shows that any $\chi^{\frac{1}{2}}\delta$ term due to tunnelling through an interfacial layer (equation 2.39) is negligible, demonstrating that these diodes are near-ideal as defined in section 2.3 (i.e. the interfacial layer, if present, offers no impediment to carrier transport). The barrier height of these diodes is .85 ± .02eV; reported values of ϕ_b for Au-n-GaAs range between .80 and 1.03 eV[4]. Adams and Pruniaux[5] have shown that the treatment with concentrated hydrochloric acid followed by a methanol rinse (as used here) produces a very thin

surface film (∿ 1.3 nm). The same authors also reported a very similar Au-n-GaAs barrier height (.83 eV) for Schottky diodes equivalent to those described in this section[6].

6.2.2 p-type GaAs

Gold Schottky barriers were prepared on LPE p on p^+ GaAs samples, again using the procedure described in section 5.3. The room temperature current-voltage characteristics are shown in fig. 6.8 (on semilogarithmic axes) and fig. 6.9. The forward log J vs. V characteristic is nonlinear because the low barrier height makes the voltage drop across the series resistance significant. The series resistance was less than 5 Ω; the dashed straight line shown in fig. 6.8 was obtained by assuming a series resistance of 4.5 Ω. The ideality factor, n, for this line was 1.05 and the effective barrier height was calculated to be .50 ± .1eV (assuming A^* = 75 A cm^{-2} K^{-2}).

The plot of reciprocal capacitance squared against bias yields a straight line (fig. 6.10), in contrast to the curve obtained for the n-type diodes discussed in section 6.2.1. This difference may be due to the lower defect density of this high purity LPE grown material. The doping density determined from the slope of the line is 2.3 x 10^{15} cm^{-3}; this is comparable to the supplied value of 1-2 x 10^{15} cm^{-3}. The intercept on the voltage axis yields a diffusion voltage, V_{do}, of .305 ± .01 V. The energy of the Fermi level below the v.b.m., as calculated from the measured doping density, is .203 eV. Therefore the barrier height obtained from the capacitance measurement is ϕ_b = .51 ± .01 eV.

In order to measure the photoresponse of these contacts it was necessary to cool the sample to 200K, using the exchange gas cryostat, to increase the impedance of these diodes. A wavelength range of .90 to 1.60 μm was covered, and the light was chopped at a frequency of 300Hz.

The resulting Fowler plot is shown in fig. 6.11. The measured effective barrier height, ϕ_e, is .49 ± .01 eV.

Using the values of doping density and diffusion potential measured above (N_a = 2.3 x 10^{15} cm^{-3}, V_{do} = .305 V), the calculated image force lowering is $\Delta \phi_{bi}$ = .012 eV. Table 6.3 gives the barrier heights calculated from this and the above data. These results are reasonably consistent with those reported for the Au-n-GaAs diodes in section 6.2.1. This demonstrates still more conclusively that Schottky diodes, prepared as described in section 5.3, are truly near-ideal.

6.3 Non-Ideal GaAs Schottky Barriers

It is comparatively simple to fabricate non-ideal diodes, in fact great care was needed in all the stages of the preparation if consistent near-ideal characteristics (as described in section 6.2) were to be obtained. We begin this section by discussing non-ideal diodes, which were produced by changing the fabrication procedures described in section 5.3. Samples were also subjected to a simulated LB film deposition process, in which no LB film layer was deposited. Schottky diodes were then fabricated on these samples, and their characteristics are discussed in the second part of this section. This procedure allows some of the effects of the LB film deposition process on the GaAs surface to be deduced.

6.3.1 Effects of Chemical Preparation

The forward bias characteristic of a typical non-ideal diode is shown in fig. 6.12. This diode was prepared by chemical polishing in bromine/methanol (1:2000 by volume), followed by a methanol rinse. Comparison with the near-ideal behaviour described in section 6.2.1 shows a decrease in current by several orders of magnitude at high bias, with an increased ideality factor (n > 1.1). At low bias a large deviation

from the exponential characteristic occurs, this is due to an 'excess current'. The high bias characteristic indicates that a substantial interfacial layer is present between metal and semiconductor. Tunnelling through this layer reduces the magnitude of the current, and the potential drop across the layer causes the increase in ideality factor (see section 2.4.1). An 'excess current', at low bias, is frequently observed in metal - tunnel insulator - semiconductor diodes. This may be due to conduction band electrons recombining into surface states and then tunnelling into the metal, as proposed by Kumar and Dahlke[7].

The above results demonstrate the importance of the HCl treatment in producing comparatively oxide free GaAs surfaces, although use of a stronger Br/methanol solution (without the HCl treatment) could produce near-ideal behaviour. Several other chemical polishes were briefly evaluated. The common SHH polish (conc. H_2SO_4 : 30% H_2O_2 : H_2O) was tried in 4:1:1 and 10:1:1 volume ratios. Near-ideal characteristics could be obtained, but the results were a little inconsistent. A three stage procedure which was claimed to leave < 1nm of oxide was tried; it consisted of a 4:1:1 SHH polish, followed by a 40% hydrofluoric acid rinse and a final 1:1 NaOH (molar) : H_2O_2 (.76 molar) polish[8]. However non-ideal diodes were produced, with similar characteristics to those described above. The final polish studied was composed of 10 parts to 1 of 50% (by weight) citric acid solution and 30% H_2O_2[9]; again non-ideal diodes were obtained. It was concluded that the Br/methanol - HCl treatment (described in section 5.3.3) was most suitable for this work because it consistently produced a relatively oxide free surface.

6.3.2 Effects of the LB Film Deposition Process

During the LB film deposition process the sample is exposed to the atmosphere for several minutes and then immersed in water for ten or more

minutes, before the first monolayer is picked up on withdrawal. It is by no means obvious that this process will not affect the surface of the semiconductor. This may be especially true for GaAs, as it has been reported that water oxidises this material[5,10]. In order to examine these effects several Schottky barrier samples were prepared on n-type GaAs, which were exposed to conditions intended to simulate various stages of the dipping process. The samples were prepared together, using the standard Br/methanol - HCL treatment, and were processed as follows:-

(a) kept under methanol for 20 minutes, blown dry with nitrogen.

(b) left in air for 20 minutes.

(c) left in air for 15 minutes, then immersed in 'millipore' water for 5 minutes, blown dry with nitrogen.

(d) left in air for 10 minutes, immersed in 'millipore' water for 10 minutes, blown dry with nitrogen.

Gold top electrodes were simultaneously evaporated onto all four samples.

The forward and reverse ln J vs. bias and the $1/C^2$ characteristics of diodes (a) to (d) are shown in fig. 6.13 and 6.14 respectively. Device (a) has current-voltage characteristics similar to those of near-ideal Schottky barriers, although the magnitude of the current is reduced by a little less than a decade. The capacitance data must be interpreted with care because there may be significant doping density variations between samples (despite the fact that they were all taken from the same wafer). However, it can be seen that the intercept of the $1/C^2$ plot of device (a) is larger than that for the near ideal case. This data could be interpreted in terms of a small increase in barrier height, but it is perhaps more probable that a thin oxide layer grew on the GaAs surface before electrode deposition. However, it should be emphasised that these effects are relatively minor ones.

Device (b) presents a rather less ideal I-V characteristic. The ideality factor has increased to 1.1, and the forward current has fallen by two orders of magnitude. This has revealed a more extensive 'excess current' region, at low bias, than that observed in near-ideal diodes. The magnitude of the 'excess current' has not increased, as can be seen in the reverse characteristic, therefore it is probably caused by the same mechanism as before, i.e. recombination in the depletion region (see sections 2.3.1 and 6.2.1). The intercept of the $1/C^2$ plot has also increased significantly. This, together with the J-V characteristic, strongly indicates the presence of an interfacial layer. Reported measurements indicate that this is probably of approximately 2 nm thickness[5].

The characteristics of devices (c) and (d) were very similar, and will be considered together. The immersion in ultra-pure water has had a pronounced effect on the log J vs. V behaviour. At high forward bias (>.5v) the current still seems to be controlled by thermionic emission and tunnelling through the interfacial layer, with an ideality factor of <1.5 . However, the reverse current and the 'excess current' at low forward bias have both increased significantly. The slope of the low forward bias characteristic ($n\sim2$) suggests that the 'excess current' is due to recombination (c.f. section 2.3.1). This change could be explained by an increase in barrier height, which would increase the minority carrier concentration in the depletion region. However the change could also be caused by an increased interface state density; this would allow electrons to recombine into these states and then tunnel into the metal[7] (c.f. section 6.3.1). The latter explanation seems more probable, because the 'excess current' increased for a longer immersion. Moreover, the intercept on the current axis (extrapolated from the high forward bias region) was larger for the longer immersion, implying that

the barrier height may even have decreased slightly. The difference in ideality factor between diodes (c) and (d) could also be explained by a difference in interface state densities. However, the differences between these samples are quite small (although they are significant). Consequently, it may be expected that a longer immersion in water would only cause minor changes in the characteristic. The non-ideal current-voltage results and the relatively large intercepts from the $1/C^2$ vs. bias plots again indicate that a significant interfacial layer has formed. Reported data suggest that this layer may be of the order of 2.5 nm thickness[5].

This investigation, although yielding little quantitative information, has given a valuable qualitative insight into the effects on the GaAs surface of the dipping process. It has demonstrated that immersion in the ultra-pure water used in the Langmuir trough allows the growth of a thin oxide layer. In addition, the surface state density at the semiconductor surface is probably increased. Roberts et al have reported that ω-TA LB films can effectively seal silicon surfaces against atmospheric attack[11]. Therefore it is expected that once the first monolayer has been deposited then the GaAs surface is largely protected against further oxidation. Thus it is reasonable to assume that in devices coated with LB films the GaAs surface is similar to that of diodes (c) and (d). These results can therefore be compared with those of devices incorporating LB films, and this allows the contribution of the LB film to be assessed.

6.4 GaAs/LB film MIS Diodes

In this section the characteristics of LB film MIS diodes on n-type GaAs are described. The discussion is in two parts, the first describes devices incorporating ω-tricosenoic acid films and the remainder is

concerned with those using phthalocyanine films. The latter are also discussed in section 7.4.3, which describes the effects of exposure to gaseous NO_2 upon devices incorporating phthalocyanine films.

6.4.1 ω-Tricosenoic Acid Devices

These devices were prepared by the method described in section 5.3, and two slightly different device structures were fabricated. The first type used large pieces of bulk n-type GaAs, which allowed the LB film to be deposited in a 'step' structure having a sequence of film thicknesses along the sample. This also left an undipped portion (referred to in this text as '0 layers'), which must not be confused with an ideal Schottky barrier. This area without a LB film was exposed for 48 hours between etching and top contact evaporation (largely under dry nitrogen in a desiccator). Only one film thickness was deposited on the smaller n on n^+ LPE samples. The results given are typical; variations between contacts on any sample were small. However, varations between samples prepared at different times were more significant, although still relatively small. This is probably due to differences in the surface oxide layers on the GaAs caused by slight variations in sample preparation.

Electrical Characteristics

The ln J vs. V characteristics of bulk n-type GaAs diodes incorporating 0, 1, 3 and 5 monolayers of ω-tricosenoic acid are shown in fig. 6.15. The reverse bias characteristics are omitted for clarity (reverse currents at .5 V:- 0 layers = 5×10^{-8} A cm^{-2}, 1 and 3 layers = 2×10^{-9} A cm^{-2} and 5 layers = 4×10^{-10} A cm^{-2}). The 0 layer diode has similar characteristics to those of the type (c) and (d) diodes discussed in section 6.3.2 (fig. 6.13). The latter devices incorporate an oxide layer which is believed to be similar to the one underneath the LB film.

Therefore it is reasonable to assume that the differences between the 0 layer device and those incorporating LB films are due to the presence of the organic layers. The diode incorporating one monolayer shows a drop in the forward current of approximately two decades, together with a reduction in slope at high bias. The three layer device exhibits a further reduction in current and slope at high forward bias. However, at low bias (< .5V) the current is significantly greater than that of the 1 layer device; this was consistent across all contacts tested. The diode incorporating 5 monolayers has similar characteristics to the 3 layer device, but with a further small reduction in current density.

The current-voltage characteristics for a device incorporating 11 layers of ω-TA, deposited on an epitaxial $n\text{-}n^+$ GaAs wafer, are shown in fig. 6.16. Comparison with the 5 layer diode described above (fig. 6.15) reveals a reduction in current density, at high forward bias, of approximately two decades. The current levels are similar for reverse and low forward bias. Although the carrier concentration in this sample is an order of magnitude less than that of the bulk GaAs, it is unlikely that this has any significant effect on the I-V behaviour.

Plots of $1/C^2$ against bias for the above bulk and epitaxial diodes are shown is fig. 6.17 and fig. 6.18 respectively. In the former case we find that the slope increases with LB film thickness and the intercept remains roughly constant. The 0 layer characteristic appears to be anomalous as it lies between those for 1 and 3 monolayers. The 11 layer device exhibits a more complex behaviour, although this becomes linear at large reverse bias. It is notable that in this latter case there is no evidence of the curved characteristic always found for devices on bulk n-type GaAs (eg. Fig. 6.5 and fig. 6.17). This indicates that the defects which cause the curvature are either absent, or much reduced in number, in the epitaxial material (see section 6.2.1).

Photoelectric measurements (in white light) on the bulk n-type diodes yielded the results shown in fig. 6.19. As might be expected, the short circuit current decreases as the LB film thickness is increased from 1 to 5 monolayers. Again the 0 layer device behaves in an anomalous fashion intermediate between that of the 1 and 3 layer diodes. The degradation of the fill factor for increasing LB film thickness is typical of the behaviour of MIS photodiodes.

Discussion

It is evident that current transport in the forward direction is considerably influenced by the ω-TA LB film, especially for high bias. It is not unexpected that the effects are more significant for large forward bias because this reduces the barrier to electron transport in the semiconductor. Therefore, for far forward bias, the insulating LB film becomes the limiting factor for current transport. For reverse bias the diffusion potential can increase greatly (providing inversion does not occur) and the semiconductor will support the majority of the bias applied across the diode. We shall now discuss the data in detail and will demonstrate that they do support these suppositions.

The continuous decrease in capacitance with increasing reverse bias (fig. 6.17 and fig. 6.18) shows that the semiconductor surface is deeply depleted at large reverse bias. To permit this the LB film must allow minority carriers (holes) to pass from the semiconductor to the metal. This then prevents minority carriers at the surface from equilibrating with the bulk of the semiconductor, thus giving rise to deep depletion. The photoelectric data also show the **LB film to be partially transparent to** holes, since the short-circuit current represents a hole current from the semiconductor to the metal. Petty et al have observed similar behaviour for GaP/LB film MIS diodes[12]. They measured the short-circuit

photocurrent and the electroluminescent efficiency, both of which depend on hole transport through the insulator (although in opposite directions). It was found that even relatively thick ω-TA films, up to approximately 13 monolayers (∿ 40 nm), were not impervious to minority carriers.

It has not been possible to determine the mechanism of hole transport in the LB film, however analysis of the forward bias characteristics yields important information concerning electron transport in the film. It is desirable to calculate the electric field, E in the insulating layer, but this is difficult because the bias is divided in a complex manner between the LB film and the semiconductor depletion region. We can simplify this relationship by assuming that a large enough forward bias has been applied to almost flatten the bands in the semiconductor. Under this condition the potential across the film, V_i, is given by

$$V_i = V - V_{do} - V_{io} \tag{6.4}$$

where V_{io} is the potential across the insulator at zero bias. For GaAs we can assume the diffusion potential, V_{do}, is .8 volts, because of the Fermi level is pinned (c.f. the Schottky barrier case, section 6.2.1). Consideration of the workfunctions of Au and GaAs suggests that V_{io} is negligible. Therefore, for large forward bias, the potential across the LB film is given by

$$V_i \sim V - .8 \tag{6.5}$$

As has been discussed in section 4.2.2, high field conduction in fatty acid LB films has been reported as being proportional to exp $(E^{\frac{1}{2}})$. This has been explained as being due to either Schottky emission or a Poole-Frenkel mechanism. Fig. 6.20 shows ln J plotted against $V_i^{\frac{1}{2}}$ ($\propto E^{\frac{1}{2}}$) for the diode incorporating 11 layers of ω-TA (c.f. fig. 6.16). For large forward bias the plot is linear, which is consistent with the above mentioned conduction mechanisms. The dielectric constant of the LB film can be calculated from the slope of this line; for the Schottky emission case (equation 3.13) then ε_i = .6 and assuming Poole-Frenkel conduction (equation 3.16) then ε_i = 2.4. The dielectric constant of ω-TA is approximately 3[13], which agrees approximately with the value calculated by assuming Poole-Frenkel conduction. For the devices with thinner LB films the linear regions in ln J vs. $V_i^{\frac{1}{2}}$ were less well defined and the degree of agreement with the Poole-Frenkel mechanism was quite poor. However in these cases the analysis is complicated by the presence of the thin oxide layer (see section 6.3.2), which becomes increasingly significant as the LB film thickness is reduced. Therefore the electron conduction in these GaAs/LB film MIS diodes is probably controlled by the Poole-Frenkel mechanism, for high forward bias.

We must also consider the apparently anomalous behaviour of the 0 layer device. Both capacitive and photoelectric measurements reveal behaviour intermediate between that of devices incorporating 1 and 3 monolayers of ω-TA. Perhaps the simplest explanation is that the oxide film in this region is considerably thicker than that in the area coated with an LB film. Another possibility is that fixed charge in the LB film causes a small decrease in the band bending in the semiconductor. This could account for the increased capacitance of the 1 monolayer LB film diode (fig. 6.17). However this does not explain the photoelectric data,

as this would be expected to give rise to a smaller photocurrent in the LB film covered regions (contrast to fig. 6.19). Therefore these discrepancies appear to be due to differences in the thickness or composition of the oxide layers in the two regions.

The characteristics of the GaAs/LB film MIS devices reported by Tredgold and El-Badawy[14] differ from those described in this section. In particular their results for devices incorporating a monolayer are more 'Schottky-like' than those described above (i.e. they correspond more closely to the behaviour described in section 2.4). Although they use stearic acid films, not ω-TA, this is unlikely to be of significance as the two materials have very similar properties. The major differences between this work and that of the above authors is in the preparation of the GaAs surface prior to LB film deposition. Tredgold and El-Badawy use a treatment that results in an oxidised GaAs surface. This oxide layer may differ from that which forms on our samples during LB film deposition (see section 6.3.2), which is possibly the cause of the differences between their work and ours.

6.4.2 CuPc Devices

Diodes incorporating 1, 2 and 4 monolayers of CuPc were fabricated on bulk n-type GaAs (using a 'step structure' as described in section 6.4.1). Fig. 6.21 shows plots of ln J vs. V for these devices; the characteristic for the 4 layer device is not shown as it is very similar to that of the 2 layer device. Variations in the characteristics of each type of diode were reasonably small. At reverse and low forward bias the characteristics are very similar. However at high forward bias there is a distinct difference between the 1 monolayer diode and those incorporating thicker films. These characteristics are not markedly different from those of the ω-TA devices shown in fig. 6.15; for a

similar number of monolayers, the high forward bias currents are slightly lower for the devices using CuPc films.

$1/C^2$ vs. bias data for these diodes are shown in fig. 6.22. As for devices incorporating ω-TA films, the slope of the curve increases as the film thickness is increased, with little change in the intercept. It is interesting to note that the 4 layer device characteristic differs significantly in slope from that of the 1 and 2 layer ones, whereas the J-V results showed a difference in behaviour between the 1 layer diode and that of those incorporating 2 and 4 layers. There does not appear to be an obvious reason for these trends.

Perhaps the most intriguing data in this chapter are those shown in fig. 6.23, the results of the photoelectric measurement of these CuPc/LB film diodes. The one monolayer device shows the expected behaviour, which is very similar to that of the device incorporating 1 layer of ω-TA (fig. 6.19). However, a completely different characteristic is found for the 2 and 4 layer diodes. Normally, to a first approximation, the current in an illuminated diode can be expressed as the dark current plus a constant photocurrent. Although the photocurrent is actually a weak function of bias, and the two currents are not independent, the variations from this simple behaviour are usually small. For the 2 and 4 monolayer CuPc MIS devices this is clearly not the case as the photocurrent appears to increase greatly from forward to reverse bias. This behaviour must be the result of a strong interaction between the effects of illumination and the dark conduction processes. Phthalocyanines are known to exhibit photovoltaic behaviour, and as the optical absorption of CuPc LB films is measurable for even a single monolayer[15], then this interesting effect may be due to the interaction of competing processes in the semiconductor and the LB film. Although

the mechanism is at present completely unknown, this interesting effect may well merit further investigation.

6.5 GaInAs/LB film MIS Diodes

In the investigation of the quaternary semiconductor alloy InGaAsP (grown lattice matched to InP) it was found that the ternary limit of $Ga_{.47}In_{.53}As$ was the most attractive material for use in high speed semiconductor devices[16,17]. Low field electron mobilities as high as 13,800 $cm^2V^{-1}s^{-1}$ at 300K have been reported[18], and from this peak electron velocities as high as 3.1×10^7 cm s^{-1} have been predicted[16]. However, fabrication of practical MESFETs on this material is not possible, because of the very low barrier height of metal contacts to n-type GaInAs. For example, the reported Au-n-GaInAs barrier height of .2eV[19] corresponds to a saturation current density (equivalent to the gate leakage in a MESFET) of approximately 300 A cm^{-2} at 300K. It is possible to increase the apparent barrier height of Schottky contacts by introducing a thin interfacial oxide layer[20], and MESFETs with 'insulator assisted' Schottky gates have been reported[21,22]. This final part of chapter 6 is concerned with GaInAs/LB film MIS diodes. Devices were fabricated using two different chemical treatments of the semiconductor surface, and monolayers of either ω-TA or SiPc were used to provide an insulating layer of tunnelling dimensions.

6.5.1 ω-TA Devices

A different chemical polishing treatment from that described in section 5.3.3 was used for the preparation of these GaInAs diodes. This is because concentrated hydrochloric acid attacks 3-5 semiconductors containing indium. A .2% bromine/methanol chemical polish was used for most of the devices fabricated (type A). This treatment is known to leave an oxide layer on the surface of both GaAs and InP[23]. Therefore

some GaInAs MIS diodes were prepared using an additional rinse in hydrofluoric acid (40%) in order to remove the oxide; these type B diodes are described in the second half of this section. Apart from the changes described above, the preparation of the two types of contact was identical (and as described in section 5.3).

Type A Devices

The forward and reverse current-voltage characteristics of a typical type A diode incorporating a monolayer of ω-TA are plotted (on semilogarithmic axes) in fig. 6.24. The error bar shows the extent of the variations between contacts on a sample. A linear region in forward bias can be discerned, with an ideality factor of between 1.5 and 1.8; the extent of this region is limited by the effects of the series resistance. The value of J_o is approximately 6×10^{-5} A cm^{-2}, more than six orders of magnitude below the theoretical value for an ideal Schottky barrier (ϕ_b = .2 eV[19]). This corresponds to an apparent barrier height of . 57eV (taking A^* = 5 A cm^{-2} K^{-2} since m^*/m = .41[24]). The reverse characteristic is quite soft, however a large reduction in reverse leakage current has still been obtained.

The $1/C^2$ vs. V characteristics are plotted in fig. 6.25, giving a fairly good straight line. The doping density, calculated as for a Schottky barrier (i.e. ignoring the effects of the interfacial layer) is 1.3×10^{17} cm^{-3}. This is larger than the supplied figure of 6×10^{16} cm^{-3}; the slope is therefore less than that for an ideal Schottky barrier, indicating that the model developed by Fonash could be valid in this case (see section 2.4.2). The intercept at .66 volts is larger than the apparent barrier height and much greater than that for an ideal Schottky barrier (where ϕ_b = .2 eV[19]). This is a strong indication that the apparent barrier height does not correspond to a true barrier

height (see section 2.3.3); this is to be expected as the thickness of the interfacial layer is at least 3nm.

Forward bias characteristics were measured over the temperature range 200-300K (fig. 6.26); the parameters determined from this are given in table 6.4. The ideality factor is independent of temperature and has a value of n = 1.73 ± .02. The apparent barrier height, calculated from the intercept on the current axis, J_o, decreases at lower temperatures. This again indicates that the true barrier height is not being measured. If the tunnel MIS model of Card and Rhoderick[25] is examined (see section 2.4.1), it can be seen (from equation 2.39) that an activation energy measurement (see section 2.3.3) should yield the true barrier height, because the term $\exp(\chi^{\frac{1}{2}}\delta)$ is constant. In this case the intercept at 1/T = 0 has a value of $\ln A^* - \chi^{\frac{1}{2}}\delta$.

The activation energy diagram for a type A diode is shown in fig. 6.27. A reasonable straight line fit can be made to this data, which yields a true barrier height of .18 eV. This is comparable to, but slightly less than, the reported Schottky barrier height of .2 eV[19]. The value of $\chi^{\frac{1}{2}}\delta$ is .15 $eV^{\frac{1}{2}}$Å; if we assume that the insulating layer thickness is equal to that of a monolayer of ω-TA (i.e. 3nm) then the barrier to tunnelling, χ, is approximately .25 eV. This is of a similar magnitude to the values reported by Card and Rhoderick for Au-SiO_2-Si diodes[25]. From their model (see section 2.4.1) the ideality factor, n, is given by equation 2.40. Since the tunnelling layer is relatively thick we will assume that all interface states equilibrate with the semiconductor (i.e. $D_{sa} = 0$), giving

$$n = 1 + \frac{\delta}{\varepsilon_i}\left(\frac{\varepsilon_s}{w} + q\,D_{sb}\right) \qquad (6.6)$$

By taking appropriate values for doping density (6×10^{15} cm^{-3}), film thickness (3nm) and dielectric constant ($\varepsilon_i = 3.0\ \varepsilon_o$) we can calculate D_{sb}. For the observed range of n = 1.5 to 1.8, we obtain an interface state density, D_{sb}, of between 1.8×10^{12} and 3.4×10^{12} cm^2 eV^{-1}.

The tunnel MIS diode model of Card and Rhoderick appears to provide quite a good description of these GaInAs/ω-TA devices. Using the model to analyse the data yields reasonable values of barrier height (.18 eV), tunnelling barrier, χ (.25 eV) and interface state density ($\sim 2.5 \times 10^{12}$ cm^2 eV^{-1}). As the barrier height is little different from that of a Schottky barrier, we can see that the substantial reduction in current density achieved by the introduction of a monolayer of ω-TA is due solely to tunnelling through this layer. The small size of the barrier height change also indicates that neither the effects of fixed charge in the LB film, nor those of the dipole layer formed by the fatty acid headgroups, are significant. Similar conclusions were drawn from unpublished work, carried out in this laboratory, on GaP/phthalocyanine MIS diodes[26]. Phthalocyanines subsituted with either copper or manganese were used; in bulk form these materials are respectively n-type and p-type semiconductors. If the electrostatic interaction with the LB film has a significant effect on the band bending in the semiconductor then we would expect differences between diodes incorporating these two materials. However, the current-voltage and photoresponse (Fowler plot) characteristics of these devices were almost identical, thus any change in the diffusion potential caused by the LB film must be insignificant. Although the reverse characteristics do not saturate, the current densities obtained are similar to those reported for other GaInAs MIS structures[20-22] and may be sufficiently low to allow practical GaInAs MESFETs to be fabricated.

Type B Devices

Ln J is plotted as a function of bias in fig. 6.28 for a typical HF treated MIS diode incorporating a monolayer of ω-TA. Comparison with the characteristic of type A diodes (fig. 6.24) reveals that the current density has increased by approximately two decades. This is accompanied by an increase in ideality factor to approximately 2. The first of these effects was not unexpected because the HF treatment removes the oxide from the semiconductor surface, thus reducing the total insulator thickness (≡ LB film + oxide). It was not possible to measure the capacitance characteristics of this device because of instrumental problems caused by its low impedance.

Examination of I-V characteristics at temperatures down to 77K (fig. 6.29) reveals very different behaviour from that seen for type A diodes (fig. 6.26). At low temperatures two distinct regions in the forward bias characteristic can be seen. At high bias the behaviour is similar to that expected and is comparable with that of type A diodes. However, at low bias a distinct 'knee' is evident, and the temperature dependence of the current in this region is quite small. Extrapolation of this region to the current axis gives an approximately constant intercept ($\sim 4 \times 10^{-3}$ A cm^{-2}) independent of temperature. This 'knee' in the curve is reminiscent of the behaviour observed by Krumar and Dahlke[7] for Cr-SiO_2-Si diodes. They attributed this to a two step recombination-tunnelling process, which occurs via interface states. The small temperature dependence of the characteristics in this region strongly suggest that the tunnelling step of the process is the rate determining step.

The parameters of the upper portion of the I-V characteristics are given in table 6.5; it is assumed that in this region the current is

controlled by thermionic emission and tunnelling through the LB film (as in the model of Card and Rhoderick[25]). The ideality factors reveal the pitfalls of this analysis. At the highest temperatures the slope may be underestimated because the two regions are indistinct, hence n may be overestimated. At low temperatures the upper region is of limited extent, making line fitting rather dubious; this may account for the increase in n with reducing temperature. These problems will also affect the activation energy plot (fig. 6.30), however a linear behaviour is found over a limited temperature range. Analysis of this portion of the curve yields a true barrier height of .14 eV and a tunnelling coefficient, $\chi^{\frac{1}{2}}\delta$, of 13 $eV^{\frac{1}{2}}$ Å, giving a tunnelling barrier, χ, of .20 eV. These values are all slightly smaller than the corresponding ones for type A diodes. As the difficulties described above would tend to cause us to underestimate ϕ_b, it is not possible to decide whether this change is significant. However the value of $\chi^{\frac{1}{2}}\delta$ is probably overestimated, implying that the tunnelling thickness, δ, is less than that in type A diodes. This would be expected if the HF treatment had removed a thin layer of oxide.

The other differences between these type B diodes and the type A diodes is the slightly higher ideality factor in the former case ($n \sim 2$ c.f $n \sim 1.7$). This indicates that the density of interface states has increased slightly (equation 6.6). This may be related to the appearance of the tunnelling-recombination limited region in the I-V characteristics. It therefore seems probable that the different behaviour of type B devices is due to a defect level which arises as a consequence of the HF treatment. Differences between bromine-methanol and HF treated surfaces have also been observed for InP/LB film MIS diodes[27] (although in this case the LB film was much thicker), and these may be due to a similar, defect related, effect.

6.5.2 SiPc Devices

These devices were prepared using the same bromine-methanol treatment as the type A ω-TA diodes (see section 6.6.1). In this case a single monolayer of silicon phthalocyanine (SiPc) was deposited prior to top electrode evaporation. The forward and reverse bias characteristics of a typical diode are plotted on semilogarithmic axes in fig. 6.31. The characteristics are similar in form to those of the type A diodes discussed previously (which used ω-TA LB films), although the current densities are a decade higher. The ideality factor is also similar at approximately 1.7. If we assume $A^* = 5$ A cm^{-2} K^{-2} then the apparent barrier height is .50 eV, approximately .07 eV less than that of comparable ω-TA devices. The plot of $1/C^2$ vs. bias is linear (fig. 6.32), with an intercept at .52 volts. The doping density calculated from the slope is 2.1×10^{16} cm^{-3}, which agrees quite well with the supplied value of 2.3×10^{16} cm^{-3}. The apparently close agreement between the current-voltage and capacitance data must be regarded cautiously because the LB film is a substantial interfacial layer (see section 2.4).

This caution is justified upon examination of the forward bias J-V characteristics over the temperature range 200-300 K (fig. 6.35). The parameters extracted from this data are given in table 6.6 As for ω-TA devices, a decrease in apparent barrier height with decreasing temperature is apparent. A notable difference from the behaviour of type A diodes is the increase in ideality factor with reducing temperature. In the tunnel MIS model the ideality factor, n, is determined by equation 2.40. Since the total density of interface states ($= D_{sa} + D_{sb}$) is unlikely to vary, the only cause of a temperature dependent n is a change in the proportion of states which equilibrate with the metal (D_{sa}) and

the semiconductor (D_{sb}). Communication between the interface states and metal is via tunnelling, which is only weakly dependent on temperature. Communication with the semiconductor occurs via recombination/generation, which decreases with falling temperature. Therefore we might expect the ratio D_{sa}/D_{sb} to increase with reduced temperature, as the relative importance of tunnelling increases. However, examination of equation 2.40 shows that this would cause a decrease in n with reducing temperature, which is contrary to the observed trend. This implies either that this model does not apply to these devices or that the model itself is invalid.

A temperature dependence of n of the form $n = 1 + T_o/T$ has been observed for many Schottky barriers[28,29], where T_o is a constant (usually < 50K). This has been ascribed to a temperature dependence of the work function of the metal[29]. In fig. 6.34, the ideality factor, n, is plotted against 1/T; it is obvious that the above behaviour does not apply. A better fit to the variation is $n = .2 + 400/T$, however there is, at present, no model that can explain this behaviour.

The activation energy diagram is shown in fig. 6.35. However, as there appear to be problems in fitting the tunnel MIS model to these data, the interpretation of this is problematical. The slope suggests a true barrier height of .15eV, comparable with that observed for ω-TA MIS devices. The intercept corresponds to a value of $\chi^{\frac{1}{2}}\delta = 14\ eV^{\frac{1}{2}}Å$. If the thickness of the SiPc monolayer is 2.2 nm then χ = .41 eV, rather larger than the corresponding value for ω-TA LB films. We can conclude that the behaviour of SiPc/GaInAs MIS diodes is slightly different from that of diodes incorporating monolayers of ω-TA. Although the differences are fairly small, this cannot be explained by the present models of device behaviour because the characteristics of the SiPc devices do not fit these models.

6.6 Conclusions

This chapter covers two themes, a systematic study of GaAs/LB film devices and a less extensive investigation of LB film tunnel-MIS devices on the ternary alloy GaInAs. The first of these began with an investigation of GaAs Schottky barriers. The semiconductor surface was prepared using a combined bromine/methanol and hydrochloric acid treatment. The characteristics of these near-ideal diodes were comparable with the best reported in the literature. This work was followed by an investigation of the effects on the GaAs surface of the LB film deposition process. It was found that a thin oxide layer is formed on the GaAs surface during immersion in the ultra-pure water used in the Langmuir trough. In addition, an apparent increase in the interface state density was observed. Study of n-type GaAs MIS devices demonstrated that even a single monolayer LB film (of either ω-TA or CuPc) had a significant effect. For the case of a diode incorporating 33 nm of ω-TA, it was shown that electron transport in the LB film occurred by a Poole-Frenkel mechanism. The ω-TA films appeared to be relatively transparent to holes, as was shown by the photoelectric measurements. For diodes incorporating CuPc films an unexplained anomalous photoelectric effect was found, which may merit further investigation.

GaInAs tunnel-MIS diodes were prepared using single monolayer LB films. The current densities in these devices were substantially smaller than in Schottky barriers on this material. Type A diodes, prepared using a bromine/methanol treatment and using ω-TA LB films, had the smallest current densities. Analysis of the results indicated that this effect was probably due to electrons tunnelling through the LB film. The band bending in the semiconductor did not appear to be increased by the presence of the LB film. The main motive for reducing current densities

is to allow the fabrication of MESFETs on GaInAs. These results indicate that LB films could be used for this purpose.

TABLE 6.1 Au-n-GaAs Schottky barrier current-voltage characteristics versus temperature

Temperature /K	Ideality Factor n	J_o/A cm^{-2}	Barrier Height (A^*=8) ϕ_e ($=\phi_b - \Delta\phi_{bi}$)/eV
350 ± 1	1.035 ± .01	7.1×10^{-7}	.841
320 ± 1	1.055 ± .01	5.6×10^{-8}	.834
290 ± 1	1.045 ± .01	1.1×10^{-9}	.850
260 ± 1	1.065 ± .01	3.2×10^{-11}	.835
230 ± 1	1.075 ± .01	2.2×10^{-13}	.833
200 ± 1	1.075 ± .01	2.0×10^{-16}	.840
190 ± 1	1.085 ± .01	1.7×10^{-17}	.836
170 ± 1	1.10 ± .01	9.2×10^{-20}	.821
150 ± 1	1.18 ± .01	2.3×10^{-21}	.739

mean ϕ_e (excluding values at 150K and 170K, see text) = 0 .839 ± .006

Table 6.2 Au-n-GaAs Barrier Height

Photoelectric Measurement (Fowler Technique)	.830 ± .005 ev
Forward Bias ln J-V measurements (A* = 8, average of measurements at several temperatures)	.869 ± .006 eV
Activation Energy	.869 ± .005 eV
Capacitance measurement	.865 ± .01 eV

Table 6.3 Au-p-GaAs Barrier Height

Forward Bias ln J-V measurement (A^* = 75)	.51 ± .01 eV
Capacitance measurement	.51 ± .01 eV
Photoelectric Measurement (Fowler Technique)	.51 ± .01 eV

TABLE 6.4 Current-Voltage characteristics for Type A GaInAs MIS diodes versus temperature

Temperature /K	Ideality Factor n	J_o/A cm^{-2}	Apparent Barrier Height ($A^* = 5$) ϕ_b/eV
300	1.75	1.4×10^{-9}	.57
290	1.70	8.8×10^{-10}	.56
280	1.71	7.3×10^{-10}	.55
270	1.77	6.1×10^{-10}	.53
250	1.73	2.7×10^{-10}	.51
230	1.70	1.0×10^{-10}	.49
215	1.73	8.1×10^{-11}	.46
200	1.73	3.8×10^{-11}	.44

TABLE 6.5 Current-Voltage characteristics for Type B GaInAs MIS diodes versus temperature

Temperature /K	Ideality Factor n (see text)	J_o/A cm^{-2}	Apparent Barrier Height ($A^* \simeq 5$) ϕ_b/eV
302	1.90	6.6×10^{-8}	.47
281	1.78	2.6×10^{-8}	.46
262	1.86	1.7×10^{-8}	.44
240	1.96	1.0×10^{-8}	.41
217	2.03	4.6×10^{-9}	.39
197	2.11	2.2×10^{-9}	.37
177	2.14	7.4×10^{-10}	.34
151	2.43	4.2×10^{-10}	.30
127	2.89	2.9×10^{-10}	.26

TABLE 6.6 Current-voltage characteristics for SiPc/GaInAs MIS diodes versus temperature

Temperature /K	Ideality Factor n	J_o/A cm^{-2}	Apparent Barrier Height (A^*=5) ϕ_b/eV
297	1.53	9.6×10^{-4}	.51
275	1.62	3.6×10^{-4}	.49
255	1.79	1.7×10^{-4}	.47
237	1.91	1.1×10^{-4}	.44
217	2.02	4.3×10^{-5}	.42
201	2.20	2.3×10^{-5}	.40

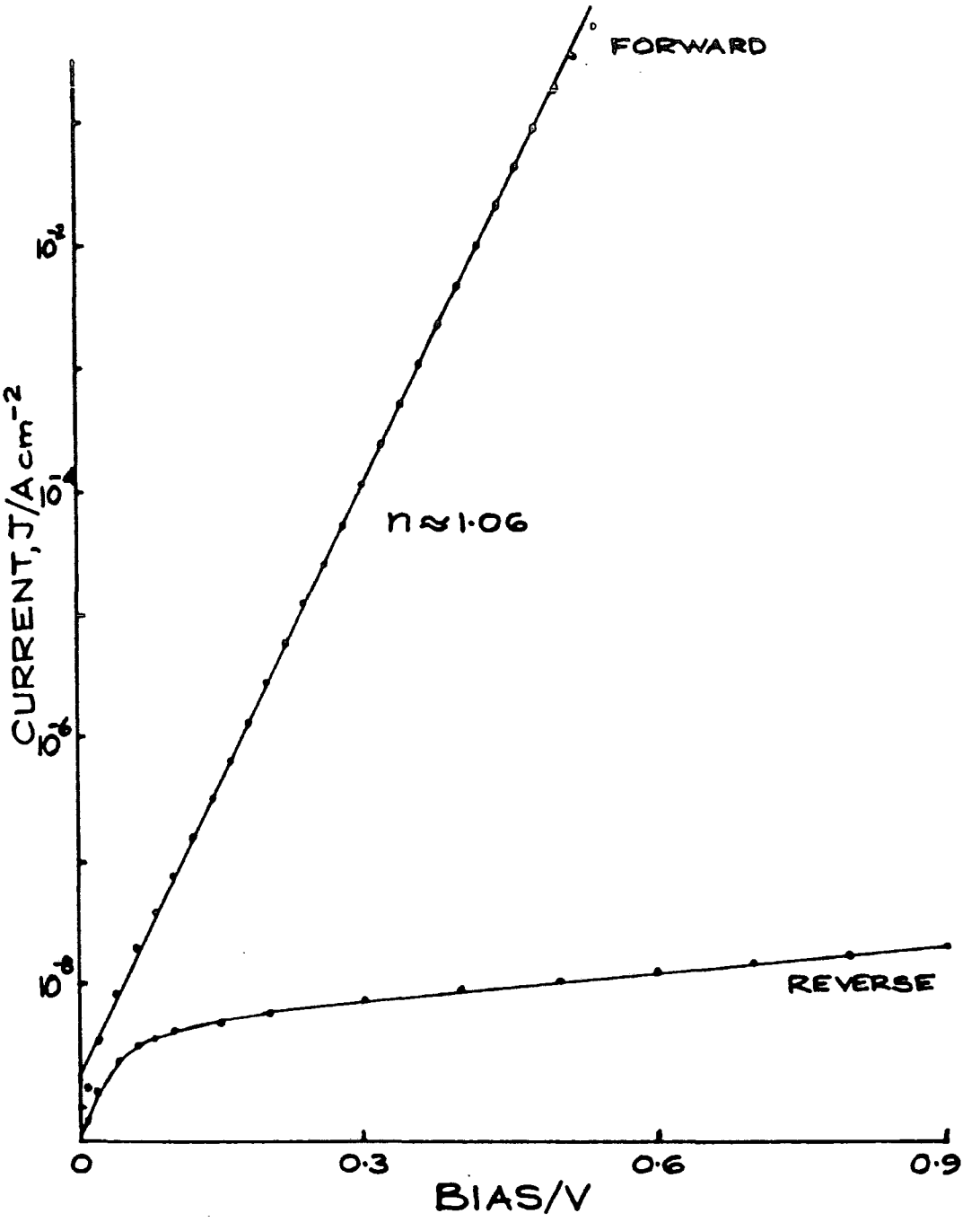

Figure 6.1 Room temperature current-voltage characteristic of a near-ideal Au-n-GaAs Schottky diode. (contact area = .013 cm^2)

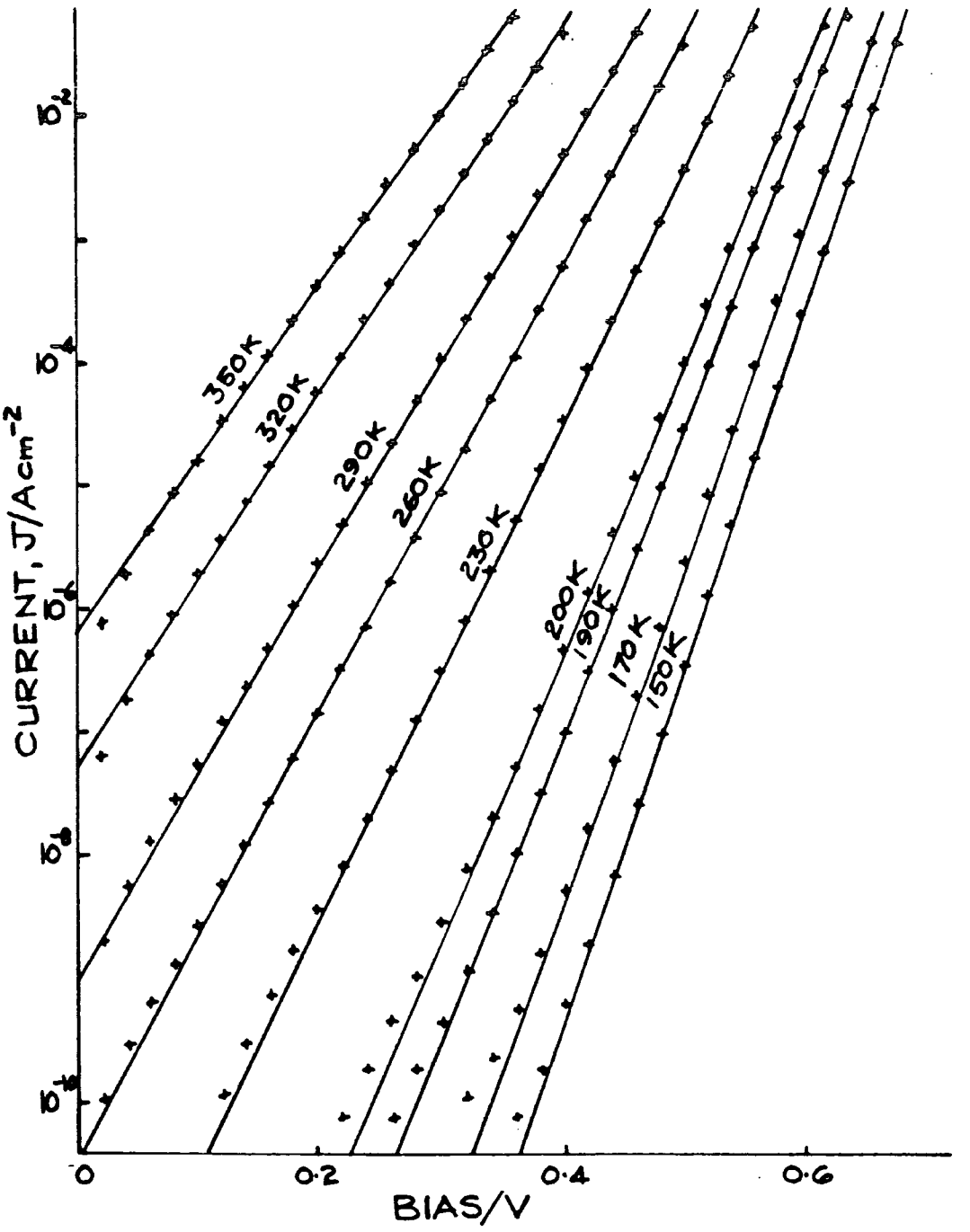

Figure 6.2 Forward bias current-voltage characteristics of a near-ideal Au-n-GaAs Schottky diode versus temperature. (contact area = .013 cm^2)

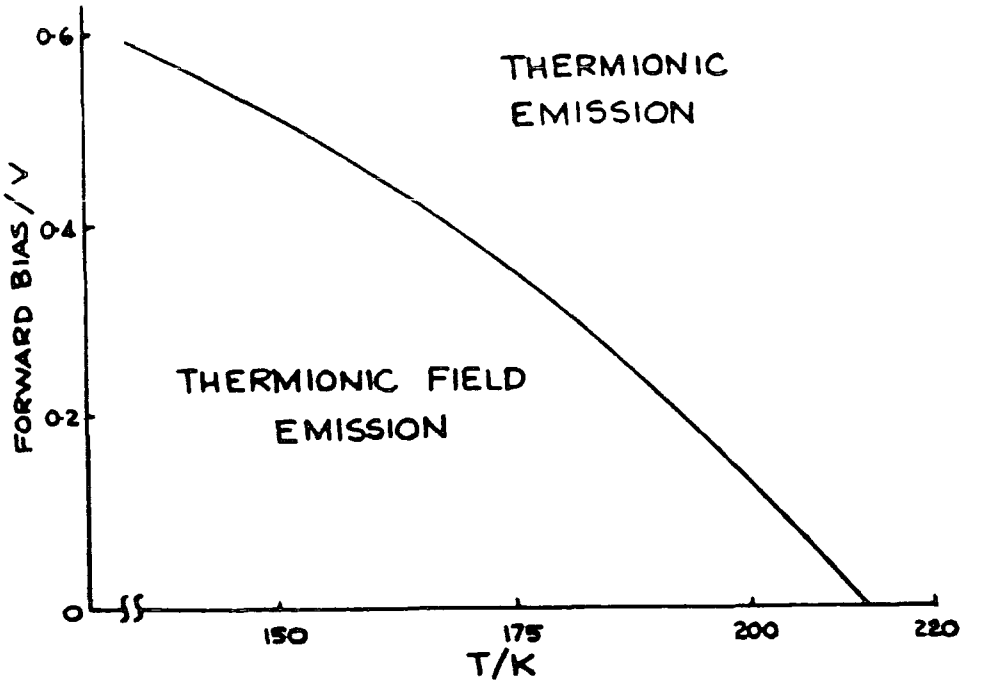

Figure 6.3 This diagram shows the boundary between the thermionic emission and thermionic field emission regimes, as a function of bias and temperature, for a Schottky diode with a diffusion voltage, V_{do} = .8V.

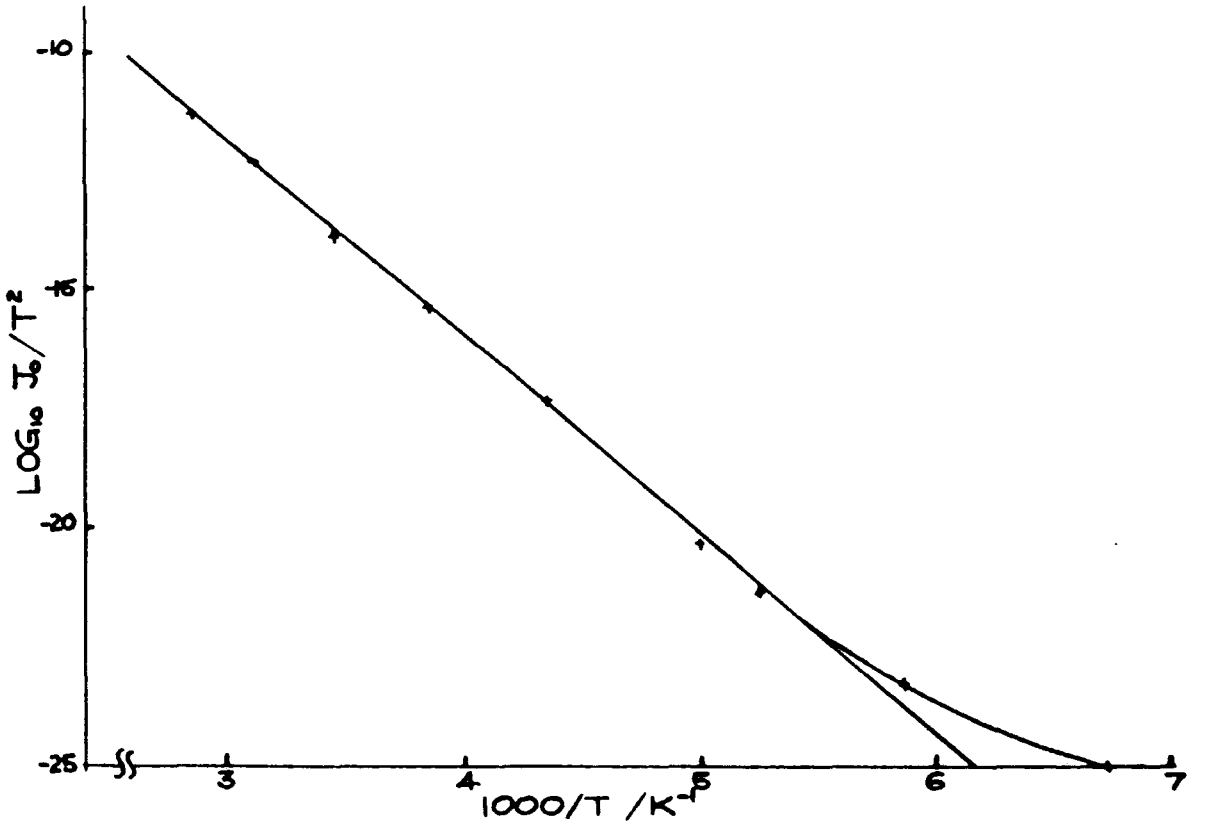

Figure 6.4 Activation energy diagram for a near-ideal Au-n-GaAs Schottky barrier. The deviation from a straight line at low temperature is due to thermionic-field emission (see text). (contact area = .013 cm^2)

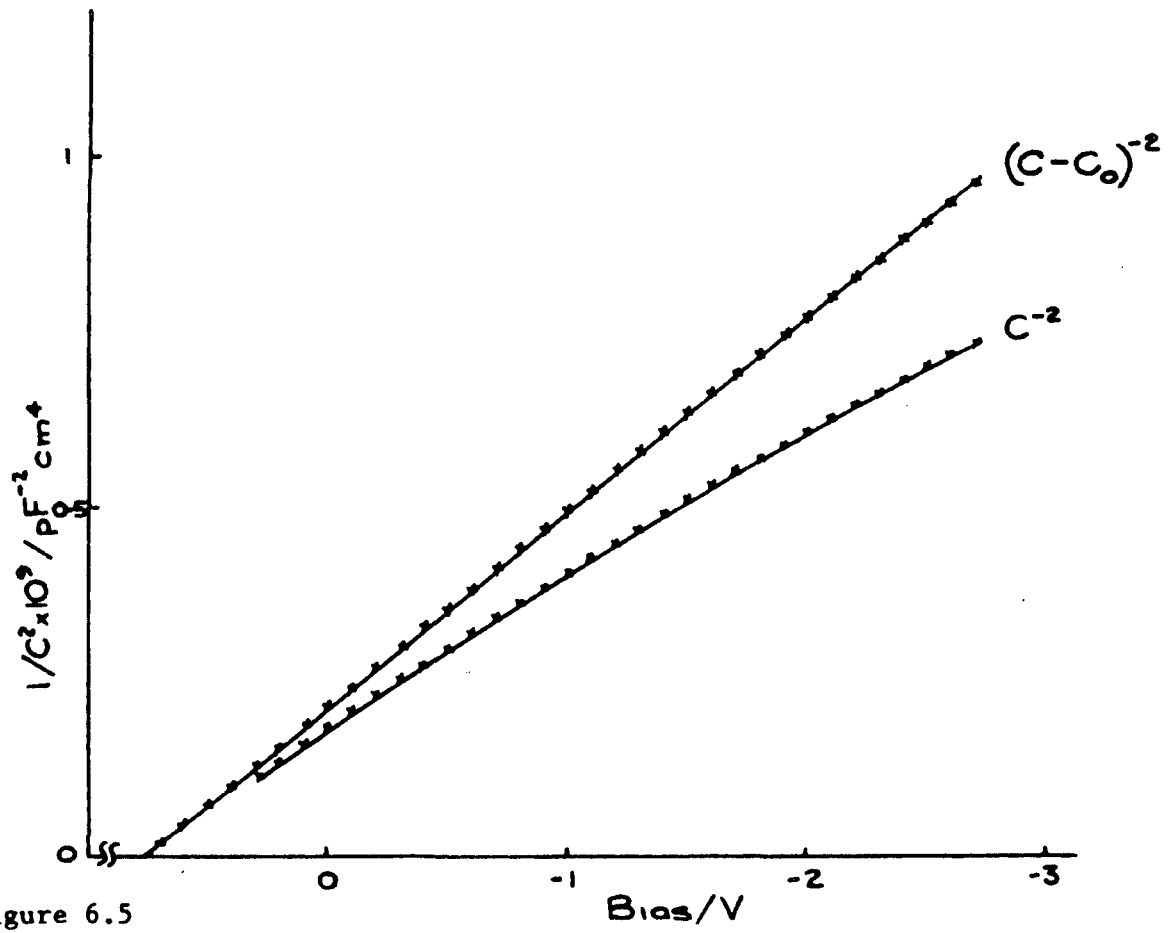

Figure 6.5

$1/C^2$ versus bias characteristics of a near-ideal Au-n-GaAs Schottky barrier. The lower curve is the experimentally observed behaviour, and the upper one is corrected according to the theory of Pellegrini and Salardi[3] (see text). (contact area = .013 cm^2)

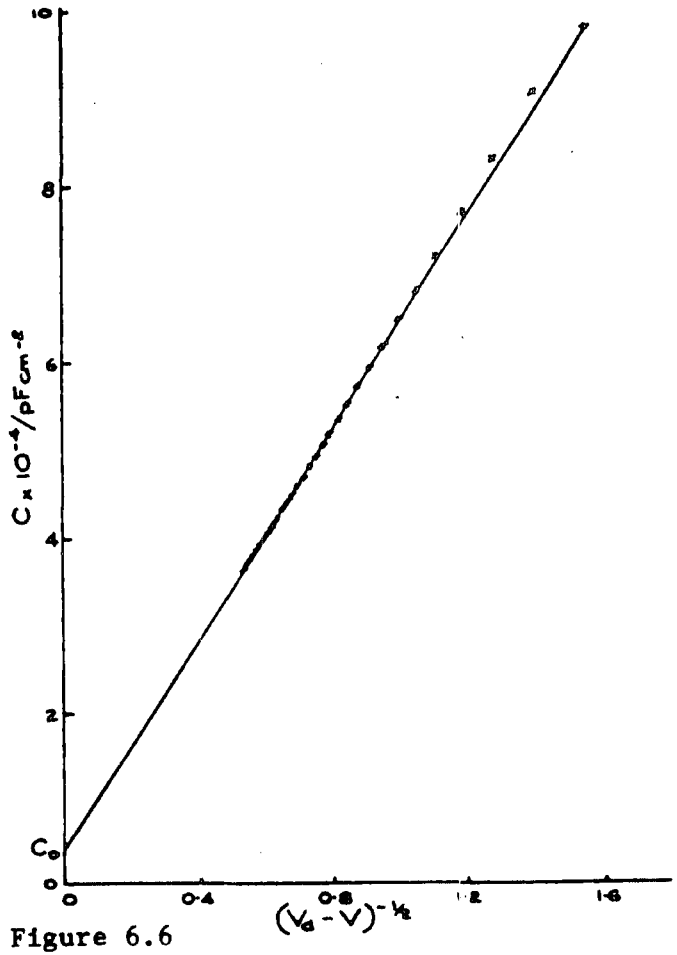

Figure 6.6

Graph showing capacitance as a function of $(V_d-V)^{-\frac{1}{2}}$ for a near-ideal Au-n-GaAs Schottky barrier. This is used to find the 'excess capacitance' (see text). (contact area = .013 cm^2)

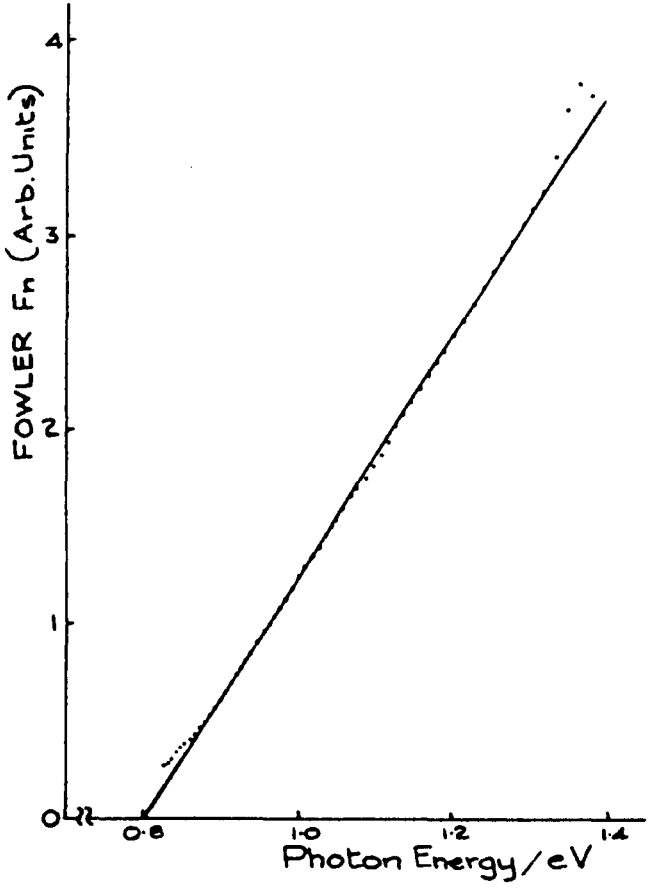

Figure 6.7

Fowler plot of the photoresponse of a near ideal Au-n-GaAs Schottky diode. The intercept on the energy axis gives the barrier height.

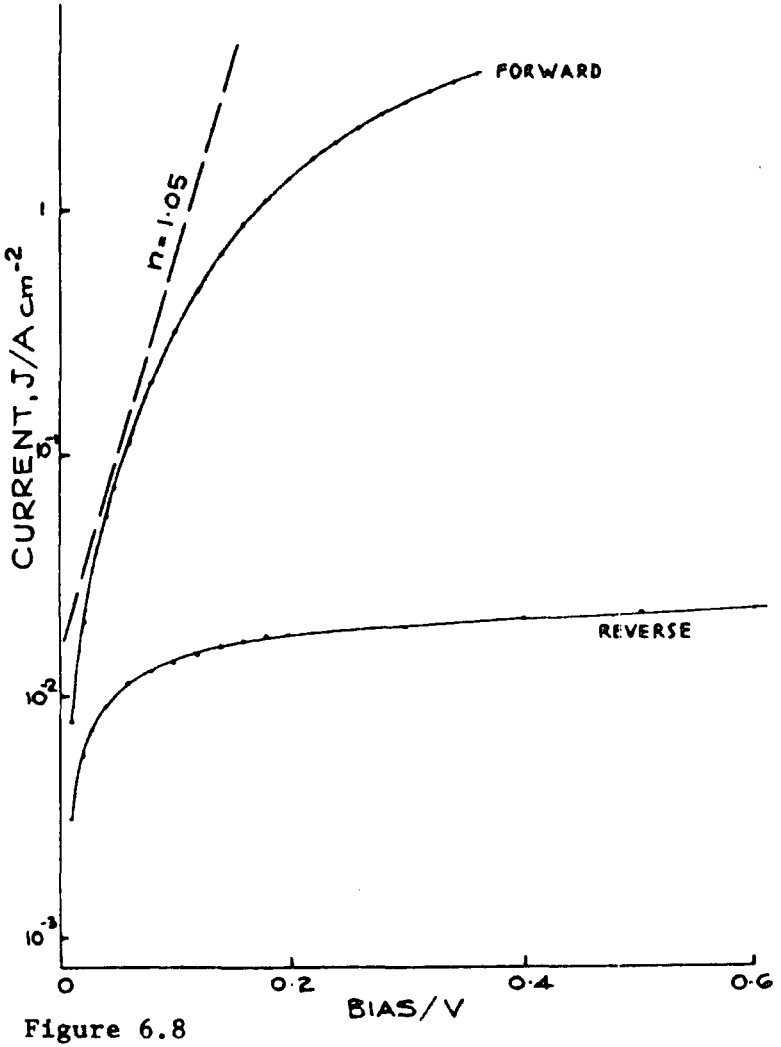

Figure 6.8

Current-voltage characteristic of a near-ideal Au-p-GaAs Schottky diode. The dashed line shows the forward bias characteristic corrected for a series resistance of 4.5Ω. (contact area = .013 cm^2)

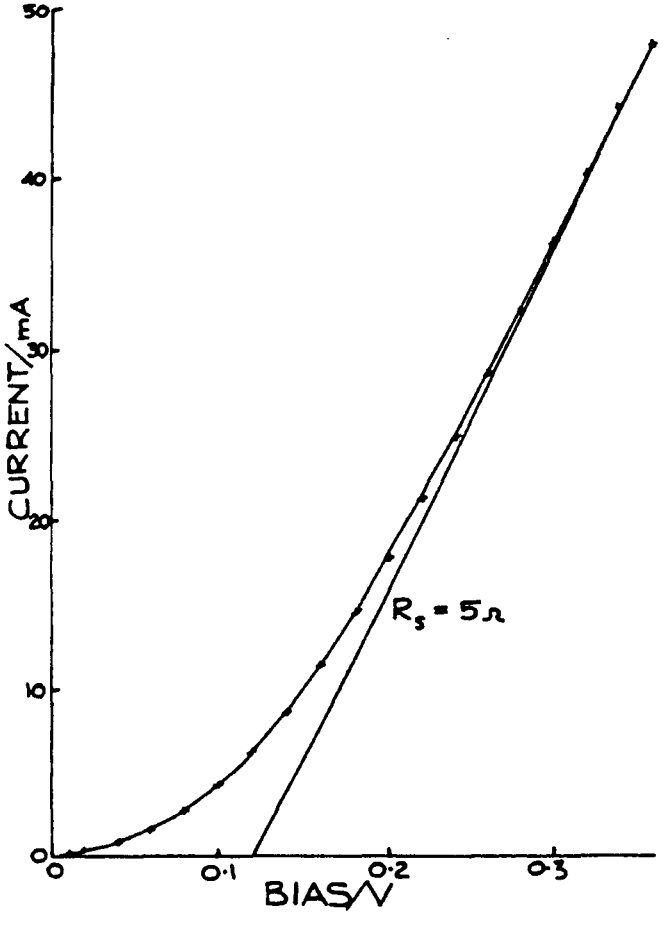

Figure 6.9

Forward bias current-voltage characteristic of a near-ideal Au-p-GaAs Schottky diode. The series resistance is less than 5Ω. (contact area = .013 cm^2)

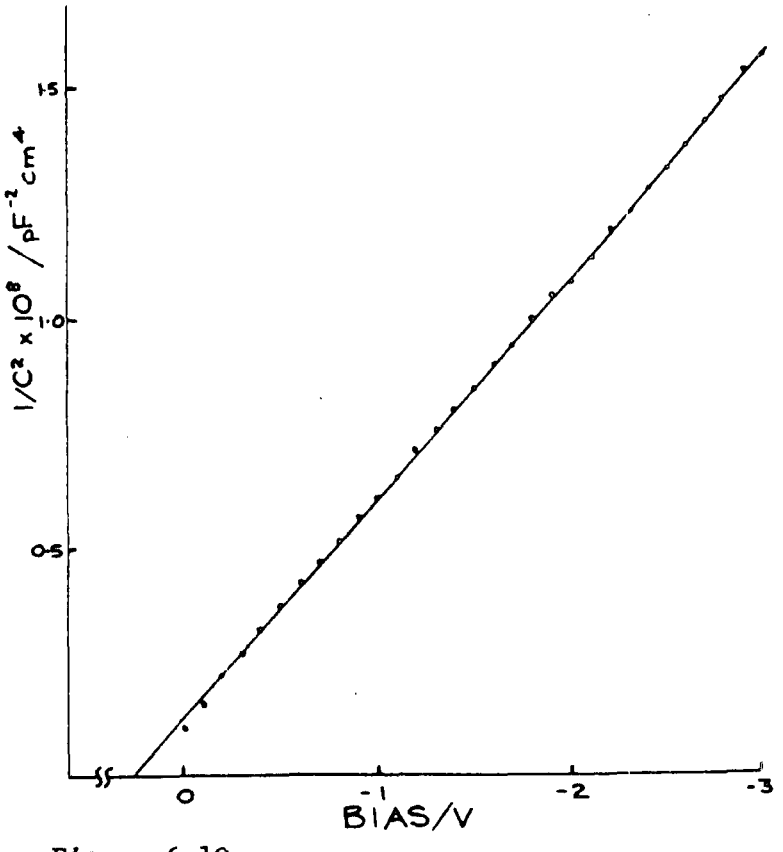

Figure 6.10

$1/C^2$ versus bias characteristic of a near-ideal Au-p-GaAs Schottky diode. (contact area = .013 cm^2)

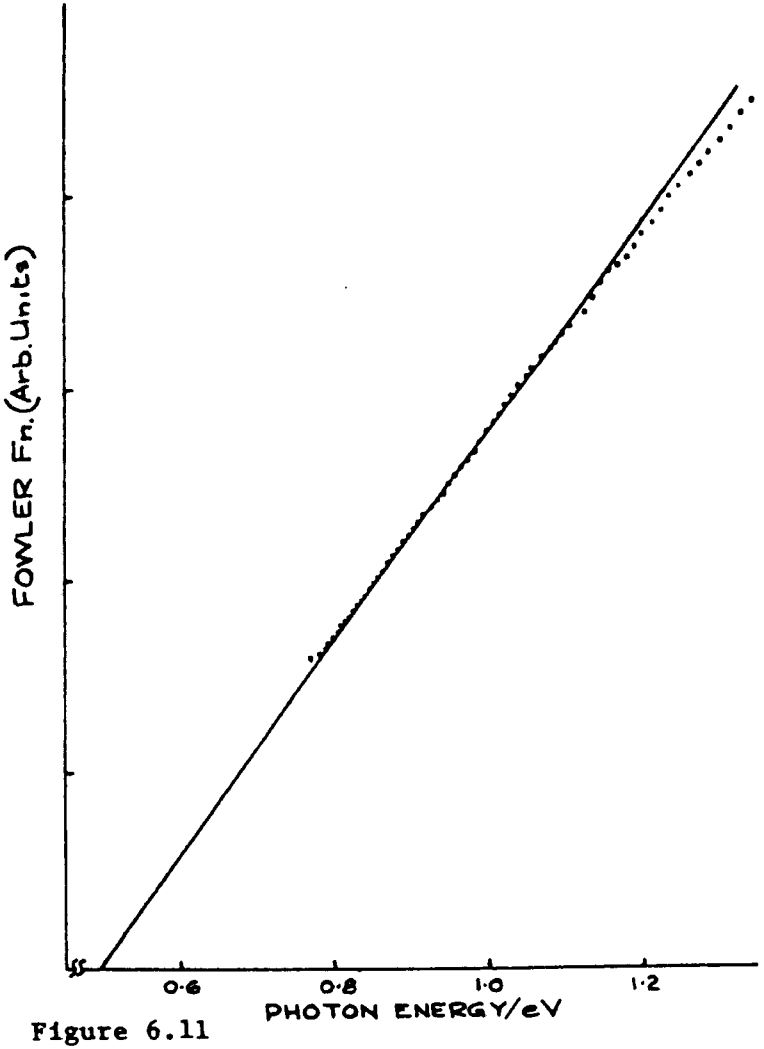

Figure 6.11

Fowler plot of the photoresponse of a near-ideal Au-p-GaAs Schottky diode at 200 K. The intercept on the voltage axis gives the barrier height.

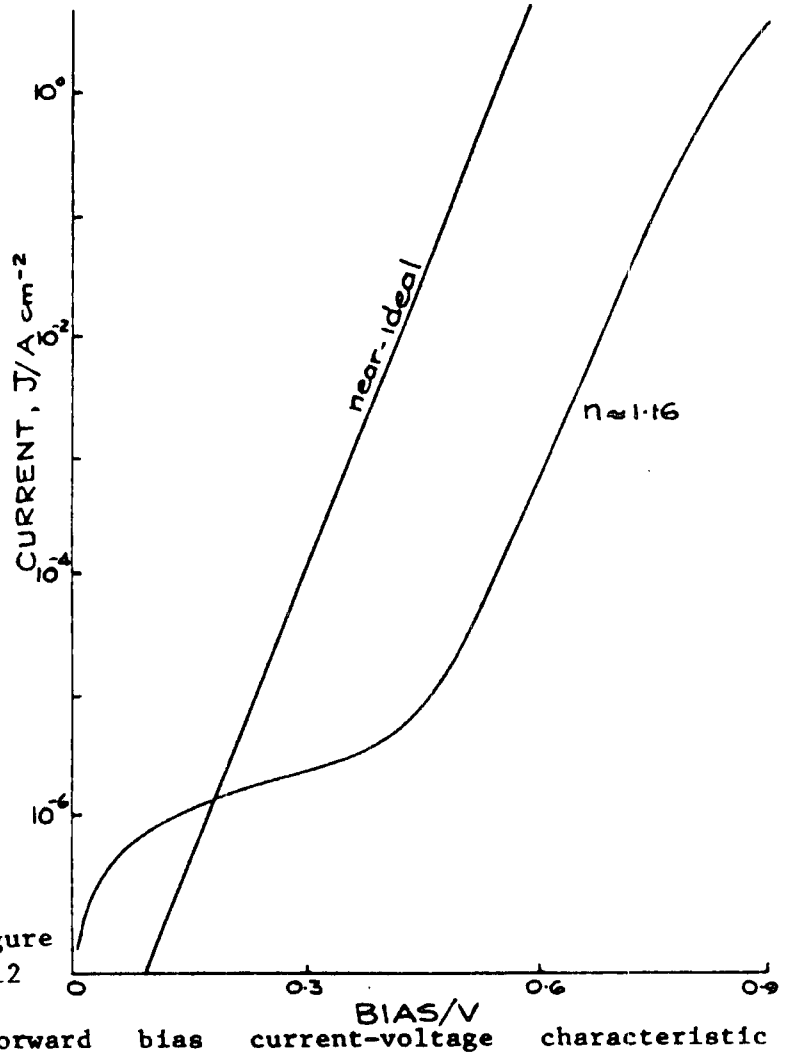

Figure 6.12

Forward bias current-voltage characteristic for a non-ideal Au-n-GaAs Schottky diode, which was prepared by omitting the hydrochloric acid treatment (see text). The characteristic of a near-ideal Au-n-GaAs diode is also shown for comparison. (contact area = 2×10^{-3} cm^2)

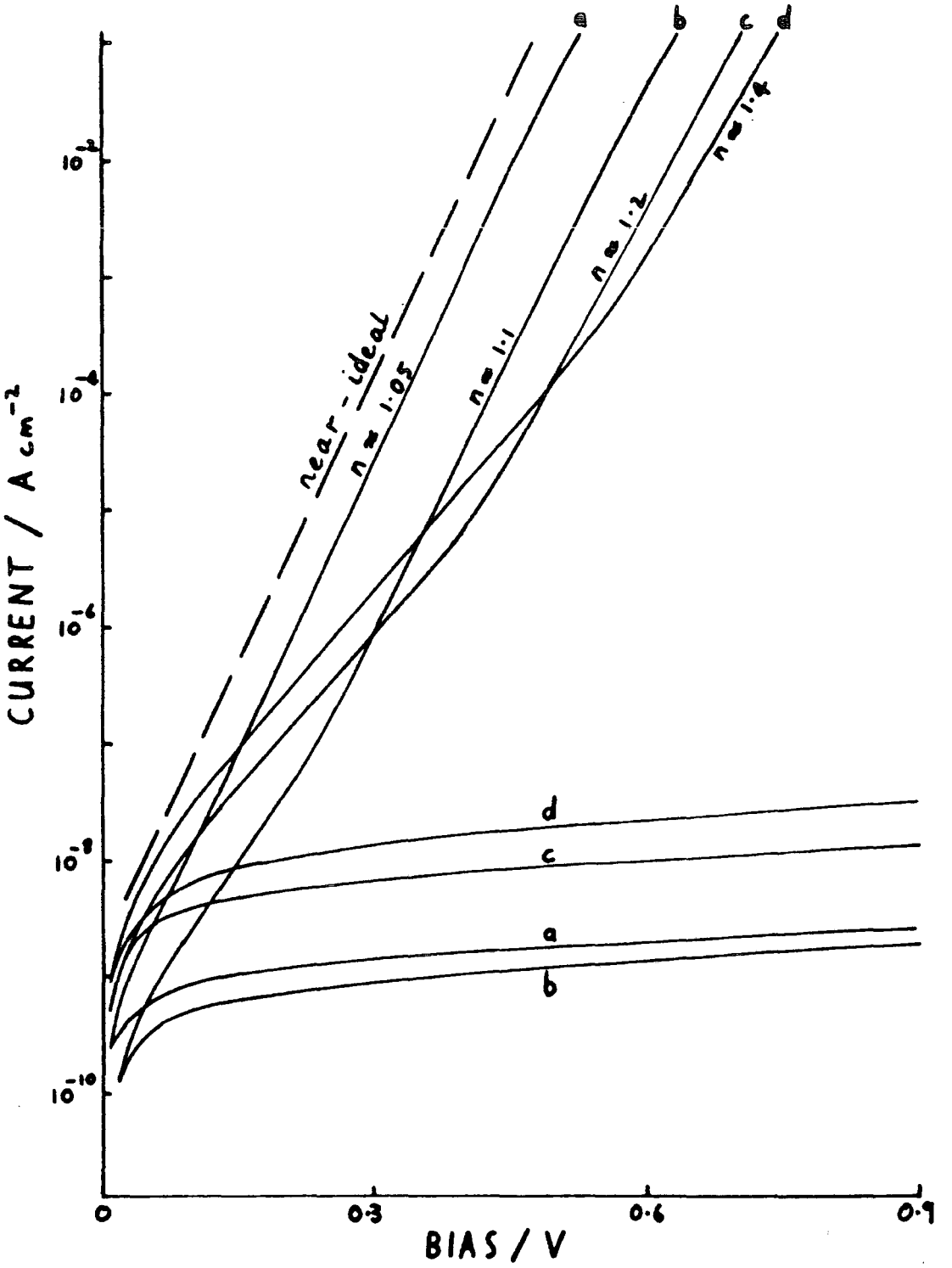

Figure 6.13 Current-voltage characteristics of Au-n-GaAs Schottky diodes which were subjected to the following surface treatments prior to electrode deposition.

(a) 20 minutes in methanol
(b) 20 minutes in air
(c) 15 minutes in air followed by 5 minutes in 'millipore' water
(d) 10 minutes in air followed by 10 minutes in 'millipore' water.

The forward bias characteristic for a near-ideal Au-n-GaAs Schottky diode is also shown for comparison. (contact areas = 8×10^{-3} cm^2)

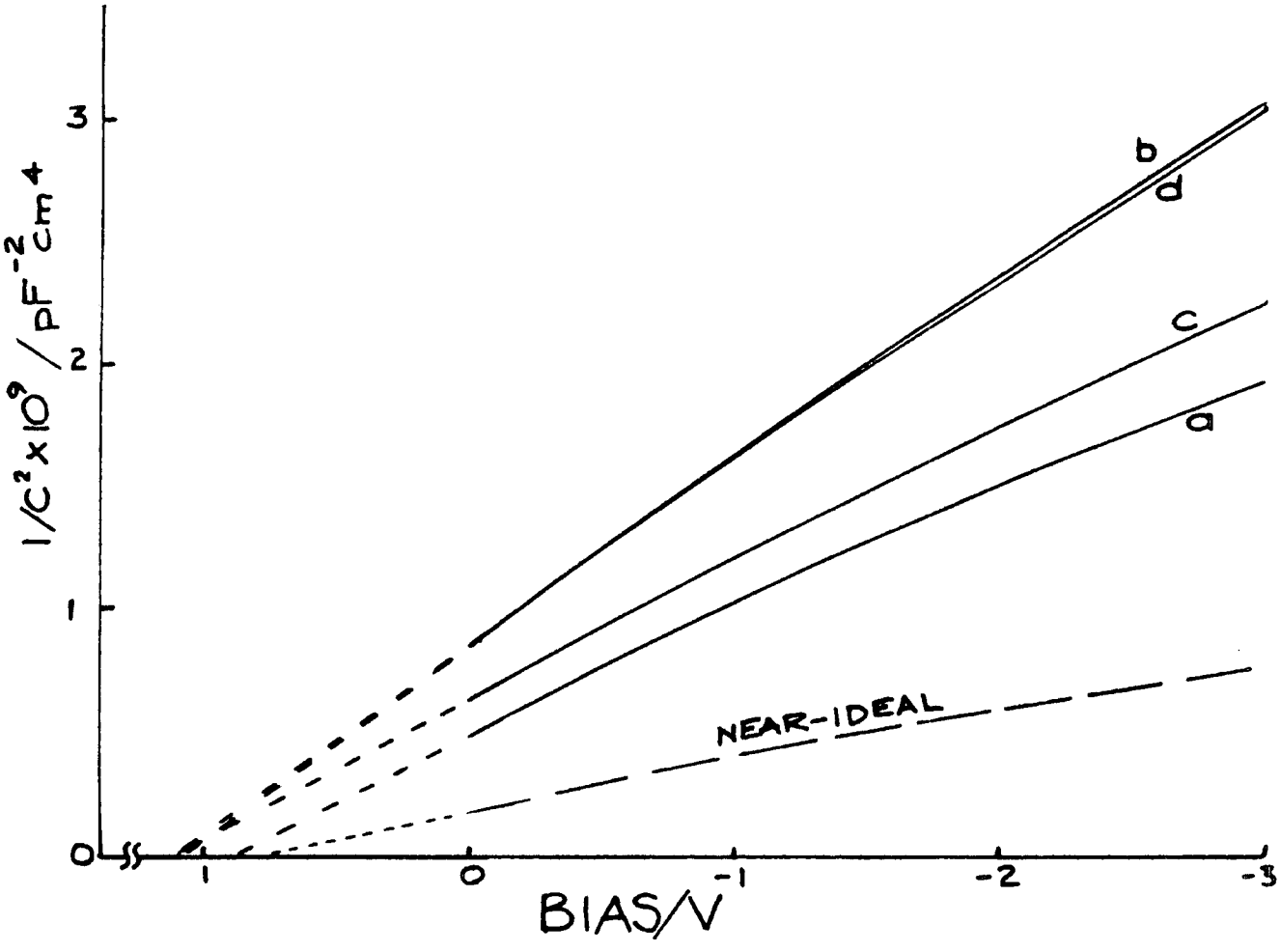

Figure 6.14 $1/C^2$ versus bias characteristics of Au-n-GaAs Schottky diodes subjected to different surface treatments prior to electrode depositon (see text). The characteristic for a near-ideal Au-n-GaAs Schottky diode is also shown for comparison. (contact areas = 8×10^{-3} cm^2)

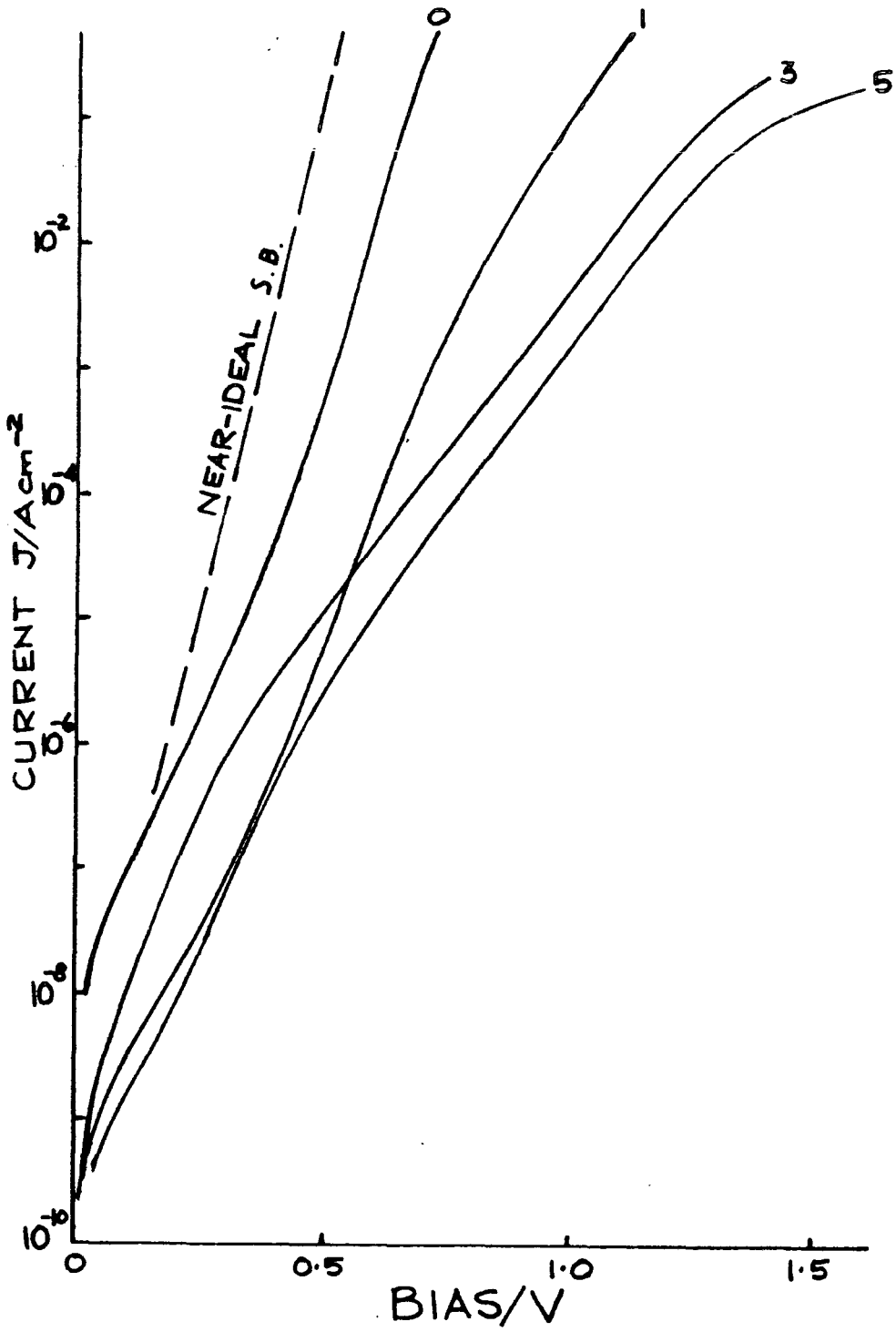

Figure 6.15 Forward bias current-voltage characteristics of LB film/n-type GaAs MIS diodes incorporating 1, 3 and 5 monolayers of ω-tricosenoic acid. The device marked '0' was on an area not coated with an LB film (see text). The characteristic of a near-ideal Au-n-GaAs Schottky barrier is also shown for comparison. (contact areas = 2×10^{-3} cm^2)

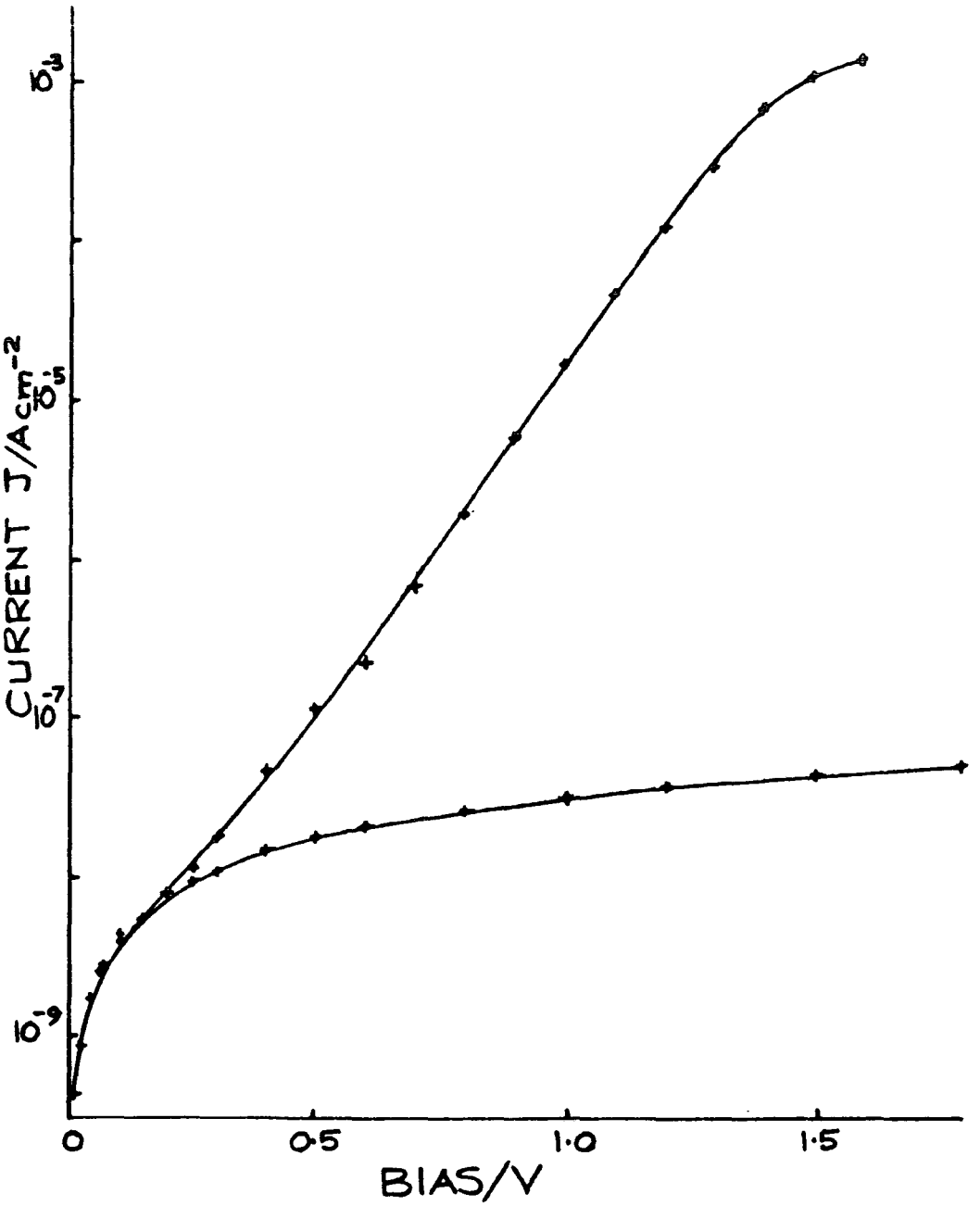

Figure 6.16 Current-voltage characteristic of an LB film/n-type GaAs MIS diode incorporating an 11 layer ω-tricosenoic acid film. (contact area = 2×10^{-3} cm^2)

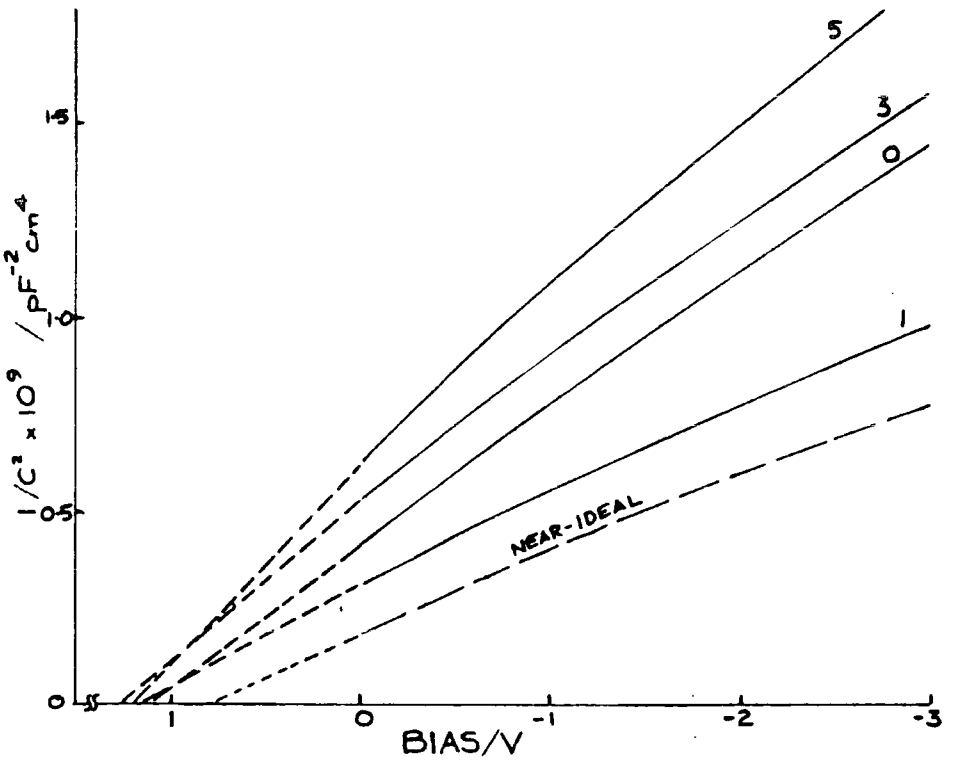

Figure 6.17 $1/C^2$ versus bias characteristics of LB film/n-type GaAs MIS diodes incorporating 1, 3 and 5 layers of ω-tricosenoic acid. The '0' layer device was on an area not coated with an LB film (see text). The characteristic for a near-ideal Au-n-GaAs Schottky diode is also shown for comparison. (contact areas = 2×10^{-3} cm^2)

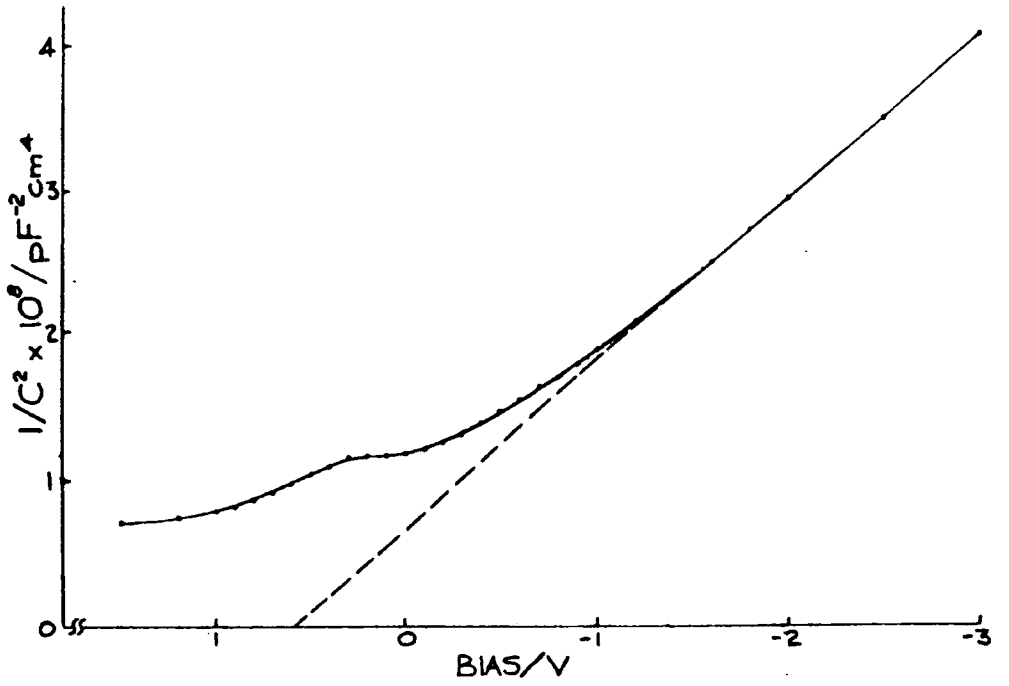

Figure 6.18 $1/C^2$ versus bias characteristic of an LB film/n-type GaAs MIS diode incorporating an 11 layer ω-tricosenoic acid film. (contact area = 2×10^{-3} cm^2)

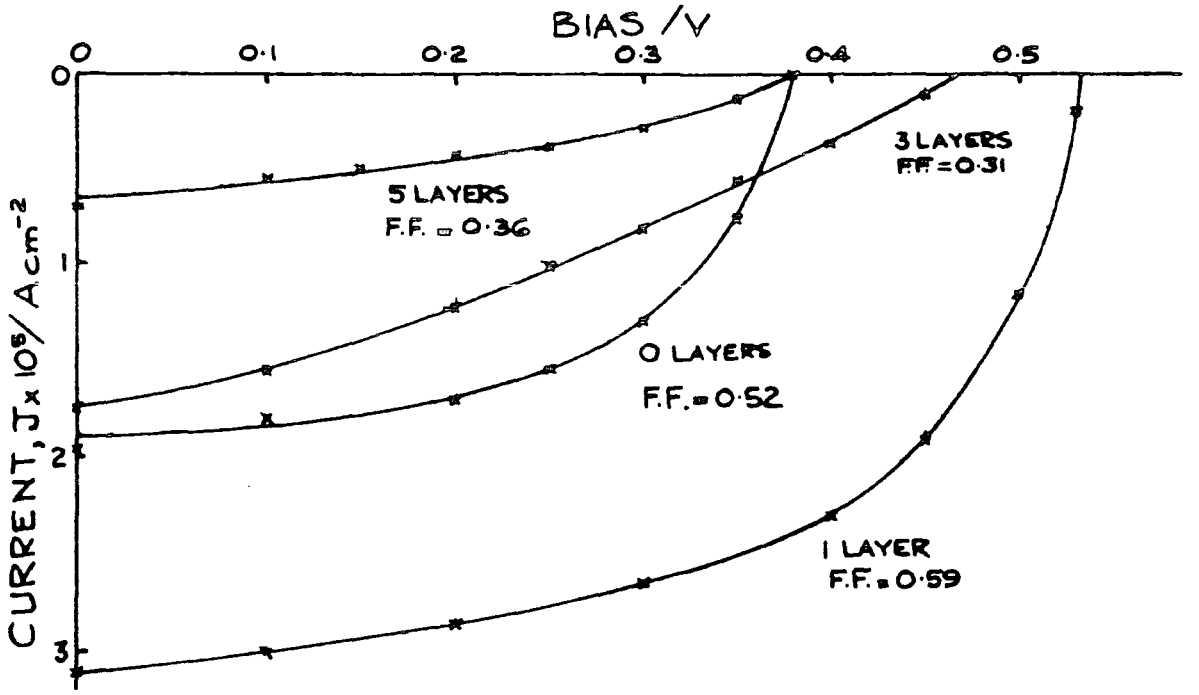

Figure 6.19 Photoelectric characteristics of LB film/n-type GaAs MIS diodes incorporating 1, 3 and 5 monolayers of ω-tricosenoic acid. The device marked '0 layers' was on an area not coated with an LB film (see text). F.F. signifies the fill factor of the characteristic. (contact area = 2×10^{-3} cm^2)

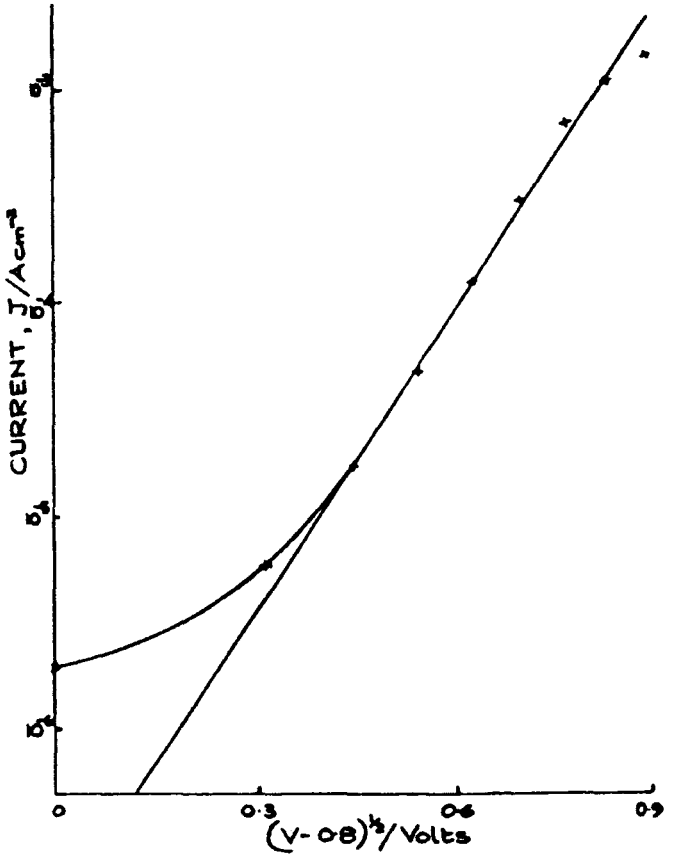

Figure 6.20 High field forward bias conduction in a LB film/n-type GaAs MIS diode incorporating 11 monolayers of ω-tricosenoic acid. The current is plotted as a function of $(V-.8)^{\frac{1}{2}}$, which is proportional to the square root of the field in the LB film (see text). (contact area = 2×10^{-3} cm^2)

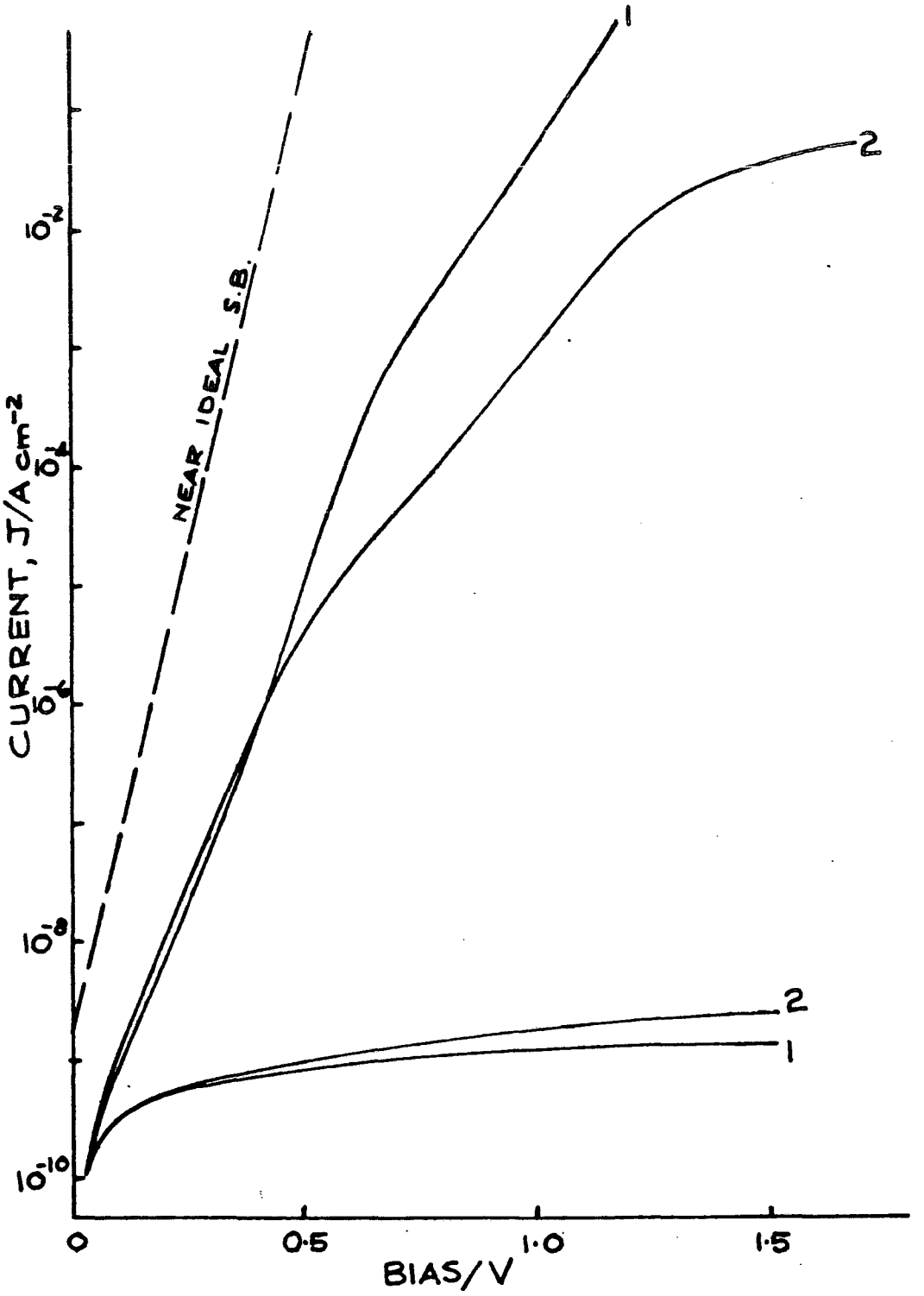

Figure 6.21 Current-voltage characteristics of LB film/n-type GaAs MIS diodes incorporating 1 and 2 monolayer copper phthalocyaine films. The characteristic of diodes incorporating 4 layer films was almost identical to that of the 2 layer device. The characteristic for a near-ideal Au-n-GaAs Schottky barrier is also shown for comparison (contact area = 2×10^{-3} cm^2)

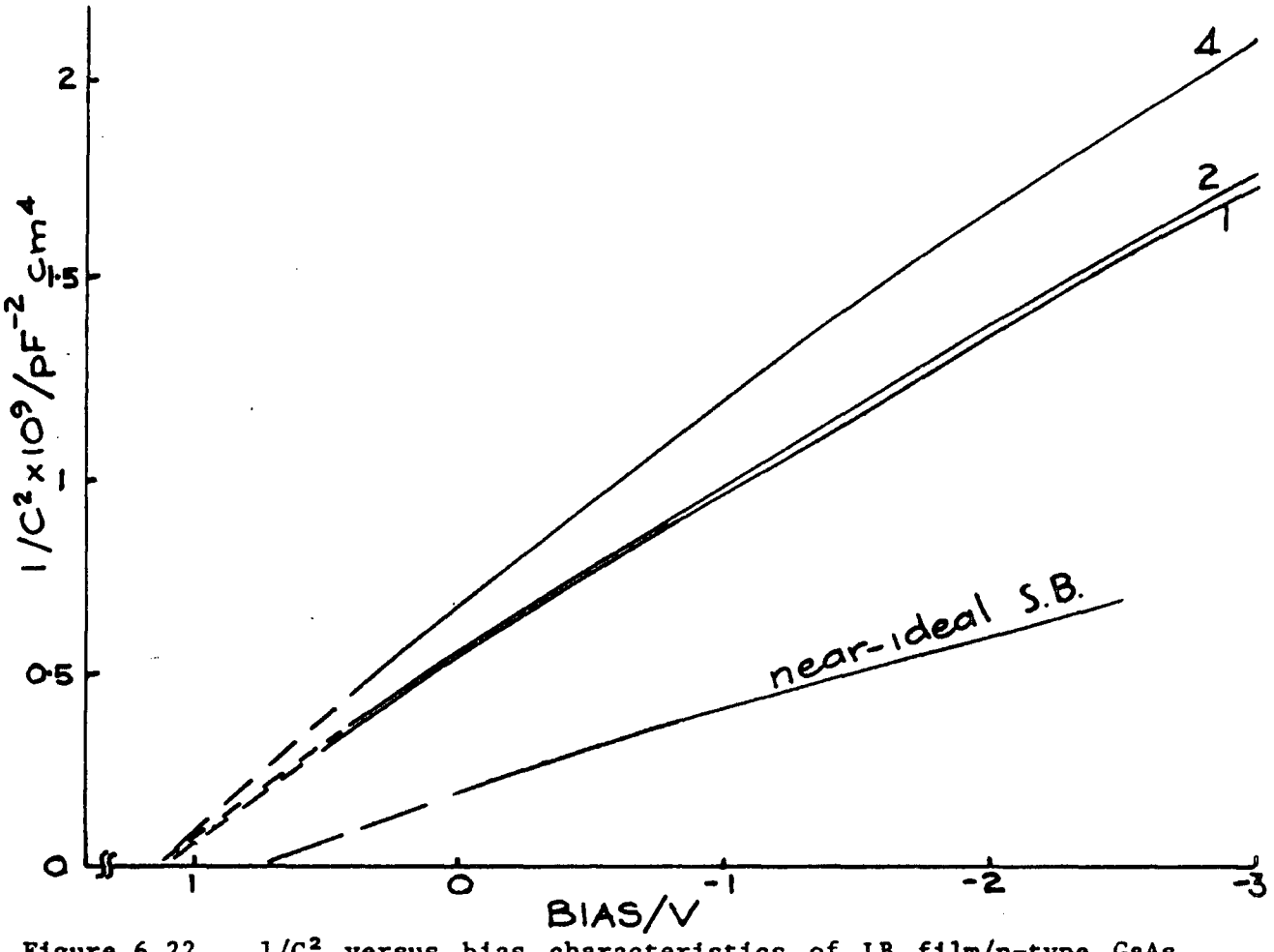

Figure 6.22 $1/C^2$ versus bias characteristics of LB film/n-type GaAs MIS diodes incorporating 1, 2 and 4 layers of copper phthalocyanine. The characteristic of a near-ideal Au-n-GaAs Schottky barrier is also shown for comparison. (contact area = 2×10^{-3} cm^2)

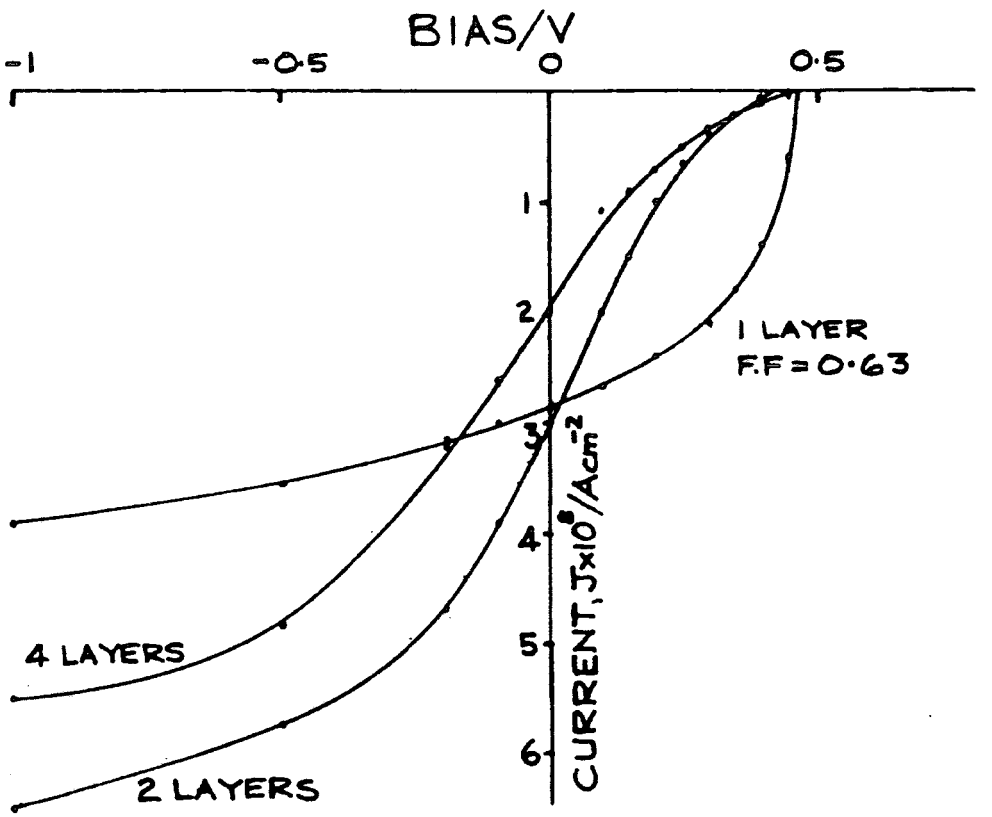

Figure 6.23 Photoelectric characteristics of LB film/n-type GaAs MIS diodes incorporating 1, 2 and 4 layers of copper phthalocyanine. F.F. signifies the 'fill factor' of the characteristic. (contact area = 2×10^{-3} cm^2)

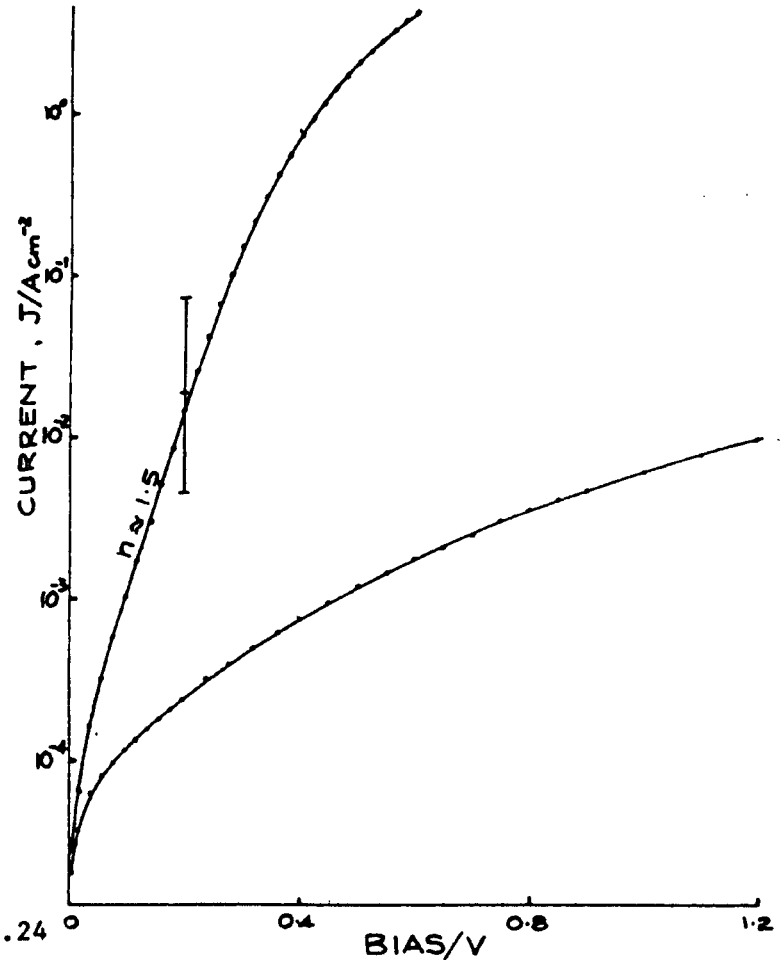

Figure 6.24

Current-voltage characteristic of a Type A LB film/n-type GaInAs MIS diode incorporating a monolayer of ω-tricosenoic acid. The error bar indicates the extent of the variations between contacts on a sample. (contact area = 8×10^{-3} cm^2)

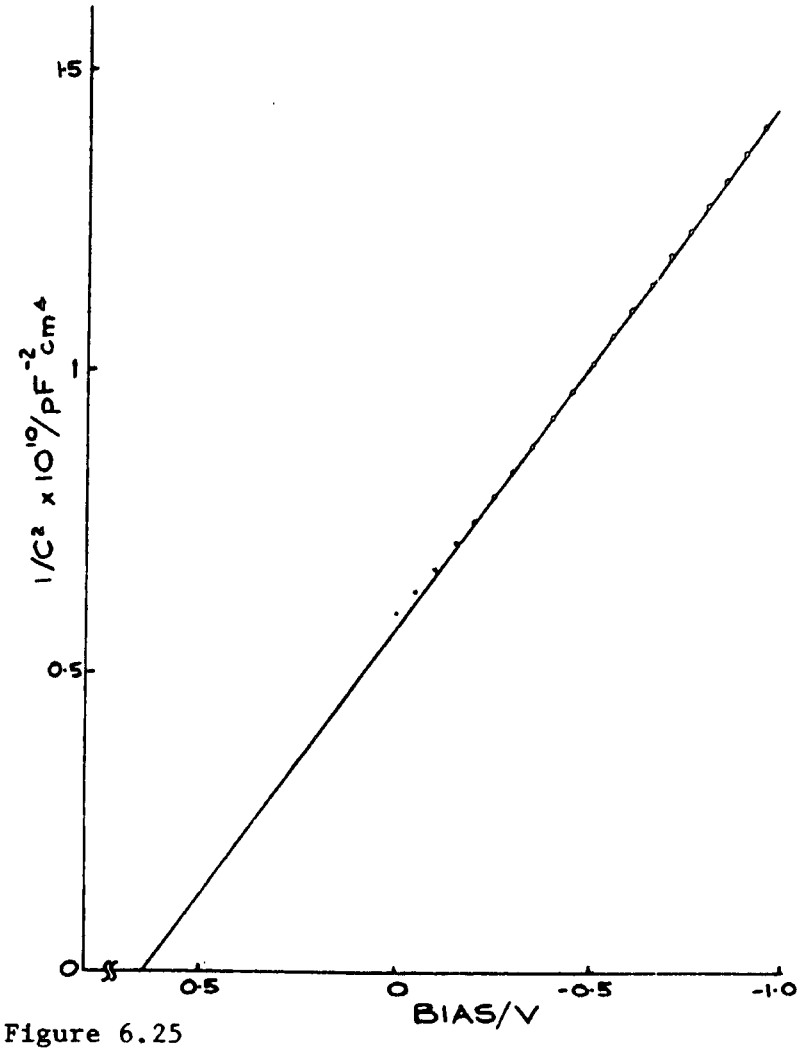

Figure 6.25

$1/C^2$ versus bias characteristic of a Type A LB film/n-type GaInAs MIS diode incorporating a monolayer of ω-tricosenoic acid. (contact area = 8×10^{-3} cm^2)

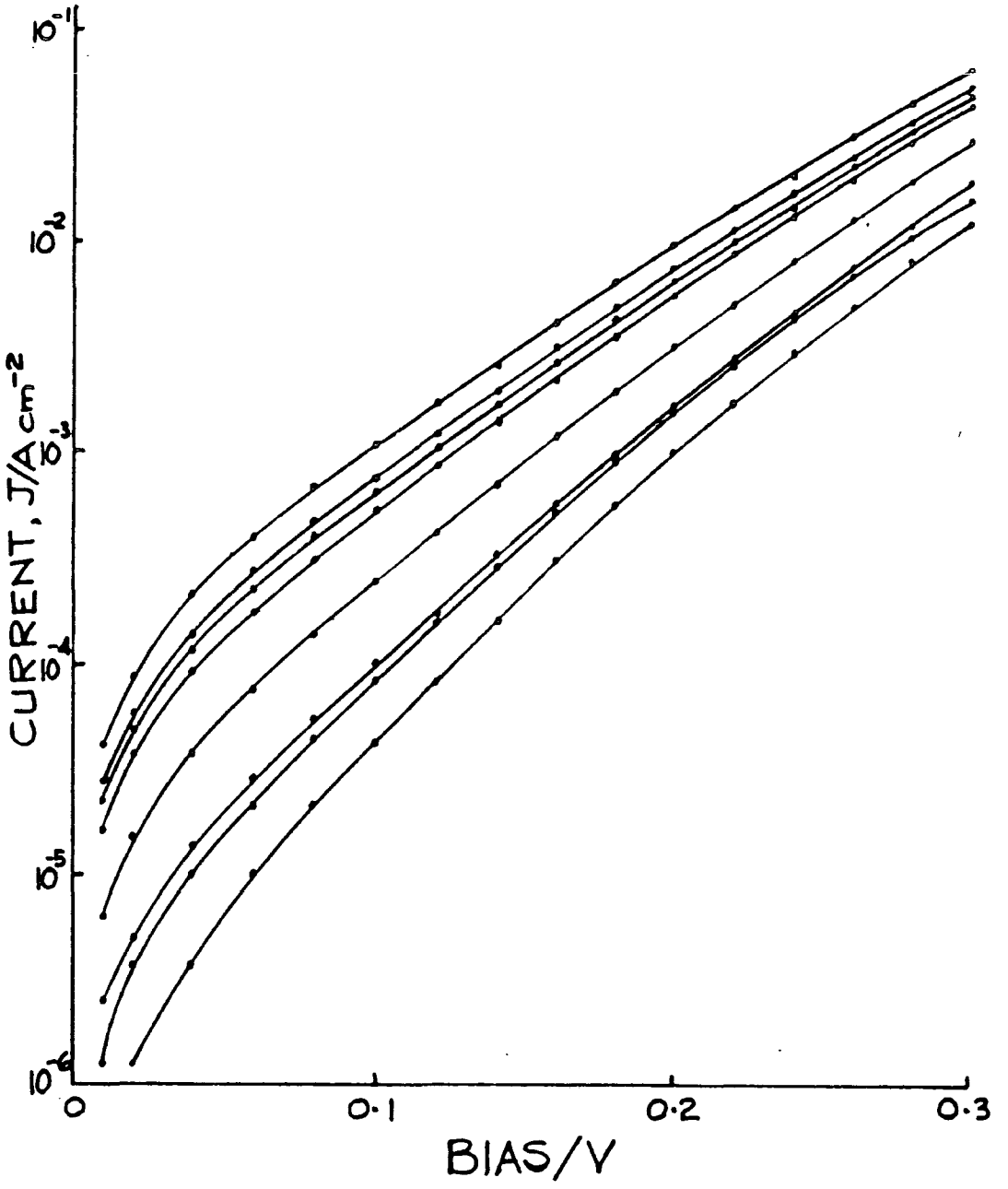

Figure 6.26 Forward bias current-voltage characteristics of a Type A LB film/n-type GaInAs MIS diode incorporating a monolayer of ω-tricosenoic acid as a function of temperature. The measurement temperatures were 300K, 290K, 280K, 270K, 250K, 230K, 215K and 200K, going from the top curve to the bottom one. (contact area = 8×10^{-3} cm^2)

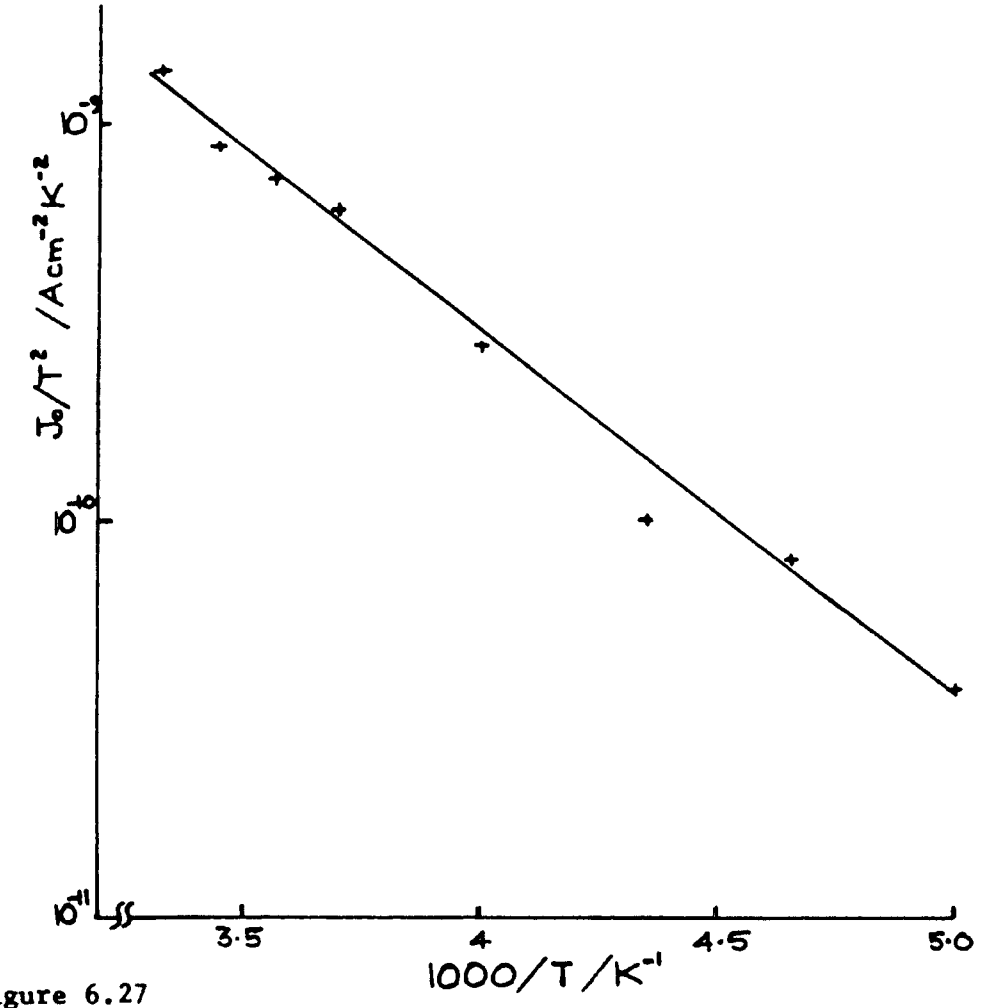

Figure 6.27

Activation energy diagram for a Type A LB film/n-type GaInAs MIS diode incorporating a monolayer of ω-tricosenoic acid.(contact area = 8×10^{-3} cm^2)

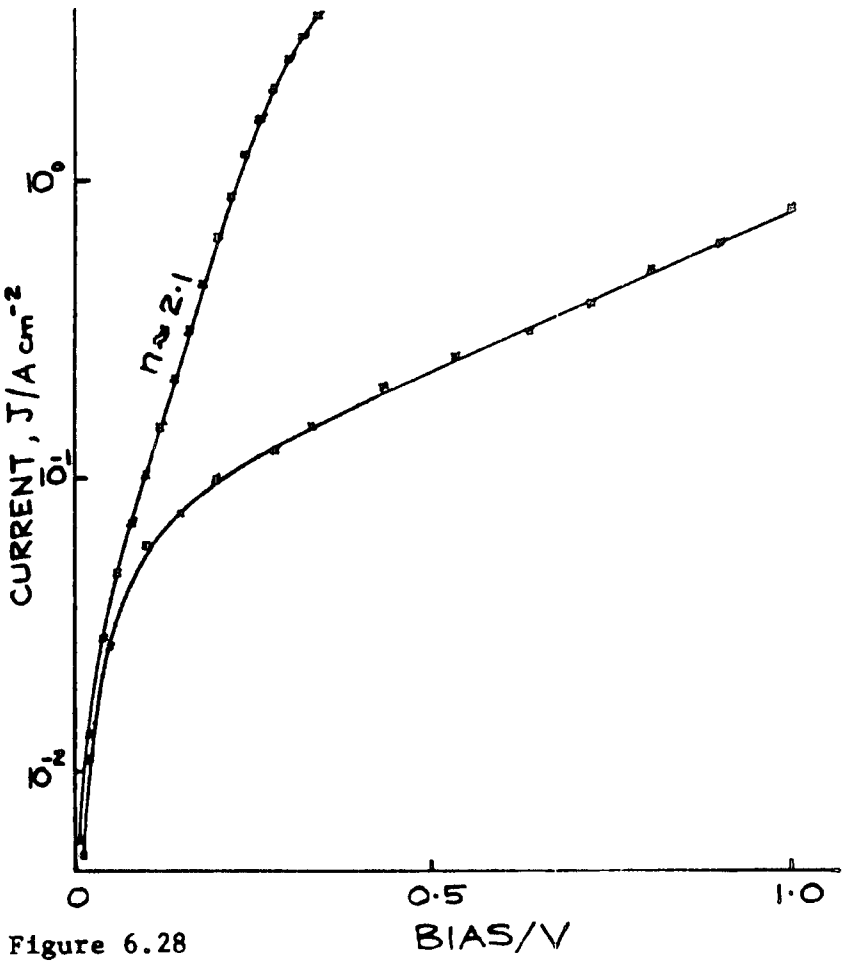

Figure 6.28

Current-voltage characteristic of a Type B LB film/n-type GaInAs MIS diode incorporating a monolayer of ω-tricosenoic acid. (contact area = .013 cm^2)

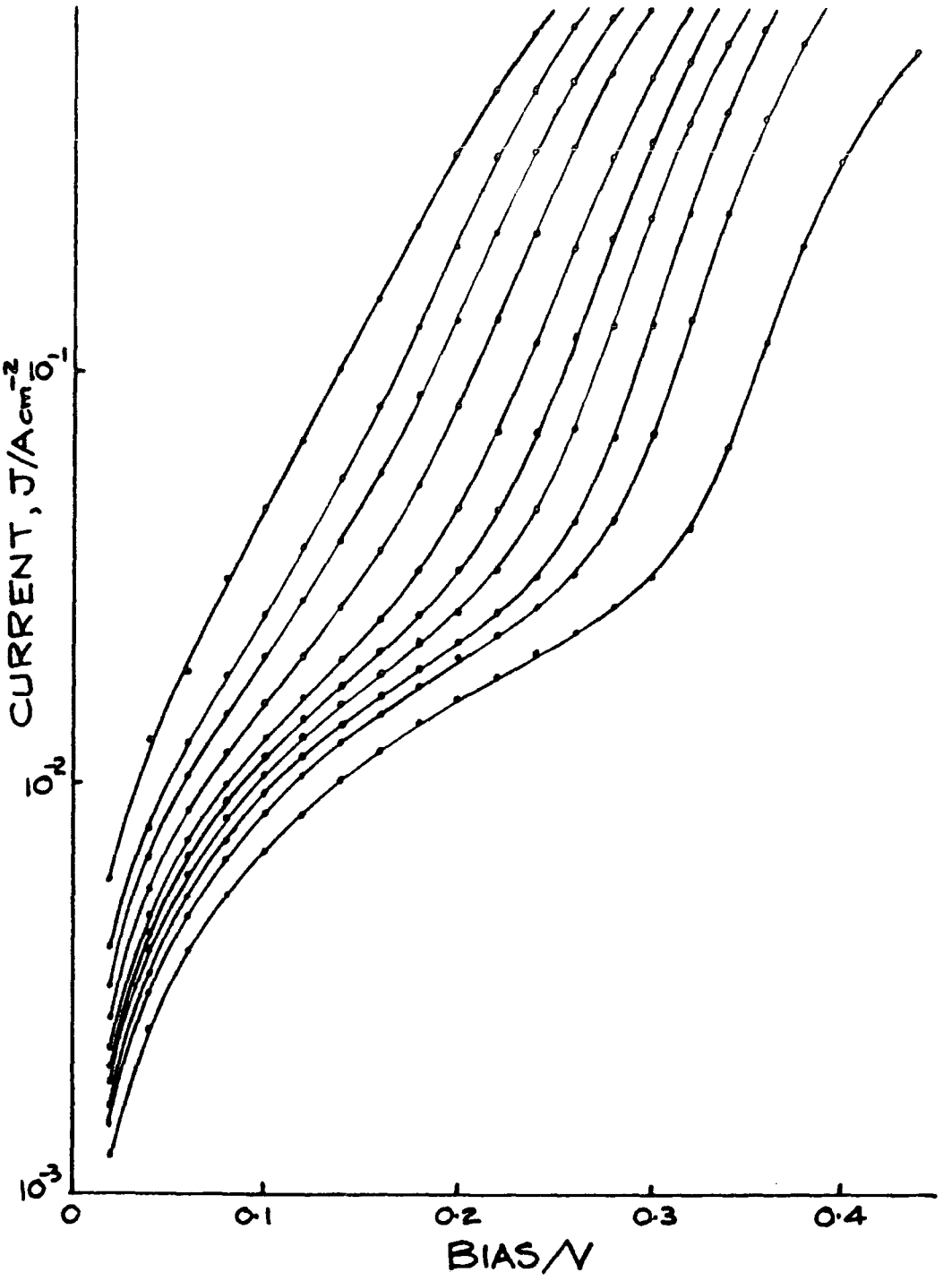

Figure 6.29 Forward bias current-voltage characteristics of a Type B LB film/n-type GaInAs MIS diode incorporating a monolayer of ω-tricosenoic acid as a function of temperature. The measurement temperatures were 302K, 281K, 262K, 240K, 217K, 197K, 177K, 151K, 127K and 77K, decreasing from the top curve to the bottom one. (contact area = .013 cm^2)

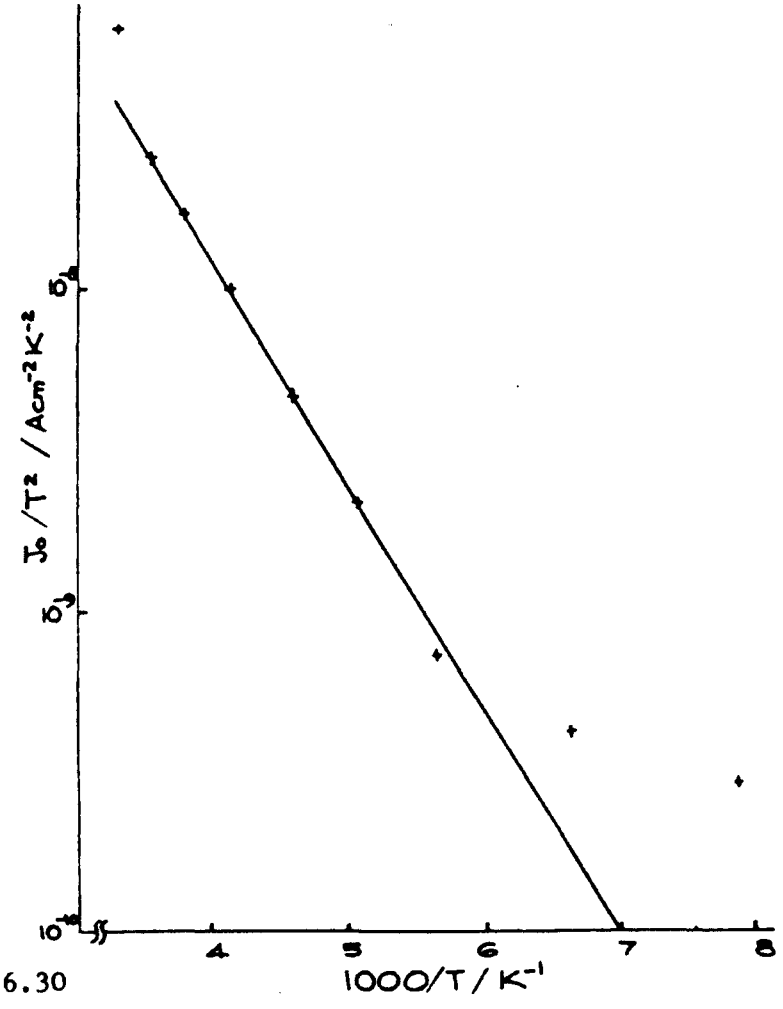

Figure 6.30

Activation energy diagram for a type B LB film/n-type GaInAs MIS diode incorporating a monolayer of ω-tricosenoic acid. (contact area = .013 cm^2)

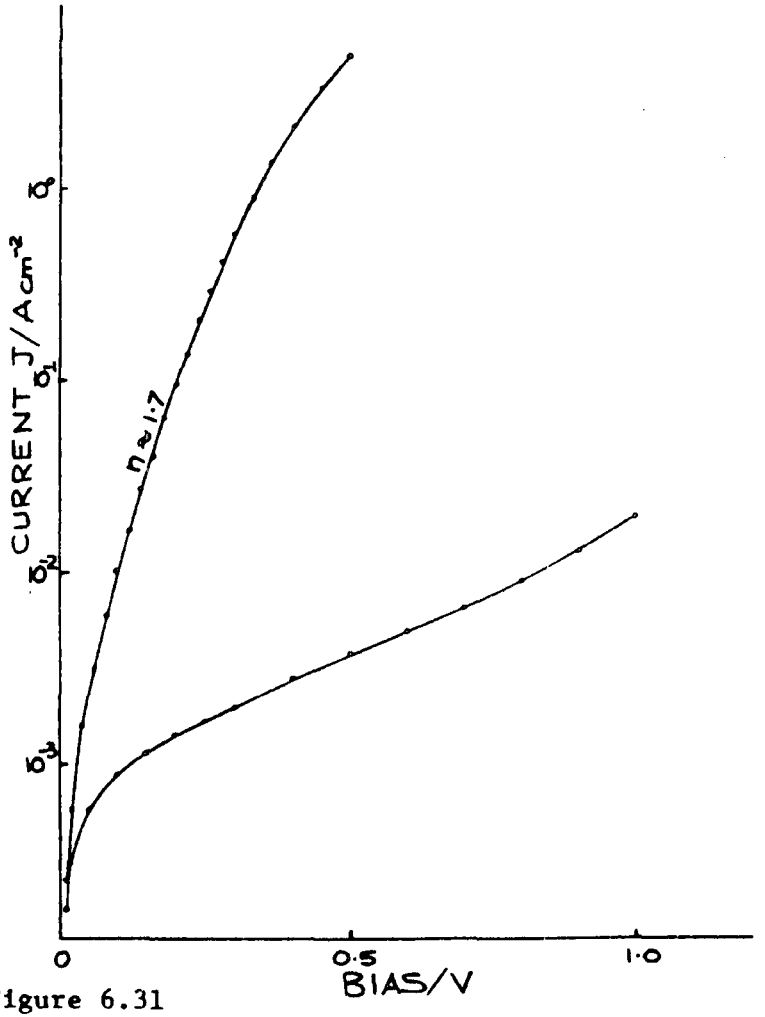

Figure 6.31

Current-voltage characteristic of an LB film/n-type GaInAs MIS diode incorporating a monolayer of copper phthalocyanine. (contact area = $8x10^{-3}$ cm^2)

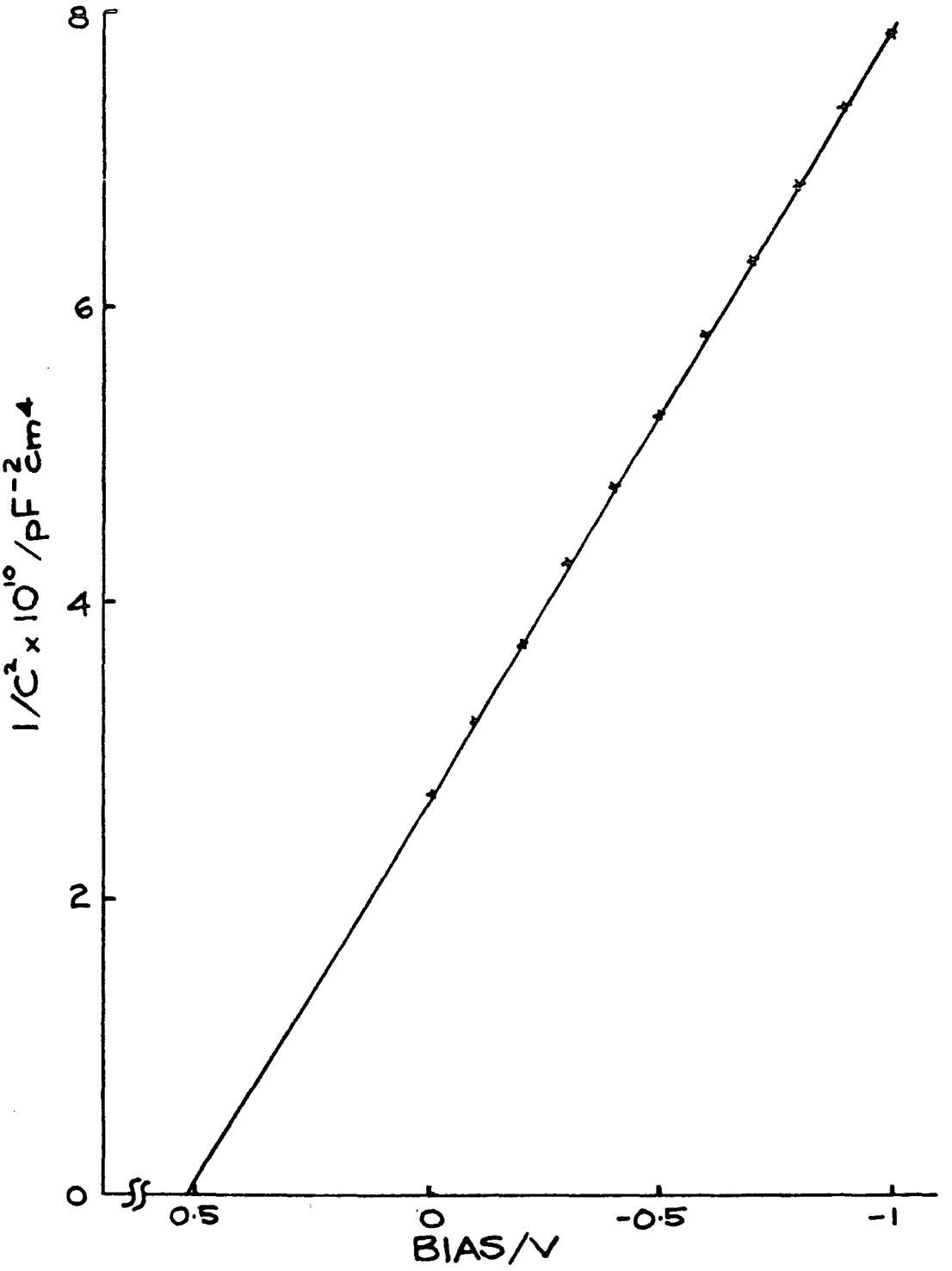

Figure 6.32 $1/C^2$ versus bias characteristic of an LB film/n-type GaInAs MIS diode incorporating a monolayer of copper phthalocyanine. (contact area = 8×10^{-3} cm^2)

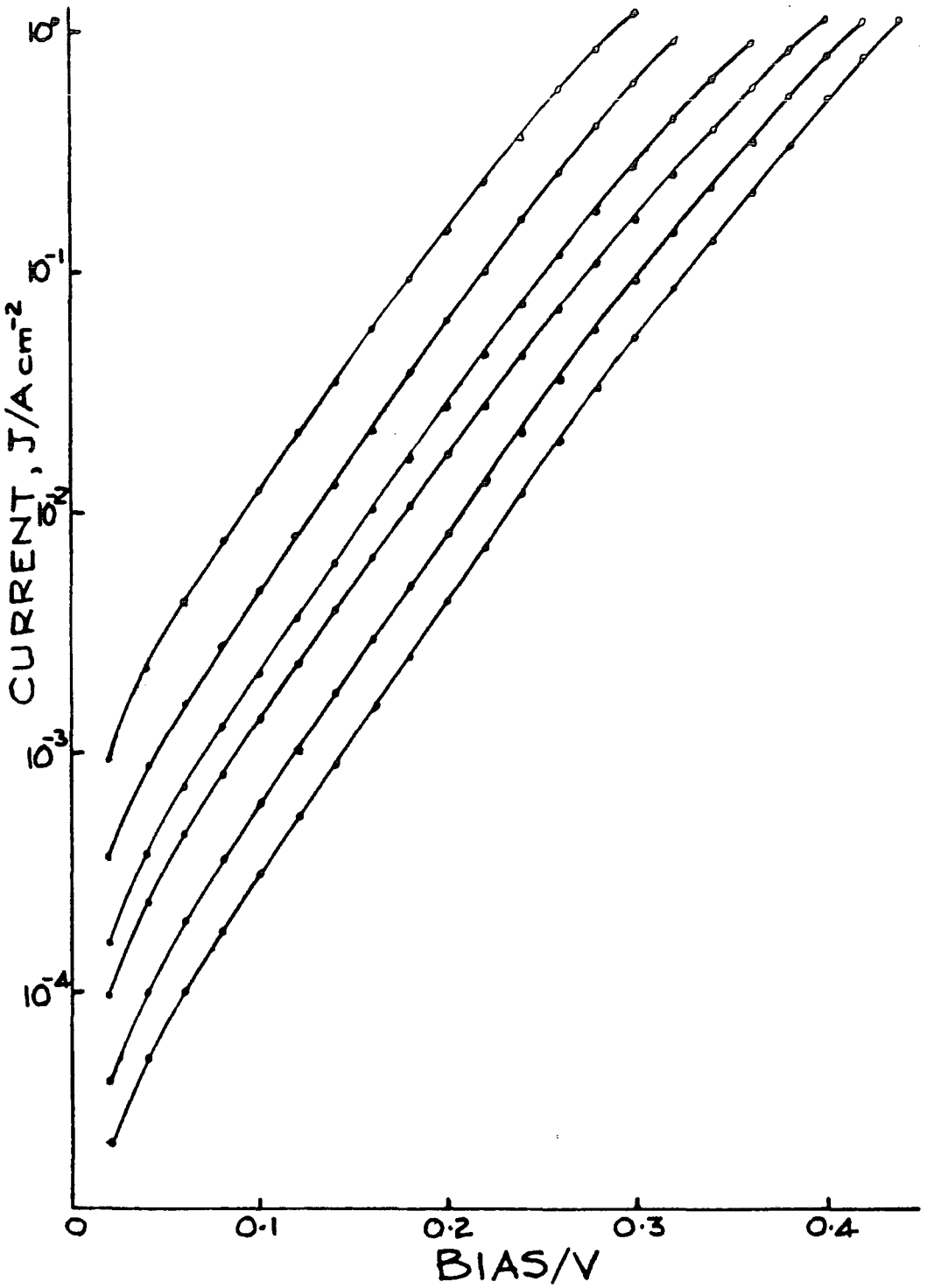

Figure 6.33 Forward bias current-voltage characteristics of an LB film/n-type GaInAs MIS diode incorporating a monolayer of copper phthalocyanine as a function of temperature. The measurement temperatures were 297K, 275K, 255K, 237K, 217K and 201K, decreasing from the top curve to the bottom one. (contact area = 8×10^{-3} cm^2)

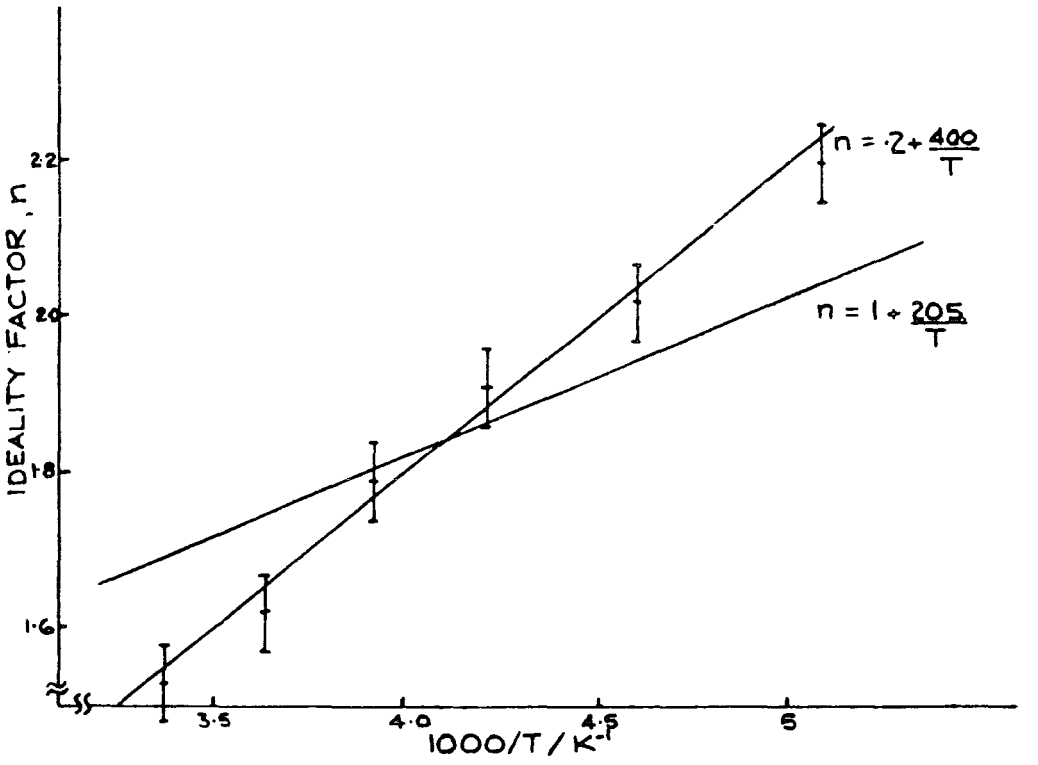

Figure 6.34 Ideality factor, n, of an LB film/n-type GaInAs MIS diode incorporating a monolayer of copper phthalocyanine plotted as a function of temperature.

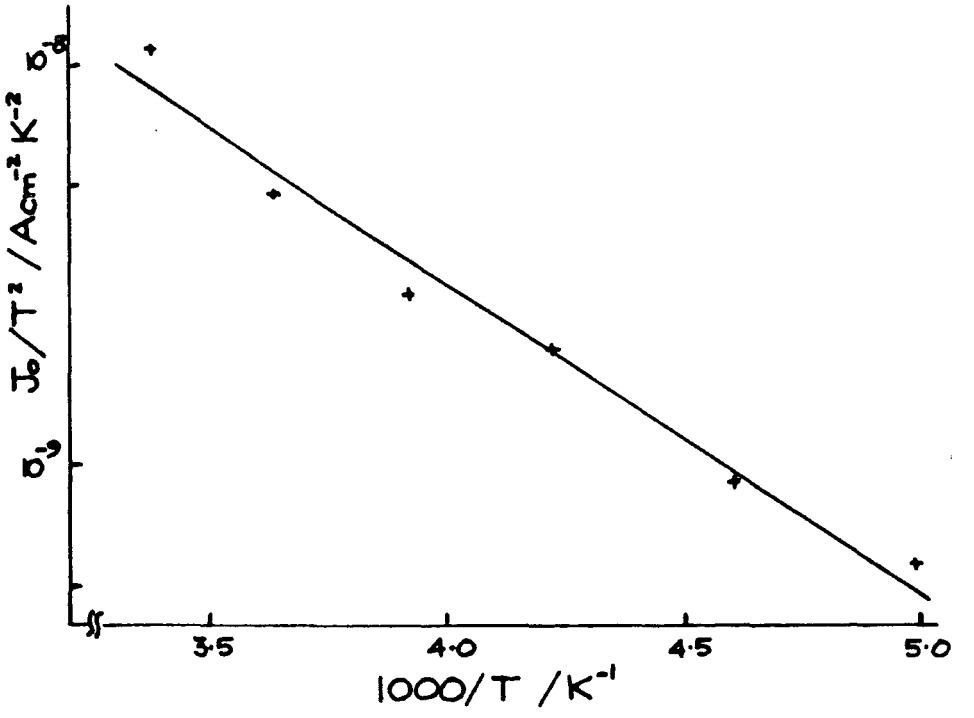

Figure 6.35 Activation energy diagram for an LB film/n-type GaInAs MIS diode incorporating a monolayer of copper phthalocyanine. (contact area = 8×10^{-3} cm^2)

CHAPTER 7

RESULTS AND DISCUSSION - MISS DEVICES

7.1 Introduction

The operation of MISS devices relies upon a thin insulating layer, which must have uniform and reproducible properties. It is well known that there are many problems associated with dielectric layers grown on or deposited on GaAs. The aim of the work reported in this chapter was to circumvent these problems, by the use of LB films, in order that GaAs MISS devices could be produced. The first section covers devices fabricated on n on p^+ GaAs using ω-tricosenoic acid LB films. The characteristics of the devices are studied to determine their dependence on film thickness and the properties of the epitaxial GaAs, which allows the switching mechanisms to be determined. The pulse response of the devices and their reliability are investigated as these are of great importance in practical applications. Devices on the complementary p on n^+ GaAs structure were also studied, although in rather less detail. A preliminary investigation of MISS diodes incorporating phthalocyanine LB films was also carried out. Of particular interest in this case is the effect upon the devices of gases to which phthalocyanines are sensitive, such as NO_2, and it was hoped that a useful sensor could be made. Finally an attempt was made to fabricate LB film MISS devices on silicon, for comparison with the GaAs diodes.

7.2 n-p^+ GaAs/ω-TA MISS Diodes

All the diodes described in this section (and most of those in subsequent sections) were prepared using the procedure described in section 5.3. The evaporated gold contacts were of .5 mm diameter and

approximately 20 nm thickness. The samples were initially examined using a transistor curve tracer, which allowed an impression of the characteristics of the contacts and the variations between them to be obtained. Typical contacts were then examined in more detail using static current-voltage and capacitance measurements. In some cases the dynamic response to a pulsed input was studied. Finally previously untouched contacts were examined in order to characterise the degradation that occurred under operating conditions.

7.2.1 Switching Characteristics

In this section the characteristics of MISS devices incorporating up to 17 monolayers of ω-TA (a thickness of 51 nm), as measured on the curve tracer, are discussed. We commence with a general survey of the results. The effects of changes in the GaAs epilayer are considered next, which then leads into a discussion of the switching mechanism. The effects on the characteristics of varying the thickness of the LB film are also described.

A General Survey

The characteristics of n-p^+ GaAs MISS devices, which incorporate between 1 and 17 monolayers of ω-TA, are summarised in table 7.1. On some samples there were areas which were not coated with an LB film (cf. the '0 layer' devices of section 6.4.1). The characteristics of MISS diodes in these areas were very variable and unstable, of these only a small proportion switched. However, in diodes incorporating a single monolayer of ω-TA no switching was observed. In this case the characteristics were reproducible, with a sharp rise in current occurring above a certain threshold voltage, without any sign of negative resistance. Diodes with LB films of three or more monolayer thickness possessed stable switching characteristics; the yield of switching

contacts on a sample could be as high as 90%. Curve tracer photographs for typical contacts from samples A and C are shown in fig. 7.1 and fig. 7.2 respectively. The characteristics appear to be ideal, with well defined on (low impedance) and off (high impedance) states.

It can be seen from the data in table 7.1 that significant variations occur between the parameters of different contacts on the same sample. These are most marked for the holding current, although the variation of holding voltage is much smaller. The switching voltage was found to vary in a systematic manner across a sample, usually increasing towards one or more of the edges. V_s does not appear to be related to the thickness of the LB film. However, it is evident that it is closely related to the characteristics of the n type epilayer, and increases in the thickness or doping density of the epilayer increased V_s (with the possible exception of sample G).

The characteristics of these MISS diodes were insensitive to illumination by white light. Measurements performed on a contact on sample C in the cryostat also showed a remarkable lack of sensitivity to temperature. Over the temperature range 100 to 300K the variation in switching voltage was insignificant (V_s = 28 ± 1V); in addition no significant changes in holding voltage or current were noted. Despite their insensitivity to temperature and illumination, the characteristics were not completely stable. When a voltage was first applied to a device, it was sometimes observed that the voltage could be increased to slightly greater than V_s, before a sudden and irreversible transition to the type of characteristic shown in fig. 7.1 occurred. This 'forming' was more noticable for thicker LB film layers and it is discussed in section 7.2.2. When devices were operated for a prolonged period a slow increase in holding voltage was noted. This degradation is discussed in section 7.2.5.

Dependence on Epilayer Properties

The dependence of V_s on the properties of the GaAs epilayer and its independence from temperature, illumination and LB film thickness, indicate that switching is probably caused by the punchthrough process (see section 3.2.3). We must discount the avalanche multiplication mechanism for two reasons, because it would produce a temperature dependent V_s (equation 3.11) and also because punchthrough must occur first for these epilayers (cf. equations 3.11 and 3.12). Inspection of equation 3.12 shows that the punchthrough voltage, V_{pt}, increases with increasing epilayer doping and thickness, which is in agreement with the observed trends in V_s. Further support for this punchthrough hypothesis is provided by the systematic variation in V_s across a sample, since LPE epitaxial layers are not usually of uniform thickness.

The hypothesis that switching occurs at punchthrough can be tested by plotting the depletion width, w_d, corresponding to the switching voltage against the thickness of the epilayer, w_e, minus the $n\text{-}p^+$ junction depletion width, w_j. The latter quantity must be calculated for small forward bias; in this case this is arbitarily assumed to be .6 volts. The depletion widths at the semiconductor surface are calculated using equations 3.3 and 3.4 (the zero bias surface potential is assumed to be .8V, equal to the Schottky barrier value). It is also assumed that the potential drop across the LB film is negligible at the switching point.

The plot of w_d against $(w_e - w_j)$ is shown in fig. 7.3 and the corresponding data are given in table 7.1. We must exercise caution in the interpretation of this graph, as there are several possible sources of error. In addition to the inaccurate knowledge of V_s and the approximations made, it should be noted that the supplied values of N_d

and w_e are not as accurate as could be hoped for. This is because these quantities were measured using a mercury probe C-V plotter, which is a relatively inaccurate technique; additional errors could arise because of the variation of epilayer thickness across samples. However, taking these factors into account, the agreement between w_d and $(w_e - w_j)$ at switching is reasonable. The deviation from this is greatest at the extremes of doping densities (samples A, G and H) as might be expected. It seems fairly certain that switching is occurring very close to punchthrough, except perhaps for the relatively heavily doped samples G and H. It is shown in section 7.2.2 that detailed static current-voltage measurements also seem to support this hypothesis.

The relationships between holding current or voltage and the epilayer properties are obscured because they are also functions of LB film thickness. In general a large value of V_H corresponds to a large value of V_s. In addition, I_H appears to increase at higher doping concentrations. However further study is required to clarify the details of these relationships.

Dependence on LB Film Thickness

It is a little easier to interpret the effects of variations in LB film thickness, as it was possible to simultaneously deposit regions of different thickness on a sample (eg. sample E). In this way the independence of V_s from LB film thickness was confirmed. However an increase from 5 monolayers to 11 monolayers caused a large decrease in holding current, which was accompanied by a significant increase in V_H. The other results seem to confirm these trends.

It is not difficult to quantitatively explain this behaviour. As the film thickness is increased then the transport of minority carriers (holes) through the film (from semiconductor to metal) is impeded (cf.

section 6.4.1). Therefore a smaller hole current can sustain the hole concentration at the GaAs surface required to maintain the on state. This implies that the total current at turn off, I_H, is smaller for thicker films, which is in agreement with the observed trend. The dependence of V_H on film thickness can also be easily explained. In the on state a significant fraction of the voltage across the device is sustained by the insulating film. The on state currents in these diodes are all of the same order of magnitude, which implies that the electric fields in the films are also similar. Therefore an increase in film thickness causes an increase in the voltage drop across the device when in the on state. Again we find agreement with the observed trend, despite the simplicity of the proposed explanation.

7.2.2 Static J-V Characteristics

The static current-voltage characteristics of these GaAs/LB film MISS diodes were measured, using a series resistance of between 1 and 20 kΩ, as described in section 5.4.1. This section begins with a description of the off state characteristics, which are explained in terms of the punchthrough model. The characteristics of the heavily doped samples (G and H) are discussed next, including the occurence of 'forming' effects. Finally the characteristics of the negative resistance region are described.

The Off State and the Punchthrough Mechanism

Current-voltage characteristics of typical contacts from samples E_2, F_1 and F_2 are plotted in fig. 7.4 on semilogarithmic axes. Qualitatively similar characteristics were measured for other samples, with the exception of those with heavily doped epilayers (ie. G and H, these are discussed later in this section). Apart from the exceptions noted above, two distinct regions can be seen in the off state. At low bias the

characteristics are similar to those of reverse biased ω-TA/n-GaAs MIS diodes (section 6.4.1). This is not unexpected because a MISS device is basically a reverse biased MIS diode in series with a forward biased p-n junction. The current densities of MIS and MISS diodes were similar in magnitude, as would be expected from the above argument. The increase in current with increasing LB film thickness seen in fig. 7.4 is also consistent with results for the MIS devices described in section 6.4.1. Therefore the low bias characteristics of these MISS devices are dominated by the reverse biased MIS diode component.

In the previous section it was shown that these MISS diodes were switching at, or close to, punchthrough. A rapid rise in current would be expected when punchthrough occurs, because the barrier to hole transport across the p-n junction is suddenly reduced. If the depletion approximation is used to calculate the potential profile then this rise would be expected to occur over a very narrow bias range, since the edges of the depletion region are abrupt. However, it can be seen from fig. 7.4 that the rise in current is much less rapid than would be expected from the above argument. The current in this region could perhaps be attributed to current multiplication in the MIS diode (see section 3.2.1), but this would have to be too weak to cause regenerative feedback, as it would otherwise trigger switching. A more attractive explanation is put forward below, in which the limitations of the depletion approximation are considered.

In the depletion approximation it is assumed that the space charge density falls abruptly to zero at the edge of the depletion region, hence the edge is sharply defined. However this is not possible as the free carrier density cannot fall abruptly to zero. Therefore the depletion region is broadened and the edge becomes poorly defined, because the space charge density falls gradually to zero. This tail region of the

depletion region has been shown to follow an approximately exponential curve[1]; the characteristic length of the exponential tail is the Debye length, L_d, which is given by

$$L_d = \left(\frac{\varepsilon_s \, kT}{N_d q^2} \right)^{\frac{1}{2}} \qquad (7.1)$$

A similar tail will also occur at the edge of the p-n junction depletion region. The effect of this broadening of the edges of the depletion regions is to make punchthrough a more gradual process and so soften the characteristic. For a doping density in GaAs of 8×10^{14} cm^{-3} the Debye length is .15 μm. This is a significant fraction of the epilayer thickness, therefore the punchthrough process will be fairly gradual. This may well account for the shape of the curves seen in fig. 7.4.

In order to test this hypothesis, an n-p^+ GaAs sample was prepared using the standard treatment (section 5.3) and gold Schottky contacts were deposited. This M-n-p^+ structure does not possess any feedback mechanism, due to the absence of an interfacial insulating layer, in contrast to the MISS device (see section 3.2.3), hence switching cannot occur. Thus any deviation from the normal Schottky barrier reverse bias behaviour must be explicable solely as an effect caused by punchthrough. The current-voltage characteristics of the M-n-p^+ diode are plotted in fig. 7.5. At punchthrough, which in this case begins at about 5 volts bias, the characteristic is remarkably similar to those of the MISS diodes shown in fig. 7.4. However, in this case, the slope of the characteristic at high current is steeper than is found for the MISS devices. This is probably due to a fraction of the applied bias being dropped across the LB film in MISS diodes at high currents.

This similarity is convincing evidence that switching occurs at punchthrough and that the off state characteristic can be explained solely in terms of this mechanism. To account for the detailed shape of these characteristics would probably require fairly sophisticated numerical modelling, which is beyond the scope of this initial study.

Heavily Doped Devices

MISS devices on samples G and H, which had comparatively heavily doped epilayers ($N_d > 5 \times 10^{15}$ cm^{-3}), do not appear to conform to the punchthrough behaviour exhibited by the other MISS diodes (see fig. 7.3). The results for these two samples are considered in turn.

For the most heavily doped sample, G, the calculated punchthrough voltage (equation 3.12) was approximately four times the observed switching voltage. This is much greater than the likely error, therefore in this case switching is not due to punchthrough. Static current-voltage measurements (fig. 7.6) appear to confirm this, since the characteristic is markedly different from those shown previously in fig. 7.4. There are no longer two distinct regions in the off state as required by the punchthrough model, instead the current rises slowly until the switching voltage is reached. It is probable that switching in this device is due to the MIS current multiplication mechanism described in section 3.2, which can occur well before punchthrough. However, it is interesting to note that the switching voltage of these diodes was insensitive to illumination, in contrast to previous reports of MISS diodes in which $V_s \ll V_{pt}$ [2].

The behaviour of contacts on sample H was rather complicated and not a little puzzling. As noted in section 7.2.1, it was sometimes noticed that some kind of 'forming' occurred during the initial application of a bias. However, for sample H this effect was very much more marked, as can be seen in fig. 7.7. This shows the off state characteristic of a

contact to sample H_2 as recorded before and after switching the device for the first time. An irreversible change has occurred, causing a significant reduction in the voltage that can be sustained across the device. It is thought that this forming process may be due to the establishment of high current paths through the insulator by a partial breakdown process. This could account for 'forming' being most noticeable for thick LB film layers, because in this case a larger potential drop is required to attain the field required to 'form' the current paths. It is not clear whether this process also occurred for diodes incorporating thin LB film layers, as no evidence of this was observed.

Another pecularity noted for this sample was the substantial difference between the switching voltages determined using curve tracer and from the static J-V measurement. The static current-voltage characteristic of an H_2 contact is plotted in fig. 7.8, which shows a switching voltage which is approximately 4 volts greater than that measured on the curve tracer (for the same contact). The off state characteristic is also a rather strange S shape. As was the case for sample G, switching in these devices does not appear to correspond to punchthrough. The unusual behaviour of contacts on sample H is probably a result of the thick LB film used. It seems that we are close to the practical upper thickness limit for LB films in MISS devices, and the film appears to be unstable under the high electric fields and current densities that occur.

The Negative Resistance Region

Measurements of J-V characteristics can be extended into the negative resistance region by using a large series resistance (i.e. a current source). However, MISS diodes biased in this region can oscillate[3], which may lead to misleading results. Unfortunately the devices were not monitored on an oscilloscope when these measurements

were made and consequently the results must be regarded with a degree of caution.

When a high series resistance was used, a smoothly curved negative resistance region was usually found, as can be seen in fig. 7.6 and fig. 7.9. In the former case (sample G) a distinct region of high negative resistance was noted when the device was measured on the curve tracer using 1kΩ series resistance; this is absent in fig. 7.6. A similar region is shown in fig. 7.10 for a contact on sample C, which was also measured using a low series resistance. It would appear that these 'third states' are an artifact, possibly caused by oscillations. To produce a genuine third stable state an additional feedback mechanism is required[4], for example avalanche multiplication[5]. There does not appear to be any such mechanism in these devices. Therefore the 'third states' frequently noted when using a low series resistance ($\sim$ 1kΩ) are probably not true stable states, but are artifacts caused by oscillations. This may also be the case in many previous reports of 'intermediate states'[6].

7.7.3 Capacitance

As a first approximation, the MISS device in the off state can be modelled as two bias dependent capacitances in series. The first of these is that of the reverse biased MIS diode; this will decrease as bias increases. The other capacitance is due to the p^+-n junction, which is slightly forward biased in the off state. The latter capacitance may be relatively large, especially as the effective junction area may be increased by two dimensional effects, hence its contribution to the total capacitance may be negligible. This model obviously breaks down at punchthrough as the two depletion regions are then no longer separate.

The characteristics of a typical contact on sample E_2 are plotted as $1/C^2$ vs. bias in fig. 7.11; results for other samples were very similar,

as were those for the M-n-p^+ sample described in section 7.2.2. For low bias the characteristic is linear and similar to that of a reverse biased MIS diode. Above 3V the slope increases before the curve flattens out at a constant capacitance (above 5.5 V). Comparison with fig. 7.4 shows that the latter voltage corresponds to the onset of punchthrough. When punchthrough occurs the epilayer is completely depleted and behaves as a dielectric. The capacitance is then between the p^+ substrate and the metal contact, and is approximately constant. Using the capacitance value from this plateau region and assuming the device can be modelled as a parallel plate capacitor, the epilayer thickness is calculated to be 4.6 μm. This agrees fairly well with the supplied figure of 5.35 μm, especially when the approximations used and possible errors are taken into account. This provides yet further evidence that switching in these structures is due to punchthrough.

7.2.4 Pulse Response

The turn on characteristics of contacts on sample D were examined using short pulses of 400 ns duration, at a repetition rate of 8×10^3 s^{-1}, applied through a series resistance of 100Ω (section 5.4.1). Fig. 7.12 and fig. 7.13 show the output of the pulse generator and the voltage across the device, as recorded from an oscilloscope trace, for two different pulse amplitudes (nb. some loading of the pulse generator occurs due to its 50Ω output impedance). As expected, the turn on process becomes more rapid as the applied pulse amplitude is increased (section 3.3.2). The three stages of the turn on process described in section 3.3.2 can be clearly seen in fig. 7.12. They are: (1) capacitive rise time, (2) inversion charge delay time and (3) feedback regeneration time. In fig. 7.13 these three phases cannot be distinguished, because of the limited time resolution of the oscilloscope that was used.

The turn on time is plotted as a function of applied pulse amplitude in fig. 7.14. The shortest turn on time obtained was approximately 40 ns, and the turn off time was of the order of 50 ns. These results are similar to those reported for silicon $n\text{-}p^+$ MISS devices[7]. It is thought that the switching speed is controlled by the transport of minority carriers through the epilayer, therefore the similarity between Si and GaAs is reasonable because their hole mobilities are nearly identical.

7.2.5 Degradation

In section 7.2.1 it was noted that some degradation of the characteristics of these devices occurred under operating conditions, with the most notable change being a gradual increase in holding voltage. A MISS diode on sample C was cycled at 100 Hz to a maximum current of 12mA, using the curve tracer, for a period of $\sim$ 48 hours, which is equivalent to more than 10^7 cycles (nb. the sample was not under vacuum). The holding voltage increased significantly over this period, from 6 to 12.5 V. In addition the holding current varied with time, although this seemed to be around a constant mean value. The change in V_H appeared to occur only during operation; storage under dry nitrogen in a desiccator for periods of several weeks did not cause any deterioration.

The initial investigation of Si MISS devices (section 7.5) showed that they deteriorated much less rapidly in vacuuo. Therefore all subsequent measurements on GaAs MISS diodes (sample D onwards) were performed under vacuum. Several contacts on sample D were left untouched when it was initially examined, in order that studies of the degradation could be performed on virgin contacts. The method used was to bias the MISS diode into the on state, with 10 volts applied through a 1kΩ series resistor. The current through and voltage across the device were recorded on x-t chart recorders. Fig. 7.15 shows the voltage across the

device as a function of time; after approximately 1000 min. the on state voltage had risen to 5.8V. The degradation was initially quite rapid and, although the rate of change gradually reduced, there was no indication that a limiting value was being approached. When the bias was removed some recovery was seen, although this was only a fraction of the total change from the original value.

There could be several causes for this degradation, indeed the partial recovery suggests that there may be two mechanisms, one of which produces an irreversible effect. The nature of these mechanisms are not clear at present. Considerable improvements are required in this area before it is feasible to consider the application of GaAs/LB film MISS devices.

7.3 $p\text{-}n^+$ GaAs/ω-TA MISS Diodes

The preparation of these devices was identical to that of the complementary $n\text{-}p^+$ devices described above (see section 5.3 for full details of the preparation). In comparison with the $n\text{-}p^+$ devices, the (p-type) epilayers were thick ($\sim$ 10μm) and had a relatively high doping density ($\sim 4\times10^{15}cm^{-3}$). Diodes incorporating one or three monolayers of ω-TA were fabricated. The one layer devices did not exhibit switching behaviour, instead a gently curved characteristic was found. The characteristic of a typical contact is shown in fig. 7.16 (reproduced from the curve tracer). Measurement in the cryostat at a temperature of 77K resulted in a characteristic of similar shape, however the voltage at the .2 mA current level had increased from .78v to 4.65v.

The behaviour of devices incorporating 3 layers of ω-TA was rather different, as can be seen from fig. 7.17(*a*). In this case a negative resistance region can be seen, however the characteristic does not correspond to ideal switching behaviour because there was no sharp transition back into the off state. Therefore a holding current and

voltage cannot be defined. These devices were quite sensitive to illumination, which reduced V_s; normal ambient lighting produced the J-V curve shown in fig. 7.17(b). This is in marked contrast to the behaviour of the $n\text{-}p^+$ devices, which were unaffected by illumination (section 7.2.1). Another difference from the $n\text{-}p^+$ diodes was the temperature dependence of the characteristics of these devices. Fig. 7.18 shows the J-V characteristic of the same contact as shown in fig. 7.17, when measured at a temperature of 77K (curve tracer data). It is evident that normal switching behaviour has emerged, in addition the switching voltage has increased to three times the room temperature value.

The changes with temperature can be described in terms of V_s, V_H, I_s and I_H. In this case, the voltage across the diode at a chosen current in the on state (V_{on}) was used instead of V_H, because of the lack of a distinct holding point at higher temperatures. These parameters are plotted as functions of temperature in figures 7.19 and 7.20. Perhaps the most interesting feature is the sudden appearance of a holding current below 100K and its very strong temperature dependence. The other three parameters all increased with decreasing temperature in a rather similar manner, with greatest slope in the region of 150K.

It is clear that neither the punchthrough nor the avalanche multiplication mechanisms can explain switching in these diodes, because V_s is too small. Therefore switching must be caused by a MIS multiplication mechanism, which triggers regenerative feedback (see section 3.2.3). In previous reports of MISS devices which were thought to operate in this fashion[8-10] it was found that V_s increased with decreasing temperature. A similar temperature dependence for V_H, I_H and I_s was also reported[8]. This is similar to the behaviour of these $p\text{-}n^+$ CaAs/LB film diodes. However the unusual disappearance of the holding point above 100K seems to be unique to these devices.

The characteristics of the p-n^+ diodes are very different from those of the complementary n-p^+ diodes (section 7.2). The greatest similarity is perhaps the absence of switching in diodes incorporating a single monolayer of ω-TA in both cases. The causes of the differences are not clear, as they could arise from the changes of carrier type, epilayer thicknesses or doping densities. It was previously noted that the most heavily doped n-p^+ MISS devices deviated from punchthrough behaviour (section 7.2.2), which suggests that the differences could be at least partly attributable to the relatively high doping in the p-n^+ structures.

7.4 GaAs/CuPc MISS Diodes

MISS diodes incorporating copper phthalocyanine LB films, on both n-p^+ and p-n^+ GaAs, were fabricated in a similar fashion to that used for ω-TA devices (see section 5.3). However, in some cases different electrode metals or chemical polishing techniques were utilised, and these variations are noted in the text. In the first section the switching characteristics of these devices are described and comparison is made with ω-TA devices. The next section covers the degradation process in these diodes. Finally the sensitivity of GaAs/CuPc structures to gaseous ambients is discussed; the effects of NO_2 on the MIS diodes of section 6.4.2 are described, as well as the effects on these MISS devices.

7.4.1 Switching Characteristics

In this section we first consider MISS diodes fabricated on n-p^+ GaAs wafers. The devices were initially examined using the curve tracer, and the results are given in table 7.2. Only samples I and J are directly comparable to the ω-TA devices (of section 7.2), because sample K had palladium top electrodes and sample L was prepared using a citric acid/H_2O_2 chemical polish. All these diodes incorporated 4 monolayers of CuPc, producing a thickness comparable to that of a 3 layer ω-TA film

(∿9nm). The characteristics of these devices are fairly similar to those of devices incorporating 3 monolayers of ω-TA; the most notable difference is the large holding voltage for CuPc diodes on heavily doped epilayers. The exceptionally high values of V_H on sample K could perhaps be due to its relatively heavy doping, although it is possible that the use of Pd contacts has some bearing on this.

The switching voltages of the CuPc MISS diodes correspond to punchthrough, as is shown by the figures for w_d (at V_s) and $(w_e - w_j)$ which are given in table 7.2. The static log J vs. V characteristic of a typical contact from sample J (fig. 7.21) provides further evidence that switching is due to the punchthrough mechanism. Similar two part off state characteristics, with a saturated low bias region and a high bias region of rapidly rising current, are discussed in section 7.2.2 and explained in terms of punchthrough. Indeed, the fact that the shapes of these curves are so remarkably similar for ω-TA and CuPc MISS diodes also supports this hypothesis.

Sample L was prepared using a 10:1 50% citric acid : 30% H_2O_2 chemical polishing treatment. The devices on this sample appeared to behave similarly to those prepared using the standard procedure. Unfortunately it was not possible to confirm this because the parameters of the epilayer on this sample were unknown. However, it seems that the difference in the preparation of the semiconductor surface does not cause any major change in device characteristics. This may perhaps be a result of immersion in the water subphase during dipping, which could leave similar oxide layers on both types of surface, even though the citric acid treated surface is already coated with a significant oxide layer (section 6.3.1).

MISS diodes were also fabricated on complementary $p\text{-}n^+$ GaAs samples ($N_a \sim 5\text{-}8 \times 10^{15}$ cm^{-3}, $w_e \sim 3\text{-}8$ μm) using LB films of 4 layers of CuPc.

Both the standard Br-methanol/HCL and the 10:1 50% citric acid : 30% w/o H_2O_2 treatments were tried. The characteristics of these devices were remarkably similar (c.f the $n\text{-}p^+$ diodes discussed above), and in both cases only a small proportion of contacts possessed even the smallest negative resistance region. Usually the behaviour was similar to that shown in fig. 7.16 (which was for a monolayer of ω-TA on $p\text{-}n^+$ GaAs), a rounded and rather featureless characteristic. This contrasts with the behaviour of $p\text{-}n^+$ MISS diodes incorporating a comparable thickness of ω-TA (i.e. 3 layers) which had a distinct negative resistance region (section 7.3). This difference is probably caused by the change in LB film material, although it should be noted that there was also a slight difference in the characteristics of the epilayers of the samples.

7.4.2 Degradation

The degradation of MISS devices on sample I ($n\text{-}p^+$ GaAs/CuPc) was examined by biasing the device into the on state and applying 10 volts through a 1kΩ series resistance (i.e. the same conditions as used in section 7.2.5). The voltage across the device is plotted against elapsed time in fig. 7.22. Comparison with fig. 7.15 (nb. difference in time axes) clearly demonstrates that the rate of change is much less for CuPc devices than for those incorporating ω-TA films. As for the latter case, a small recovery occurred when the bias was removed, however upon reapplication of the bias the recovery soon disappeared. After 70 hours of nearly continuous operation the on state voltage had increased to approximately 6.2 V. Thus the use of CuPc LB films allows a useful improvement in device lifetime to be obtained. Phthalocyanine films have been reported as conferring an improvement in the stability of GaP/LB film electroluminescent MIS diodes, when compared to those incorporating ω-TA[11]. The fact that similar effects are found for LB film devices on

two different semiconductors suggests that the degradation must be related to changes occurring in the LB film, although the mechanism is not yet known.

7.4.3 Gas Effects

The measurements of the effects of nitrogen dioxide upon devices incorporating CuPc LB films were performed using the equipment described in section 5.4.3. The discussion in this section is in two parts, the first of which covers CuPc MIS diodes (which are also the subject of section 6.4.2) and the remainder is devoted to CuPc MISS devices.

n-type GaAs MIS Diodes

These measurements were performed on a MIS diode incorporating 4 monolayers of CuPc on an n-bulk GaAs sample. This was mounted in the stainless steel chamber connected to the gas blender (see section 5.4.3). The sample was allowed to reach a stable equilibrium with the flow of pure N_2 from the gas blender (nb. the internal temperature of the gas blender is maintained at 40°C). The electrical characteristics of the device in this ambient were not significantly different from those of the similar devices described in section 6.4.2.

For the first measurement sequence a forward bias of .6 V was applied, which gave a current density of 1.2×10^{-5} Acm^{-2}. The gas flow was then rapidly changed to one containing 50 v.p.m. of NO_2 in the N_2 carrier gas; the time dependence of the resulting change in current density is shown in fig. 7.23. The initial rapid rise began almost instantaneously and peaked after approximately 3.5 minutes, at 5 times the initial current density. The response then began to decay. Eventually a constant current density was approached; after 15 hours in 50 v.p.m. NO_2 the current density was 1.05×10^{-5} Acm^{-2}, which is almost identical to the initial value before NO_2 was admitted. A quick check on the J-V characteristics of the diode was performed once it had reached

equilibrium with the flow of NO_2. This revealed that a substantial change had occurred at reverse bias, although for forward bias the characteristics were little changed from their initial state (i.e. in equilibrium with N_2). The gas flow was then changed back to one of pure N_2. When equilibrium was reached the characteristics of the diode reverted to their original form.

For the next measurement sequence a reverse bias of 1 V was used. The current through the device was then monitored as 50 v.p.m. of NO_2 was again introduced into the flow of N_2. After 230 minutes the gas flow was changed back to one of pure N_2. The effects of this sequence are plotted in fig. 7.24. As for forward bias, an initial rapid rise which peaked after a few minutes was found. However, in this case the increase in current density was much greater, approximately 100 fold. The rapid rise was followed by a slower decay, which appeared to approach an equilibrium value at least an order of magnitude higher than the initial value. This is in marked contrast to the forward bias case, where the equilibrium currents under 0 v.p.m. and 50 v.p.m. of NO_2 were almost identical. After the flow reverted to one of pure N_2 the current density fell quite rapidly and then returned slowly towards its initial value; after 15 hours in the pure N_2 flow the current density had stabilised at its original value (i.e. before NO_2 was admitted).

After the above measurements and after equilibrium with the flow of N_2 was reached, the J-V characteristics of the diode were measured, as shown in curve (1) of fig. 7.25. As expected this is quite similar to the original characteristic (c.f. fig. 6.22). The full reverse characteristic was not measured, but at 1V bias the reverse current density was approximately 4×10^{-9} Acm^{-2}. The sample was then exposed to 50 v.p.m. of NO_2 for long enough to allow a stable equilibrium to be achieved. The J-V characteristic when in this state is plotted in fig.

7.25 as curve (2). Comparison with curve (1) shows that there is little difference above about .4V forward bias. However, a large increase in current density has occurred at small forward and reverse bias. These observations are in agreement with the behaviour shown in fig. 7.23 and 7.24 and described above, as expected. The sample was then left under a flow of pure N_2 for long enough for a stable equilibrium to be reached, then the J-V characteristic shown in fig. 7.25 as curve (3) was measured. It appears that some permanent damage has now occurred, with a significant and irreversible change in the forward bias characteristics. This is possibly due to the NO_2 (an oxidising agent) attacking the GaAs surface beneath the LB film, hence causing an irreversible degradation. Attempts were also made to measure the effects of NO_2 upon the SiPc/GaInAs MIS diodes which were described in section 6.5.2. For these diodes a small reversible effect was apparent, but this was overwhelmed by an irreversible fall in current density. This could also be explained by the growth of an oxide on the GaInAs surface as a result of exposure to NO_2.

The large increase in the conductivity of CuPc LB films upon exposure to NO_2 is thought to be due to an increase in the hole concentration, which is caused by electrophilic attack on the delocalised electronic states of the phthalocyanine molecule by NO_2[12]. However, it is difficult to analyse what effects this process would have on the MIS structures described above. It is possible that the creation of charged acceptor states in the LB film, which could affect the potential distribution in the system, are of more importance than the increased hole density. The transient effects are particularly puzzling. It was initially thought that they might be due to the mobile charge created in the CuPc being 'swept out' in the electric field. However, the number of electrons in the transient can be estimated from the charge defined by

the curve in fig. 7.23. As this is approximately a factor of 10^3 greater than the number of phthalocyanine molecules under the contact then this possibility must be discounted.

Under far forward bias the current in these devices is thought to be limited by electron transport through the LB film (section 6.4.2). Under equilibrium conditions, exposure to NO_2 has little effect at far forward bias, therefore electron transport through the CuPc film cannot be significantly altered. Under reverse bias the current is thought to be controlled by the band bending in the semiconductor. Therefore the significant gas effect suggests that the band bending has been altered by exposure to NO_2, which could be due to the generation of fixed charge in the LB film. However, there is at present no satisfactory theory that fits these proposals and can also explain the transient effects.

n-p^+ GaAs MISS Diodes

The effects upon n-p^+ MISS samples I, J and K of exposure to NO_2 were investigated, using the equipment described in section 5.4.3. The curve tracer was used to monitor the current-voltage characteristics. The devices were exposed to concentrations of NO_2 up to 100 v.p.m. (in N_2) for a duration of at least two hours. Sample I was kept in an atmosphere of 100 v.p.m. of NO_2 for over 48 hours. No significant changes in V_s, V_H, I_H or the general shape of the characteristics were observed. This is rather strange because the only difference from the MIS diodes described above is in the choice of GaAs substrate. It is almost certain that this does not affect the processes which occur in the CuPc LB film upon exposure to NO_2. Therefore we must assume that the changes that occur in the CuPc film do not significantly alter the characteristics of these MISS diodes.

In these diodes V_s is determined by the bias required for punchthrough of the epilayer (section 7.4.1). This can explain the

insensitivity of the switching voltage to NO_2 exposure because, for this mechanism, V_s is only weakly dependent on the properties of the insulating layer. A large change in the band bending in the semiconductor would significantly alter V_s, however this is unlikely to occur for GaAs as the Fermi level at the surface is pinned by a high density of surface states. It is more difficult to explain the insensitivity of the on state characteristics to the NO_2, because they are controlled by conduction through the insulating film, which is mainly electron transport. We can perhaps draw a comparison with far forward bias conduction in the MIS diodes of section 6.4.2, which is also controlled by electron transport through the LB film (but in the opposite direction). Earlier in this section, we noted that the far forward bias characteristics of the MIS diodes are only slightly altered by exposure to NO_2. Therefore it seems possible that the on state of CuPc MISS diodes is insensitive to NO_2.

Measurements were also performed to examine the effects of exposure to hydrogen on MISS sample K, which had palladium contacts. Absorption of hydrogen causes a change in the work function of palladium[13], and this has been reported as producing significant changes in the switching voltage of silicon MISS devices[14]. The mechanism proposed to explain this effect was an alteration of the barrier height for tunnelling through the oxide, due to the Pd work function change. This varies the gain of the MIS multiplication process (see section 3.2.1), which therefore influences V_s through its effect on the regenerative feedback process (section 3.2.3). In these LB film MISS devices switching usually occurs at punchthrough, therefore only a small change in V_s would be expected due to the work function modification. However, if the effect is large enough to allow switching to occur via a different mechanism then V_s could be significantly altered. When diodes on sample K were

exposed to 5% H_2 in N_2 for 135 minutes no significant changes in the current-voltage characteristics could be discerned using the curve tracer. Although a small voltage shift would be expected, even for the punchthrough model, this could have been obscured since V_s for devices on sample K was very large (table 7.2).

7.5 Si MISS Diodes

LB film MISS devices on n-p^+ silicon were briefly investigated. They were fabricated using the techniques described in section 5.3. A step structure of ω-TA was deposited on the first sample, producing areas with no film and 2, 4 and 6 monolayers. No switching was observed for diodes without an LB film or for those incorporating 2 layers of ω-TA; for these devices the current remained low until punchthrough occurred. Devices incorporating 4 or 6 layers did possess switching characteristics, with V_s ($\sim$ 12V) corresponding to punchthrough. However, it was impossible to characterise these diodes because of the rapid changes that occurred during operation, although the changes were retarded slightly under vacuum. The degradation also appeared to progress even during storage in vacuuo. The changes began with increases in V_H, I_H and I_s, although V_s was little changed, then the on state became unstable and finally the on state disappeared completely.

In an attempt to produce a more stable interface between the silicon and the LB film it was decided to allow a thin oxide to form on the silicon surface. This was done by leaving the sample in air (at room temperature) for several days after the treatment with 40% HF. This sample was then dipped with 3 monolayers of ω-TA (nb. no deposition occurs upon oxidised silicon surfaces during the first insertion into the trough). The characteristics of diodes on this sample resembled those of HF treated devices that had partially degraded. This perhaps suggests

that the rapid degradation in Si/LB film MISS diodes may be caused by the growth of an oxide layer beneath the LB film.

CuPc films were also deposited on n-p^+ silicon samples. Diodes incorporating 1, 2, 4 and 8 monolayers of CuPc exhibited switching characteristics; V_s again corresponded to punchthrough ($\sim$ 12V). Degradation of these devices was similar to that in ω-TA diodes, although it was not quite so rapid; the characteristic changed distinctly within 30 minutes when operated under vacuum. LB films of SiPc were also used in Si MISS diodes, which switched at punchthrough ($V_s \sim$ 12V). In these structures a slightly different type of degradation occurred; I_s initially rose very rapidly and within 5 minutes the on state had also changed substantially.

7.6 Conclusions

In this chapter the characteristics of MISS diodes incorporating LB films were described, and an attempt was made to explain the various kinds of behaviour observed. Several different structures on both GaAs and silicon substrates were examined. Good switching characteristics were obtained, with relatively high yield, for MISS diodes on n-p^+ GaAs which incorporated between 3 and 11 monolayers of ω-TA (9-33 nm) or 4 monolayers of CuPc. No switching was observed for similar diodes incorporating a single ω-TA layer, which demonstrates that the LB film plays a crucial role in the operation of these devices. MISS structures incorporating ω-TA films of more than 11 monolayers were also fabricated, but they possessed unstable characteristics. Therefore the useful range of LB film thickness in these devices was from 9 - 33 nm.

The switching mechanism in these structures was usually a punchthrough process, however this did not seem to apply for the most heavily doped epilayers. The evidence supporting the punchthrough model included the dependence of switching voltage on the properties of the

epilayer, the J-V and capacitance characteristics of the off state, and the independence of switching voltage from temperature, illumination and the thickness of the LB film. No attempt was made to optimise the switching speed of these structures, but this was measured as 40 ns, which is comparable to that reported for Si MISS diodes. The most significant problem of these LB film devices was the gradual degradation during operation. The CuPc LB films were significantly better in this respect than the ω-TA films, but a further significant improvement is required before practical devices can be fabricated.

Diodes on $p\text{-}n^+$ GaAs incorporating 3 monolayers of ω-TA also possessed switching characteristics. These were less than ideal at room temperature, although a significant improvement occurred at low temperature (< 100K). In this case switching was not attributable to the punchthrough mechanism. Similar devices incorporating either a monolayer of ω-TA or 4 layers of CuPc did not exhibit switching characteristics.

The brief investigation of MISS diodes on $n\text{-}p^+$ silicon was plagued by the rapid degradation of the devices. Even the most robust structures, incorporating CuPc films and measured in vacuuo, deteriorated too rapidly for significant results to be obtained. The reasons for the difference in lifetime between Si and GaAs devices is not yet understood, and this area should be more fully investigated.

One of the aims of this work was to produce a gas sensitive MISS device by the use of phthalocyanine LB films. This was not achieved, although it was shown that similar MIS diodes were significantly affected by exposure to NO_2. This apparent difference between the behaviour of MIS and MISS structures is a little puzzling. A tentative explanation for this difference is proposed, but if a better understanding of these gas effects could be obtained it would be a very useful aid to the design of LB film sensors.

TABLE 7.1 $n\text{-}p^{+}$ GaAs/ω-TA MISS Devices

Sample	ω-TA Film Thickness (monolayers)	Switching Voltage V_s/V	Holding Voltage V_H/V	Holding Current I_H/mA	Epilayer Doping Density N_d/cm^{-3}	Effective Epilayer Thickness $(w_e-w_j)/\mu m$	Calculated Depletion Width at Switching $w_d/\mu m$
A	3	9.1 (20%)	4.7 (11%)	1.9 (45%)	3×10^{14}	4.7 ± .9	6.9 ± .7
B	5	10.5 (35%)	6.0 (25%)	1.4 (81%)	6×10^{14}	4 ± .8	5.2 ± .8
C	3	25.3 (27%)	6.9 (23%)	3.6 (27%)	1×10^{15}	5.9 ± 1.2	6.1 ± .8
D	3	17.9 (25%)	4.1 (15%)	3.4 (65%)	7.5×10^{14}	5.4 ± 1.1	6 ± .7
E_1	1	-	-	-	7.9×10^{14}	4.3 ± .8	-
E_2	7	10.4 (36%)	3.5 (11%)	2.5 (28%)	7.9×10^{14}	4.3 ± .8	4.5 ± .7
F_1	5	10.8 (30%)	3.4 (6%)	4.0 (10%)	1.5×10^{15}	3.1 ± .6	3.3 ± .5
F_2	11	11.6 (60%)	5.3 (32%)	0.9 (55%)	1.5×10^{15}	3.1 ± .6	3.4 ± 1.0
G	3	14.5 (26%)	5.1 (14%)	3.6 (47%)	$6\text{-}8 \times 10^{15}$	3.6 ± .8	1.8 ± .2
H_1	13	12.8 (10%)	9.7*(14%)	~3*	$4\text{-}5 \times 10^{15}$	3.2 ± .7	2.1 ± .1
H_2	17	12.2 (13%)	9.0*(16%)	~3*	$4\text{-}5 \times 10^{15}$	3.2 ± .7	2.0 ± .1

Notes: Percentages in brackets are the variation between contacts on the sample
* For this sample the holding point was not clearly defined, therefore V_H is the on state voltage and I_H is an approximate value.

TABLE 7.2 $n\text{-}p^+$ GaAs/CuPc MISS Devices

Sample	CuPc Film Thickness (monolayers)	Switching Voltage V_s/V	Holding Voltage V_H/V	Holding Current I_H/mA	Epilayer Doping Density N_d/cm^{-3}	Effective Epilayer Thickness $(w_e-w_j)/\mu m$	Calculated Depletion Width at Switching $w_d/\mu m$
I	4	10.3 (40%)	4.9 (18%)	1.6 (44%)	6×10^{14}	4 ± .8	5.1 ± .9
J	4	24.6 (15%)	14.4 (39%)	6.3 (48%)	1×10^{15}	4.9 ± 1.0	6 ± .4
K*	4	38.6 (8%)	35.1 (9%)	2.5 (25%)	3×10^{15}	3.2 ± .6	4.3 ± .2
L+	4	5.1 (18%)	4.4 (16%)	1.2 (33%)	N.K.	N.K.	-

Notes: Percentages in brackets are the variation between contacts on the sample
* top contacts Pd not Au
\+ chemically polished in 1:10 50% Citric Acid : 30% H_2O_2.

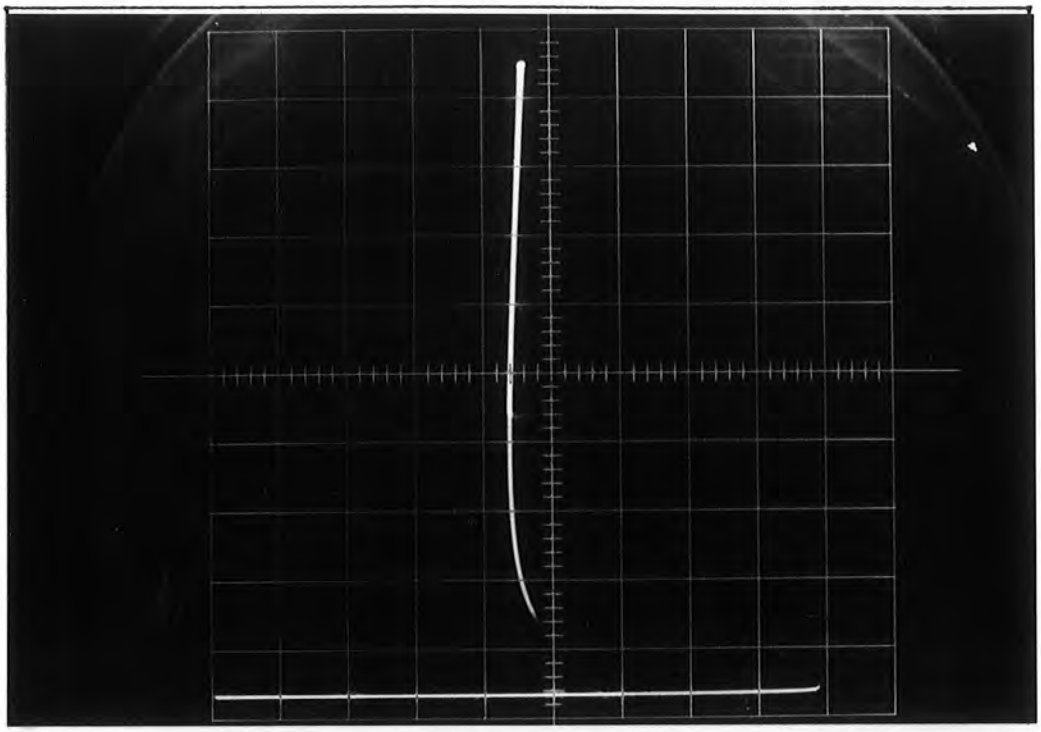

Figure 7.1 Current-voltage characteristic of an LB film/n-p^+ GaAs MISS diode, as recorded on a curve tracer. This diode, from sample A, incorporated a 3 layer ω-tricosenoic acid film. The vertical scale is 1 mA/division, the horizontal scale is 1 V/division, and the series resistance was 500Ω. (contact area = 2×10^{-3} cm^2)

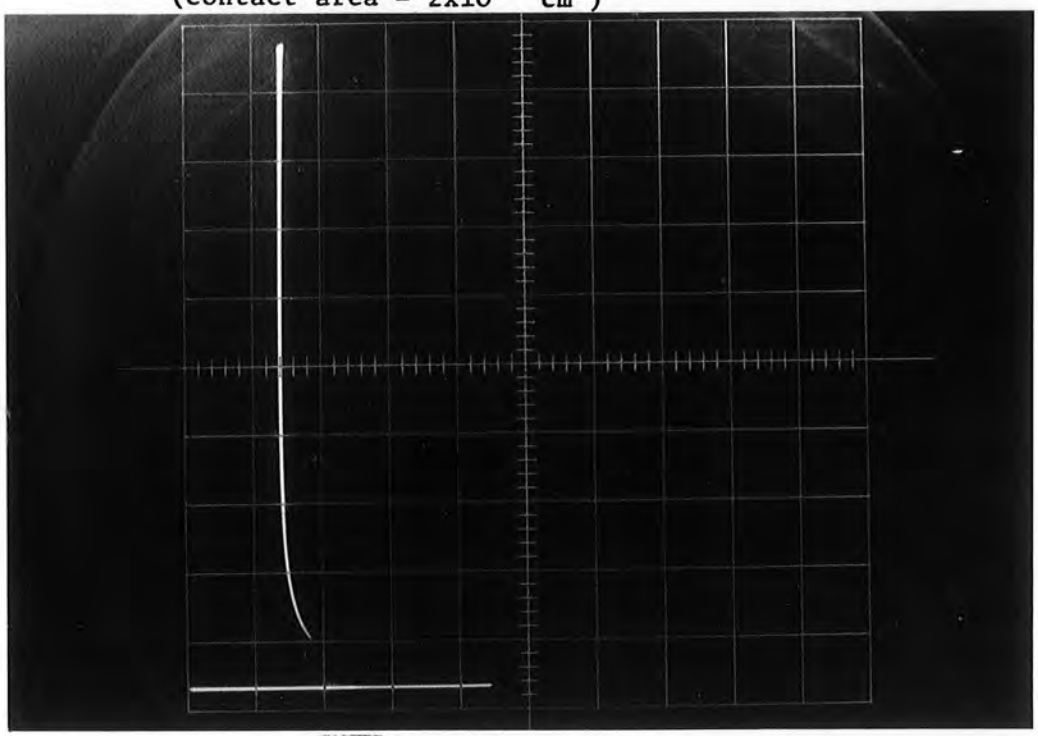

Figure 7.2 Current-voltage characteristic of an LB film/n-p^+ GaAs MISS diode, as recorded on a curve tracer. This diode, from sample C, incorporated a 3 layer ω-tricosenoic acid LB film. The vertical scale is 5 mA/division, the horizontal scale is 5 V/divison, and the series resistance was 1KΩ. (contact area = 2×10^{-3} cm^2)

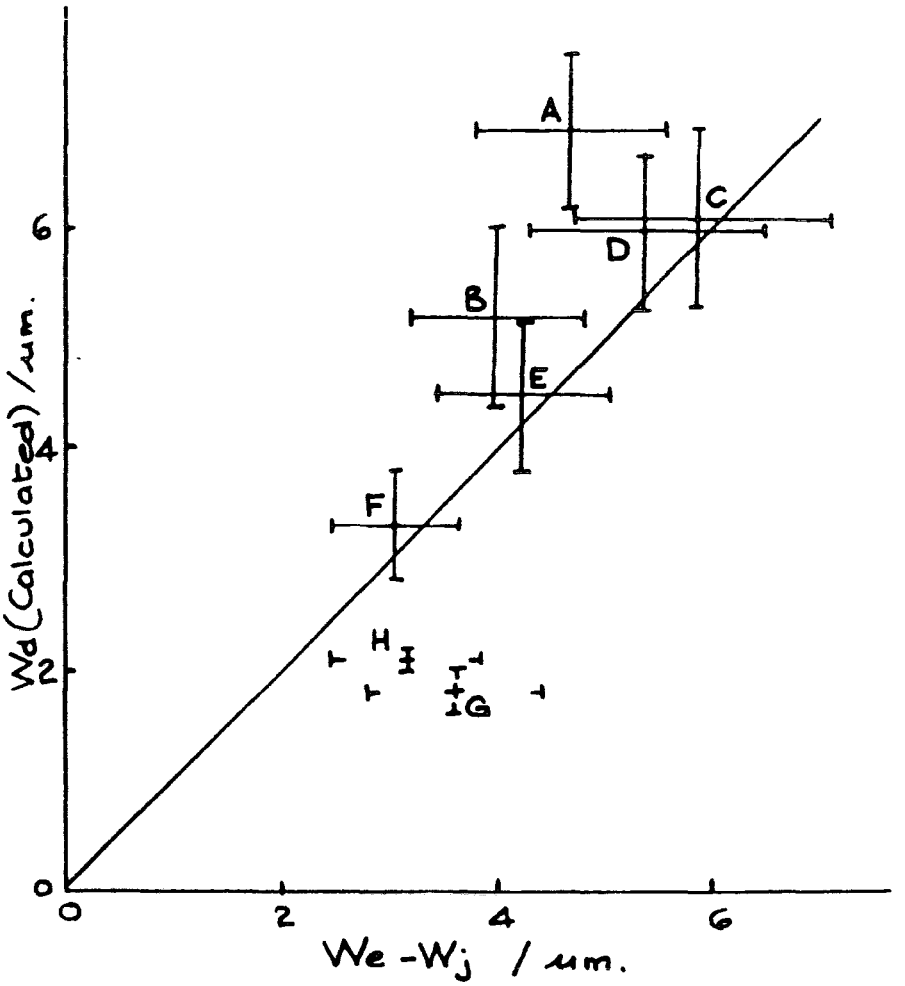

Figure 7.3 Plot of the depletion width at the switching voltage, W_d, versus the thickness of the epitaxial layer, W_e, for LB film/n-p^+ GaAs MISS diodes incorporating ω-tricosenoic acid LB films. The epitaxial layer thickness is modified to take into account the depletion width of the p^+-n junction, W_j. This graph indicates that switching probably occurs via a punchthrough mechanism, for the majority of devices (see text).

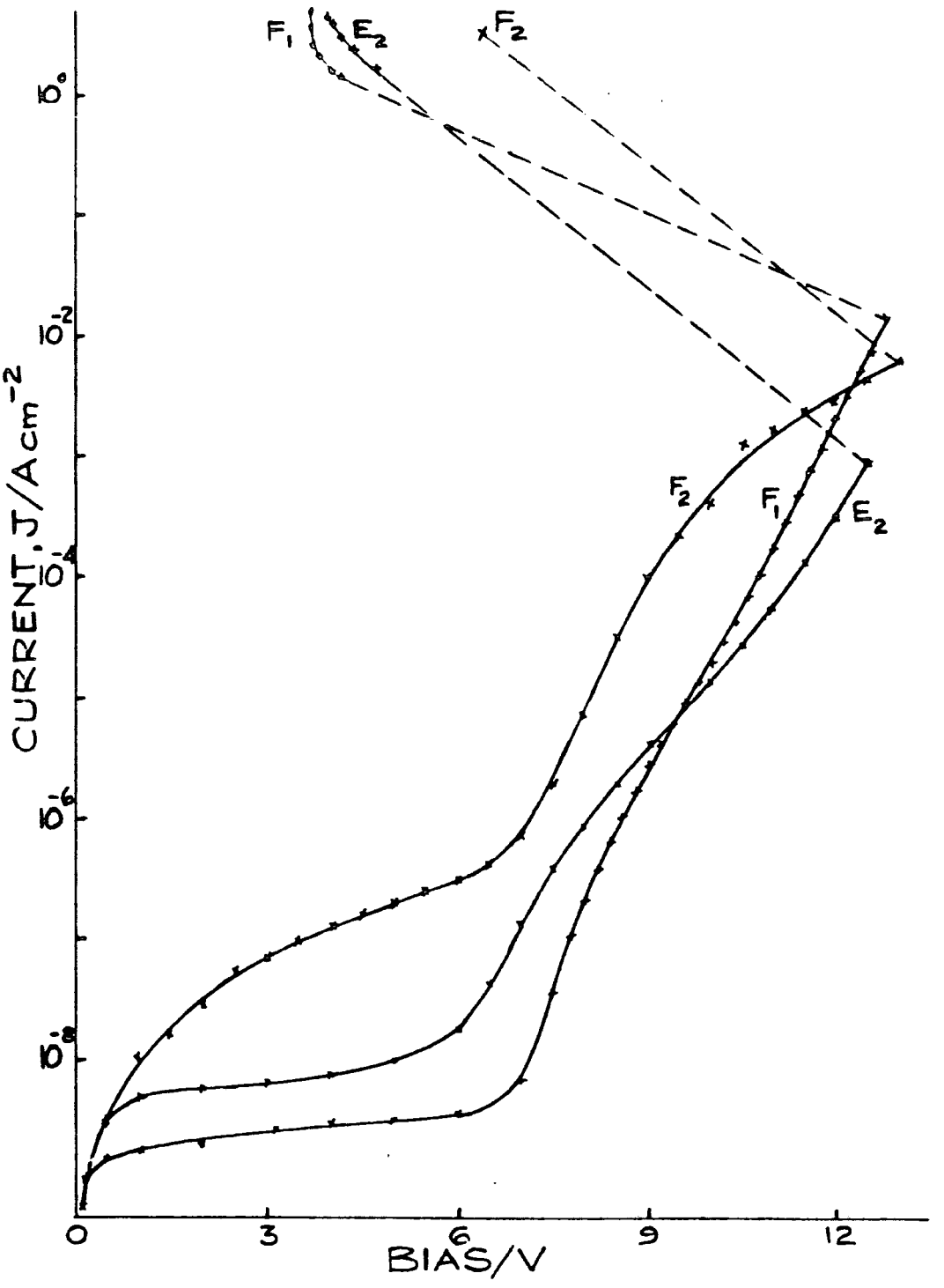

Figure 7.4 Current-voltage characteristics of LB film/n-p^+ GaAs MISS diodes incorporating ω-tricosenoic acid LB films. The device from sample E_2 had a 7 layer film, that from F_1 had a 5 layer film and the diode from sample F_2 incorporated 11 monolayers. In all cases the series resistance was 1KΩ. (contact areas = 2×10^{-3} cm^2)

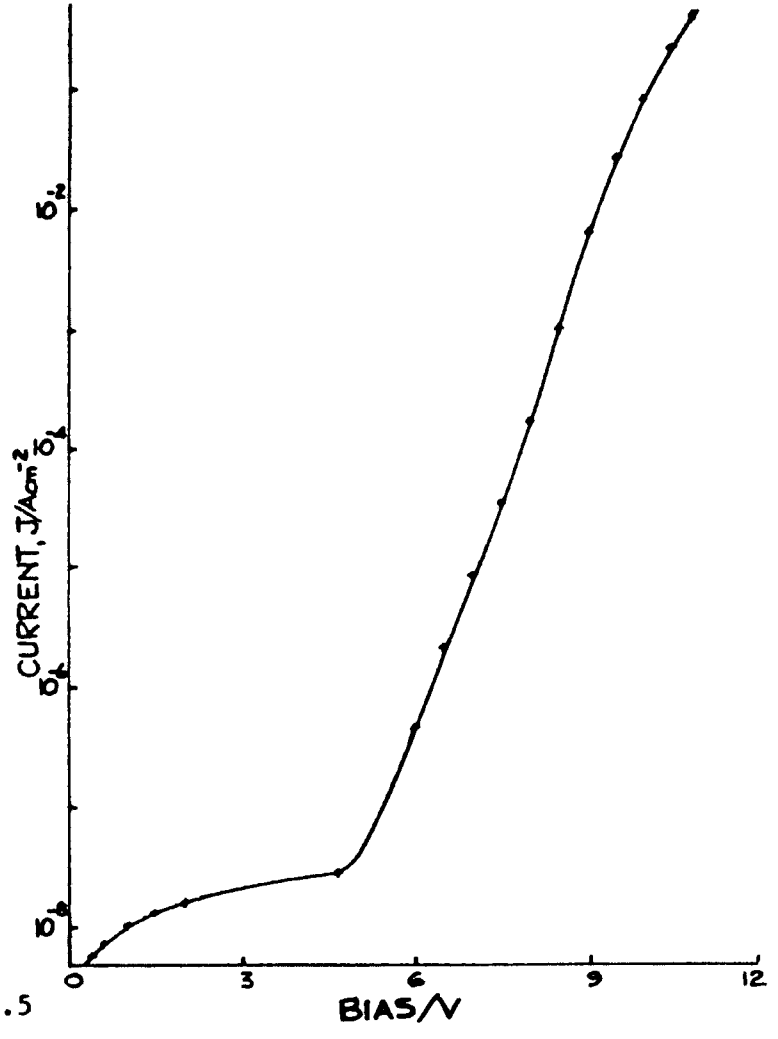

Figure 7.5

Current-voltage characteristic of a metal/n-p^+ GaAs diode. This is equivalent to a MISS diode without an insulating layer, and it shows the effects of punchthrough (see text). (contact area = 2×10^{-3} cm^2)

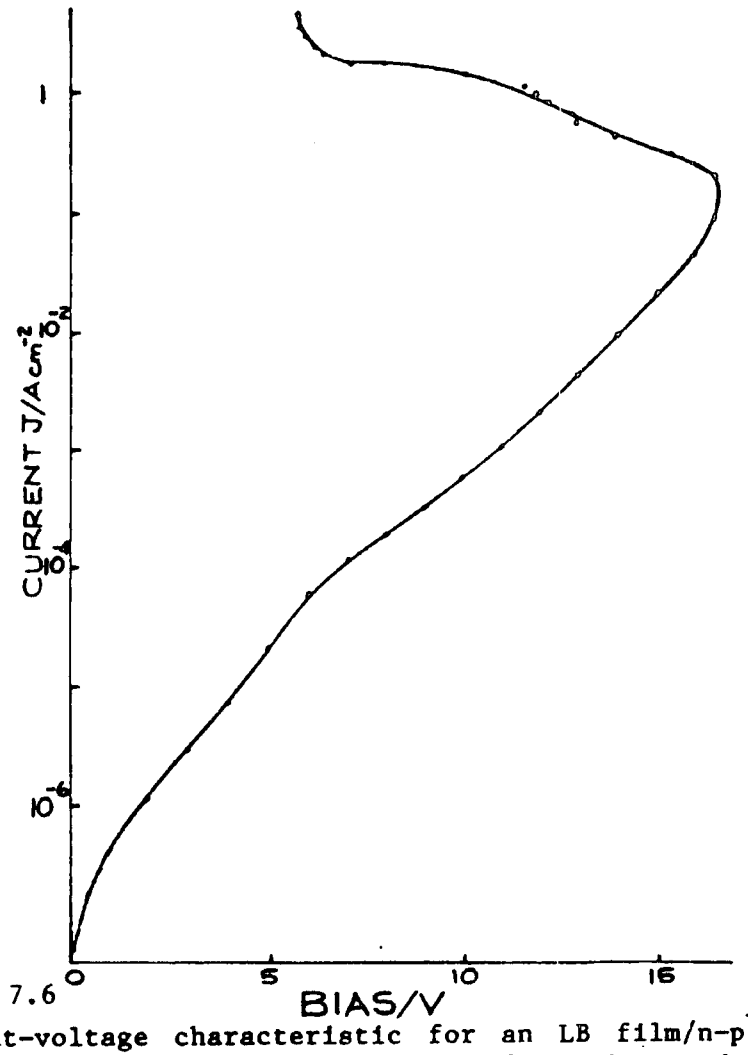

Figure 7.6

Current-voltage characteristic for an LB film/n-p^+ GaAs MISS diode incorporating 3 layers of ω-tricosenoic acid. This device was from sample G, which had a relatively heavily doped epilayer. The series resistance was 10KΩ. (contact area 2×10^{-3} cm^2)

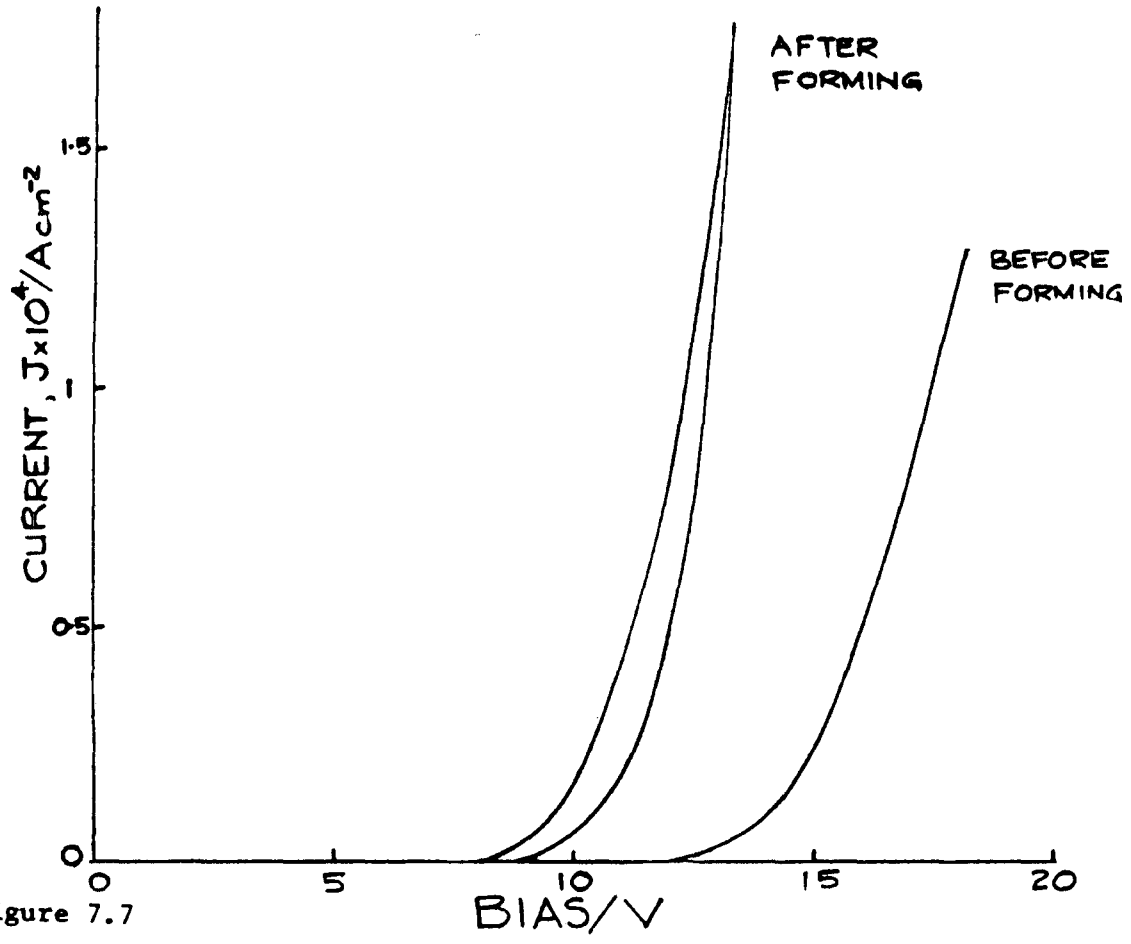

Figure 7.7

Off state current-voltage characteristics of an LB film/n-p^+ GaAs MISS diode (taken from a curve tracer photograph). These are from sample H_2, which had a 17 layer ω-tricosenoic acid film, and show the difference between the behaviour before and after 'forming' (see text). (contact area = 2×10^{-3} cm^2)

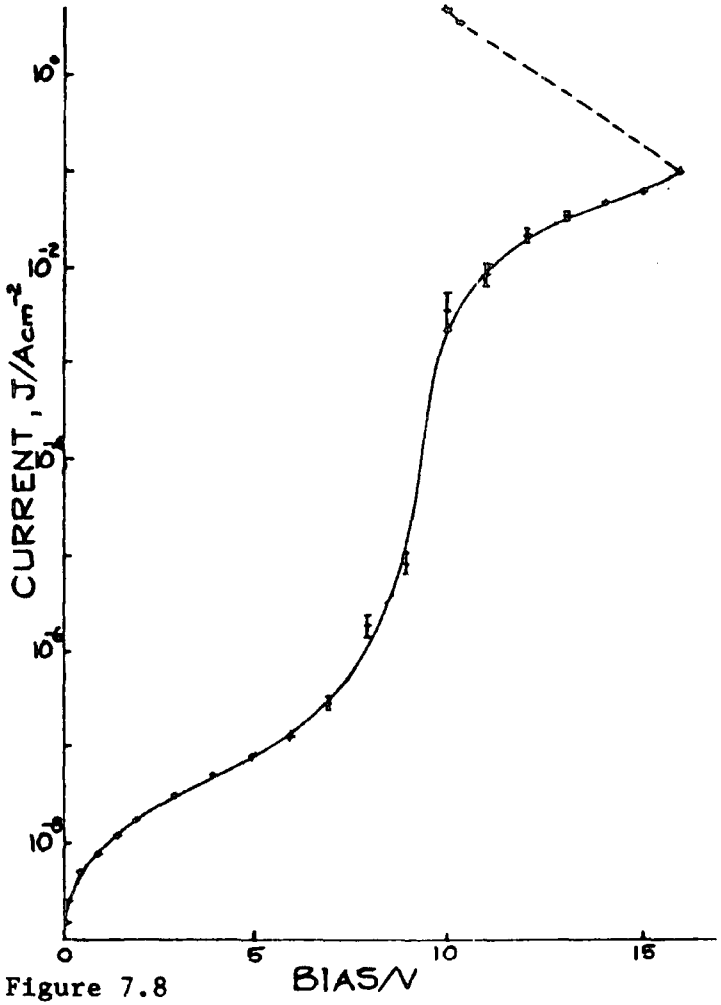

Figure 7.8

Current-voltage characteristic of an LB film/n-p^+ GaAs MISS diode. This device, from sample H_2, incorporated 17 monolayers of ω-tricosenoic acid. The series resistance was 10KΩ . (contact area = 2×10^{-3} cm^2)

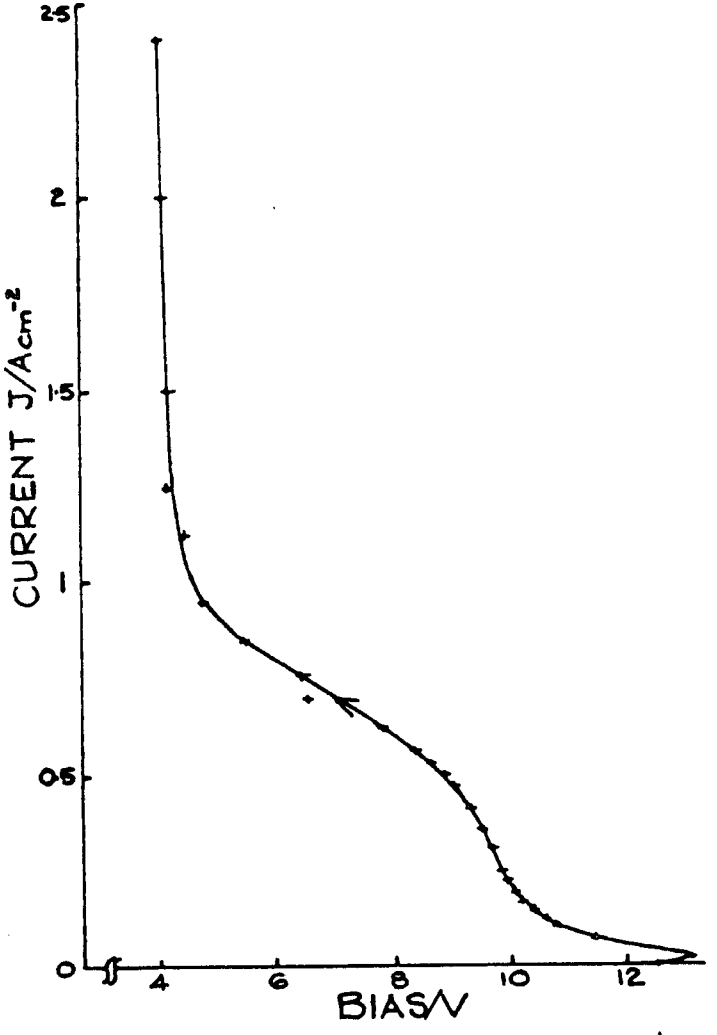

Figure 7.9

Current-voltage characteristic of an LB film/n-p^+ GaAs MISS diode incorporating 5 monolayers of ω-tricosenoic acid, from sample F_1. The high series resistance of 20KΩ permits the shape of the negative resistance region to be discerned. (contact area = 2×10^{-3} cm^2)

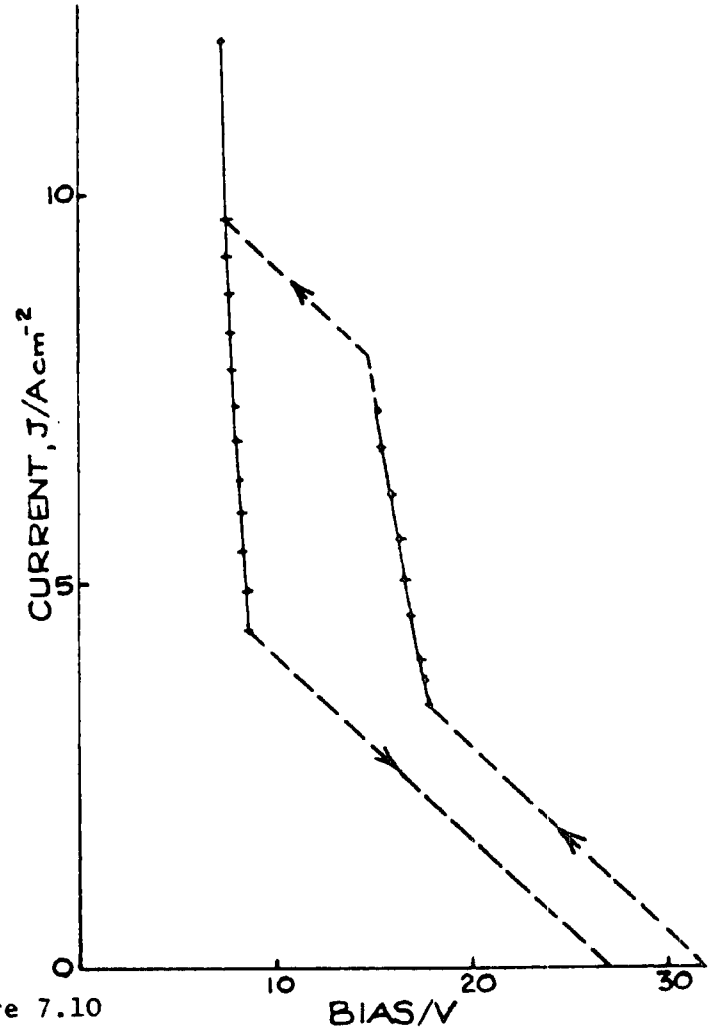

Figure 7.10

Current-voltage characteristic of an LB film/n-p^+ GaAs MISS diode incorporating 3 layers of ω-tricosenoic acid, from sample C. The series resistance was 2.2KΩ. The intermediate state which can be seen is believed to be an artifact produced by oscillations (see text). (contact area = 2×10^{-3} cm^2)

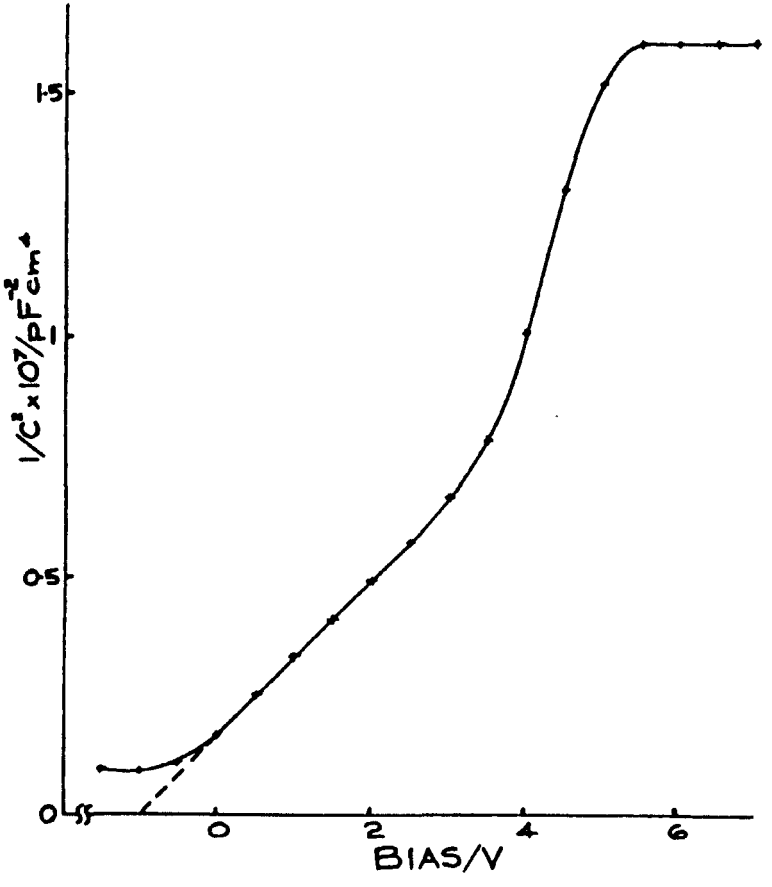

Figure 7.11

$1/C^2$ versus bias characteristic for the off state of an LB film/n-p^+ GaAs MISS diode. This device, incorporating 7 layers of ω-tricosenoic acid, was from sample E_2. (contact area = 2×10^{-3} cm^2)

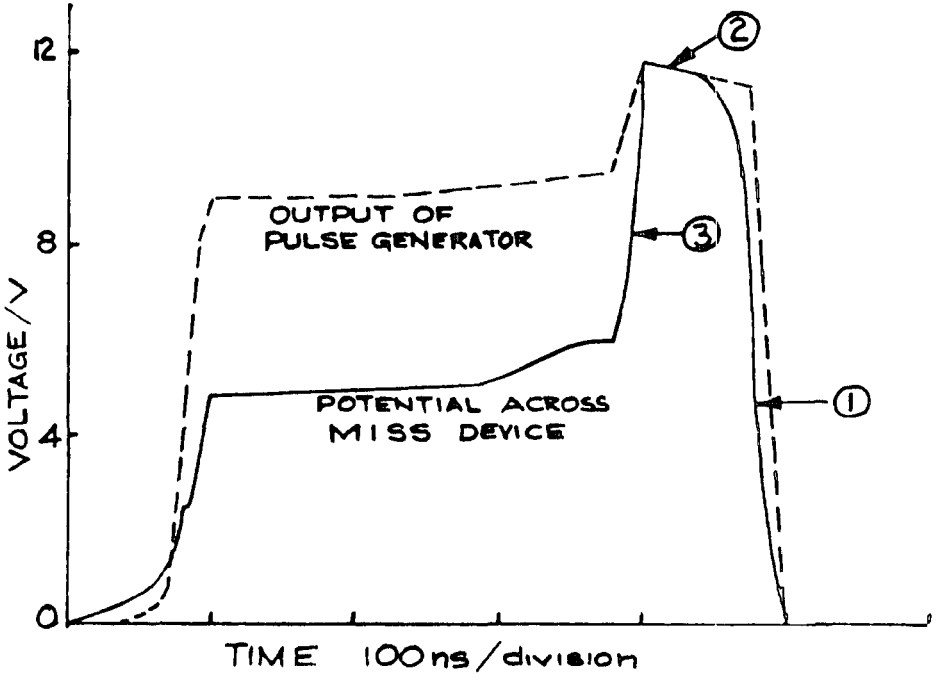

Figure 7.12

Response to a small amplitude pulse of an LB film/n-p^+ GaAs MISS diode. This device was from sample D and incorporated 3 layers of ω-tricosenoic acid. The series resistance was 100Ω and the pulse generator had an output impedance of 50Ω. The three numbered regions of the initial transient are;
(1) the capacitive rise time,
(2) the inversion charge delay time and
(3) the feedback regeneration time
(contact area = 2×10^{-3} cm^2)

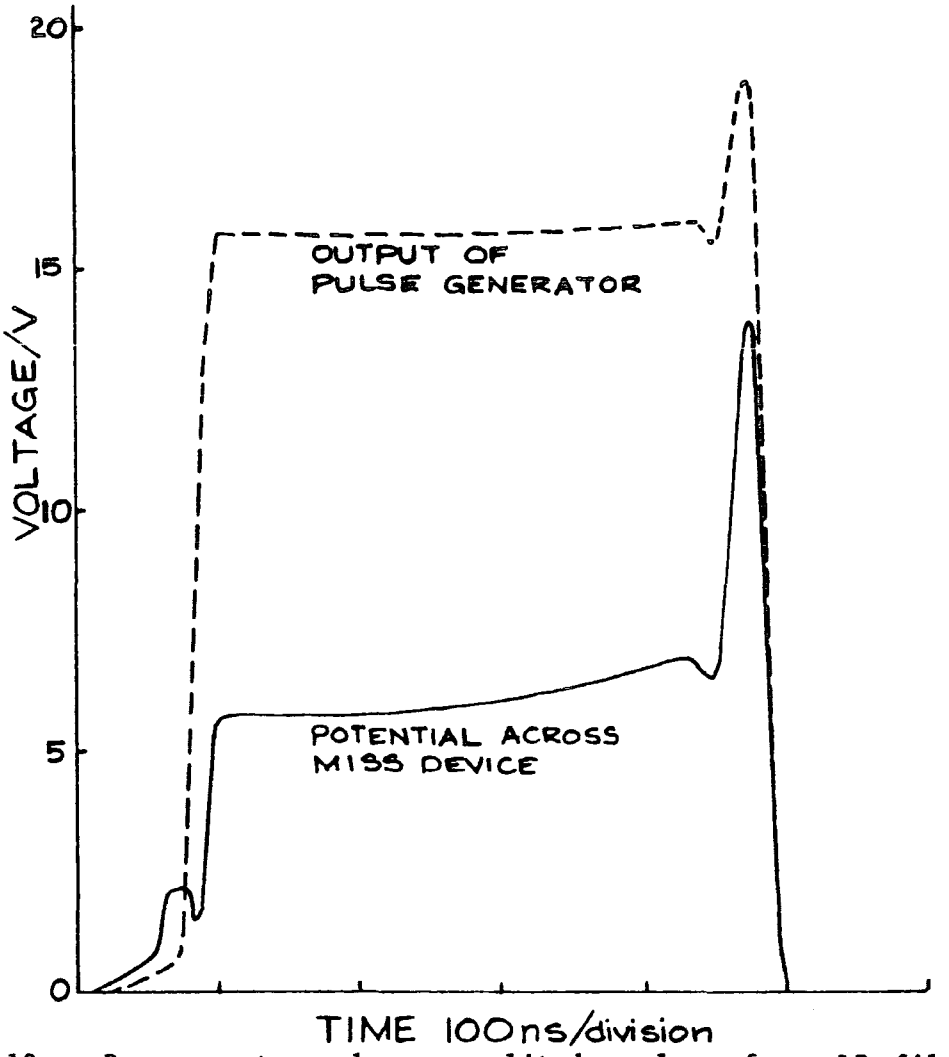

Figure 7.13 Response to a large amplitude pulse of an LB film/n-p^+ GaAs MISS diode incorporating 3 layers of ω-tricosenoic acid, from sample D. The series resistance was 100Ω and the pulse generator had an output impedance of 50Ω. (contact area = 2×10^{-3} cm^2)

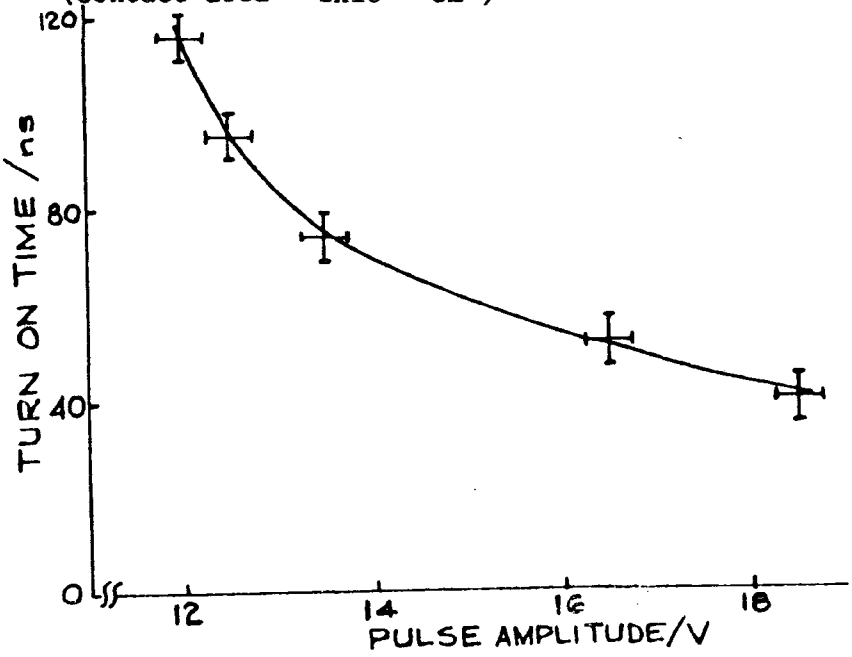

Figure 7.14 Turn on time as a function of pulse amplitude for an LB film/n-p^+ GaAs MISS diode incorporating 3 layers of ω-tricosenoic acid. This device, from sample D, was in series with a total resistance of 150Ω.

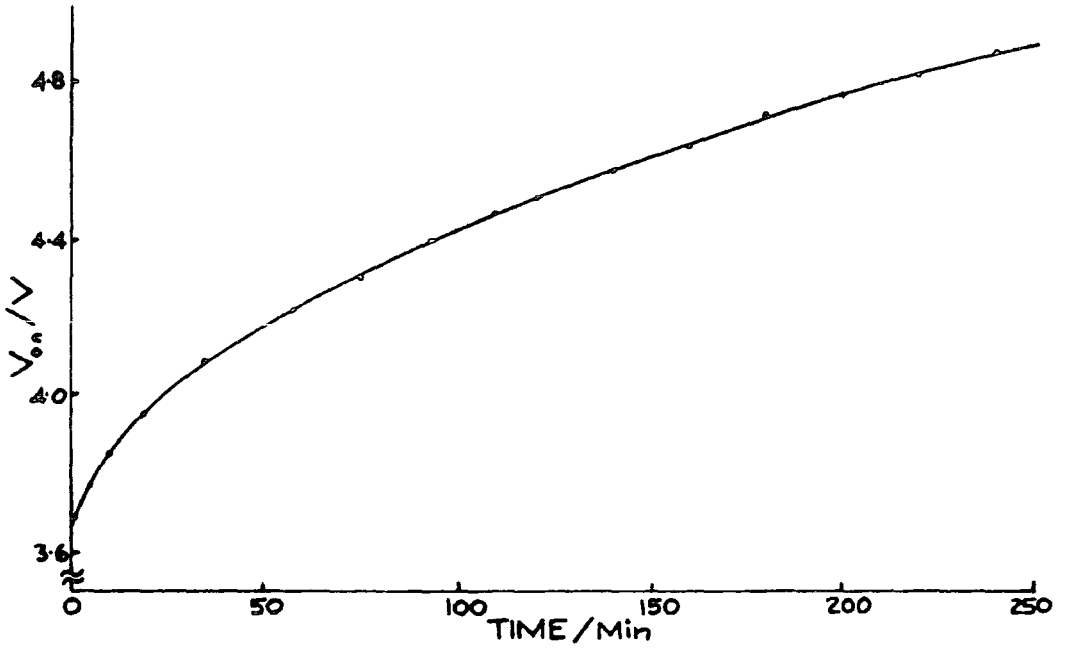

Figure 7.15 Plot of on state voltage versus time for a 3 layer ω-tricosenoic acid LB film/n-p^+ GaAs MISS diode from sample D. This illustrates the degradation of the characteristics that occurred in these devices. This was obtained by applying 10V bias through a series resistance of 1KΩ. (contact area = 2×10^{-3} cm^2)

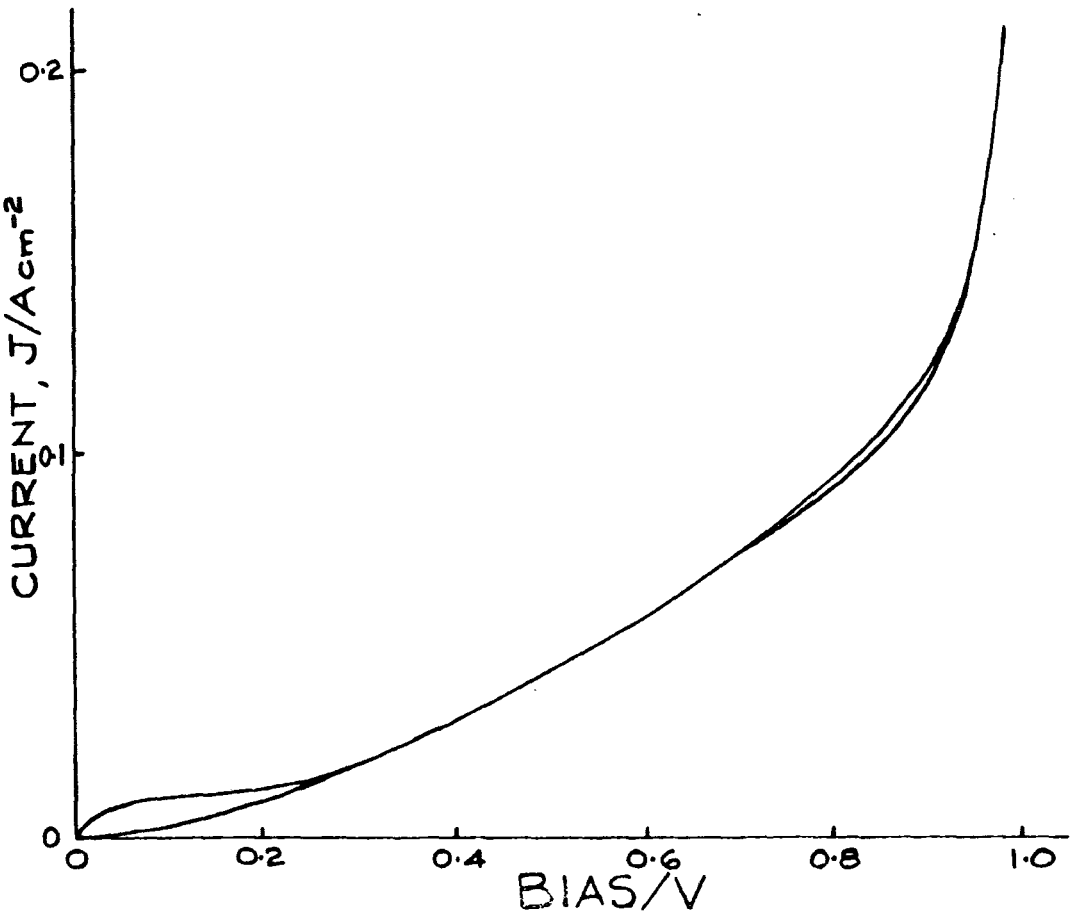

Figure 7.16 Current-voltage characteristic of an LB film/p-n^+ GaAs MISS diode, taken from curve-tracer data. This device incorporated 1 layer of ω-tricosenoic acid. (contact area = 2×10^{-3} cm^2)

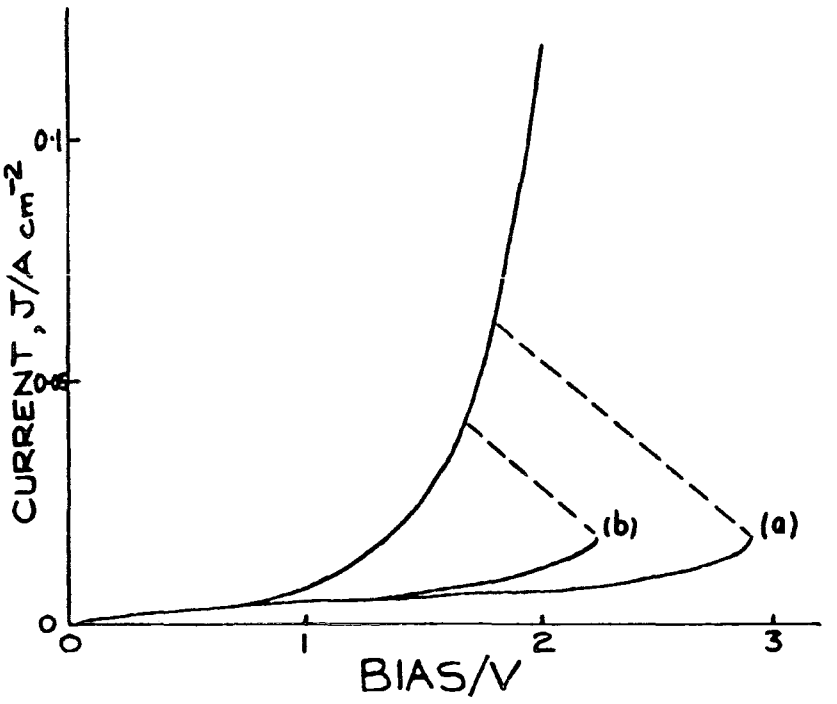

Figure 7.17 Current-voltage characteristic of an LB film/ p-n^{+} GaAs MISS diode incorporating 3 layers of ω-tricosenoic acid. These curves were taken from curve-tracer data recorded at room temperature. Curve (a) was measured in the dark and curve (b) shows the effect of illumination (contact area = 2×10^{-3} cm^2, series resistance 10KΩ)

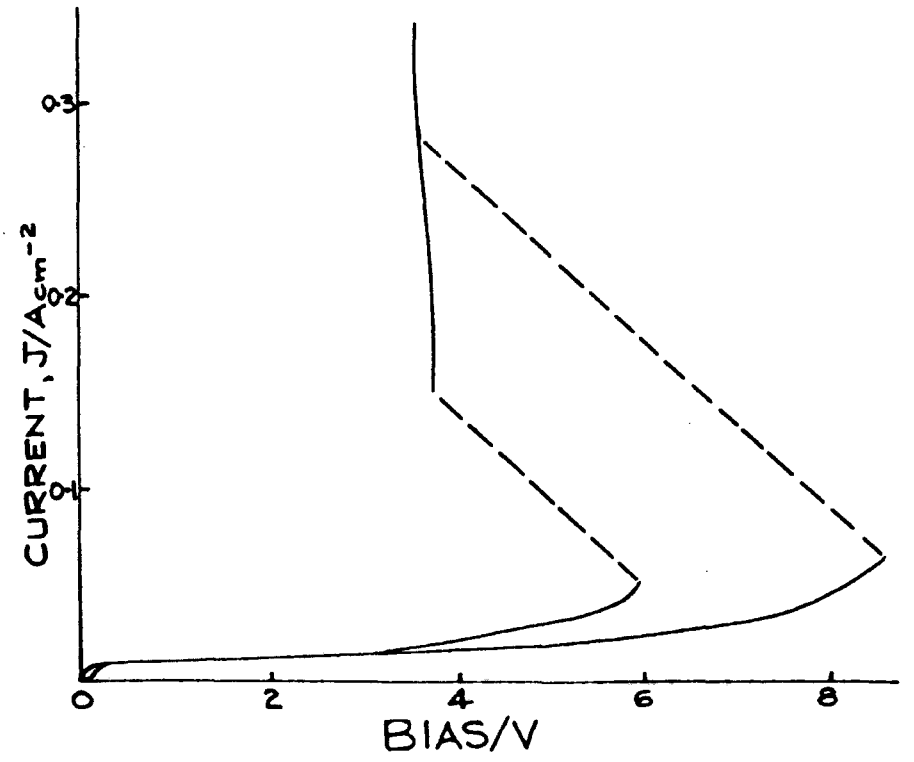

Figure 7.18 Current-voltage characteristic of an LB film/p-n^{+} GaAs MISS diode incorporating 3 layers of ω-tricosenoic acid. These curves were taken from curve-tracer data recorded at 77K. (contact area = 2×10^{-3} cm^2, series resistance 10KΩ)

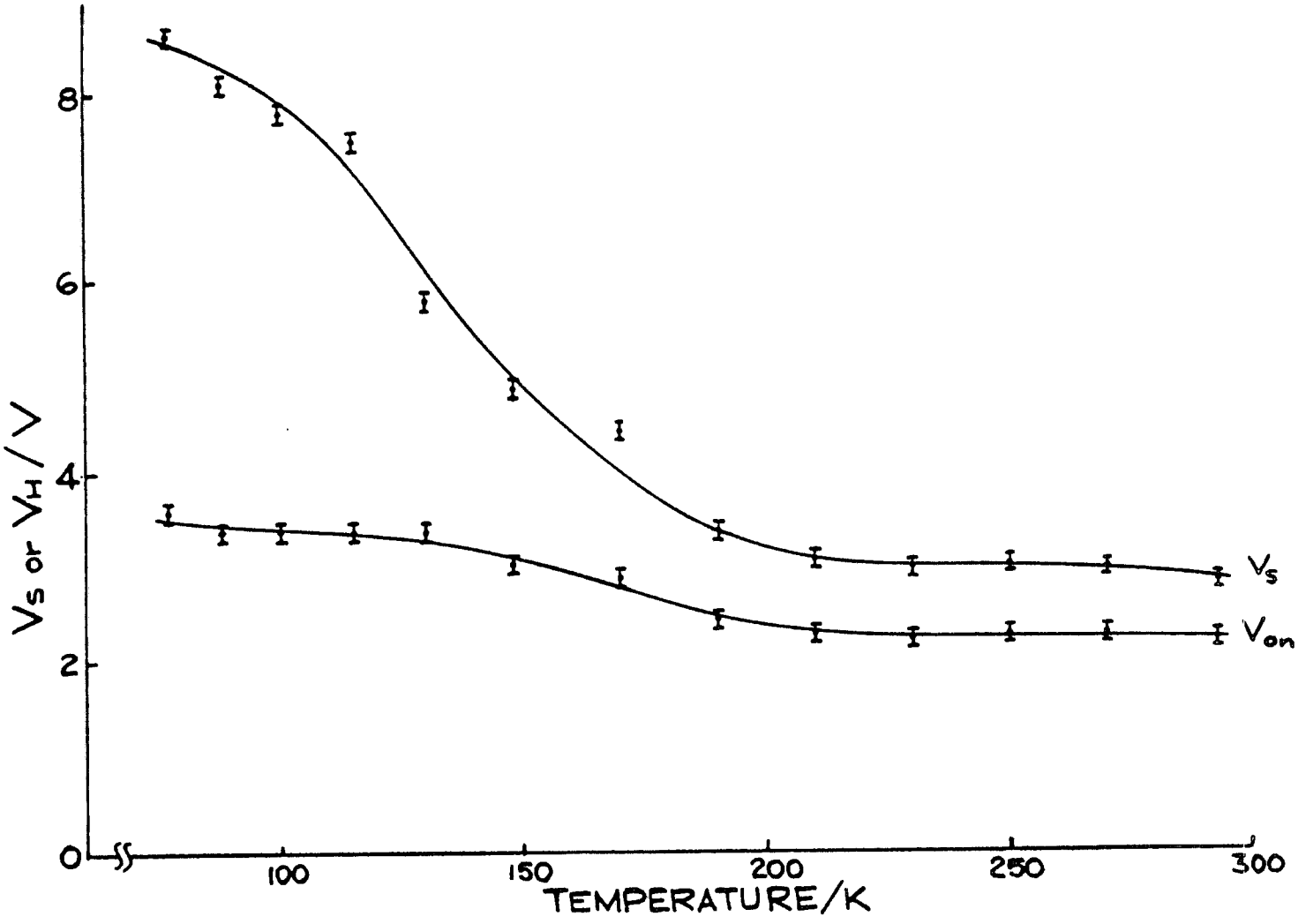

Figure 7.19 Switching voltage, V_s, and on state voltage, V_{on}, plotted as functions of temperature for an LB film/p-n GaAs MISS diode incorporating 3 layers of ω-tricosenoic acid.

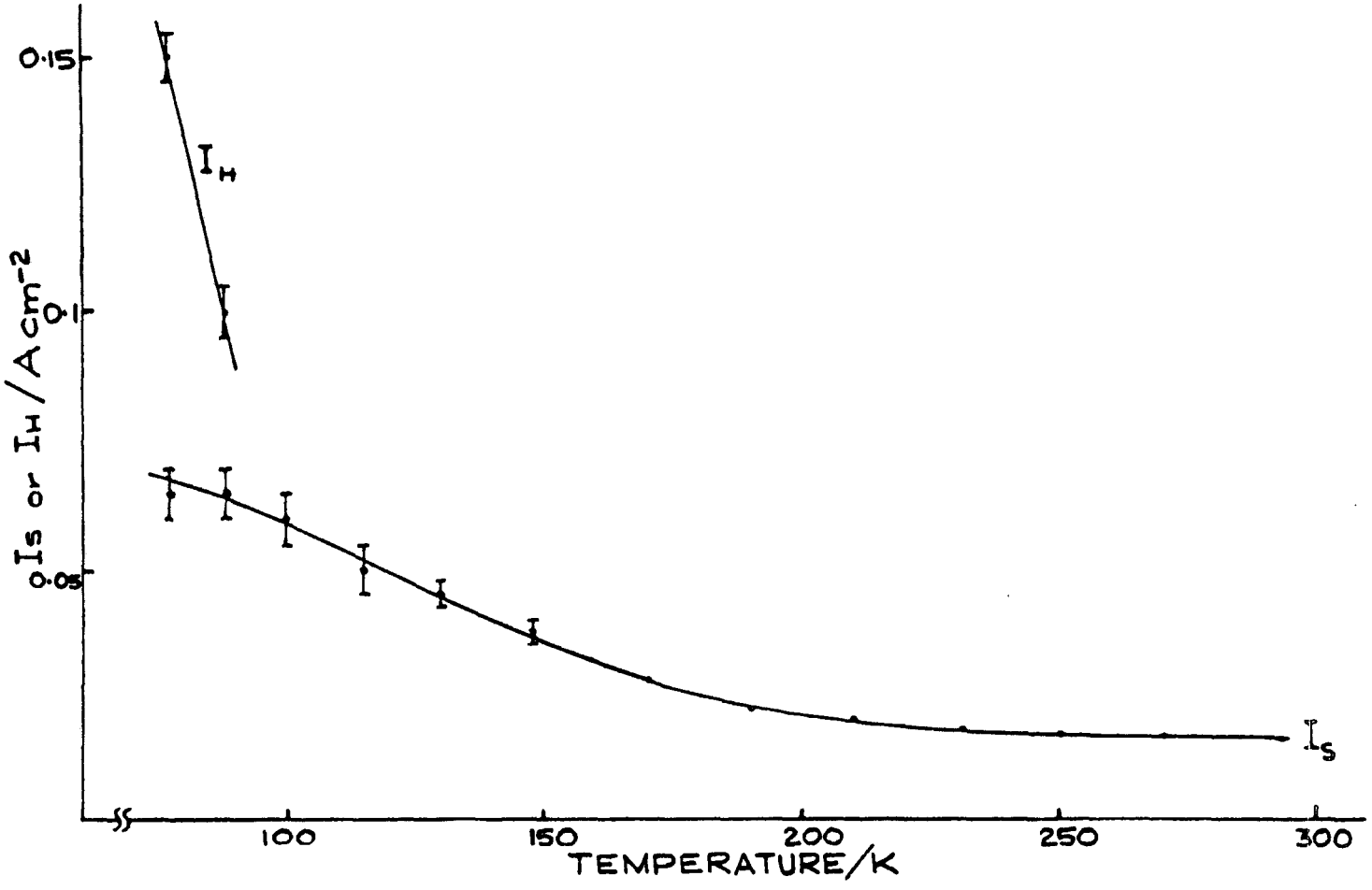

Figure 7.20 Switching current, I_s, and holding current, I_{H+} plotted as functions of temperature for an LB film/p-n$^+$ GaAs MISS diode incorporating 3 layers of ω-tricosenoic acid.

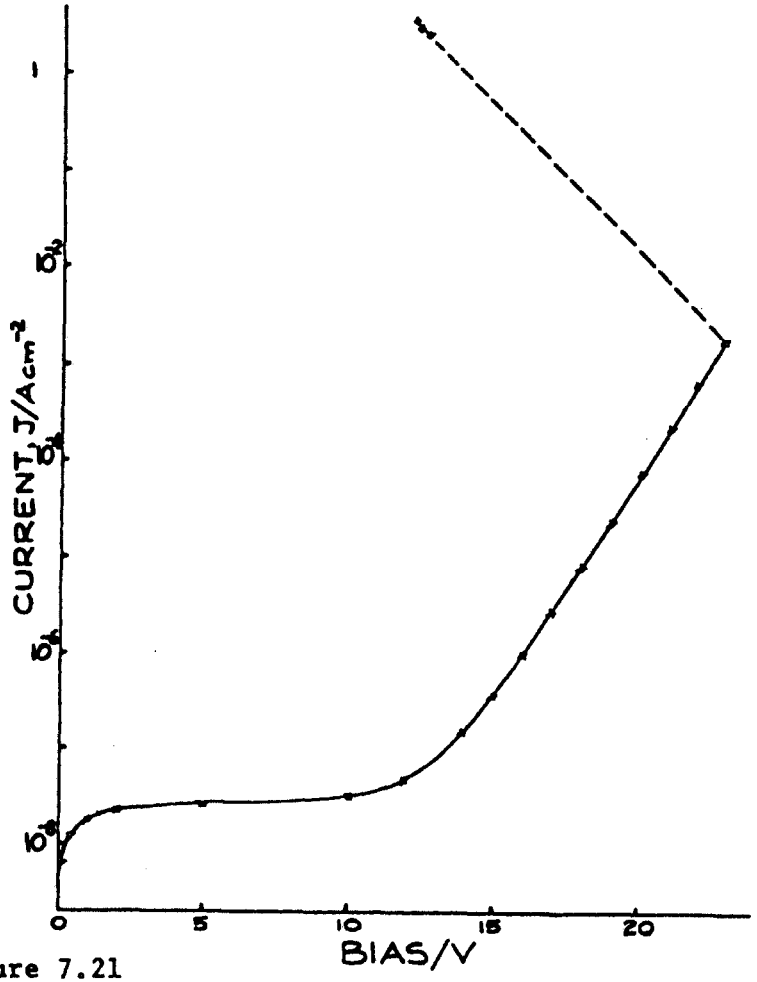

Figure 7.21

Current-voltage characteristic of an LB film/n-p^+ GaAs MISS diode. This device from sample J used a 4 monolayer film of copper phthalocyanine. (contact area 2×10^{-3} cm^2, series resistance 1KΩ)

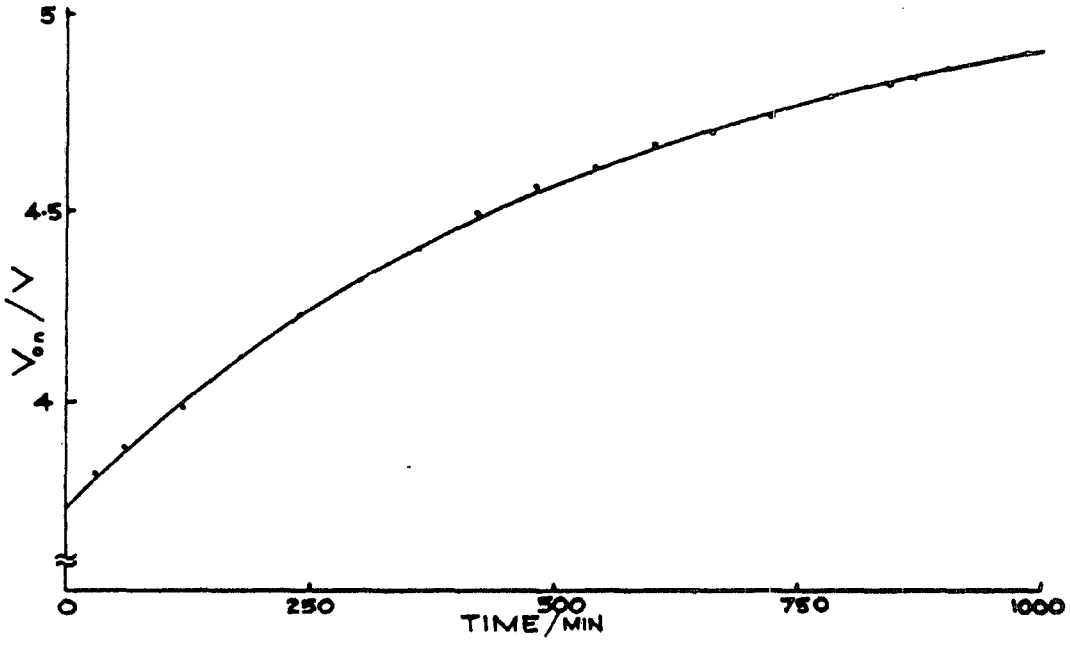

Figure 7.22

Plot of on state voltage versus time for a 4 layer copper phthalocyaine LB film/n-p^+ GaAs MISS diode from sample J. This illustrates the degradation of the characteristics that occurred in these devices. This was obtained by applying 10V bias through a series resistance of 1KΩ. (contact area = 2×10^{-3} cm^2)

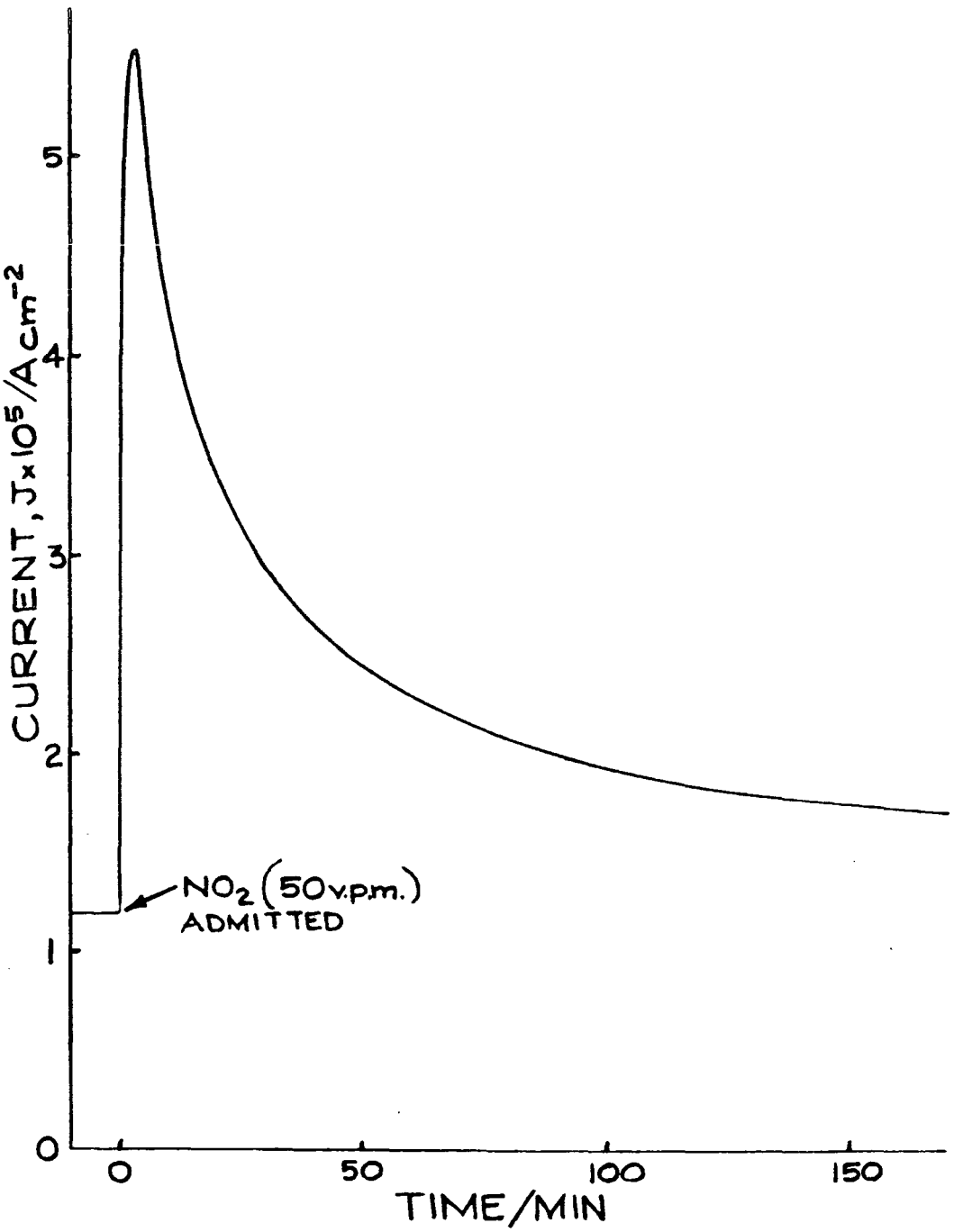

Figure 7.23 The effect of exposure to NO_2 upon the forward bias (.6V) current in an LB film/n-type GaAs MIS diode incorporating 4 layers of copper phthalocyanine. (contact area = 2×10^{-3} cm^2)

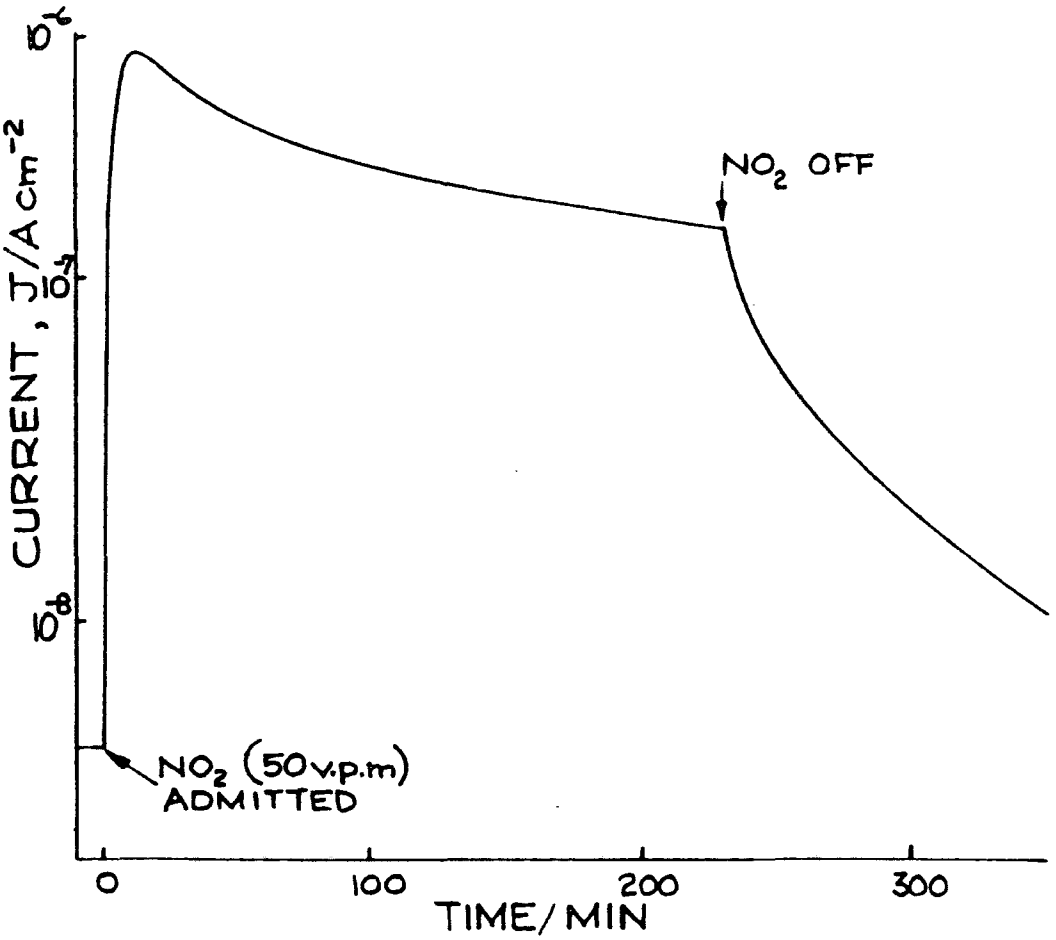

Figure 7.24 The effect of exposure to NO_2 upon the reverse bias (1V) current in an LB film/n-type GaAs MIS diode incorporating 4 layers of copper phthalocyanine. (contact area = 2×10^{-3} cm^2)

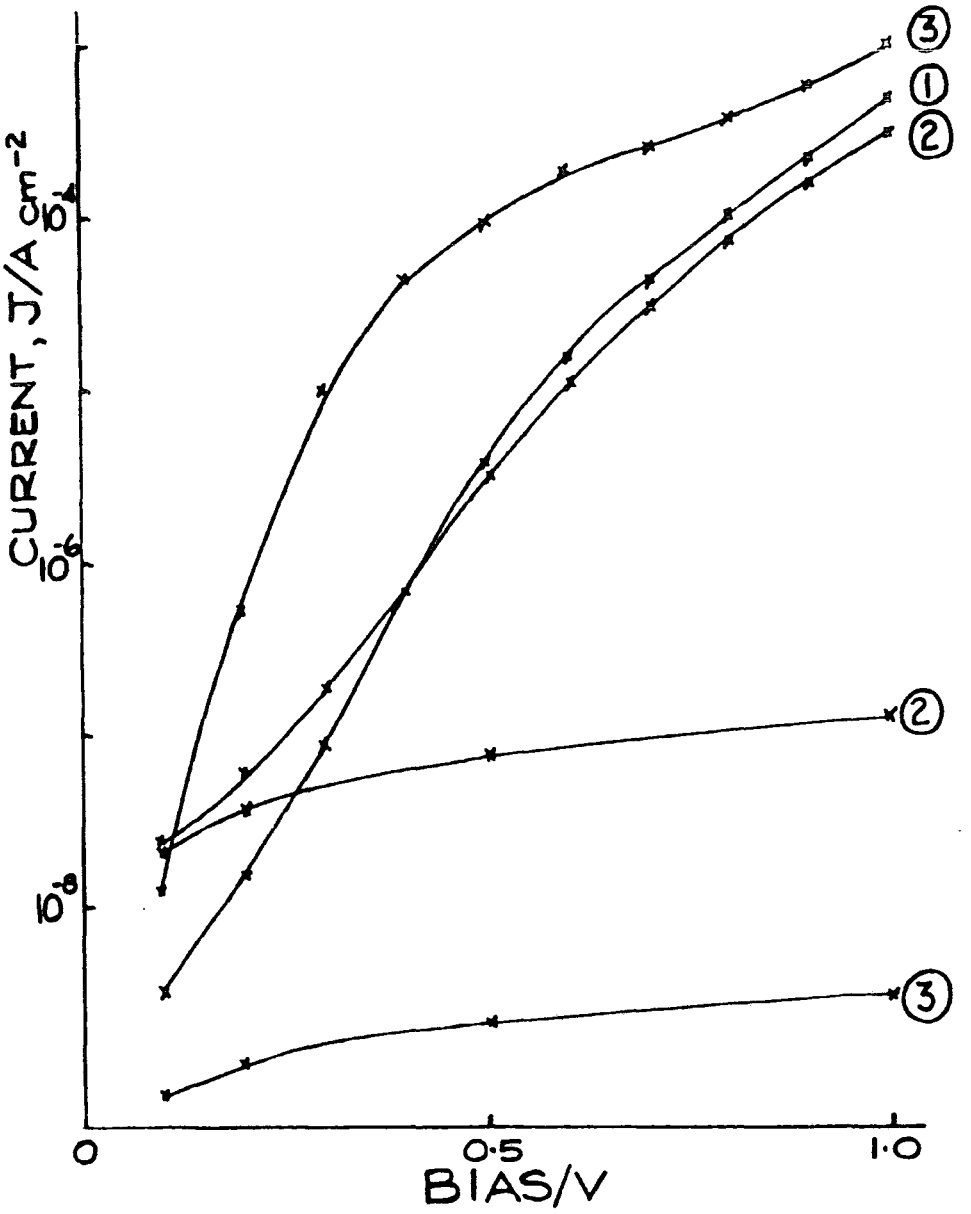

Figure 7.25 The effects of exposure to NO_2 upon the current-voltage characteristics of an LB film/n-type GaAs MIS diode incorporating 4 layers of copper phthalocyanine.
(1) in equilibrium with an N_2 atmosphere,
(2) in equilibrium with an atmosphere containing 50 v.p.m NO_2
(3) in equilibrium with an N_2 atmosphere, after degradation had occurred (see text)
(contact area = 2×10^{-3} cm^2).

CHAPTER 8

CONCLUSION

The objective of this work was to investigate the properties of gallium arsenide/Langmuir-Blodgett film MIS devices. The systematic study of these devices required a knowledge of the properties of freshly etched GaAs surfaces, together with an appreciation of the effects upon these surfaces of the LB film deposition process. The electrical characteristics of Schottky barriers can be used to help determine the nature of the metal-semiconductor interface, and by extension the nature of the semiconductor surface. Measurements indicated that a freshly etched, relatively clean, GaAs surface becomes coated with a thin oxide layer as a consequence of the LB film deposition procedure. These experiments enabled the influence of this oxide layer upon the characteristics of the MIS devices to be separated from that of the LB film.

Two different LB film materials were used to fabricated MIS diodes : ω-tricosenoic acid and a substituted copper phthalocyanine. The characteristics of devices incorporating these two materials were qualitatively similar, and corresponded to leaky 'non-equilibrium' MIS diode behaviour of the kind described in chapter 3. This type of behaviour suggested that LB films could be used to fabricate bistable MISS diodes. The GaAs MIS diodes incorporating phthalocyanine LB films exhibited an anomalous photoelectric behaviour, which did not occur for similar diodes incorporating layers of ω-tricosenoic acid. The origin of this interesting phenomenon is not known, but it must be related to an interaction between the LB film and the semiconductor. It would be

informative to determine whether this effect is unique to the system under study, or if it also occurs for other combinations of semiconductor and LB film. At present further work is required to determine whether this effect could have any practical applications.

The ternary semiconductor alloy $Ga_{.47}In_{.53}As$ has very desirable electronic and optical properties, but one of its technological limitations is the extremely low barrier height of metal/GaInAs contacts. An attempt was made to remedy this problem by producing 'Schottky-like' tunnel MIS contacts incorporating LB films. The use of single monolayers of ω-tricosenoic acid or silicon phthalocyanine gave rise to a substantial increase in the effective barrier height for this material. This effect appeared to be caused by electrons tunnelling through the LB film (and not due to increased band bending in the semiconductor caused by fixed charge in the LB film, as has been previously suggested). The reverse leakage current of these contacts was apparently small enough for their use as the gate in field effect transistors, analogous to MESFETs (which cannot be made on GaInAs). Future work in this area is necessary in order to devise FET structures and processing sequences that are compatible with LB films (or vice versa).

The core of the thesis describes an investigation of the GaAs/LB film bistable MISS device. This was the first time that an organic insulating layer had been used in MISS structures, and it was only the second report of GaAs MISS devices. Good switching characteristics were obtained for either ω-tricosenoic acid or copper phthalocyanine LB films on $n\text{-}p^{+}$ GaAs, with a reasonably high yield of working diodes (up to 90%). No switching was noted for devices incorporating single monolayers, which showed that the organic layer plays an important role in the operation of these MISS diodes. In contrast, there did not appear to be a clearly

defined upper limit to the LB film thickness, beyond which switching would not occur. However, the characteristics of diodes incorporating layers of greater than 30nm thickness were less well behaved.

The switching characteristics of these MISS devices were relatively insensitive to LB film thickness (within the limits noted above), temperature and illumination. However, the switching voltage was clearly related to the properties of the n-type epilayer. The form of this relationship suggested that switching in these structures occurred by a 'punchthrough' mechanism. A considerable body of evidence supporting this hypothesis was amassed, including the detailed form of the I-V and C-V characteristics. However, this behaviour did not apply for devices on the more heavily doped epilayers.

LB film MISS diodes on $p\text{-}n^+$ GaAs possessed rather different characteristics. This was not totally surprising because of the comparatively large doping density and thickness of the p-type epilayers, which would give rise to very high switching voltages for the 'punchthrough' mechanism. The characteristics of these devices were sensitive to temperature and illumination, hence confirming that the operation of these devices is rather different from that of the complementary $n\text{-}p^+$ structures.

One of the significant drawbacks to the use of LB films as active layers in semiconductor devices is the fairly rapid degradation that occurs. At this early stage in the development of LB film devices it is unreasonable to expect high reliability and long lifetimes. It has been shown in this work that improvements can be made in this area by the use of a more robust film material, i.e. phthalocyanine. It was also discovered that LB film MISS diodes fabricated on silicon had very short lifetimes, indicating that degradation in LB film devices is dependent on

the substrate, as well as the film material itself. It should be noted in this context that MISS devices based on more conventional insulating materials are not without reliability problems. It remains to be seen whether devices incorporating LB films can be made sufficiently reliable to be of practical use, but at this early stage of development improvements in this area must be possible.

One of the subsidiary aims of this work was to investigate the possibility of producing sensors based on GaAs MIS (or MISS) devices incorporating phthalocyanine LB films. The ultimate objective of this type of development is to produce small, low cost, accurate, fast reacting microelectronic sensors for a wide variety of organic and inorganic chemicals. In this area the results of this work were a little disappointing as the MISS devices were unaffected by exposure to the appropriate ambient, nitrogen dioxide. This was perhaps a consequence of the 'punchthrough' mode of operation of the MISS diodes incorporating phthalocyanine LB films, since this resulted in a switching voltage which was determined by the properties of the epilayer, not by those of the LB film.

In principle, LB film technology does possess several significant advantages for use as the active layer in sensors. Many active materials, especially biological ones such as enzymes and proteins, could be prepared as LB film forming derivatives; others can be incorporated into a matrix of film material, as has been done for several kinds of dye molecule. Such films offer precise control of the quantity of material deposited, a high degree of structural perfection (it may also be possible to control or modify the structure) and very good uniformity over a large area. These attributes could prove invaluable for the mass production of high quality sensors, although a considerable long term effort will be required before this technique can be exploited effectively.

REFERENCES - CHAPTER 2

1. K. F. Braun
   Pogg. Ann. 153 (1874) 556.

2. W. Schottky, R. Stormer and F. Waibel
   Zeits. f. Hochfrequenztechn. 37 (31) 162.

3. A. H. Wilson
   Proc. Roy. Soc. (A) 136 (32) 487.

4. W. Schottky and W. Hartmann
   Zeits. f. techn. Physik. 16 (35) 512.

5. W. Schottky
   Naturwiss 26 (38) 843.

6. N. F. Mott
   Proc. Cambridge. Phil. Soc. 34 (38) 568.

7. H. A. Bethe
   M.I.T. Radiation. Lab. Rep. 43-12 (42).

8. J. Bardeen
   Phys. Rev. 71 (47) 717.

9. H. K. Henisch
   'Rectifying Semi-conductor Contacts' Clarendon, Oxford (57).

10. E. Spenke
    'Electronic Semiconductors' McGraw-Hill, New York (58).

11. S. M. Sze
    'Physics of Semiconductor Devices' Wiley, New York (81).

12. E. H. Rhoderick
    'Metal Semiconductor Contacts' Clarendon, Oxford (80).

13. H. K. Henisch
    'Semiconductor Contacts' Clarendon, Oxford (84).

14. B. L. Sharma (Ed.)
    'Metal-Semiconductor Schottky Barrier Junctions and their Applications' Plenum, New York (74).

15. L. J. Brillson
    Surface Science Reports 2 (82) 123.

16. V. L. Rideout
    Thin Solid Films 48 (78) 261.

17. E. H. Rhoderick
IEE Proc. I 129 (82) 1.

18. W. Schottky and E. Spenke
Wiss. Veroff. Siemens-Werken 18 (39) 225.

19. A. M. Cowley and S. M. Sze
J. Appl. Phys 36 (65) 3212.

20. V. Heine
Phys. Rev. 138A (65) 1689.

21. R. J. Archer and T. O. Yep
J. Appl. Phys. 41 (70) 303.

22. C. A. Mead
Phys. Rev. 134A (64) 713.

23. C. A. Mead
Solid St. Electron. 9 (66) 1023.

24. S. Kurtin, T. C. McGill and C. A. Mead
Phys. Rev. Lett 22 (69) 1433.

25. M. Schluter
Phys. Rev. B 17 (78) 5044.

26. R. H. Williams
Surface Sci. 132 (83) 122.

27. J. M. Andrews and J. C. Phillips
Phys. Rev. Lett 35 (75) 56.

28. L. J. Brillson
Phys. Rev. Lett. 40 (78) 260.

29. L. J. Brillson, C. F. Brucker, N. G. Stoffel, A. D. Katnani and G. Margaritondo
Phys. Rev. Lett. 46 (81) 838.

30. W. E. Spicer, I. Lindau, P. Pianetta, P. W. Chye and C. M. Garner
Thin Solid Films 56 (79) 1.

31. W. E. Spicer, I. Lindau, P. Skeath and C. Y. Su
J. Vac. Sci. Technol. 17 (80) 1019.

32. S. Krawczyk and P. Viktorovitch
Thin Solid Films 111 (84) 1.

33. A. Zunger
Thin Solid Films 104 (83) 301.

34. J. M. Woodall and J. L. Freeouf
J. Vac. Sci. Technol. 21 (82) 574.

35. B. W. Lee, D. C. Wang, R. K. Ni, G. Xu and M. Rowe
J. Vac. Sci. Technol. 21 (82) 577.

36. C. R. Crowell and S. M. Sze
Solid St. Electron 9 (66) 1035.

37. F. A. Padovani and R. Stratton
Solid St. Electron 9 (66) 695.

38. A. Y. C. Yu and E. H. Snow
J. Appl. Phys 39 (68) 3008.

39. C. T. Sah, R. N. Noyce and W. Shockley
Proc. IRE. 45 (57) 1228.

40. H. Norde
J. Appl. Phys. 50 (79) 5052.

41. T. Chot
Phys. Stat. Sol. A. 66 (81) K43.

42. C. D. Lien, F. C. T. So and M. A. Nicolet
IEEE Trans. Electron Dev. 31 (84) 1502.

43. S. Ashok. J. M. Borrego and R. J. Gutmann
Electronics Lett. 14 (78) 332.

44. A. M. Goodman
J. Appl. Phys. 34 (63) 329.

45. R. H. Fowler
Phys. Rev. 38 (31) 45.

46. W. G. Spitzer, C. R. Crowell and M. M. Atalla
Phys. Rev. Lett. 8 (62) 57.

47. B. M. Arora, A. K. Srivastava and S. Guha
J. Appl. Phys. 53 (82) 1820.

48. S. J. Fonash
J. Appl. Phys. 48 (76) 3597.

49. R. C. Jaklevic, D. K. Donald, J. Lambe and W. C. Vassell
Appl. Phys. Lett. 2 (63) 7.

50. P. O'Connor, T. P. Pearsall, K. Y. Cheng, A. Y. Cho. J. C. M. Hwang and K. Alavi
IEEE Electron. Dev. Lett. 2 (82) 64.

51. H. C. Card and E. H. Rhoderick
J. Phys. D. 4 (71) 1589.

52. A. M. Cowley
J. Appl. Phys. 37 (66) 3024.

53. S. J. Fonash
J. Appl. Phys. 54 (83) 1966.

54. D. V. Morgan, M. J. Howes and W. J. Devlin
J. Phys. D. 11 (78) 1341.

55. O. Wada, A. Majerfeld and P. N. Robson
Solid St. Electron 25 (82) 381.

REFERENCES - CHAPTER 3

1. T. Yamamoto and M. Morimoto
   Appl. Phys. Lett. 20 (72) 269.

2. H. Kroger and H. A. R. Wegener
   Appl. Phys. Lett. 23 (73) 397.

3. C-Y Wu and Y-T. Huang
   Solid State Electron. 27 (84) 203.

4. H. Kroger and H. A. R. Wegener
   Solid State Electron. 21 (78) 643.

5. A. Adan and K. Dobos
   Solid State Electron. 23 (80) 17.

6. T. Yamamoto, K. Kawamura and H. Shimzu
   Solid State Electron 19 (76) 701.

7. H. Kroger and H. A. R. Wegener
   Appl. Phys. Lett. 27 (75) 303.

8. H. Kroger and H. A. R. Wegener
   Solid State Electron 21 (78) 655.

9. K. C. Chik and J. G. Simmons
   Solid State Electron 22 (79) 589.

10. A. G. Nassibian
    IEEE Electron Device Lett. 1 (80) 67.

11. J. M. Dell, M. J. Davis and A. G. Nassibian
    IEEE Electron Device Lett. 2 (81) 121.

12. J. G. Simmons and A. El-Badry
    Solid State Electron. 20 (77) 955.

13. A. El-Badry and J. G. Simmons
    Solid State Electron 20 (77) 963.

14. J. Buxo, A. E. Owen, G. Sarrabayrouse and J. P. Sebaa
    Revue Phys. Appl. 13 (78) 770.

15. M. M. Darwish and K. Board
    Electron. Lett. 14 (78) 482.

16. K. Kawamura and T. Yamamoto
    IEEE Trans. Electron. Dev. 28 (81) 1078.

17. J. G. Simmons and A. A. El-Badry
    Radio and Electronic Engineer 48 (78) 215.

18. A. G. Nassibian, R. B. Calligaro and J. G. Simmons
    IEE J. Solid State and Electron. Dev. 2 (78) 149.

19. S. Moustakas, J. M. Dell, R. B. Calligaro, A. G. Nassibian and J. L. Hullet
IEE Proc. I 128 (81) 92.
20. K. Kawamura and T. Yamamoto
IEEE Electron Device Lett. 4 (83) 88.

21. T. Tamara, Y. Yamamoto and Y. Mizushima
IEEE Trans. Electron. Dev. 30 (83) 929.

22. C. E. C. Wood, L. F. Eastman, K. Board, K. Singer and R. Malik
Electron. Lett. 18 (82) 676.

23. J. M. Suzbert and K. E. Singer
J. Vac. Sci. Technol. B 3 (85) 794.

24. W. F. Croydon and E. H. C. Parker
'Dielectric Films on Gallium Arsenide', Gordon and Breach (81)

25. H. C. Card and E. H. Rhoderick
J. Phys. D. 4 (71) 1602.

26. R. A. Clarke and J. Shewchun
Solid State Electron. 14 (71) 957.

27. S. Kar and W. E. Dahlke
Solid State Electron. 15 (72) 869.

28. V. A. K. Temple, M. A. Green and J. Shewchun
J. Appl. Phys. 45 (74) 4934.

29. C. W. Jen, C. L. Lee and T. F. Lei
Solid State Electron, 24 (81) 949.

30. J. Shewchun and R. A. Clarke
Solid State Electron. 16 (73) 213.

31. M. A. Green and J. Shewchun
Solid State Electron. 17 (74) 349.

32. M. A. Green, V. A. K. Temple and J. Shewchun
Solid State Electron 18 (75) 745.

33. W. Shockley
Bell. Sys. Tech. J. 28 (49) 435.

34. A. M. Sekela, D. L. Feucht and A. G. Milnes
Inst. Phys. Conf. Ser. 24 (75) 245.

35. J. L. Moll
Proc. IRE 46 (58) 1076.

36. C. T. Sah, R. N. Noyce and W. Shockley
Proc. IRE 45 (57) 1956.

37. I. Zolomy
Solid State Electron 28 (85) 537.

38. S. E-D. Habib and J. G. Simmons
Solid State Electron 23 (80) 497.

39. S. M. Sze
'Physics of Semiconductor Devices' Wiley, New York (81).

40. M. J. Morant
'Introduction to Semiconductor Devices' Harrap, London (64).

41. K. A. Duncan, P. D. Toner, J. G. Simmons and L. Faraone
Solid State Electron. 24 (81) 941.

42. L. Faraone, J. G. Simmons, F-L. Hsueh and U. K. Mishra
Solid State Electron 25 (82) 335.

43. J. Millan, F. Serra-Mestres and J. Buxo
Revue. Phys. Appl. 14 (79) 921.

44. S. E-D. Habib and J. G. Simmons
Solid State Electron. 22 (79) 181.

45. S. E-D. Habib and J. G. Simmons
IEE Proc. I 127 (80) 111.

46. G. Sarrabayrouse, J. Buxo, A. E. Owen, A. Munoz-Yague and J-P. Sebaa
IEE Proc. I 127 (80) 119.

47. G. Sarrabayrouse, J. Buxo, J-P. Sebaa and A. Essaid
IEE Proc. I. 128 (81) 53.

48. S. E-D. Habib and A. A. Eltoukly
J. Appl. Phys. 52 (81) 3027.

49. J. Millan, F. Serra-Mestres and X. Aymerich-Humet
Solid State Electron. 25 (82) 565.

50. I. Zolomy
Solid State Electron. 26 (83) 643.

51. J. Martinez and J. Piqueras
Solid State Electron. 27 (84) 937.

52. A. C. Fiore de Mattos and G. Sarrabayrouse
Phys. Stat. Sol. (a) 87 (85) 699.

53. G. Sarrabayrouse, J. Buxo, A. Munoz-Yague, A. E. Owen and J. P. Sebaa
Inst. Phys. Conf. Ser. 50 (79) 179.

54. I. Zolomy and A. Adan
Solid State Electron. 24 (81) 19.

55. J. G. Simmons and G. W. Taylor
in 'Solid State Devices 1981' Editions de Physique (81).

56. R. Straton
J. Phys. Chem. Solids 23 (62) 1177.

57. J. W. Gadzuk
J. Appl. Phys. 41 (70) 286.

58. R. H. Fowler and L. Nordheim
Proc. Royal Soc. A 119 (28) 173.

59. J. C. Anderson
J. Vac. Sci. Technol. 9 (72) 1.

60. J. J. O'Dwyer
'The Theory of Electrical Conduction and Breakdown in Solid Dielectrics' Clarendon, Oxford (73).

61. J. Frenkel
Phys. Rev. 54 (38) 647.

62. J. G. Simmons
Phys. Rev. 155 (67) 657.

63. R. M. Hill
Phil. Mag. 23 (71) 59.

64. N. F. Mott and R. W. Gurney
'Electronic Processes in Ionic Crystals' O.U.P., Oxford (48).

65. A. Rose
Phys. Rev. 97 (55) 1538.

REFERENCES - CHAPTER 4

1. B. Franklin
Phil. Trans. R. Soc. London 64 (1774) 445.

2. A. Pockels
Nature 43 (1891) 437.

3. Lord Rayleigh
Phil. Mag. 48 (1899) 321.

4. I. Langmuir
J. Am. Chem. Soc. 39 (17) 1848.

5. K. M. Blodgett
J. Am. Chem. Soc. 57 (35) 1007.

6. H. Kuhn, D. Mobius and H. Bucher
'Spectroscopy of Monolayer Assemblies' in A. Weissberger and B. Rossiter, (Eds) 'Physical Methods of Chemistry' Vol. 1, pt. 3b, Wiley, New York (72).

7. G. L. Gaines, Jr.
'Insoluble, Monolayers at Liquid-Gas Interfaces' Wiley, New York (66).

8. P. S. Vincett, W. A. Barlow, F. T. Boyle, J. A. Finney and G. G. Roberts
Thin Solid Films 60 (79) 265.

9. C. W. Pitt and L. M. Walpita
Thin Solid Films 68 (80) 101.

10. L. Blight, C. W. N. Cumper and V. J. Kyte
J. Coll. Sci. 20 (65) 393.

11. J. Jaffe, G. Bricman and A. Gelbecke
J. de Chim. Phys. 46 (67) 942.

12. L. Wilhemly
Ann. Physic 119 (1863) 177.

13. G. G. Roberts, P. S. Vincett and W. A. Barlow
Phys. Technol. 12 (81) 69.

14. H. Bucher, K. H. Drexhage, M. Fleck, H. Kuhn, D. Mobius, F. P. Schafer, J. Sondermann, W. Sperling, P. Tillman and J. Wiegand
Mol. Cryst. 2 (67) 199.

15. P. Christie
Ph.D. Thesis, Durham (85).

16. I. R. Peterson, G. J. Russell and G. G. Roberts
Thin Solid Films 109 (83) 371.

18. Unpublished Data, Dr. R. K. Thomas (Oxford University).

19. G. G. Roberts, P. S. Vincett and W. A. Barlow
J. Phys. C. 11 (78) 2077.

20. D. Allara and J. D. Swalen
J. Phys. Chem. 86 (82) 2700.

21. C. Mori, H. Noguchi, M. Mizuno and T. Watanabe
Jpn. J. Appl. Phys 19 (80) 725.

22. C. A. Brown, F. C. Burns, W. Knoll and J. D. Swalen
J. Phys. Chem. 87 (83) 3616.

23. S. Baker, M. C. Petty, G. G. Roberts and M. V. Twigg
Thin Solid Films 99 (83) 53.

24. S. Baker, G. G. Roberts and M. C. Petty
IEE Proc. I 130 (83) 260.

25. Y. L. Hua, G. G. Roberts, M. M. Ahmad, M. C. Petty, M. Hanack and M. Rein
Phil. Mag. B 53 (86) 105.

26. P. S. Vincett and G. G. Roberts
Thin Solid Films 68 (80) 135.

27. E. P. Honig
Thin Solid Films 33 (77) 231.

28. B. Mann and H. Kuhn
J. Appl. Phys. 42 (71) 4398.

29. B. Mann, H. Kuhn and L. V. Szentpaly
Chem. Phys. Lett. 8 (71) 82.

30. E. E. Polymeropoulos
J. Appl. Phys. 48 (77) 2404.

31. M. A. Careem and R. M. Hill
Thin Solid Films 51 (78) 363.

32. J. L. Miles and H. O. McMahon
J. Appl. Phys. 32 (61) 1176.

33. A. Leger, J. Klein, M. Belin and D. Deformeau
Thin Solid Films 8 (71) R51.

34. G. L. Larkins Jr., E. D. Thompson, F. Ortiz, C. W. Burkhart and J. B. Lando
Thin Solid Films 99 (83) 277.

35. T. M. Ginnai, D. P. Oxley and R. G. Prichard
Thin Solid Films 68 (80) 241.

36. M. H. Nathoo and A. K.Jonscher
J. Phys. C. 4 (71) L301.

37. A. K. Jonscher and M. H. Nathoo
Thin Solid Films 12 (75) 515.

38. G. G. Roberts, P. S. Vincett and W. A. Barlow
J. Phys. C. 11 (78) 2077.

39. M. Sugi, K. Membach, D. Mobius and H. Kuhn
Solid St. Comm. 13 (73) 603.

40. M. Sugi, T. Fukui and S. Iizima
Appl. Phys. Lett. 27 (75) 559.

41. M. Sugi, T. Fukui and S. Iizima
Chem. Phys. Lett. 45 (77) 163.

42. M. Sugi, T. Fukui and S. Iizima
Phys. Rev. B 18 (78) 725.

43. M. H. Nathoo
Thin Solid Films 16 (73) 215.

44. R. W. Sykes
Ph.D. Thesis, Durham (81).

45. J. Batey, M. C. Petty and G. G. Roberts
Proc. Int. Conf. Insulating Films on Semiconductors, Eds. J. F. Verwey and D. R. Walters, Elsevier (83) 141.

46. K. K. Kan, M. C. Petty and G. G. Roberts
'The Physics of MOS Insulators', Eds. G.Lucovsky, S. T. Pantilides and F. L. Galeener, Pergamon (80).

47. S. Baker
Ph.D. Thesis, Durham (75).

48. G. G. Roberts
Advances in Physics 34 (85) 475.

49. J. Tanguy
Thin Solid Films 13 (72) 33.

50. G. G. Roberts, K. P. Pande and W. A. Barlow
Electron. Lett. 13 (77) 581.

51. G. G. Roberts, K. P. Pande and W. A. Barlow
Solid State and Electron Devices 2 (78) 169.

52. R. W. Sykes, G. G. Roberts, T. Fok and D. Clark
Proc. IEE I. 127 (80) 137.

53. M. C. Petty and G. G. Roberts
Inst. Phys. Conf. Ser. 50 (80) 186.

54. K. K. Kan, G. G. Roberts and M. C. Petty
Thin Solid Films 99 (83) 291.

55. J. P. Lloyd, M. C. Petty, G. G. Roberts, P. G. LeComber and W. E. Spear
Thin Solid Films 99 (83) 297.

56. G. G. Roberts, M. C. Petty and I. M. Dharmadasa
Proc. IEE. I. 128 (81) 197.

57. R. H. Tredgold and G. W. Smith
IEE. Proc. I. 129 (82) 137.

58. J. Batey, G. G. Roberts and M. C. Petty
Thin Solid Films 99 (83) 489.

59. J. Batey, M. C. Petty, G. G. Roberts and D. R. Wight
Electron. Lett. 20 (84) 489.

60. C. S. Winter, R. H. Tredgold, P. Hodge and E. Koshdel
IEE Proc. I. 131 (84) 125.

61. C. S. Winter and R. H. Tredgold
J. Phys. D. 17 (84) L123.

62. M. C. Petty, J. Batey and G. G. Roberts
IEE Proc. I. 132 (85) 133.

63. G. G. Roberts, M. C. Petty, S. Baker, M. T. Fowler and N. J. Thomas
Proc. 2nd Int. Conf. on LB films, Schenectady 1985.

64. R. H. Tredgold and Z. I. El-Badawy
J. Phys. D. 18 (85) 103.

REFERENCES - CHAPTER 5

1. V. L. Rideout
Solid State Electron 18 (75) 541.

2. B. Schwartz (Ed.)
'Ohmic Contacts to Semiconductors'
Electrochemical Society, New York (69).

3. W. Kern
RCA Review 39 (78) 278.

4. D. J. Stirland and B. W. Straughan
Thin Solid Films 31 (76) 139.

5. B. Tuck
J. Mat. Sci. 10 (75) 321.

6. Y. Tarui, Y. Komiya and Y. Harada
J. Electrochem. Soc. 118 (71) 118.

7. A. C. Adams and B. R. Pruniaux
J. Electrochem. Soc. 120 (73) 408.

8. I. R. Peterson, G. J. Russell and G. G. Roberts
Thin Solid Films 109 (83) 371.

9. J. Batey
Ph.D. Thesis, Durham (83).

CHAPTER 6 - REFERENCES

1. F. A. Padovani and R. Stratton
   Solid State Electron 9 (66) 695.

2. J. M. Borrego, R. J. Gutmann and S. Ashok
   Solid State Electron 20 (77) 125.

3. B. Pellegrini and G. Salardi
   Solid State Electron 21 (78) 465.

4. A. K. Srivastava, B. M. Arora and S. Guha
   Solid State Electron 24 (81) 185.

5. A. C. Adams and B. R. Pruniaux
   J. Electrochem. Soc. 120 (73) 408.

6. B. R. Pruniaux and A. C. Adams
   J. Appl. Phys. 43 (72) 1980.

7. V. Kumar and W. E. Dahlke
   Solid State Electron 20 (77) 143.

8. I. Shiota, K. Motoya, T. Ohmi, N. Miyamoto and J. Nishizawa
   J. Electrochem. Soc. 124 (77) 155.

9. M. Otsubo, T. Oda, H. Kumabe and H. Miki
   J. Electrochem. Soc. 123 (76) 676.

10. B. Schwartz
    J. Electrochem. Soc. 118 (71) 657.

11. G. G. Roberts, M. C. Petty, M. C. Caplan and E. H. Poindexter
    Proc. Int. Conf. Insulating Films on Semiconductors, Eds. J. F. Verweij and D. R. Walters, Elsevier (83).

12. M. C. Petty, J. Batey and G. G. Roberts
    IEE Proc I 132 (85) 133.

13. N. J. Evans
    Ph.D. Thesis, Durham (86).

14. R. H. Tredgold and Z. I. El-Badawy
    J. Phys. D. 18 (85) 103.

15. S. Baker, G. G. Roberts and M. C. Petty
    IEE Proc. I 130 (83) 260.

16. J. H. Marsh, P. A. Houston and P. N. Robson
    Inst. Phys. Conf. Ser. 56 (81) 621.

17. A. Cappy, R. Fauquembergue, E. Constant, G. Salmer and B. Carnez
    Inst. Phys. Conf. Ser. 56 (81) 175.

18. J. D. Oliver and L. F. Eastman
    21st Electronic Materials Conf. (1979), Boulder, Colorado.

19. K. Kajiyama, Y. Mizushima and S. Sakata
Appl. Phys. Lett. 23 (73) 458.

20. D. V. Morgan and J. Frey
Electron. Lett. 14 (78) 737.

21. P. O'Connor, T. P. Pearsall, K. Y. Cheng, A. Y. Cho. J. M. C. Hwang and K. Alavi
IEEE Electon. Device Lett. 3 (82) 64.

22. C. L. Cheng, A. S. H. Liao, T. Y. Chang, E. A. Caridi, L. A. Coldren and B. Lalevic
IEEE Electron. Device Lett. 5 (84) 511.

23. D. T. Clark, T. Fok, G. G. Roberts and R. W. Sykes
Thin Solid Films 70 (80) 261.

24. Landolt-Bornstein New Series, 17a Semiconductors, Springer-Verlag, Berlin (82).

25. H. C. Card and E. H. Rhoderick
J. Phys. D. 4 (71) 1589.

26. Private Communication, Y. L. Hua (Permanent Address:- Changchun Institute of Physics, Chinese Academy of Sciences, Changchun, China).

27. R. W. Sykes, G. G. Roberts, T. Fok, D. T. Clark
IEE Proc. I. 127 (80) 137.

28. F. A. Padovani and G. G. Sumner
J. Appl. Phys. 36 (63) 3744.

29. A. N. Saxena
Surface Science 13 (69) 151.

REFERENCES - CHAPTER 7

1. Y. Moreau, J-C. Manfacier and H. K. Henish
Solid State Electron. 25 (82) 137.

2. G. Sarrabayrouse, J. Buxo, A. E. Owen, A. Munoz Yague and J-P. Sebaa
IEE Proc. I 127 (80) 119.

3. J. G. Simmons and A. A. El-Badry
The Radio and Electronic Engineer 48 (78) 215.

4. I. Zolomy
Solid State Electron 28 (85) 537.

5. S. E-D. Habib and J. G. Simmons
Solid State Electron 21 (78) 643.

6. H. Kroger and H. A. Wegener
Solid State Electron 23 (80) 497.

7. G. Sarrabayrouse, J. Buxo, A. Munoz Yague, A. E. Owen and J-P. Sebaa
Inst. Phys. Conf. Ser 50 (80) 179.

8. J. Buxo, A. E. Owen, G. Sarrabayrouse and J-P. Sebaa
Revue. Phys. Appl. 13 (78) 767.

9. H. Kroger and H. A. R. Wegener
Solid State Electron. 21 (78) 643.

10. C-Y, Wu and Y-T. Huang
Solid State Electron. 27 (84) 203.

11. J. Batey, M. C. Petty, G. G. Roberts and D. R. Wight
Electron. Lett. 20 (84) 489.

12. S. Baker, G. G. Roberts and M. C. Petty
IEE Proc. I 130 (83) 260.

13. I. Lunstrom, S. Shiraraman, C. Svenson and L. Lundkvist
Appl. Phys. Lett. 26 (75) 55.

14. K. Kawamura and T. Yamamoto
IEEE Electron. Device Lett. 4 (83) 88.

LIST OF FIGURES

LIST OF TABLES